HYDRODYNAMIC DETACHMENT OF DEPOSITED PARTICLES IN FLUIDIZED BED FILTER BACKWASHING

A Dissertation
Presented to
The Academic Faculty

By

Barbara Maria Brouckaert

In Partial Fulfillment
Of the Requirements for the Degree
Doctor of Philosophy in Civil and Environmental Engineering

Georgia Institute of Technology

July, 2004

HYDRODYNAMIC DETACHMENT OF DEPOSITED PARTICLES IN FLUIDIZED BED FILTER BACKWASHING

Approved by:

Dr. Appiah Amirtharajah, Advisor

Dr. J. Carlos Santamarina

Dr. Terry W. Sturm

Dr. Costas Tsouris

Dr. Sotira Yiacoumi

May 21, 2004

To my family, especially Enrico.

AKNOWLEDGMENTS

The research presented in this work was partially funded by the South African Water Research Commission. Experimental facilities were provided by by Umgeni Water. Some additional instrumentation was provided by the University of Natal School of Chemical Engineering and the Pollution Research Group. Funding for my graduate studies was provided by Georgia Department of Natural Resources, USEPA and the Cobb-Marrietta Water Authority.

During the course of my studies, I had the great privilege of working with a large number of people who contributed to my research and understanding of my topic in many different ways. Working under the guidance of my advisor, Dr Amirtharajah, has been an opportunity of a lifetime. Not only have I benefited from his vast knowledge and experience in the context of my doctoral studies, but he also supported me in the risky decision to move the research component of my Ph.D. home to South Africa and has continued to provide support and advice to our research and academic programs at the University of KwaZulu-Natal.

I would also like to thank my other committee members: Dr Carlos Santamarina, Dr Terry Sturm, Dr Sotira Yiacoumi and Dr Costas Tsouris for their helpful criticisms and insights. I would also like to acknowledge the contributions of two of my original committee members, Dr Christine Tiller and Dr Jeffrey Morris who moved from Georgia Tech before my I completed my research program.

The research presented in this document would not have been possible without the support and assistance of the staff of the Umgeni Water Process Evaluation Facility, in particular Martin Pryor and Rachi Rajagopaul. I would like to extend my sincere thanks and appreciation to all my friends and colleagues in Umgeni Water's Scientific Services Division.

I would also like to thank my fellow Tech students, in particular, Timmerly Richman, Vasethuvan "Ravi" Ravisangar, James Amburgey and Jeffrey Huang, with whom I worked most closely, and Dr Guangxuan Zhu who was both a mentor and a friend. In addition I would like to thank my three closest friends at Georgia Tech, Becky Pascual, Myrna Jacobson and Rosy Krajmalnik Brown, who helped me through the highs and lows of graduate student life.

In September 1998 and August 2000 I had the privilege of visiting Dr Caroline Fitzpatrick's Environmental Engineering Group at University College, London in order to learn more about their filter backwash studies. Both trips were extremely informative and helpful to me in developing my own research project. I would like to thank Dr Fitzpatrick, David Hall and Ian Sturtevant for their assistance and hospitality.

I would like to express my gratitude to the late Dr Joseph P. Gould who assisted me in applying to Georgia Tech, and to both him and his wife Julia for their hospitality and friendship when I first arrived in the U.S.

Finally, the completion of my Ph.D would not have been possible without the active support and encouragement of my family, particualry my father Chris, a fellow water engineer, and my husband Enrico.

TABLE OF CONTENTS

LIST OF TABLES

LIST OF FIGURES

SUMMARY

Rapid or depth filtration is an integral part of most water treatment facilities around the world. Particulate contaminants including viruses, bacteria and pathogenic protozoa are removed from the filter influent by collision and adhesion to the filter media. Over time, filters clog and have to be cleaned by reversing the flow to detach and flush away the accumulated deposits.

Over the last few decades, there has been a substantial amount of research on modeling the filtration phase of the filter operating cycle. However, there has been little fundamental research into the backwash process. Theoretical and experimental studies on backwash fundamentals have tended to focus on the behaviour of relatively simple model systems and the mechanisms of detachment in real filters are still not well understood. Most of the backwash models that have been developed are for up-flow wash with full bed fluidization. The effect of auxiliary backwash on particle detachment is generally not modeled although most modern treatment works now use some kind of auxiliary system to increase the agitation and abrasion of the filter media.

The primary objective of the current study was to investigate the backwashing behavior of filters under more realistic conditions and to develop a quantitative model or models of the backwash process based on both fundamental and practical considerations. The focus of this

study was on water only backwash but the applicability of the results to auxiliary backwash systems is discussed.

The experimental part of the study was carried out at the Umgeni Water Process Evaluation Facility in South Africa using a pilot-scale filtration plant drawing raw water from the head of Umgeni's Wiggins Water Treatment Works. The effects of filter backwash rate, coagulant used, degree of filter clogging and age of filter deposits on backwash behavior and efficiency was investigated. Several of the backwash experiments were also recorded on video tape to facilitate the analysis of the backwash behavior. The results of these experiments and their implications both for modeling and managing filter backwash are discussed.

The initial stages of backwashing were found to be dominated by mixing and flow localization effects not accounted for in existing models of backwash. These effects appeared to be dependent on both the equipment and the experimental conditions making the development of an accurate model of backwash transient behavior extremely difficult. However, it is shown that the overall efficiency of backwash can be predicted based on data about the filter and backwash design and operation that should be available at any treatment plant. This is an important first step in the development of modeling tool for the design and optimization of the complete filter cycle.

A significant finding of this study is that the average age of filter deposits is one of the most important factors determining the ease with which they are detached during backwashing.

Deposits become more difficult to remove the longer they remain in the filter. This has important implications for the robust design and operation of filters in applications where optimal backwash cannot be guaranteed. The rate of accumulation of mud in a filter over multiple filter cycles was determined experimentally for one set of backwash conditions and a procedure for estimating the useful life of a filter bed with sub-optimal backwash is proposed.

CHAPTER 1

INTRODUCTION AND OVERVIEW

1.1. Granular media filtration and filter backwashing in water treatment

Granular media filtration is an integral part of conventional water treatment and is mandated by the USEPA for the treatment of surface water (Cortruvo and Vogt, 1990). In rapid filtration, the type of filtration most commonly used in water treatment, floc particles are typically 1 or 2 orders of magnitude smaller than the pore spaces between clean filter media grains. Particles are removed from suspension primarily by transport to, collision with and adhesion to the filter grains. Since a significant fraction of the influent particles will penetrate some way into the filter bed before being removed, this type of filter operation is also referred to as "depth" filtration.

During the filter run, floc deposits accumulate on the surface of the filter media and in the pore spaces resulting in an increase in headloss through the media and/or a decrease in flow. Periodic washing is required to unclog the filter and to avoid turbidity break through when its floc holding capacity is exceeded. Failure to clean a filter adequately can lead to the formation of agglomerates of filter media and floc known as mudballs, solidified subsurface accumulations and the development of cracks in the surface of the filter bed and between the media and the

filter walls (Cleasby, 1990). The deterioration of the state of the filter bed may eventually result in excessively short filter run times and/or a decline in filtrate quality.

1.1.1. Filter Backwash Options

For many years it was believed that rapid filters should be washed very gently so as not to remove the biological film that supposedly coated the media. However, during the first part of the 20th century it came to be appreciated that a clean filter bed performed better than a film coated one (Baylis, 1954).

Rapid filters in the United States have traditionally been washed with full bed fluidization. High rate water wash alone is usually adequate for applications where no coagulant is added to the filter influent (Martin, 1998). Rapid filtration without coagulation is generally limited to the treatment of very low turbidity waters filters to remove dissolved iron, manganese and/or organics by chemical oxidation, precipitation and filtration. Most rapid filters require the use of coagulants to achieve acceptable turbidity removals. Extensive experience has shown that high rate up flow wash alone cannot maintain filter beds in a reasonably clean condition for longer than several months when coagulants are used (Kawamura, 2001).

Consequently, several different auxiliary wash systems have been developed to increase the energy dissipation in the filter during backwash. The different backwash options are described below.

1.1.1.1. Upflow water wash without auxiliary wash

This system relies on the expansion of the bed and drag forces on attached suspended particles to affect cleaning. It is now widely accepted that using water alone is a weak washing method that does not solve all dirty filter-related problems. Amirtharajah (1978) argued that this is due to the lack of abrasion occurring between the grains in a fluidised bed.

Water only backwash without some form of auxiliary backwash is seldom employed in modern treatment plants (Haarhoff, 1997). There are however a few remaining applications of this method. The current study was conducted in parallel with an investigation into the suitability of autonomous valveless filters (AVF's) for use in rural treatment plants in South Africa (Brouckaert et al., 2003). The unique hydraulic design of the AVF allows it to backwash automatically when a certain terminal headloss is reached, without any operator intervention or electronic controls. However, autonomous backwash is restricted to water wash only. Despite the relative inefficiency of the backwash, valveless filters have become a popular choice for rural treatment works where auxiliary backwash systems often do not function correctly and operators fail to backwash filters regularly.

1.1.1.2. Upflow water wash with air scour

Air scour systems supply air to the full area of the filter from orifices under the filter medium (Cleasby, 1990). Air scour has been used alone (consecutive air and water wash) or together with low-rate water backwash in an unexpanded or slightly expanded bed

(simultaneous air and water wash). Both air scour alone and combined air and water wash have been found to be fairly effective in preventing filter mudballing (Martin, 1998).

When air is used alone, most of the scouring occurs near the bed surface. Agitation deeper in the bed is only observed in the first minute or so while discrete air bubbles moves through the mixture of water and sand in the bed. Gradual displacement of water from the pore spaces results in compaction of the bed and the formation of fixed channels through which air travels directly to the bed surface (Haarhoff and Malan, 1983). As a result, this system is not very effective in cleaning the lower sections of the filter bed and there have been a few cases of significant mud accumulation in the lower regions of filters in which sequential air and water wash have been used (Kawamura, 2001).

By contrast, simultaneous air and water flows in the correct ratios result in the formation and collapse of pockets of air throughout the filter bed, or "collapse pulsing" of the filter bed (Amirtharajah, 1993). This has been established as the most effective filter cleaning method as it produces the greatest amount of abrasion between the media grains throughout the depth of the bed.

Air scour alone followed by low rate water wash is typically used in monomedia filters with 0.6 to 1.2 mm effective size media (Martin, 1998). Air scour alone followed by high rate water backwash is used in dual and multimedia filters. Simultaneous air and water wash is usually reserved for deep bed coarse-grained filters (effective size 1 – 2 mm).

1.1.1.3. Upflow water wash with surface/ sub-surface wash

Surface wash systems have been extensively used to improve the effectiveness of fluidised-bed backwashing in the USA (Haarhoff, 1997) but are little used elsewhere in the world (Haarhoff and Malan, 1983).

Surface wash uses jets of water located about 5cm above the fixed bed media surface to increase the agitation of the media during backwash and thus assist the release of attached particles (Cleasby, 1990). Fixed systems discharge auxiliary washwater from equally spaced nozzles in a pipe grid while rotary arms have pipe arms which swivel on a central bearing (Martin, 1998). Rotary systems provide a better cleaning action but are more likely to fail due to mechanical problems. Subsurface wash systems are sometimes used in dual or multimedia filters and have jets below the surface of the fixed bed.

The effectiveness of surface wash has been found to be comparable to consecutive air and water wash (Cleasby et al., 1977). Both systems may be ineffective in cleaning certain areas of the bed (Kawamura, 2001; Martin, 1998), especially if mudballs sink into the fluidised media away from the zone of maximum agitation.

1.2. Modeling filter backwash

Over the last few decades, there has been a substantial amount of research on modeling the filtration phase of the filter operating cycle. However, there has been little fundamental

research into the backwash process. A better understanding of backwashing would assist in the optimization of existing filters as well as improving filter design for more robust operation, particularly in applications where optimum backwash cannot be guaranteed.

Previous modeling efforts have tended focus on either the mechanism of detachment of filter deposits from the fluidized filter media or on attempting to relate the rate of detachment to the backwash concentration profile (backwash effluent concentration as a function of backwash time).

Limitations of existing modeling approaches include the following:

- Theoretical and experimental studies on backwash fundamentals have tended to focus on the behavior of relatively simple model systems and the mechanisms of detachment in real filters are still not well understood.

- Most of the backwash models that have been developed are for up-flow wash with full bed fluidization. Amirtharajah (1985) developed a model of the condition for optimum backwash with simultaneous air and water and Kawamura (1975b) developed formulae to calculate the energy input to the filter for different backwash options. However, as far as the author is aware, no existing models include the effect of auxiliary backwash on the rate of particle detachment.

- Available modeling tools for the design of filter backwash are currently limited to correlations that predict filter media expansion during backwash and models of the theoretical optimum backwash rates. There are currently no models available that can provide quantitative predictions of backwash efficiency or which can predict the long-term impact of backwash conditions on filter performance.

1.3. Aims and Objectives

The primary objective of the current study was to investigate the backwashing behavior of filters under realistic operating conditions and to develop a quantitative model or models of backwash that could be more easily applied to the design and optimization of the complete filter cycle (filtration + backwash) than existing models. Such a model or models should integrate fundamental considerations of microscopic attachment and detachment forces and mechanisms with observations of the macroscopic behavior during both filtration and backwashing (e.g. headloss development, filter media expansion, filter mudballing, backwash effluent concentration).

Specific research objectives were to:

- Assess the assumptions on which existing backwash models are based and identify their limitations.

- Develop a better conceptual framework for understanding and modeling filter backwash, including the mechanisms by which inefficient backwash leads to filter mudballing.

- Investigate the effect of filtration and backwash conditions on backwash efficiency.

- Develop a model for predicting backwash efficiency under realistic operating conditions.

- Develop a model of the long-term impact of inefficient backwash on the state of the filter media.

1.4. Approach

In this study, three different aspects of filter backwash performance were investigated: (i) the behavior of the filter bed during backwash and the rate and mechanisms of floc detachment; (ii) the factors affecting the accumulation of residual mud in a filter over multiple backwash runs (iii) the factors which affect the overall efficiency of a single backwash. This section describes the approach taken to each topic. The focus of this investigation was on water only backwash (fluidised backwash without auxiliary wash). However, the implications of the results obtained for systems with auxiliary backwash are also discussed.

1.4.1. Filter backwash behavior and the kinetics of detachment

The fundamental purpose of filter backwash is to detach the maximum amount of floc from the filter grains with the smallest possible cost in water and energy. A key issue in the overall optimization of backwash is the intrinsic rate of detachment of floc from the filter media. The rate of detachment at any point in the filter cannot be measured directly or predicted using any existing models of particle detachment. Therefore, several authors have attempted to relate the detachment rate to the measured backwash concentration profile (concentration of solids in the backwash effluent as a function of time).

Unfortunately, the backwash concentration profile is also affected by the distribution of filter deposits at the end of the filter run and by mixing effects both within and above the filter bed. These effects have to be taken into account if models of the concentration profile are to be useful for determining the intrinsic rate of detachment.

A set of experiments was designed to study the backwash concentration profile and the behavior of the backwashing filter in detail. The concentration of the backwash effluent leaving the filter bed was measured as a function of backwash time using an on-line opacity meter. These experiments were also recorded on videotape in order to facilitate the analysis of various phenomena observed during filter backwashing.

Floc deposits retained in the filter after water backwash were subsequently detached using a vigorous regime of combined air and water wash. The mass detached during each wash was measured separately to determine the efficiency of the water only wash.

Backwash experiments were carried out at a range of backwash rates (varying the hydrodynamic forces) and for different degrees of filter clogging using two different coagulants (varying the attachment forces and initial distribution of deposits).

1.4.2. Accumulation of mud in filters due to inefficient backwash

During the course of the parallel investigation into the operation of the AVF, it became apparent that what happens to residual floc deposits in a filter between one backwash and the next may be as or more important as what happens during a single backwash. Mudball formation was observed after as few as one or two filter runs with water only backwash. Furthermore, the appearance of the mudballs was strikingly different to residual chunks of clogged media observed in the filter during backwash after a single filter run. As a result, a second line of investigation was undertaken to determine the rate of accumulation of residual deposits over multiple filter runs and the role of changes in deposit characteristics in the formation of mudballs.

Five series of experiments were carried out in which the filtration and backwash conditions were maintained as constant as possible and the filter was operated for 1, 2, 4, 6 and

9 consecutive runs with water only backwash. At the end of each series, the total residual mass left behind in the filter after water only backwash was measured. The results were then analyzed to determine which factors influenced the rate of accumulation of mud in the filter and whether mudballing itself affected backwash efficiency.

A separate series of experiments was conducted in which backwash of a clogged filter was delayed between 0 and 66 hours after the end of the filter run in order to prove that the adhesive of the floc deposits increased with age.

1.4.3. Factors affecting the efficiency of backwash

The experiments described in Sections 1.4.1 and 1.4.2 were also analyzed to determine the effect of various factors on overall backwash efficiency. The goal was to identify specific parameters that were indicators of both the hydrodynamic detachment forces and the floc attachment forces.

The filtration parameters within each set of experiments were kept as consistent as possible. The only factors varied deliberately were filter backwash rate, coagulant used, number of consecutive runs with water only backwash, filter run time and terminal headloss. However, it was not possible to control the quality or temperature of the raw water quality coming into the plant. Temperature and influent water turbidity varied within a fairly narrow range (19 to 26 ^{o}C and 0.8 to 3 NTU). However, in some cases there were significant variations in rate of headloss

development, filtrate quality and total mass of floc deposited within each set of experiments. These variations indicated that changes in the quantity and characteristics of the influent floc may also have had an impact on backwash efficiency.

Multiple linear regression analysis was used to look for correlations between backwash efficiency and various parameters relating to the operation and performance of the filter in filtration mode. Since the experiments were not designed to look at these effects and the ranges of parameter values were fairly small, few statistically significant correlations were found. However, some interesting results were obtained which contributed to a broader understanding of how the operation of the filter affected backwash efficiency.

1.5. Thesis structure

The starting point for this work is a review of previous attempts to model the backwash process. Chapter 2 " A Critical Review of the Literature Filter Backwash Modeling" describes the various approaches to backwash modeling in the literature. Three different aspects of backwash modeling are discussed: (a) predicting the optimum backwash rate based on hydrodynamic conditions, (b) modeling the effect of adhesive forces on the detachment mechanism and rate, and (c) modeling the backwash concentration profile.

Chapter 3 “Experimental Methodology” describes the experimental apparatus and instrumentation used in this study and the procedures for determining the efficiency of backwash.

Chapters 4 and 5 present calculations used in the analysis of the experimental results. Chapter 4 “Filter Media Characteristics, Fluidization and Theoretical Optimum Backwash Conditions” describes the calculation of the theoretical optimum backwash conditions as a function of the properties of the clean filter media. The results of these calculations are compared with trends in measured backwash efficiency in Chapter 9.

Chapter 5 “Material Balance Calculations” describes the calculation of the total mass deposited during filtration, mass detached during and mass retained after backwashing.

The major experimental results are presented in Chapters 6 to 9. Chapter 6 and 7 present experimental results on the behavior of the filter bed and the rate of particle detachment during backwash and discuss the implication of the results for filter backwash modeling while Chapters 8 and 9 present results on backwash efficiency. The implications of the results for backwash modeling are discussed in each chapter.

Chapter 6 “Behavior of Real Filters During Backwashing” focuses on macroscopic phenomena observed during backwashing while Chapter 7 “The Backwash Concentration

Profile and the Kinetics of Detachment" focuses on the analysis of the backwash concentration profile.

Chapter 8 "Mass Accumulation and the Growth of Mudballs in Filters" discusses the mechanisms of mudball formation and growth and presents experimental data on the rate of accumulation of mud in a filter over multiple filter runs. A model of mud accumulation is proposed.

Chapter 9 "Factors Affecting the Efficiency of Backwash" presents experimental results on the effects of various filtration and backwash parameters on backwash efficiency. Stepwise multiple linear regression is used to identify which filter operation and performance parameters are the best indicators of the adhesive properties of the floc.

Chapter 10 "Conclusions and Recommendations" summarizes the results of this study and presents recommendations for future work.

CHAPTER 2

A CRITICAL REVIEW OF THE LITERATURE ON FILTER BACKWASH MODELING

2.1. Introduction

This Chapter reviews various approaches to modeling the backwash process described in the literature. The focus is on models that deal with the detachment of floc particles from media grains. Modeling the expansion of clean fluidized beds is discussed separately in Chapter 4. The backwash models presented in this chapter have been developed with one or more of the following objectives:

- Predicting the conditions for optimum backwash (Amirtharajah, 1971; Kawamura, 1975b; Sakkas and Lekkas, 1989).

- Determining the effect of floc, clay and bacteria surface properties on backwash efficiency (Huang and Basagoiti, 1989; Ahmad, 1996; Raveendran, 1993; Mahmood, 1996; Richman, 1999).

- Increasing the efficiency of washwater usage. Backwashing utilizes filtered water and can consume up to 10 % of plant production even with well-managed filters

(Bhargava and Ojha, 1989). In addition, the costs of treatment and/or disposal of the backwash effluent have to be considered. Prolonging backwash results in increased washwater usage for diminishing returns in terms of cleaning efficiency.

- Predicting the impact of backwash remnants on filter ripening on the following filter run. Analysis of the backwash effluent concentration profile can be used to predict the concentration of detached particles remaining in and above the filter media towards the end of backwash (Amirtharajah and Wetstein, 1980). Amburgey et al. (2003) found that the spike in filtrate turbidity during filter ripening could be reduced by modifying the backwash procedure.

Although most treatment plants now employ auxiliary backwash, modeling efforts have tended to focus on water only fluidized backwash. It has been assumed that the water only fluidized backwash regime would be the simplest to model and the results could later be extrapolated to systems including auxiliary wash. Furthermore, there is already a large body of literature on the behavior of fluidized beds because of their widespread use in the chemical and mineral processing industries.

Efforts to model particle detachment during backwashing can be divided into three categories:

1. Earlier attempts to analyze backwash from a theoretical point of view focused on the hydrodynamic aspects of the detachment mechanisms and the prediction of the optimum backwash rate.

2. Advances in colloid science have prompted several researchers to study the physico-chemical forces that cause particles to adhere to surfaces and their impact on the backwash process.

3. Several authors have attempted to model and analyze the backwash effluent concentration profile with time in order to better understand the backwash process and/or predict its impact on the following filter run.

The first part of this chapter focuses on the mechanisms of detachment in filter backwashing while the second part looks at progress in modeling the backwash concentration profile. The models presented here are revisited in Chapter 6 and Chapter 7. Chapter 6 considers the behavior of real filters during backwashing and how this impacts attempts to model the backwash process. Chapter 7 explores whether information about the intrinsic rate of detachment of floc from the filter grains can be extracted from the backwash concentration profile in practice.

2.2. Mechanisms involved in filter cleaning

During rapid filtration, influent particles collide with and adhere to the surface of media grains and to other particles already attached. Detaching deposited particles requires the application of a force that exceeds the strength of their attachment to the media grains. Therefore the probability of detachment occurring is a function of both the attachment forces and the forces tending to result in detachment. Both the attachment and detachment forces vary with time and depend on the structure of floc deposits and media-floc composites.

Theoretical work on the factors affecting the efficiency of backwash has tended to deal with the two types of forces separately. Sections 2.2.1 to 2.2.5 focus on the hydrodynamic aspects of detachment while Section 2.2.6 discusses the interaction between attachment and detachment forces at the microscale.

2.2.1. Turbulent effects in filter backwashing

Predicting and modeling detachment mechanisms in fluidized filters requires some understanding of the flow regime. There has been extensive theoretical and experimental analysis of particle detachment from planar surfaces for both laminar and turbulent flows (Ziskind et al., 1995). However, the situation in beds of fluidized grains is very much more complicated.

The flow in the vicinity of an isolated particle may be characterized in terms of the particle Reynolds number, which is defined as

$$\mathrm{Re}_t = \frac{v_t d}{n} \qquad 2.1$$

Re_t = Particle Reynolds number

v_t = Particle free settling velocity, m/s

d = Particle diameter, m

n = Kinematic viscosity, m^2/s

Particle Reynolds numbers for filter media are typically of the order of 1 to 10 and therefore fall in the transitional regime between laminar and turbulent flow ($0.2 < Re_t < 500 – 1000$). However, particles in a fluidized bed are in continuous motion and the interaction between the particles and fluid phase results in a fluctuating velocity field that is in some respects analogous to turbulent flow (Amirtharajah, 1978). This has led to the idea that the mechanisms of detachment may be similar to detachment in turbulent boundary layers in the sense that fluctuating velocity components play a key role. There have been several attempts to relate the efficiency of detachment to the rate of energy dissipation in the flow, which is in turn related to the turbulent characteristics of the flow (Amirtharajah, 1978; Sakkas and Lekkas, 1989). These ideas will be explored further in Sections 2.2.3 and 2.2.4.

2.2.2. The debate over the dominant cleaning mechanism during fluidized backwash

Over the years, there has been some debate about the dominant mechanism involved in the cleaning of filter grains during water backwashing. At the heart of the debate, was the need

to develop a model of filter backwash that could be used to optimize backwash design and operation. It was originally believed that fluidization resulted in abrasion between grains. However, during the sixties and seventies, several authors (Camp et al., 1971; Cleasby, 1977; Amirtharajah, 1971) concluded that collisional interactions in fluidized beds had to be negligible. Some of the arguments against the occurrence of inter-grain collisions in fluidized beds included the following:

- Nearly all the energy dissipated in a fluidized bed is required to suspend the grains (Camp et al., 1971), implying that there is little energy available for grain collisions.

- Particle attrition is negligibly small in fluidized beds (Zenz and Othmar, 1960).

- Significant pressure increases are expected to occur in the layer of liquid between two grains as they approach each other (Buevich and Markov, 1970). This would tend to prevent direct contact between grains in a manner analogous to lubrication theory.

Camp et al. (1971), Cleasby (1977) and Amirtharajah (1971) therefore concluded that detachment of particles in backwashing filters must be primarily due to shearing forces. Based on this assumption, Amirtharajah (1971) developed a theoretical model of fluid shear during backwashing, which predicted optimum cleaning at expanded bed porosities of around 0.70 for uni-sized particles. Other authors have presented variations on the same idea. These models are presented in Section 2.2.4.

Kawamura (1975b) argued that the optimum backwash rates predicted based on maximum fluid shear were much higher than those used in practice. Furthermore, the shear forces on deposits near the top of the beds towards the end of a filter run are greater than the maximum shear developed during backwashing (Camp, 1965). Kawamura interpreted this to mean that fluid shear cannot be an important mechanism in cleaning and that grain collisions had to be dominant.

One of the corollaries to the fluid shear vs grain collision debate is that most authors agree that air scour backwash is more effective than water fluidization because more grain collisions occur (Amirtharajah, 1978). In fact, since air scour is carried out in conjunction with sub-fluidized water wash or with no water flow at all, most of the filter grains remain in direct contact with each other and the shock waves resulting from the collapse of air bubbles are transmitted through the bed structure. It could be argued that the shock waves themselves break the floc bonds between individual grains in a manner analogous to the liquefaction of soil during earthquakes. However, the abrasion of adjacent grains moving relative to each other could strip away residual deposits more effectively than shear forces in a fluidized bed.

More recently, researchers at University College London have studied interactions between media grains and the detachment of filter deposits during backwashing using video endoscopy. Fitzpatrick (1993) reported that in fluidized beds:

"Video observations revealed apparently random behavior of grains with velocities varying in both space and time. There were intermittent periods of high and low velocities in different directions…Grains appeared to collide but may only approach very closely…Grain to grain contact is evident during periods of low activity."

Fitzpatrick (1993) commented that even if grains remained separated by a thin film of fluid, high local shearing forces could develop as the grains approach each other. Therefore, the distinction between grain collisions or abrasion and fluid shear as cleaning mechanisms is not very clear. However, the endoscope videos showed a marked difference in media grain motion during simultaneous air and water wash as compared to water fluidization. Simultaneous air and water wash resulted in the pulsation of the entire filter bed resulting in much more rapid and abrupt changes in grain velocity magnitude and direction than in fluidized beds.

Video footage of the detachment of kaolinite deposits from sand grains during both water only backwash and backwash with air suggested that detachment was primarily due to fluid shear in both cases. The deposits appeared to shear off the grains as the flow started as opposed to being jolted or gouged off as a result of grain collisions (Fitzpatrick, 1991). Fitzpatrick (1990, 1993) argued that high instantaneous local fluid and grain velocities during backwash with air were the main reason for the increase in cleaning efficiency. However, she also pointed that the kaolinite deposits were not very adhesive (compared to typical water treatment flocs) and were relatively easy to remove by shear. Up to 90 % of the deposits could be removed by water wash only at close to the minimum fluidization velocity of the filter bed (Fitzpatrick, 1990).

2.2.3. Fluid shear and energy dissipation in fluidized beds

If fluid shear is the dominant mechanism in the detachment of deposits in fluidized beds then maximum detachment efficiency should correspond to conditions of maximum shear. Several authors (Amirtharajah, 1971; Kawamura, 1975b, Sakkas and Lekkas, 1989) have developed models intended to predict the backwash velocity, v_{bms}, and expanded bed porosity, e_{ms}, at which fluid shear in the fluidized bed is maximized. All of these models are based on the implicit or explicit assumption that maximum fluid shear corresponds to maximum power dissipation per unit volume of either the fluid or the expanded bed. This section discusses the relationship between power dissipation and fluid shear. Section 2.2.4 discusses the derivation of models of the optimum backwash rate.

Camp and Stein (1943) argued that energy dissipation in fluids (headloss or friction loss) corresponds to the work done by shear stresses only. For laminar flow in a Newtonian fluid, the shear stress at a point is related to the local velocity gradient as follows:

$$\vec{t} = m \frac{\partial \vec{v}}{\partial \vec{r}} \qquad 2.2$$

$\vec{t}$ = Shear stress vector, N/m^2

$\frac{\partial \vec{v}}{\partial \vec{r}}$ = Fluid velocity gradient vector, s^{-1}

m = Dynamic viscosity, kg/(m.s)

Camp and Stein (1943) considered the work done on an incremental element of fluid undergoing distortion due to shear forces and calculated the rate of energy dissipation to be

$$\Phi = m\left[\left(\frac{\partial v_x}{\partial y}+\frac{\partial v_y}{\partial x}\right)^2+\left(\frac{\partial v_x}{\partial z}+\frac{\partial v_z}{\partial x}\right)^2+\left(\frac{\partial v_y}{\partial z}+\frac{\partial v_z}{\partial y}\right)^2\right] = mG^2 \qquad 2.3$$

Φ = Dissipation function = total work done by shear per unit volume per unit time, J/m^3/s

v_x, v_y, v_z = Components of the local fluid velocity in Cartesian co-ordinates, m/s

G = $\sqrt{\left(\frac{\partial v_x}{\partial y}+\frac{\partial v_y}{\partial x}\right)^2+\left(\frac{\partial v_x}{\partial z}+\frac{\partial v_z}{\partial x}\right)^2+\left(\frac{\partial v_y}{\partial z}+\frac{\partial v_z}{\partial y}\right)^2}$, 1/s

Camp and Stein (1943) described G as the "absolute local velocity gradient" at a point in the fluid. It must not be confused with the time averaged velocity gradient in flow (e.g. the universal velocity gradient for turbulent flow in a pipe or channel) although the magnitudes of the two quantities at any given point may be similar in the vicinity of phase boundaries.

Strictly speaking Equation 2.3 is not valid for turbulent flows. For a Newtonian fluid with constant density and viscosity, the rate of viscous dissipation is given by (Hinze, 1975):

$$\Phi = m\left(\frac{\partial v_i}{\partial x_j} + \frac{\partial v_j}{\partial x_i}\right)\frac{\partial v_i}{\partial x_j}$$

$$= m\left\{2\left[\left(\frac{\partial v_x}{\partial x}\right)^2 + \left(\frac{\partial v_y}{\partial y}\right)^2 + \left(\frac{\partial v_z}{\partial z}\right)^2\right] + \left(\frac{\partial v_x}{\partial y} + \frac{\partial v_y}{\partial x}\right)^2 + \left(\frac{\partial v_y}{\partial z} + \frac{\partial v_z}{\partial y}\right)^2 + \left(\frac{\partial v_x}{\partial z} + \frac{\partial v_z}{\partial x}\right)^2\right\} \quad 2.4$$

In practice, the average G value for a system is evaluated as

$$\overline{G} = \sqrt{\frac{\overline{\Phi}}{m}} = \sqrt{\frac{P}{mV}} \quad 2.5$$

$\overline{G}$ = Root mean square velocity gradient, 1/s

$\overline{\Phi}$ = Mean rate of power dissipation, J/m^3/s

P = Power dissipated in the fluid, J/s

V = Fluid volume, m^3

In other words, Camp and Stein's G value is essentially an index of power dissipation in a flow, which happens to have the units of velocity gradient (1/s). If it is understood in this way then the discrepancy between Equations 2.3 and 2.4 is not important. The rationale is that the greater the intensity of power dissipation, the sharper the velocity fluctuations and hence the greater the velocity gradients.

Camp and Stein (1943) originally applied the G value concept to the analysis and design of mixing, coagulation and sedimentation processes but suggested that it was applicable to all phenomena involving fluid friction losses. Camp (1965) later extended the G concept to the analysis of energy loss and shear stresses in filter pores during filtration and backwashing. In this case, the power dissipated is

$$P = Q\Delta p = v_z A \rho g \Delta h \qquad 2.6$$

Q = Volumetric flowrate, m^3/s

A = Filter cross section, m^3

v_z = Superficial velocity = Q/A, m/s

Δp = Pressure drop across the filter bed = $\rho g \Delta h$, Pa

ρ = Density of water, kg/m^3

G = Gravitational acceleration constant = 9.81 m/s^2

Δh = Headloss across the filter bed, m

The volume of fluid in the pores is

$$V = eAl \qquad 2.7$$

e = Porosity

Substituting Equations 2.6 and 2.7 into Equation 2.5 yields.

$$\overline{G} = \sqrt{\frac{\Delta h}{l}\frac{g v_z}{e n}} \qquad 2.8$$

v_z = Superficial velocity (filtration or backwashing), m/s

n = Kinematic viscosity, m^2/s

By analogy with Equation 2.2, Camp (1965) defined the average shear stress in the filter pores as

$$\bar{\tau} = m\overline{G} \qquad 2.9$$

$\bar{\tau}$ = Theoretical shear stress in the filter pores, N/m^2

Strictly speaking, Equation 2.2 is only valid for laminar flow. Like $\overline{G}$, $\bar{\tau}$ should be regarded as a characteristic of the energy dissipation in the system rather than the shear stress at any particular point.

2.2.4. Models of the optimum backwash rate

The backwash rate corresponding to maximum shear/power dissipation can be calculated by relating the intensity of energy dissipation to the expansion of the filter media. The headloss across a fully fluidized bed remains essentially constant and can be related to the bed height and porosity using Fair and Hatch's (1933) relation

$$\rho g \Delta h = g(\rho_s - \rho)(1-e)l \tag{2.10}$$

l = Fluidized bed height, m

ρ_s = Media grain density, kg/m^3

e = Fluidized bed porosity

Substituting Equation 2.10 into Equation 2.8 yields the hypothetical mean velocity gradient in the pores.

$$\overline{G} = \left[\frac{v_b g(\rho_s - \rho)(1-e)}{\mu e} \right]^{\frac{1}{2}} \tag{2.11}$$

v_b = Superficial backwash velocity, m/s

The relationship between backwash velocity and expanded bed porosity can be represented by the empirical Richardson and Zaki equation (1954).

$$v_b = k e^n \tag{2.12}$$

k, n = Constants for a given temperature, grain size, shape and density

Typical values of n for the various types of filter media range from 2.5 to 4.5 (Cleasby and Fan, 1981) depending on the size, shape and density of the media. Substituting Equation 2.12 into Equation 2.11 and differentiating with respect to e to obtain the porosity at which the

maximum value of $\overline{G}$ (or equivalently, the maximum power dissipation per volume) occurs yields (Amirtharajah, 1971).

$$e_{ms} = \frac{n-1}{n} \qquad 2.13$$

e_{ms} = Porosity at the maximum shear condition

From Equation 2.12, the corresponding backwash velocity is

$$v_{ms} = k\left(\frac{n-1}{n}\right)^n \qquad 2.14$$

For n = 2.5 to 4.5, the theoretical optimum porosity is 0.6 to 0.78. However, Amirtharajah (1978) focused his discussion on sand filters. Typical values of n for silica sand are 3.1 to 3.4 which means that the optimum porosity would fall in the region e = 0.68 to 0.71. Assuming fixed bed porosities of 0.4 to 0.5, an average backwash porosity of 0.7 would correspond to bed expansions of 67 to 100 %. Bed expansions used in practice are generally much lower than this (typically around 25 %) for two reasons.

The first reason relates to the size distribution of the filter media. Filter beds in water treatment plants always consist of a range of particle sizes. Fluidization results in stratification of the media with the finest grains tending to move to the top of the bed as a result of bulk density

effects (the bed porosity is higher for fine grains then coarse grains at any given backwash rate). Amirtharajah (1978) argued that for graded filter beds, the upper sections of the bed where the heaviest floc loadings occur would approach the optimum porosity at overall bed expansions of 40 to 50%.

The second reason for using lower than optimum backwash rates is that the theoretical shear stress/rate of energy dissipation is not very sensitive to backwash porosity in the region of the optimum. Amirtharajah (1978) estimated that the theoretical shear stress (Equation 2.9) would increase by only 7.8 % when a filter bed with an fixed porosity of 0.42 expanded from e = 0.52 (~ 25 % expansion) to the optimum porosity of e = 0.68. From Equations 2.3 and 2.9, a 7.8 % increase in $\bar{\tau}$ corresponds to a 16 % increase in the dissipation function, $\overline{\Phi}$. Economic considerations combined with experience have therefore favored the use of lower than optimum backwash rates.

Sakkas and Lekkas (1989) took a slightly different approach to Amirtharajah (1971) and derived a model of the maximum power dissipation per unit volume without invoking the G value concept. They would however, have arrived at the same result as Amirtharajah (1971) except that they chose to divide the power dissipated by total bed volume instead of the pore volume. The total volume of the expanded bed is

$$V' = Al \qquad 2.15$$

This resulted in a calculated optimum porosity and backwash rate of

$$e'_{ms} = \frac{n}{n+1} \tag{2.16}$$

$$v'_{bms} = k\left(\frac{n}{n+1}\right)^n \tag{2.17}$$

The equivalent root mean square velocity gradient would have been

$$\overline{G}' = \left[\frac{v_b g\left(r_s - r\right)(1-e)}{m}\right]^{\frac{1}{2}} \tag{2.18}$$

Assuming values of n ranging from 2.5 to 4.5, Sakkas and Lekkas (1989) predicted that the optimum porosity would vary from 0.71 to 0.81. These values were 5 to 16 % higher than the predictions of Equation 2.13 with greatest deviation at the lowest values of *n*.

Although some fraction of the power dissipated must be associated with the movement of particles in the fluidized bed, these movements are both induced and damped by the motion of the fluid. No energy is actually dissipated within the grains themselves therefore the use of Equation 2.18 in place of Equation 2.11 does not appear to be supported by theory.

Kawamura (1975b) took a similar approach to Sakkas and Lekkas (1989). However, he used Fair and Geyer's (1954) equation to express the relationship between backwash velocity and porosity.

$$e = \left(\frac{v_b}{U_t} \right)^{0.22} \qquad 2.19$$

U_t = Terminal velocity of a free settling media grain, m/s

Solving for the backwash velocity at maximum power dissipation per volume of the fluidized bed yielded

$$v'_{bms} = 0.46 U_t \qquad 2.20$$

Had he used Equation 2.7 instead of 2.15, the result would have been

$$v_{bms} = 0.56 U_t \qquad 2.21$$

Kawamura (1975b) argued that the d_{60} size (mesh size through which 60 % of the mass of the sand would pass), a value usually specified in the design of a filter, was a convenient basis for the calculation of the optimum backwash rate since it is reasonably representative of the average media size. The backwash rate calculated for theoretical maximum shear for a sand bed with d_{60} = 0.7 mm was four times the normally accepted backwash rate and Kawamura

therefore concluded that conditions of optimum shear therefore did not exist under typical backwash conditions. In the same paper, Kawamura (1975b) presented a model of the backwash rate that would theoretically maximize grain abrasion.

$$v_{bmg} = 0.1U_t \qquad 2.22$$

The predictions of this model corresponded closely to backwash rates used in practice and Kawamura (1975b) argued that this supported the view that grain abrasions are the dominant cleaning mechanism. Equation 2.22 is the basis of the curves of the appropriate backwash rate presented in Kawamura's design text (Kawamura, 1991).

However, if Kawamura (1975b) had applied his models to the media in the top sections of the filter bed instead of the average size, the predicted optimum velocities would obviously have been lower. Furthermore, his results were biased by the use of Equation 2.19 to describe the bed expansion. When Equations 2.12 and 2.19 are compared, U_t and the exponent 0.22 correspond to k and $\frac{1}{n}$ respectively. In Fair and Geyer's (1954) relationship, $n = \frac{1}{0.22} = 4.54$ as opposed to 3.1 – 3.4 assumed by Amirtharajah (1971). Substituting Equations 2.20 and 2.21 into Equation 2.19 yield theoretical optimum porosities of e'_{ms} = $(0.46)^{0.22}$ = 0.84 and e_{ms} = $(0.56)^{0.22}$ = 0.88 respectively. Substituting Equation 2.22 into

Equation 2.19 yields a theoretical optimum porosity of $e_{mg} = (0.1)^{0.22} = 0.60$ which is closer to Amirtharajah's (1971) result for maximum shear.

Furthermore, Dharmarajah and Cleasby (1986) have shown that $k < U_t$. Consequently, Kawamura's models would tend to overestimate the velocities corresponding to both the theoretical maximum shear and maximum grain abrasions.

The lesson to be drawn from these comparisons is that the prediction of the optimum backwash porosity is very sensitive to the filter media expansion characteristics. Using an inappropriate value for n will produce misleading results. Since Fair and Geyer (1954), there have been several advances in the modeling of filter bed expansion. In Chapter 4, Dharmarajah and Cleasby's (1986) correlation for predicting fluidized bed porosity for various types and sizes of media is used to calculate the theoretical optimum backwash conditions for the sand beds used in the current study.

2.2.5. Experimental evidence supporting the existence of an optimum backwash rate

Several authors have presented experimental evidence to support optimum backwashing at expanded bed porosities of $\varepsilon = 0.65$ to 0.75. Amirtharajah (1978) presented experimental results showing optimum cleaning of a relatively uniform sand bed (0.5 - 0.6 mm) at $e = 0.65$ to 0.7. For graded sand (effective size 0.455, uniformity coefficient 1.52)

optimum porosity of the top 3 inches of the expanded media was approximately 0.74. The overall bed expansion at this point was 50 %. Turan (1992) verified that the optimum porosity for 0.5-0.6 mm sand fell in the range 0.7 to 0.75.

Therefore, the calculation of the optimum backwash conditions based on the intensity of power dissipation in the fluid does appear to be valid. Amirtharajah (1978) quoted several authors in the fluidization literature (Hanratty et al., 1956; Cairns and Prausnitz, 1960; McCune and Wilhem, 1949; Beek, 1971) who found that maximum turbulent diffusion for a variety of fluidized materials occurred at expanded bed porosities of 0.65 to 0.75. Hanratty et al. (1956) suggested that at lower porosities, turbulence is fluid generated and increases with flowrate, but above the critical porosity, turbulence is particle generated and decreases as the particles move further apart. This supports the view that detachment efficiency is related to the intensity of turbulence.

2.2.6. Modeling detachment at the microscale

Developing a model of the hydrodynamic detachment force(s) involved in stripping floc off filter grains requires some assumptions be made about the mechanisms of detachment at the microscale. Advances in colloid science have made it possible to both measure and model the adhesive forces between various types of particles in a few well-defined systems. For example, Amirtharajah and co-workers (Mahmood et al., 1998) have developed a micromechanical force model that explains differences in detachment efficiency of kaolinite particles at different

pH's and ionic strengths and between kaolinite and bacteria. Mahmood (1996) showed that differences in efficiency of detachment of asymmetric kaolinite particles from fluidized glass beads was a function of both the interparticle bond strengths and the microstructure of the kaolinite flocs. The limitations of this approach are that the micromechanical force model has so far only been applied to relatively simple model systems and that the actual mechanism of particle detachment is still not well understood.

There have been some preliminary attempts to model the mechanism of detachment for a single particle. For example, Amirtharajah and Giourgas (1981) assumed that detachment occurred when lift forces due to "turbulent bursts" exceeded the forces attaching a floc particle to a surface.

According to turbulent boundary layer theory, viscous effects become dominant in the region close to a phase boundary (the viscous sub-layer). However, turbulent events further away from the interface induce velocity fluctuations that are felt even in the viscous sublayer. These velocity fluctuations have components both tangential and perpendicular to the interface, giving rise to both lift and drag forces. Amirtharajah and Giourgas (1981) assumed that particles were detached from filter grains due to lift forces arising from turbulent bursts.

However, Ziskind et al. (1995) showed that in the viscous sub-layer, drag forces are much greater than lift forces and consequently, adhesive bonds are more likely to be broken by hydrodynamic moments than lift forces. Corino and Brodkey (1969) observed that particles

embedded deep within the viscous sub-layer of a turbulent boundary layer would move away from the wall in sympathy with a turbulent burst but rarely acquired sufficient momentum to escape from the viscous sub-layer within the time period of that burst. Usually a second burst was required to transport the detached particles to the bulk flow.

The larger question, however, is whether it is valid to focus on the detachment of single particles when considering filter backwash. The applied hydrodynamic force depends on the size and shape of the structure being detached while the total adhesive force that has to be overcome depends on the number of and orientation of the interparticle bonds that have to be broken. The endoscope studies carried out at University College London showed kaolinite deposits detaching from the filter media in chunks or shearing off en mass rather than as individual flocs (Fitzpatrick, 1991).

Regardless of the exact mechanisms involved, the rate and efficiency of detachment from fluidized particles are expected to be related to the intensity of the local velocity fluctuations. Therefore, in so far as $\overline{G}$ and $\overline{\Phi}$ in Section 2.2.3 are correlated with the intensity of velocity fluctuations in the fluid between media grains, they should also be indicators of the intensity of the detachment forces whatever the mechanism involved.

2.3. Models of backwash effluent quality

Backwash effluent quality as a function of backwash time is relatively easy to measure and can be used as a qualitative indicator of backwash efficiency (Kawamura, 1991). Figure 2.1 shows a typical backwash concentration profile with time. There is a short lag period before the backwash turbidity peaks followed by an exponential decay in turbidity. A high initial peak and rapid decline in backwash turbidity usually indicates relatively efficient backwash while a low peak and slow decline in turbidity usually indicates inefficient backwash. Backwash efficiency here relates to the rate at which floc is detached from the media grains. The more rapidly and completely floc detaches, the sooner it can be flushed out of the bed.

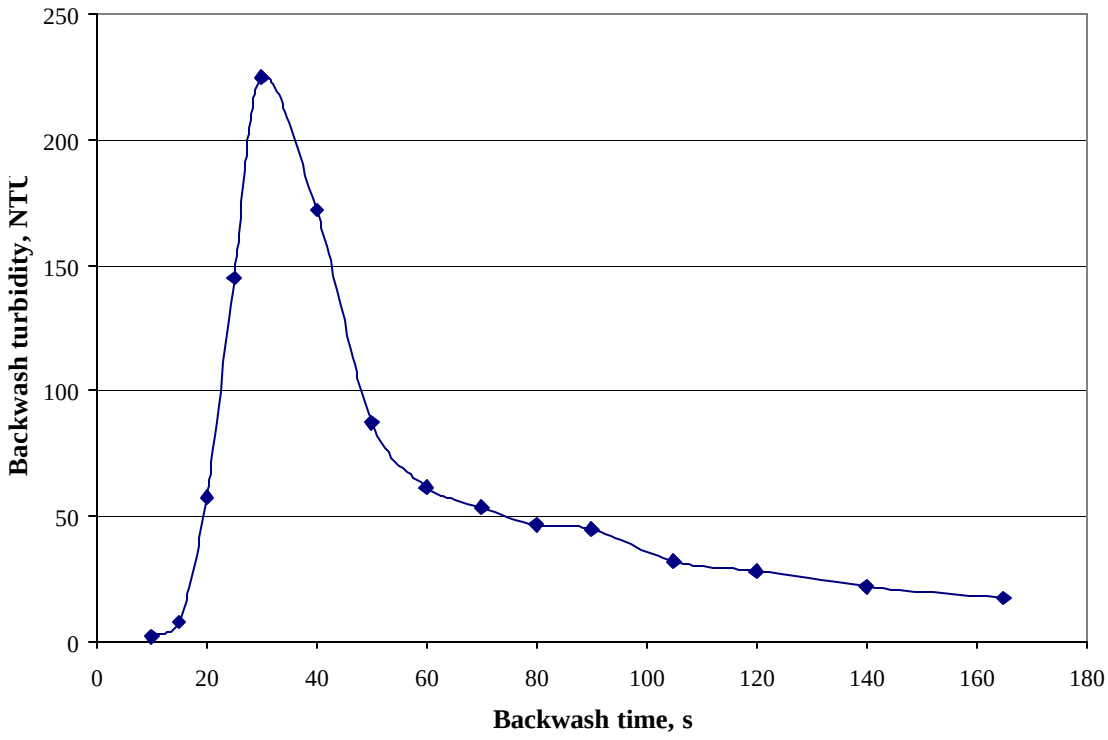

Figure 2.1 Typical backwash concentration profile with time

Theoretically, if the rate of detachment of floc from the media grains is known, it can be coupled with a model of flow through the filter in order to predict the backwash concentration profile. Conversely, the backwash concentration profile can theoretically be used to calculate the intrinsic rate of detachment, which could in turn provide information about the mechanism of detachment. However, there are several complications.

Detachment rate is not the only factor that affects the backwash turbidity profile. Filtration results in a non-uniform distribution of deposits throughout the filter bed with the highest concentrations towards the top of the bed. The deposit concentration with depth profile varies with filtration conditions and is difficult to measure directly.

The other factor which can significantly affect the measured backwash turbidity profile is mixing and dispersion both in and above the filter bed. This complicates any attempts to extract information about the intrinsic rates of detachment from media grains from the backwash turbidity profile, particularly near the beginning of the backwash. The effect of mixing on the backwash effluent concentration is discussed in detail in Chapter 7.

This section examines several models that attempt to relate the rate of detachment from media grains to the measured backwash concentration. The models are presented in order of increasing complexity.

2.3.1. Amirtharajah and Giourgas (1981), Amirtharajah (1985)

Amirtharajah and Giorgas (1981) developed a model of floc detachment from filter grains where detachment was assumed to be due to lift forces caused by turbulent bursts. This process was seen as being analogous to the surface renewal mechanism in Dankwerts (1951) surface renewal theory for mass transfer across turbulent boundary layers. Based on Dankwerts model, the rate of surface renewal was assumed to be

$$A(t) = A_0 s \exp(-st) \qquad 2.23$$

$A(t)$ = Rate of surface renewal at time t, m^2/s

A_0 = Deposit surface area at time $t = 0$, m^2

S = Surface renewal frequency, 1/s

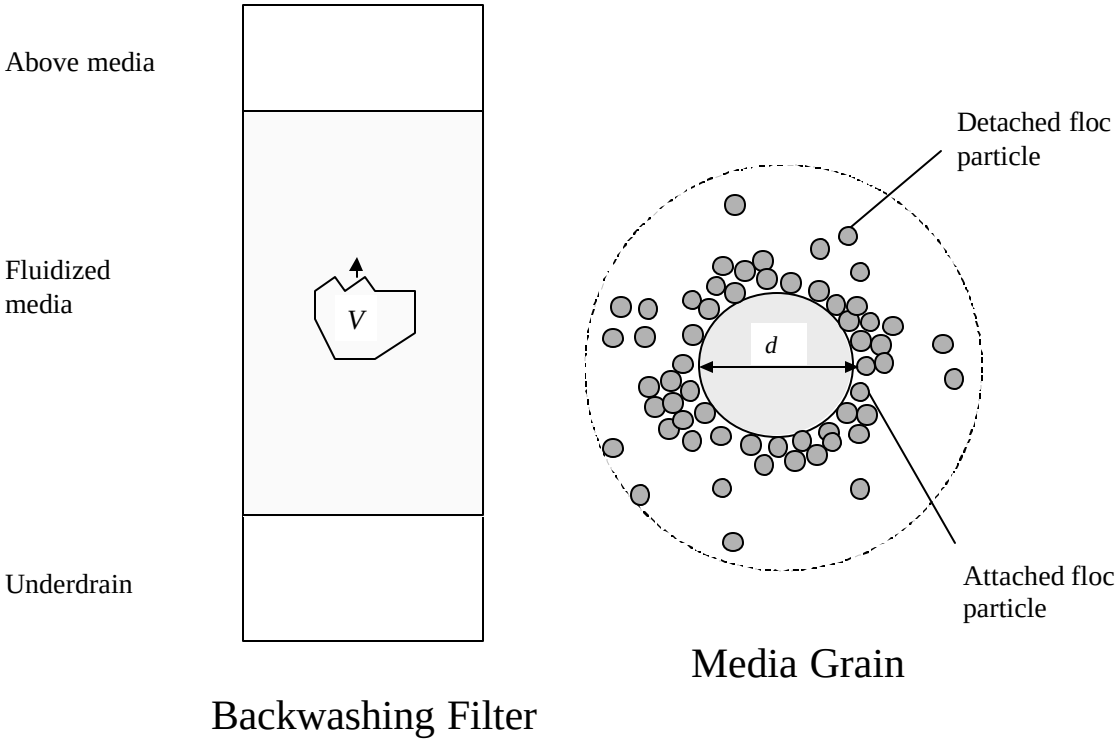

Figure 2.2 Conceptual model of filter backwash

Amirtharajah (1985) formulated the material balance on an arbitrary control volume V traveling up through the filter bed as shown in Figure 2.2

The rate of accumulation of detached floc in V is given by

$$-V\frac{dc}{dt} = \overline{M}A(t) = \overline{M}A_0 s\exp(-st) \qquad 2.24$$

V = Control volume, L

c = Concentration of detached solids in V, mg/L

$\overline{M}$ = Mass detached per unit area renewed, mg/m^2

Integration leads to a solution of the form

$$c = K \exp(-st) \tag{2.25}$$

Where

$$K = \frac{\overline{M} A_0}{V}$$

There is substantial evidence in the literature that confirms the exponential relationship between backwash concentration and time. As a first approximation, Amirtharajah (1985) assumed the renewal frequency was

$$s = \frac{v_b}{d} \tag{2.26}$$

d = Media grain diameter, m

Substituting Equation 2.26 into Equation 2.25 yields

$$c = f(v_b t) \tag{2.27}$$

The product $v_b t$ is the cumulative volume of washwater used per unit filter area. Amirtharajah (1985) provided experimental evidence from different filters (graded and uniform sand) at expanded porosities of 0.55 to 0.78 which suggested that the volume of washwater required to achieve a particular terminal washwater quality was independent of the backwash

rate. This tends to support the assumption in Equation 2.26 that the surface renewal frequency is proportional to the backwash velocity. This result represented a shift in emphasis to an earlier published analysis of the same experimental data (Amirtharajah, 1978), which indicated that optimum backwash efficiency occurred at a porosity of 0.7. The differences in backwash efficiency were small, however, and resulted in less than 1 mg/L (~ 0.5 % of the peak concentration) difference in effluent concentration for a given backwash volume towards the end of backwash.

Amirtharajah (1985) did not discuss the impact of the initial non-uniform filter deposit profile on the backwash concentration. The main contribution of this paper to backwash modeling was that it indicated how the backwash concentration profile and intrinsic rate of detachment could be related to the mechanism of detachment.

2.3.2. Bhargava and Ojha (1989)

Bhargava and Ojha investigated the rate of change of thickness of a clay coating on wheat flour balls during backwashing. The rate of change of the average diameter of the coated balls was found to be

$$\frac{dD}{dt} = -k_2 D \qquad 2.28$$

D = Average diameter of balls, m

K_2 = Rate constant, 1/s

k_2 was found to be 8.066 x 10^{-4} /s The authors assumed that this rate law could also be used to describe the rate of decrease of deposit layer thickness during filter backwashing. The solution of Equation 2.28 is

$$D = D_{\max}\left[\exp\left(-k_2 t\right)\right] \tag{2.29}$$

D_{max} = Initial diameter of coated particle, m

Alternately, Equation 2.29 could be written in terms of particle volume

$$V = V_{\max}\left[\exp\left(-3k_2 t\right)\right] \tag{2.30}$$

V_{max} = Initial volume of coated particle, m^3

The authors assumed that complete removal of deposit coating would be achieved in time t_w, therefore the rate constant k_2 could be expressed as

$$V = V_{\max}\left[\exp\left(-3k_2 t\right) - \exp\left(-3k_2 t_w\right)\right] + V_{\min} \tag{2.31}$$

V_{min} = Volume of clean particle, m^3

The total volume of deposit removed from a particle at time t was denoted as

$$T = V_{\max} - V = V_{\max}\left[1 - \exp\left(-3k_2 t\right)\right] \qquad 2.32$$

Bhargava and Ojha (1989) accounted for the non-uniform distribution of deposits with filter depth by dividing the bed into layers based on the sieve analysis of the media (See Figure 2.3) and calculating a separate V_{max} for each layer. The V_{max} values were calculated based on the reduction of porosity in the clogged filter bed. Details of the calculation were not given.

The authors assumed that the rate constant k_2 was the same for all layers. This seems to be a reasonable first approximation. However, the method the authors used to evaluate k_2 was questionable. They argued that since there is almost no deposit in the bottom most layer, the time required to clean this layer, t_w is approximately equal to its hydraulic retention time. Once t_w is known for one layer, then k_2 can be calculated for the whole bed. There are several problems with this reasoning.

1. Flushing detached floc out of the bottom layer is a different mechanism to detaching it. There is no physical reason why the intrinsic rate constant should be the same.

2. The depth of the bottom layer in Bhargava and Ojha's model and hence the calculated value of k_2 depends on the sieve analysis and the particular sieve sizes used (See Figure 2.3). This has no relationship to the actual rate of detachment.

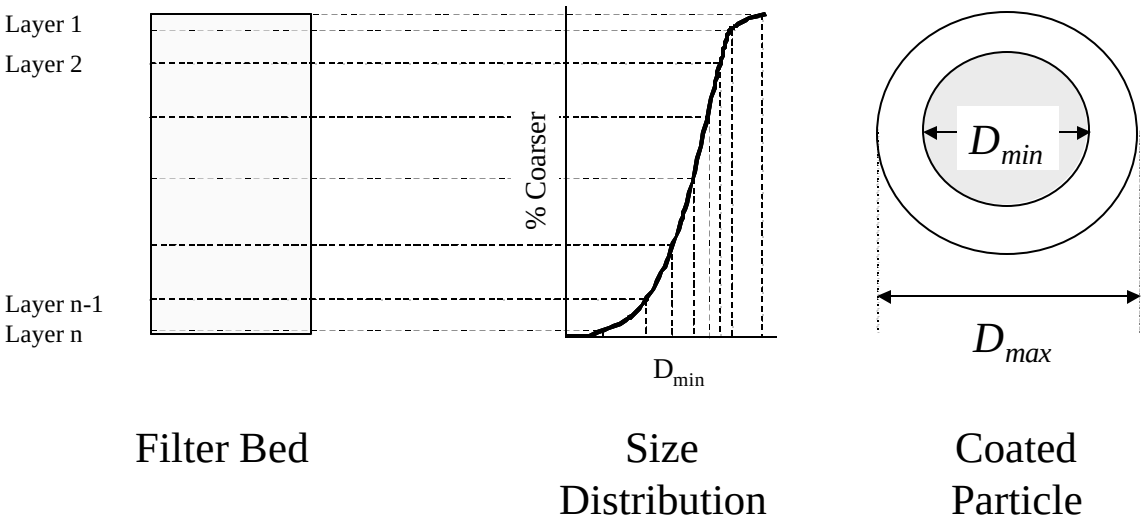

Figure 2.3 Bhargava and Ojha's (1989) conceptual model

The authors provided experimental data comparing measured backwash turbidity and calculated volume of deposit detached from the various layers, however, they did not explain how the two quantities were related nor did they account for the effect of travel time from the various layers to the point where backwash concentration was measured.

The main contribution of this work therefore appears to be that it provided experimental evidence of the exponential decay of deposit volume over time (assumed but not proven by other authors.) and that it attempted to account for the effect of the initial floc deposition profile.

2.3.3. Huang and Basagoiti (1989)

Huang and Basagoiti (1989) presented a model of backwash effluent concentration that explicitly included the travel time from various parts of the fluidized bed to the backwash sampling point. Solutions for both $t < q$ and $t > q$ were provided, where q is the hydraulic retention time within the expanded bed. The model included the following assumptions:

- The intrinsic rate of detachment was given by

$$\frac{\partial s_t(z)}{\partial t} = -k_3 s_t(z) \qquad 2.33$$

$s_t(z)$ = Specific deposit at time t and depth z, $\left(\frac{\text{volume floc particles}}{\text{volume bed}}\right)$

z = Filter depth measured from top of bed, m

k_3 = Rate constant, 1/s

- There was no detachment during expansion of the bed. The bed was fully expanded at $t = 0$.

- Although, the deposit profile at the end of backwashing was non-uniform, the authors assumed that bed expansion led to a more uniform profile. To simplify the model equations, they assumed a uniform deposit profile at backwash time $t = 0$, i.e.

$$s_0(z) = s_a \tag{2.34}$$

s_a = Average deposit concentration at t = 0, $\left(\frac{\text{volume floc particles}}{\text{volume bed}}\right)$

The last assumption appears to be unrealistic. The authors implicitly assumed that porosity was uniform throughout the expanded bed, hence the assumption of uniform deposit profile implied instantaneous complete mixing of all media grains in the bed. This seems unlikely to occur under normal circumstances. There is, however, some justification for assuming that substantial mixing occurs in the top most heavily clogged section of the bed as it is fluidized. This is discussed further in Chapter 6. The model obtained was

$$c_{out}(t) = \frac{s_a}{e}\{1 - \exp(-k_3 t)\} \qquad \text{for} \quad t < q \tag{2.35}$$

$$c_{out}(t) = \frac{s_a}{e}\exp(-k_3 t)\{\exp(k_3 q) - 1\} \qquad \text{for} \quad t > q \tag{2.36}$$

Where

$$q = \frac{L}{\left(\frac{v_b}{e}\right)} \tag{2.37}$$

L = Expanded bed height, m

Equations 2.35 and 2.36 were integrated with respect to time to obtain expressions for the total mass of solids detached. Huang and Basagoiti (1989) ran several experiments using

filters clogged with one of three different floc suspensions: clay/alum, ferric chloride or clay/ polymer. The polymer used was 1,165 L, a high molecular weight cationic polyelectrolyte supplied by Betz Laboratories Inc. (Trevosa, Pennsylvania). The filters were backwashed at various rates and the model fitted to the measured backwash concentration profile and total solids detached to obtain values of the parameter k_3.

The authors found that the clay/alum and ferric floc suspensions tended to have lower k_3 values than the clay/polymer suspension i.e. alum and ferric floc detached more rapidly than polymer floc. The backwash rate and bed expansion required to achieve a given solids removal efficiency were also greater for polymer floc than for the other two suspensions.

2.3.4. Hall and Fitzpatrick (1998)

Hall and Fitzpatrick (1998) presented the most comprehensive model of backwash concentration profile to date. This model was part of a larger effort to model the entire filtrer cycle (filtration and backwash) with the filtration model providing the initial condition for the backwash model. Model features included:

- The initial filter deposit profile was calculated using Ives' (1975) model of filtration.

- The process of bed expansion ("transient stage") was included in the model. Previous models had ignored this stage. The filter bed was divided into *n* equal volume layers and each layer underwent expansion in sequence, starting with the lowest layer and moving up the bed.

- Some fraction, a, of the initial deposit was assumed to dislodge during expansion.

- Filter deposits were assumed to form uniform coatings on the filter grain. Once each layer was fully expanded, the rate of detachment within the layer was expressed in terms of reduction of coated grain diameter (adapted from Bhargava and Ojha (1989))

$$-\frac{dD}{dt} = k_4\left(D - D_{cg}\right) \qquad 2.38$$

D_{cg} = Clean grain diameter, m

k_4 = Rate constant, 1/s

The final result of the theory was

$$c(t)_n = c(t)_{n-1} - \frac{gD_{cg}^2 \exp\left[-k_4\left(t - n \cdot t_{beL}\right)\right]}{k_4 - \frac{Q}{V_f}} - \frac{gD_{cg}B_n \exp\left[-2k_4\left(t - n \cdot t_{beL}\right)\right]}{2k_4 - \frac{Q}{V_f}}$$
$$- \frac{gD_{cg}B_n^2 \exp\left[-3k_4\left(t - n \cdot t_{beL}\right)\right]}{3k_4 - \frac{Q}{V_f}} + A_n \exp\left[-\frac{Q\left(t - n \cdot t_{beL}\right)}{V_f}\right] \quad 2.39$$

$$g = \frac{\Delta LA(1 - e_0)pB_n k_4}{2V_f \cdot V_{cg}} \quad 2.40$$

$$A_n = c_{in} + \frac{gD_{cg}^2}{k_4 - \frac{Q}{V_f}} - \frac{gD_{cg}B_n}{k_4 - \frac{Q}{V_f}} - \frac{gB_n^2}{3k_4 - \frac{Q}{V_f}} - c\left(n \cdot t_{beL}\right)_{n-1} \quad 2.41$$

$$B_n = D_{gn\max} - D_{cg} \quad 2.42$$

Where

$c(t)_n$ = Concentration of suspended solids in the n^{th} layer at time t, (vol/vol) ppm

n = Layer number. Bottom layer is $n = 1$

ΔL = Layer depth before expansion, m

A = Filter cross section, m^2

e_0 = Fixed bed porosity

V_f = Fluid volume in expanded layer, m^3

t_{beL} = Layer expansion time, s

c_{in} = Initial concentration in n^{th} layer, (vol/vol) ppm

D_{gnmax} = Theoretical maximum coated grain diameter in the n^{th} layer, calculated from the filtration model, m

Hall and Fitzpatrick's model was conceptually straight forward but the inclusion of the transient phase and the initial deposit profile led to substantially more complicated mathematical expressions than previous models. This illustrates the difficulties involved in attempting to accurately depict the process of filter backwashing in a mathematical model.

2.3.5. Effect of mixing and flow localization on the backwash concentration profile

Of the four models discussed in Section 2.3, Hall and Fitzpatrick (1998) provided the most comprehensive description of the early stages of filter backwash. However, one important effect was omitted: the effect of mixing and dispersion on the backwash concentration profiles. Subsequent experimental work by the same authors (Hall and Fitzpatrick, 2000) revealed that the smooth expansion assumed in their model was too simplistic. During the expansion of the bed, the top most clogged sections tended to collapse into the lower layers, often resulting in a double concentration peak in the backwash effluent.

Filter underdrains are designed to minimize flow maldistribution (differences in flow at different points) during backwashing as this is critical for maintaining the long-term performance of filters (Getting et al., 2001). Therefore, the commonly used assumption of plug flow (no axial mixing) may be justified once steady state fluidization has been achieved. However, the presence of relatively impermeable clogged regions in the filter at the beginning of backwash can result in transient flow localization and mixing of the initial turbidity peak.

Hall and Fitzpatrick (2000) found that the effect of mixing on the backwash profile appeared to increase with increasing backwash rate. The authors suggested that other factors such as filter nozzle design and layout, uneven flow through gravel support layers, grain size,

sphericity and the rate at which the backwash valve was opened could also affect flow localization and the degree of mixing.

This has important implications for the interpretation and backwash turbidity profiles in general. First, rate constants (s, k_2, k_3, k_4) determined empirically from experimental backwash profiles will reflect not only the intrinsic rate of detachment but also the degree of mixing. Since flow localization and mixing is induced by the presence of clogged regions, the degree of mixing probably depends to some extent on the initial deposition profile. Secondly, the hydraulic conditions at any given backwash rate are likely to vary from one experimental setup to another.

Greater amounts of mixing, like more adhesive floc, will produce lower peaks and less rapid decay in concentration, i.e. lower rate constants. If backwash efficiency is defined to mean both the ease with which floc is detached from the media (intrinsic rate of detachment: Equations 2.23, 2.28, 2.33 and 2.38) and the ease with which it is flushed out of the bed, then lower *k*'s can be interpreted to mean less efficient backwash. However, the hydraulic situation has to be taken into account when attempting to relate *k* to the intrinsic rate of detachment.

2.4. Applying backwash theory to real filters

Despite its importance in water treatment, there has been relatively little progress made in the theoretical analysis and modeling of filter backwash. This is largely because of the complexity of the processes. For example, in filtration modeling, the sand bed structure can be considered a constant and only variations in deposit volume and distribution need be

considered. However, during backwashing the media grains as well as the fluid phase and the detachable floc become mobile, affecting both the mechanisms of detachment and the transport of floc out of the bed.

This chapter has reviewed the various approaches to modeling floc detachment described in the literature. A number of important issues have been identified. The models of the optimum backwash rate and porosity (Section 2.2.4) were shown to be very sensitive to the model of the bed expansion used. Chapter 4 discusses the calculation of the bed expansion parameters for filters based on water temperature and media properties (size, shape and density). The results of the bed expansion model are then used to calculate the optimum backwash rates and porosities as a function of media properties. The calculation of the optimum backwash rates for graded beds is also discussed.

Chapter 6 discusses the behavior of real filter beds during backwashing and re-examines the assumptions made in the models discussed in Section 2.3. Chapter 7 looks at the estimation of the rate of detachment from experimental backwash concentration profiles.

CHAPTER 3

EXPERIMENTAL METHODOLOGY

3.1. Introduction

Two different types of experiments were carried in this study. The first group of experiments looked at the effect of backwash rate, type of floc and degree of clogging of a filter on the efficiency of backwash and the kinetics of detachment. The behavior of the clogged bed during the backwash step of these experiments in described in Chapter 6. The backwash concentration and detachment kinetics are analyzed in Chapter 7. Chapter 9 discusses the effect of various parameters on the overall efficiency of backwash.

The second group of experiment was designed to track the accumulation of floc in a filter over multiple filter runs with inadequate backwash. These experiments are presented in Chapter 8. Factors affecting the efficiency of backwash for individual runs in this set of experiments are also analyzed and discussed in Chapter 9.

This chapter describes the laboratory filters, instrumentation, operating procedures and methods for determining backwash efficiency used in the current study. The characteristics and fluidization behavior of the filter media are described in Chapter 4.

3.2. Laboratory Filters

Filtration and backwashing experiments were carried out at a pilot filtration plant located at the Umgeni Water Process Evaluation Facility in Durban, South Africa. The plant consisted of four laboratory filters constructed from 200 mm diameter clear PVC tubes. The media in each filter was supported on a PVC orifice plate drilled with 5 mm holes and covered by a wire mesh to prevent sand passing through the orifices. A scale marked on the front of each column was used to estimate bed height (in mm). The clear PVC walls of the laboratory filters also allowed direct observation of the backwash behavior of the filter beds. The laboratory filters are shown in Figure 3.1.

Experiments into the effect of backwash rate and degree of clogging on backwash performance were carried out using a filter bed consisting of sand sieved between 1 and 1.4 mm to provide a relatively uniform size distribution in the filter bed. Experiments to measure the accumulation of mud over multiple filter cycles were carried out in a 0.7 mm sand filter that had been used to monitor the effect of mudballing on filter performance in an investigation into the operation of autonomous valveless filters (Brouckaert et al., 2003).

A sampling point located above each filter bed was used to collect samples for analysis of coagulated influent turbidity and pH during filtration and was connected to the opacity meter for on-line monitoring of backwash turbidity.

Each filter column was also fitted with nine manometer ports. The piezometric head at each port could be measured off the scale on a manometer board located next to each filter (See Figures 3.1 and 3.2). The scale interval was 2 mm. The manometers were used for measuring the headloss profile across the filter bed during filtration and also during fluidization tests carried out to characterize the behavior of the clean fluidized beds (Described in Chapter 4). During regular backwash, valves on the manometer tubes were shut off to prevent flow being diverted out of the filter.

The filter bed heights and locations of the manometer ports are listed in Table 3.1. Port "a" was located below the orifice plate. During the fluidization tests, the 1 – 1.4 mm sand filter expanded to a maximum of 0.555 m (between points h and i). Fluidization tests for the 0.7 mm sand bed were carried out with a shorter bed than the floc accumulation experiments (l_{fx} = 0.47 m instead of 0.64 m) and the maximum expanded height was 0.605 m (also between h and i).

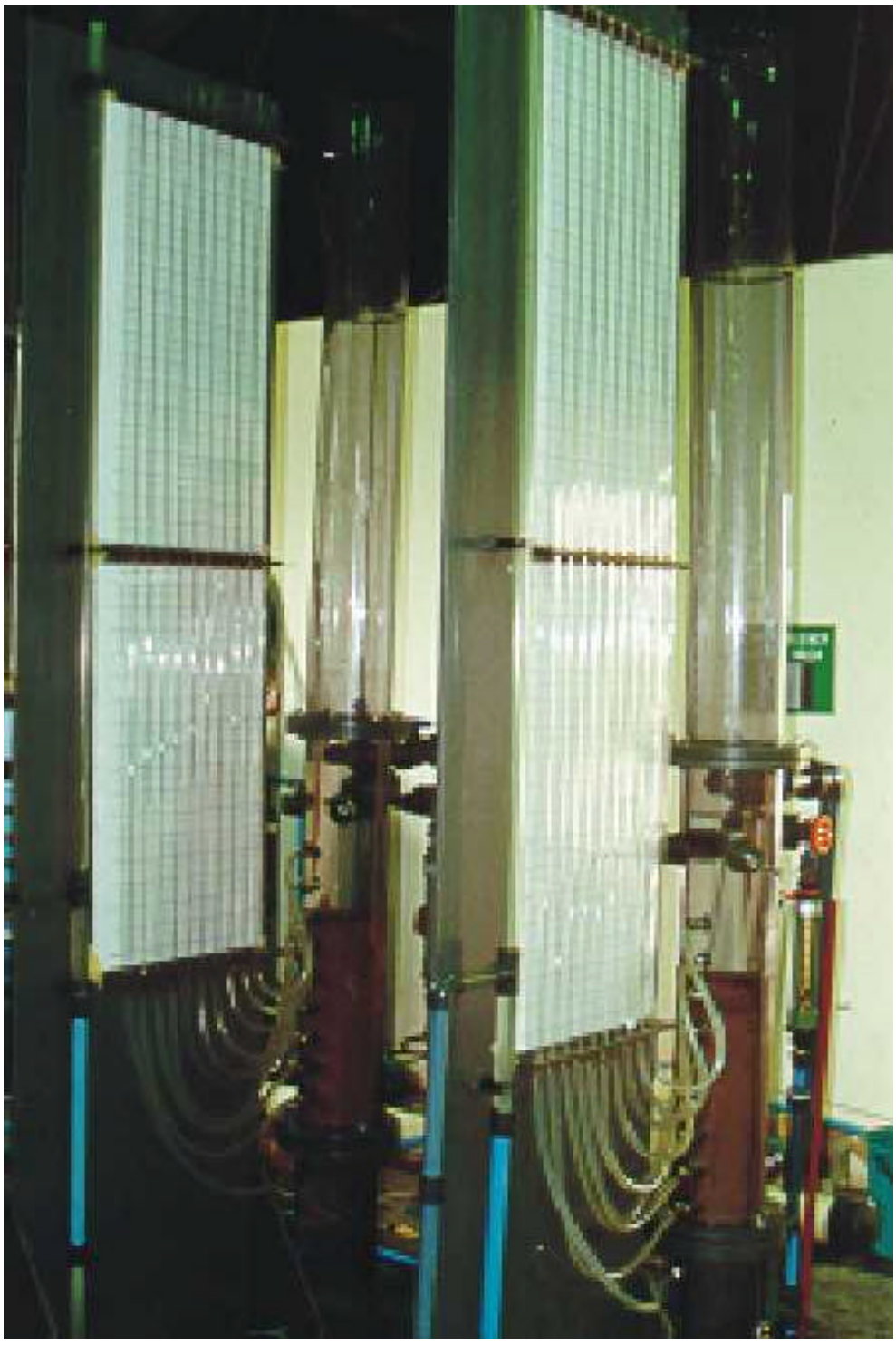

Figure 3.1. Laboratory filters

Table 3.1 Fixed bed heights and locations of manometer ports

	Distance from orifice plate, m	
	Filter 1 (1 – 1.4 mm sand)	Filter 3 (0.7 mm sand)
Fixed bed height, l_{fx}	0.47	0.64
b	0.055 (0.12 l_{fx})	0.098 (0.15 l_{fx})
c	0.138 (0.29 l_{fx})	0.178 (0.28 l_{fx})
d	0.217 (0.46 l_{fx})	0.253 (0.40 l_{fx})
e	0.288 (0.61 l_{fx})	0.328 (0.51 l_{fx})
f	0.363 (0.77 l_{fx})	0.403 (0.63 l_{fx})
g	0.438 (0.93 l_{fx})	0.478 (0.75 l_{fx})
h	0.512 (> l_{fx})	0.558 (0.87 l_{fx})
i	0.586 (> l_{fx})	0.628 (0.98 l_{fx})
j	0.66 (> l_{fx})	0.703 (> l_{fx})

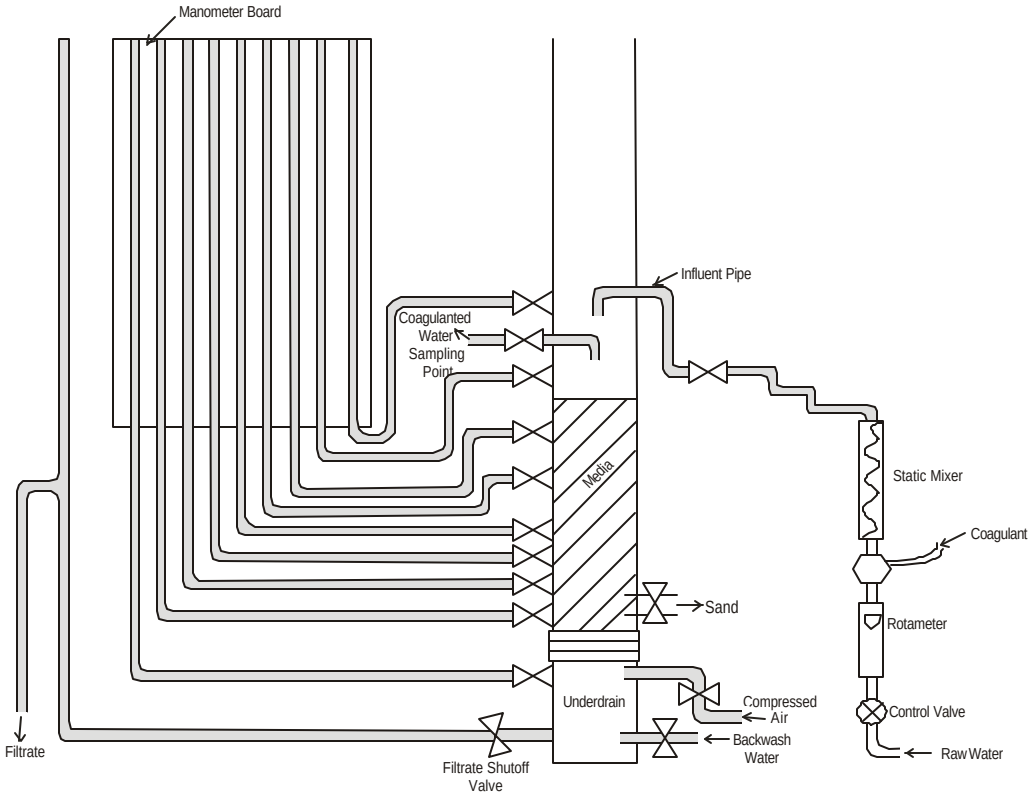

Figure 3.2. Sand filtration pilot plant schematic

3.2.1. Operation in filtration mode

The pilot plant was operated in in-line filtration mode (no flocculation or sedimentation steps). Raw water from the head of the Wiggins Water Treatment Works was supplied to a constant tank level feed tank and was then pumped to individual filters by a common feed pump. Each filter had a separate coagulant pump. Coagulant was dosed into the influent line ahead of a static mixer as shown in Figure 3.2.

The filters were operated at constant rate with rising level. The flow to each filter was regulated using a rotameter and diaphragm valve located ahead of the coagulant dosing point.

The target filtration rate for all experiments in the current study was 6.7 m/h, however there was tendency for the filtration rate to drop slightly over time, especially if more than one filter was operating in parallel. The flow tended to become more stable the longer the filters were operated.

3.2.2. Operation in backwash mode

During backwash, clean water was pumped into the filter underdrain and entered the filter via the orifice plate. The orifice plate was designed with over 1 m of headloss to ensure even distribution of the backwash flow. The dirty backwash water overflowed into a backwash trough and exited the filter via the backwash effluent pipe. The backwash trough consisted of a 75 mm pipe sealed at one end and with a 75 X 150 mm notch cut in its upper surface and was located approximately 1 m above the orifice plate.

The backwash flow was manually controlled with the aid of 0 to 4000 L/h rotameter marked off in increments of 100 L/h.

3.3. Filter influent

3.3.1. Raw water characteristics

The raw water used in this study was supplied to Wiggins Water Treatment plant from the Inanda Dam on the uMngeni River about 25 km northwest of the port of Durban. The

catchments of uMgeni River and its tributaries upstream of the dam include both commercial and communal farm land and the city of Pietermaritzburg (CSIR, 2004).

Filter backwash experiments were carried out in two time blocks. The first set of experiments was conducted over the course of February 2001. The remaining two sets of experiments were conducted in parallel between September and November 2001. Table 3.2 summarizes the raw water quality for the Wiggins Water Treatment Plant during these two periods (data supplied by Umgeni's Water Quality Division). The lag time between water reaching the head of the works and arriving at the experimental filters was a few hours at most.

Table 3.2 Raw water characteristics

	February	September – November
Turbidty, NTU	1.6 – 2.8	0.8 – 3.1
pH	7.3 – 7.9	7.3 – 8.4
Temperature, ^{0}C	22 – 25	17 – 25
Conductivity, mS/m	20 – 21	19 – 22
Hardness, mg/L as $CaCO_3$	50	53
Total organic carbon, mg/L as C	2.3 – 3.6	1.9 – 3.6
E.coli, cfu/100ml	0 - 4	0 – 6
F. strep, cfu/100ml	0 - 8	0 – 6

3.3.2. Coagulants

The coagulants used in this study were alum and Z464N (Zetachem, South Africa), a proprietary blend of a poly-DADMAC (poly diallyl dimethyl ammonium chloride) and aluminum chlorohydrate used at the Wiggins Water Treatment Plant. Poly-DADMACs (also known as poly-DMDAACs) are formed by the reaction and polymerization of a stoichiometric mixture of allyl chloride and dimethylamine in aqueous solution. The monomeric unit is shown in Figure 3.3. A typical molecular weight for a poly-DADMAC is 2-3 x 10^6 (Nozaic et al., 2001).

Poly-DADMACs have a constant positive charge below a pH of about 10 because of the acidity of the quaternary nitrogen atoms in the molecules (Amirtharajah and O'Melia, 1990). Consequently, their performance as coagulants is fairly insensitive to pH under typical water treatment conditions.

Aluminum chlorohydrate (ACH) is a specific form of poly-aluminium chloride (PACl) with a chemical formula of $Al_2(OH)_5Cl$ (Gabilech et al, 2004). PACl is manufactured by partially neutralizing solutions of aluminium salts by the addition of a base to produce highly charged polymeric aluminum hydroxide species. The polymeric species are more effective as coagulants than the primarily monomeric species formed during coagulation with alum. The solubility of ACH is fairly constant above pH 7.

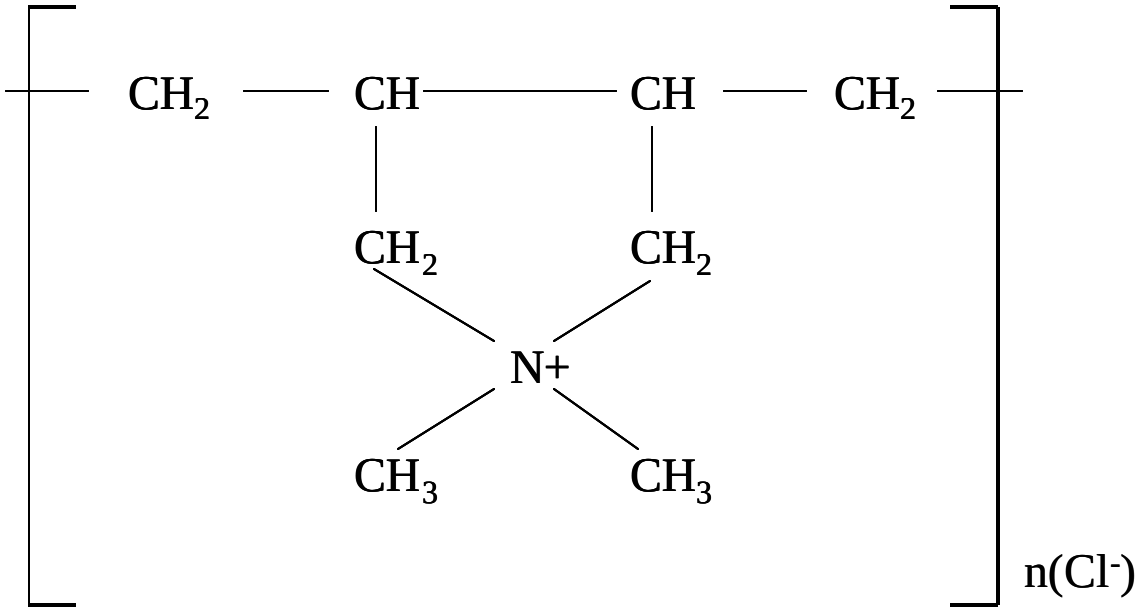

Figure 3.3 Poly-DADMAC monomeric unit

Alum was supplied as 48 % by weight (as $Al_2SO_4.14.3H_2O$) aqueous solution (density = 1.3 kg/m^3). Alum doses were calculated in mg/L as $Al_2SO_4.14.3H_2O$. Z464N was supplied as an aqueous solution with ~ 26% by weight of solids and density 1070 to 1090 kg/m^3. Since the exact composition of the stock solution was not known, the dose was calculated as mg of stock solution per liter of raw water.

The minimum flowrate the dosing pumps could supply while still allowing adequate mixing of the coagulant with the raw water was 6 mL/min. The dosing solutions were prepared by diluting coagulant stock in tap water in a 20 L plastic drum calibrated in increments of 5 L. The concentration of the dosing solution was selected to give the required dose at a dosing rate of 6 mL/min.

3.4. Instrumentation

3.4.1. Differential pressure probe

The variation in headloss across the top part of the filter during backwash was measured using a 0 – 200 mbar differential pressure (DP) probe. The probe produced a 4 – 20 mA signal output that was linearly related to the differential pressure. During preliminary test of the probe, it was found that a sharp increase in pressure resulted in a damped oscillation in the signal. This was assumed to be due to the vibration of the diaphragm in the differential pressure cell. The oscillation was very reproducible and could be modeled as an underdamped vibration. Using the model, the signal output could be deconvolved to obtain the original step change in pressure. The deconvolution procedure is discussed in detail in Appendix 1.

The DP probe pressure tappings were connected to the filter via tee connections at ports "f" and "j" on the 1 – 1.4 mm sand filter as shown in Figure 3.4 (see Table 3.1 for location of ports). The signal output could then be calibrated against piezometric headloss using the readings from the manometers. During backwash experiments, the branches connected to the manometers were shut off but the branches connected to the DP probe were left open.

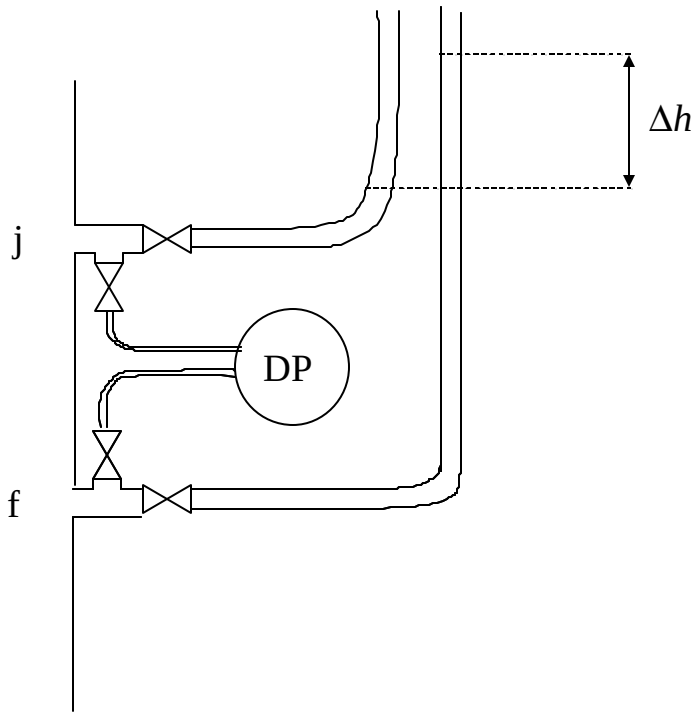

Figure 3.4 Pressure tappings

The DP probe was originally connected between ports “b” and “j” in order to record the headloss over as much of the bed as possible. However, it was found that once the flow started, the headloss remained essentially constant for the duration of the backwash and consequently did not provide much useful information about the behavior of the bed. The differential headloss across the section f-j provided information on the expansion of filter media above port “f” and on flow disruptions that occurred towards the end of the expansion process. The interpretation of the on-line headloss measurements is discussed in detail in Section 6.3.2. Chapter 6 deals with various phenomena observed during the backwashing of clogged filters.

The signal output was recorded using an RR1010-D four channel Rustrack Scout Datalogger (Rustrak, ISC, Inc., Cleveland, OH) with the logging frequency set at 0.25 /s. The calibration of the probe was checked at the beginning of each series of experiments. The slope of the calibration line was found to be fairly consistent from day to day but the signal at zero headloss tended to drift. Consequently, the signal output at zero headloss was recorded before each backwash experiment and the calibration equation adjusted accordingly.

3.4.2. The Opacity Meter

3.4.2.1. Meter description and principle of operation

Backwash turbidity concentrations for the 1 – 1.4 mm sand filter were measured on-line using a simple online opacity meter constructed by the Mechanical Workshop staff at the School of Chemical Engineering, University of Natal. The device was originally intended for measuring solids concentrations in sludges and was more suited for concentrated suspensions than low turbidity samples.

The opacity meter measured the reduction in light transmitted through a flowing sample as a result of turbidity in the sample. The detector consisted of a glass tube through which the sample flowed. An LED on one side of the tube transmitted light perpendicular to the direction of flow. The intensity of the transmitted light was measured by a photodiode on the opposite side of the tube as shown in Figure 3.5. The detector was housed in a black plastic box and the

inlet and outlet tubing were wrapped with insulating tape to minimize interference from stray light. The voltage signal from the photodiode was fed to the Rustrak Scout Datalogger.

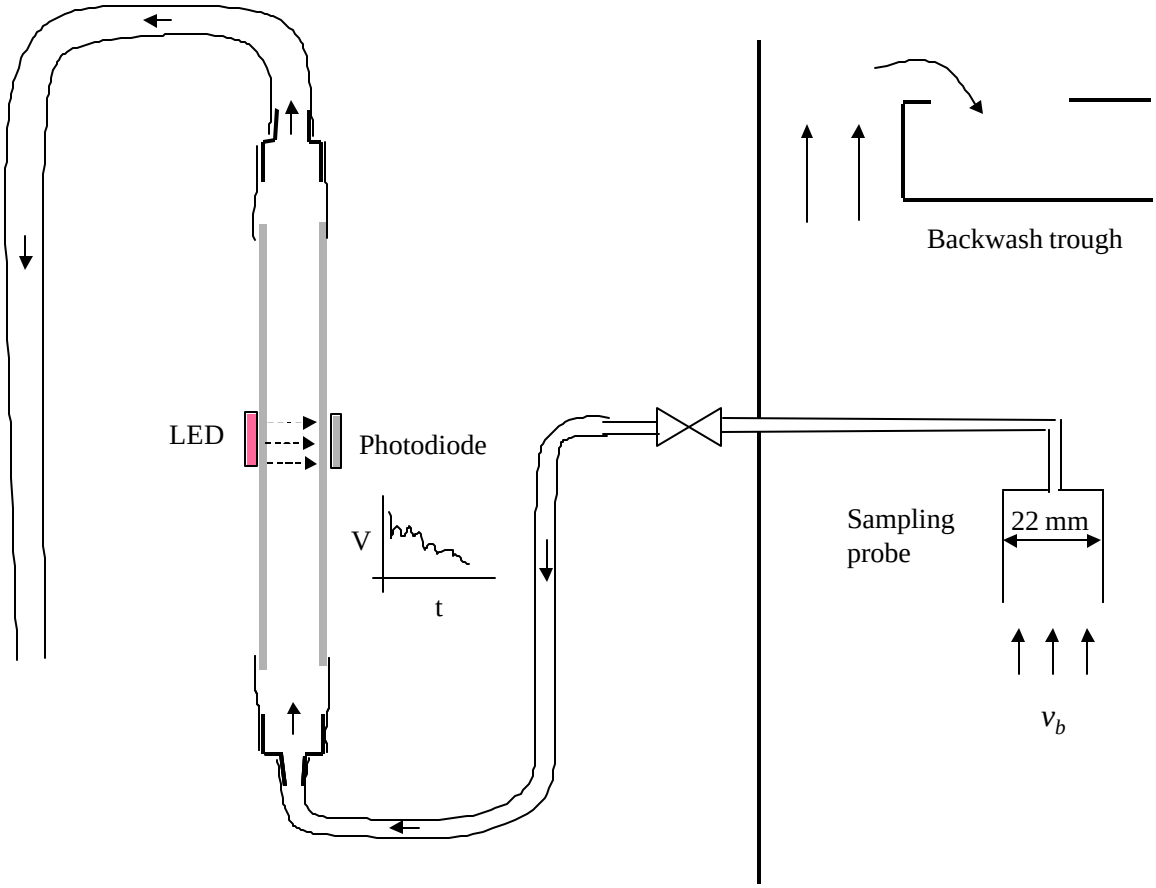

Figure 3.5 Opacity meter and sampling probe

Turbidity in the samples absorbed and scattered light, resulting in a reduction in the incident light on the photodiode and hence also the voltage signal output. This signal could then be calibrated against turbidity readings using a standard laboratory turbidimeter.

3.4.2.2. Calibration

The meter was calibrated using settled backwash effluent. Samples of both the sludge and the supernatant were collected and mixed in different ratios to produce a range of solids concentrations. A detailed description of the calibration procedure is given in Appendix 2.

During backwash, sample for the opacity meter was drawn from above the surface of the backwashing filter through a 22 mm diameter sampling probe located 0.705 m above the base of the filter bed. The flow of sample was set to approximately 1.2 % of the total backwash flow by adjusting the level of the discharge from the opacity meter. This ensured that the average velocity entering the probe was approximately the same as the backwash rate.

There was no indication of saturation of the signal output at the highest backwash concentrations observed in this study. The meter was calibrated up to 1400 NTU (output voltage ~ 4.5 V compared to ~ 10.6 V for clean water) while the maximum turbidity observed during a backwash experiment was 1088 NTU (output voltage ~ 5.3 V).

However, the calibration at low turbidity (< 10 NTU) was found to be very sensitive to temperature. Upon further investigation it was found that heat generated by the LED driver circuit tended to cause the detector to heat up, particularly when there was no sample flowing through the meter. Conversely, liquid flow through the meter tended to cause the detector to cool down resulting in a shift in the calibration. It was therefore important to ensure that the

detector temperature remained reasonably constant throughout the backwash. At the end of the filter run, the water above the filter had to be drained down to the level of the backwash trough. During this period the sampling valve was opened so that part of the water drained through the meter to cool it down in time for the start of the backwash. When this procedure was followed, the shift in baseline was 0.02 V or less which corresponded to a ~ 4 mg/L differential in calculated backwash concentration in the low concentration range.

3.5. Experimental procedures

3.5.1. Filtration

Filtration rate, temperature and headloss profile were recorded manually during the course of each run. Grab samples of the raw water, coagulated influent and filtrate were collected at intervals and analyzed for turbidity and pH. The total volume of water filtered during each run was calculated from the flow rate measurements.

3.5.2. Backwashing

At the end of each filter run, the filter was backwashed with a pre-determined volume and backwash rate using domestic tap water. The clean water was stored overnight in a 1000 L tank PVC tank to minimize variations in temperature at the beginning of backwash.

Prior to the start of backwash, the manual flow control valve was set with the flow being pumped to one of the filters not in use at the time. Once the flow was set, the backwash pump was switched off until the start of the backwash of the clogged filter. The water level in the backwash tank was adjusted so that there was no flow between the tank and the filter when the inlet valve to the filter underdrain was opened prior to switching the pump back on.

After the backwash was complete, the down flow fixed bed headloss profile was measured (using raw water without coagulant). The porosity of the fixed bed and hence also the headloss profile was found to be sensitive to the conditions under which the bed settled out. The most reproducible results were generally obtained when the backwash rate was reduced gradually rather than shut off abruptly. At the end of each experiment, the backwash flow was reduced at a rate of 100 L/h per 5 seconds (0.64 m/h/s) to 500 L/h (16 m/h) before the pump was shut off. The turn down period was timed so that the total volume of backwash water used in each experiment was approximately the same (134 L = 4.27 m^3/m^2 for the 1 – 1.4 mm sand bed and 100 L = 3.18 m^3/m^2 for the 0.7 mm sand bed).

The backwash effluent was collected in 120 L plastic drums calibrated in 5 L increments. The volume of effluent collected in a given drum could be determined to an accuracy of approximately ± 0.9 L. Once backwash was complete, the volume of water collected was recorded and then the contents of each bin were stirred up with a length of plastic pipe to obtain a uniform concentration. Samples of the mixed effluent were collected for turbidity and suspended solids measurements.

Floc retained in the bed after fluidized bed backwash was dislodged by backwashing with a combination of air and water. The air flow from the compressor could be measured using a rotameter on the air line, however, the flows of both the air and water were usually varied to maximize the agitation of the bed rather than set to predetermined rates. The water level in the filter was drawn down to just above the bed surface before the start of air scour and the flow was shut off before the water reached the backwash trough in order to prevent media losses. The bed was then flushed with water at high rate to remove the detached floc. This process was repeated until the amount of additional floc being removed from the bed became negligible. The effluent from combined air and water wash was collected and analyzed in the same way as the fluidized backwash effluent.

Once all the residual floc had been removed, the bed was backwashed at high rate to flush out any remaining bubbles and then settled out by gradual reduction of the flowrate in preparation for the next filter run.

3.5.3. Recording the filter backwash on video

Backwash experiments in the 1 – 1.4 mm sand bed were taped using a Sony CCDTR2000E home video camera in order to record the rate of bed expansion and the disintegration of the filter bed. The camera was set up on a tripod to one side of the filter and was focused on a measurement scale (in mm) on the side of the filter column. The zoom was adjusted to ensure that the surface of the filter bed was visible throughout the expansion

process. A stopwatch was attached to the filter column adjacent to the scale so that the camera recorded the time on the watch corresponding to each position of the bed as it expanded. This is shown in Figure 3.6.

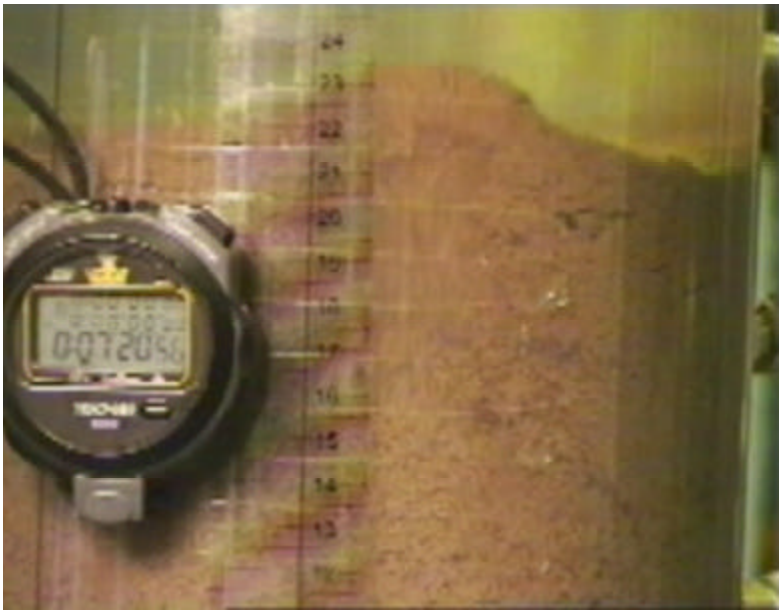

Figure 3.6 View of side of filter showing stopwatch and measurement scale

The watch on the filter column was synchronized with a second ten lap stop watch which was used to time the start of the data logger session and the time that the backwash pump was turned on. The time shown on the stopwatch in the video could then be related to the time since the start of backwash using the lap times recorded on the second stopwatch.

The video footage was downloaded onto a computer using Pinnacle Studio Version 8 (Pinnacle Systems, 2002). Selected clips were converted to short movies using the same

software and saved as mpeg files. The mpeg files can be downloaded from the dissertation website and be viewed using Windows Media Player.

3.6. Water quality analysis

Raw water, filter influent, filtrate and backwash samples were analyzed for turbidity using a Hach 2100N Turbidimeter (Hach Company, Loveland, CO). Backwash samples were shaken up to break the floc before measurements were made as this procedure gave more reproducible results. pH was measured using the Process Evaluation Facility laboratory's meter. The calibrations of the turbidity and pH meters were checked daily.

Total suspended solids (TSS) concentrations were measured using Standard Method 2540 D (American Public Health Association, 1999). Samples were measured out using appropriately sized plastic measuring cylinders and filtered through pre-dried and pre-weighed 45 mm Whatman glass fibre filters using a vacuum pump. The filters were dried overnight at 105 ^{o}C and then stored in a dessicator to cool. Once cooled, the filters were weighed to +/- 1 mg accuracy on a 0 to 2000 g balance. The filters were returned to the dessicator and later re-weighed to ensure their mass had stabilized. The solids concentration of the original sample was calculated from the sample volume and the change in mass of the filter. The volume of sample used was selected to obtain a maximum of 10 mg of residue for the most concentrated samples. A maximum of 3 L was used for the most dilute samples.

The results of the suspended solids analysis were used to develop a correlation between TSS and turbidity. Separate correlations were developed for alum and Z464N floc. The calibration curves are given in Appendix 2.

CHAPTER 4

FILTER MEDIA CHARACTERISTICS, FLUIDIZATION AND THEORETICAL OPTIMUM BACKWASH CONDITIONS

4.1. Introduction

Specification of filter media characteristics (grain size distribution, density and shape) is an important part of filter design. The effect of media characteristics on filtration performance, specifically turbidity removal and filter headloss development, is well documented. Media characteristics also determine filter backwash requirements. For fluidized backwash, large and heavy grains require higher backwash rates than smaller and less dense grains. The expansion of filter bed at a given backwash rate is also a function of the media properties. The effect of filter media characteristics on the backwash rates required to fluidize the media and the expansion of the bed once fluidized has been dealt with in some detail in the water treatment literature since they affect the design of the filter box and backwash facilities. However, the effect of media properties on backwash efficiency has received relatively little attention.

Amirtharajah (1971) calculated that the optimum backwash rate (see Section 2.2.4) corresponded to an expanded bed porosity of

$$e_{ms} = \frac{n-1}{n} \qquad 4.1$$

e_{ms} = Porosity at the maximum shear condition

where n is the expansion coefficient in the Richardson – Zaki relationship between backwash rate and porosity.

$$v_b = k_{iTy} e_i^{n_{iTy}} \qquad 4.2$$

v_b = Superficial backwash velocity, m/s

k_{iTy}, = Constants for size fraction i , temperature T and sphericity y

n_{iTy}

Amirtharajah (1971) assumed n = 3.1 to 3.4 for sand beds, leading to the much quoted result that optimum backwash occurs in the region e = 0.68 to 0.71. However, since n is in fact a function of grain size, density and shape (Cleasby and Fan, 1981; Amirtharajah and Cleasby, 1972; Dharmarajah and Cleasby, 1986), both the optimum backwash rate and optimum porosity are expected to be a function of media characteristics.

Furthermore, the efficiency of backwash at the optimum backwash conditions is likely to be different for different media. It is generally agreed that fine media is more prone to mudballing than coarse media (Kawamura, 1975b). For example, the City of Kyoto found that

0.45 mm filters accumulated ten times more mud than 0.7 mm sand filters over a period of 4 years with backwash at the same rate (Water Dept., City of Kyoto, 1956).

The theoretical optimum porosity and corresponding backwash rate for any given set of media characteristic can be calculated using Equations 4.1 and 4.2 if appropriate values of k and n are available. k and n can either be determined experimentally or calculated using one of several available correlations. Furthermore, the expanded bed porosity is known, the rate of power dissipation per unit volume can be calculated. From Equations 2.3 and 2.11, the dissipation function for a given media size and backwash rate can be calculated as

$$\overline{\Phi} = m\overline{G}^2 = m\left[\frac{v_b g(r_s - r)(1-e)}{me}\right] \qquad 4.3$$

$\overline{\Phi}$ = Mean rate of power dissipation, J/m^3/s

Chapter 4 presents the calculation of the theoretical optimum backwash conditions and rate of energy dissipation for the filter media used in the current study. Section 4.2 discusses the effect of media and fixed bed properties on fluidization behavior. Section 4.3 describes the experimental determination of the characteristics of the filter media. Section 4.4 presents the calculation of the minimum fluidization velocities and bed expansions for the two filter beds used in the investigation. Section 4.5 presents the calculation of the optimum backwash conditions and dissipation functions for the range of media sizes in each filter bed. The selection of the optimum backwash conditions for graded filter beds is also discussed. The theoretical values of

the dissipation function calculated in Section 4.5 are compared to experimentally determined backwash efficiencies in Chapter 9.

4.2. Fluidized bed hydraulics and the effect of filter media characteristics on fluidization

This section presents the models of minimum fluidization velocity and bed expansion used in this investigation, and discusses their sensitivity to the media characteristics. More comprehensive reviews of filter media characteristics and fluidization are available elsewhere (Amirtharajah and Cleasby, 1972; Dharmarajah and Cleasby, 1986; Ceronio and Haarhoff, 1994).

4.2.1. Fluidization

Fluidization of a bed of solid particles occurs when the drag forces on the particles due to the upward flow of a fluid exactly balance the buoyant weights of the particles. A slight increase in the velocity above the minimum required to achieve the critical drag force (the minimum fluidization velocity, v_{mf}) results in the particles moving apart and becoming suspended in the fluid. Any further increase in velocity causes the particles to move further apart from each other until the forces on the particles are again balanced or the particles are ultimately washed away.

4.2.2. Media and packed bed characteristics relevant to fluidization

4.2.2.1. Media size

Filter grain size (and shape) determines the ratio of surface area to weight and consequently is an important factor in determining fluidization behavior. Smaller grains fluidize at lower velocities than larger grains and undergo greater bed expansion. All real filters contain a range of grain sizes and this complicates modeling the fluidized bed. In practice, the size distribution of media samples is determined by a standard sieve test, which measures the weight of sample passed through successively finer sieves. The size distribution is usually characterized in terms of its d_{10} and d_{60} sizes (sieve sizes through which 10 % and 60 % respectively of the sample mass passes). The uniformity coefficient of the media sample is defined to be the ratio between the d_{60} and d_{10} sizes.

$$UC = \frac{d_{60}}{d_{10}} \qquad 4.4$$

d_{60} = Mesh size through which 60 % of sample mass passes, mm

d_{10} = Mesh size through which 10 % of sample mass passes, mm

d_{10} is also known as the effective size.

4.2.2.2. Grain density

Grain density r_s in combination with grain size determines the weight of individual particles and hence the magnitude of the drag force required to suspend them. Denser media such as silica sand (2650 kg/m^3) fluidizes at higher backwash velocities and tends to undergo less expansion at a given backwash rate than lighter media such as anthracite and GAC (1450 to 1730 kg/m^3 and 1300 to 1500 kg/m^3 respectively).

4.2.2.3. Particle shape and sphericity

Particle shape also affects the surface area to weight ratio of filter grains and hence their fluidization behavior. Angular grains have a higher surface area than spherical grains and consequently fluidize at lower velocities and undergo greater bed expansion than more spherical grains.

Modeling the effect of grain shape on backwash behavior is difficult. Many definitions for media grain shape factors have been proposed in the literature. The most commonly used shape factor is sphericity, y, defined to be the ratio of the surface area of an equal volume sphere to the surface area of a grain (McCabe and Smith, 1976). y = 1 for perfectly spherical grains and y < 1 for angular particles. The equivalent spherical diameter, d_{eq}, can be obtained from measurements of the media density and masses of individual grains. Cleasby and Fan (1981) showed that the filter media sphericity can be determined indirectly by measuring the down flow headloss through a clean filter bed and fitting the data to the Ergun equation.

$$\frac{\Delta h}{l} = 4.17\frac{n}{g} v_z \frac{(1-e_0)^2}{e_0^3} S_v^{\ 2} + 1.75\frac{n}{g} v_z^2 \frac{(1-e_0)}{e_0^3} S_V \qquad 4.5$$

Δh = Piezometric headloss, m

l = Bed height, m

n = Kinematic viscosity, m^2/s

v_z = Superficial velocity, m/s

e_0 = Fixed bed porosity

S_v = Specific surface (surface per volume), m^2/m^3

The specific surface is defined as

$$S_v = \frac{6}{y d_{eq}} \qquad 4.6$$

y = Surface area sphericity

For graded media, the total piezometric headloss across the filter bed can be assumed to be the linear sum of the contributions of each size fraction based on the sieve analysis. Equation 4.5 becomes

$$\frac{\Delta h}{l} = 4.17\frac{n}{g} v_z \frac{(1-e_0)^2}{e_0^3} \sum_i x_i S_{vi}^{\ 2} + 1.75\frac{n}{g} v_z^2 \frac{(1-e_0)}{e_0^3} \sum_i x_i S_{vi} \qquad 4.7$$

$$S_{vi} = \frac{6}{y d_i} \qquad 4.8$$

d_i = Geometric mean mesh size for the ith mass fraction, m

x_i = ith mass fraction

d_i and x_i are the media sieve analysis results. x_i refers to the sample mass fraction retained between two sieves and d_i is the geometric mean of the mesh sizes of those two sieves. d_i is assumed to be a reasonable approximate of d_{eq}. Values of y obtained from Equations 4.5 and 4.7 are quite sensitive to e_0, the porosity of the fixed bed (Dharamarajah and Cleasby, 1986). It is important for the fixed bed to be in a loosely packed state when the headloss is measured.

4.2.2.4. Fixed bed porosity and porosity at incipient fluidization

Grain shape tends to affect the loose settled bed porosity, which is an important parameter in bed expansion models. The more angular particles are, the lower their settling velocity and the higher the settled bed porosity.

The loose bed porosity also depends on the degree of stratification of the filter media and to some extent on the size of the filter column or box (Logsdon et al., 2002). A stratified bed typically occupies a greater volume than an unstratified bed, since smaller grains can occupy

the voids between bigger grains. Filter media will not settle back completely for filter columns with diameters less than 15 cm and, in some cases, slightly larger, resulting in higher porosities in smaller filters.

The actual porosity of a fixed bed, e_0, is typically lower than the loose settled bed because any vibration or shock that the filter is subjected to tends to cause the bed to compact (Cleasby and Fan, 1981, Logsden et al., 2002). A reduction in e_0 results in an increase in clean bed headloss (e.g. See Equation 4.5).

For beds of particles of non-uniform size, the porosity at incipient fluidization, e_{mf}, is generally not the same as the fixed bed porosity. This is because smaller grains fluidize at lower velocities than the rest of the bed. Therefore, when the point of incipient fluidization is reached, a small amount of expansion has already occurred. However, e_0 is often used to approximate e_{mf} in models of fluidization (e.g. Amirtharajah and Cleasby, 1972; Dharmarajah and Cleasby, 1986).

4.2.3. Minimum fluidization velocity

A bed of particles becomes fluidized when the average drag forces on the particles exactly balance the buoyant weight of the particles and each particle becomes separated from every other particle by a layer of fluid. For a bed of uniform particles, the particle characteristics that determine the point of incipient fluidization are particle size, shape and density. For filters

beds consisting of a range of particle sizes, the point at which the bed becomes fluidized is less well defined and the overall bed expansion is strongly affected by the particle size distribution. The point at which bed expansion occurs in both uniform and graded beds is also affected by the fixed bed porosity. Depending on the degree of compaction of the bed, expansion may precede fluidization.

The minimum fluidization velocity for a given media size and water temperature can be estimated using the model of Wen and Yu (1966).

$$V_{mf} = \frac{\mu}{\rho\, d_{eq}}\left(33.7^2 + 0.048Ga\right)^{0.5} - \frac{33.7\mu}{\rho\, d_{eq}} \qquad 4.9$$

V_{mf} = Minimum fluidisation velocity

μ = Water viscosity

ρ = Water density

d_{eq} = Equivalent media diameter

G_a = Galileo number

Ga is defined by:

$$Ga = d_{eq}^3 \frac{r(r_s - r)g}{m^2} \qquad 4.10$$

r_s = Media density, kg/m^3

g = Gravitational acceleration constant = 9.81 m/s^2

Equations 4.9 and 4.10 are valid for any dimensionally consistent set of units. Equation 4.19 was derived by solving for the velocity at which the headloss across the fixed bed became equal to the headloss across the fluidized bed.

The fixed bed headloss was modeled using the Ergun equation for flow through packed beds (Equation 4.5) while the fluidized bed headloss was modeled using Equation 2.10. The simultaneous solution of the fixed and fluidized bed equations is quite sensitive to the values of e_{mf} and y (Cleasby, 1990). When this calculation is carried out for design purposes, the value of the bed porosity at incipient fluidization, e_{mf}, and y are often not known. Wen and Yu (1966) eliminated both parameters from the solution by using the following approximate empirical relationship between them.

$$\frac{1 - e_{mf}}{y^2 e_{mf}^3} = 11 \qquad 4.11$$

e_{mf} = Porosity at incipient fluidization

Cleasby and Fan (1981) measured v_{mf} for various size fractions of different filter media and found that it agreed well with the predictions of Equation 4.9 when the passing size (mesh size through which each media sample passed) was used in place of d_{eq}. For graded beds, they recommended using the d_{90} mesh size to represent the coarsest fraction of the grains. d_{90} can either be determined directly from the sieve analysis data or estimated from d_{10} and d_{60} (Cleasby, 1990).

$$d_{90} = d_{10}\left(10^{1.67 \log UC}\right) \qquad 4.12$$

d_{90} = Mesh size through which 90 % of the sample mass passes, m

4.2.4. Modeling the expansion of fluidized beds

The expansion of the filter bed during backwashing is an important design consideration. Consequently, several authors have developed models of the relationship between backwash velocity and fluidized bed porosity. After a comprehensive review of the literature on fluidized bed expansion, Dharmarajah and Cleasby (1986) used dimensional analysis to develop the following semi-empirical correlation for calculating expanded porosity.

$$\log(A1) = 0.56543 + 1.09348 \log \mathrm{Re}_1 + 0.17979(\log \mathrm{Re}_1)^2 - 0.00392(\log \mathrm{Re}_1)^4 - 1.5(\log y)^2 \qquad 4.13$$

Where

$$A1 = \left[\frac{e^3}{(1-e)^2}\right]\left\{\frac{r(r_s - r)g}{\left(\frac{6}{yd}\right)^3 m^2}\right\} \quad 4.14$$

$$\mathrm{Re}\,1 = \frac{rv_b}{\left(\frac{6}{yd}\right)m(1-e)} \quad 4.15$$

Equation 4.13 applies to situations where wall effects can be neglected. Wall effects will have no discernable impact on expansion of full-scale filters. However, they can be significant in laboratory columns. According to the authors, the porosity in smaller equipment can be predicted by replacing v_b, the actual backwash velocity, by v_0, the hypothetical backwash velocity free of wall effect, in Equation 4.13.

$$v_0 = v_b \times 10^{a\left(\frac{d}{D_t}\right)} \quad 4.16$$

$$a = \frac{5.18}{\mathrm{Re}_{t,\infty}^{0.585}} \quad 4.17$$

$\mathrm{Re}_{t¥}$ is the Reynolds number based on the particle free settling velocity in an infinite medium.

Equation 4.13 was calibrated using a range of granular materials of various sizes, shapes and densities. The sphericity values were determined by fitting the Ergun Equation (Equation

4.5) to the downflow headloss in loosely packed beds of uniform particles. The correlation was found to give a good fit to the experimental data for $Re_1 > 0.2$ and $e < 0.85$ for particles with $Re_t < 100$ and for $e < 0.9$ for particles with $Re_t > 100$ but did not work outside these porosity ranges. Re_t was the particle Reynolds number based on the terminal settling velocity of a particle measured in a column of diameter D_t.

4.3. Characteristics the filter media used in the current investigation

Backwashing experiments were carried out using two different sand gradings: 0.7 mm sand (UC =1.36) and 1 to 1.4 mm sand. The 0.7 mm sand was a standard grading available from B&E Silica (Brtiz, South Africa). The 0.7 mm sand bed had been used to observe the development of filter mudballs in an earlier project that simulated the operation of valveless sand filters (Brouckaert et al., 2003). The 1 – 1.4 mm sand bed was prepared by sieving 1.0 mm graded sand (UC = 1.4) sand purchased from B&E Silica to remove the fractions less than 1 mm and greater than 1.4 mm to create a more uniform size distribution. The size range 1 – 1.4 mm was selected to allow backwashing at a range of sub-fluidized and fluidized up flow rates within the operating range of the plant backwash system.

Samples of the sand used in each filter were characterised in terms of size distribution, density and surface area sphericity.

4.3.1. Size distribution

The media size distributions for each of the filters were determined by sieve analysis using a mechanical shaker. Representative sampling techniques were used and multiple determinations were made for each filter. Because of the narrow size distributions of the media samples, a $\sqrt[4]{2}$ series of sieves was used to ensure adequate resolution in the measured size distribution. The mass of sand in each size fraction was summed for replicate determinations and the totals in each fraction used to determine the average size distribution. The size distribution results are presented in Figure 4.1.

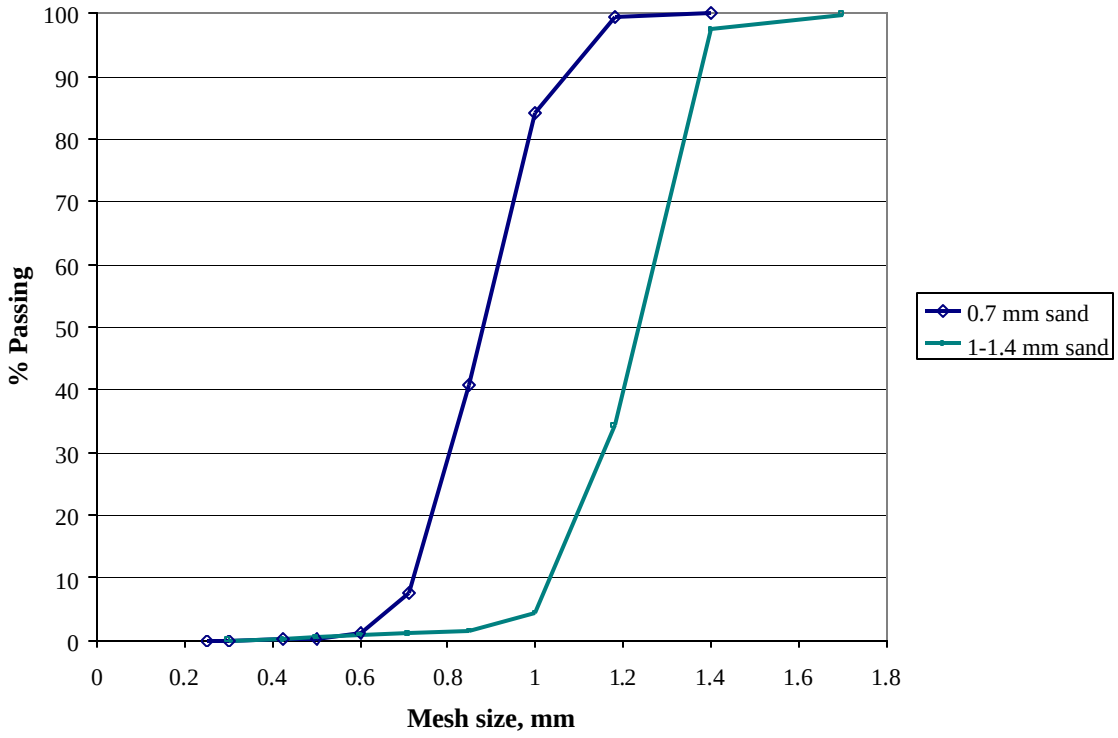

Figure 4.1 Media size distributions

The d_{10}, d_{60}, d_{90} and uniformity coefficient (Equation 4.4) of each filter media was calculated from its average cumulative size distribution. The sieve sizes and corresponding geometric mean sizes and mass fractions are listed in Table 4.1.

Table 4.1 Size fraction analysis

Mesh size, mm	Geometric mean size d_i, mm	Mass fraction x_i	
		0.7 mm sand	1 –1.4 mm sand
> 1.7	1.84		0.0012
1.4 – 1.7	1.54	0.0005	0.0253
1.18 – 1.4	1.29	0.0068	0.6307
1.00 – 1.18	1.09	0.1521	0.2987
0.85 – 1.00	0.92	0.4326	0.0285
0.71 – 0.85	0.78	0.3312	0.0051
0.60 – 0.71	0.65	0.0654	0.0023
0.50 – 0.60	0.55	0.0093	0.0025
0.425 – 0.50	0.46	0.0008	0.0045
0.30 – 0.425	0.36	0.0009	0.0011
0.25 – 0.30	0.27	0.0004	

4.3.2. Density

Sand samples were rinsed several times in deionised water to remove dust and clay and then dried overnight at 110 ^{o}C. Samples were stored in a dessicator while cooling. 200 mL volumetric flasks were weighed to 1/100th of 1 g and then half filled with deionised water. 100 g samples of sand were transferred to the volumetric flasks which were then sealed and shaken to eliminate air bubbles. The flasks were then topped up to the 200 mL mark with deionised water and re-weighed. The density of the media could then be determined by calculating the volumes of the water and media in the flask.

4.3.3. Surface area sphericity

Surface area sphericities of the various media samples were calculated from clean bed down flow headloss measurements using Equation 4.7

Media characteristics and filter bed depths for the different sand gradings are presented in Table 4.2.

Table 4.2. Media Characteristics

	0.7 mm sand	1 – 1.4 mm sand
d_{10}	0.72 mm	1.04 mm
d_{60}	0.91 mm	1.27 mm
d_{90}	1.04 mm	1.38 mm
Uniformity coefficient (UC)	1.36	1.22
Density (r_s)	2642 kg/m^3	2643 kg/m3
Surface area sphericity (from Equation 4.7)	0.86	0.81
Fixed bed height	0.64 m	0.47 m
Fixed bed porosity, e_0	0.48	0.48
Porosity at incipient fluidization, e_{mf} (from fluidization tests Section 4.4.1)	0.51	0.5

4.4. Modeling the fluidization of the clean filter media

Several experiments were carried out to determine the minimum fluidization velocity and bed expansion of the experimental filter beds at different temperatures. The filter set up was described in Chapter 3. The results were then compared to Wen and Yu's (1966) correlation for the minimum fluidization velocity and Dharmarajah and Cleasby's (1986) correlation for backwash rate and bed expansion.

4.4.1. Minimum fluidization velocity, V_{mf}

The minimum fluidization velocity of a media sample can be determined experimentally from the intersection of the fixed (upflow) and fluidized bed headloss curves (Cleasby, 1990). At sub-fluidization velocities, the headloss increases linearly with backwash rate whereas the headloss across a fully fluidized bed remains constant. The experimentally determined value of v_{mf} depends on the degree of compaction of the filter media at incipient fluidization (Fitzpatrick, 1998). The more compacted the bed, the lower the backwash rate at which the maximum headloss is achieved. In this study, headloss measurements were made with the bed contracting from a fully fluidized state rather than expanding from an initially fixed state as this gave more reproducible results.

Figure 4.2(a) and Figure 4.2(b) show the fluidization curves for the two filter beds at various temperatures, with the regression lines used to estimate v_{mf}. Values predicted from Wen and Yu's equation (based on the d_{90} size) are also shown.

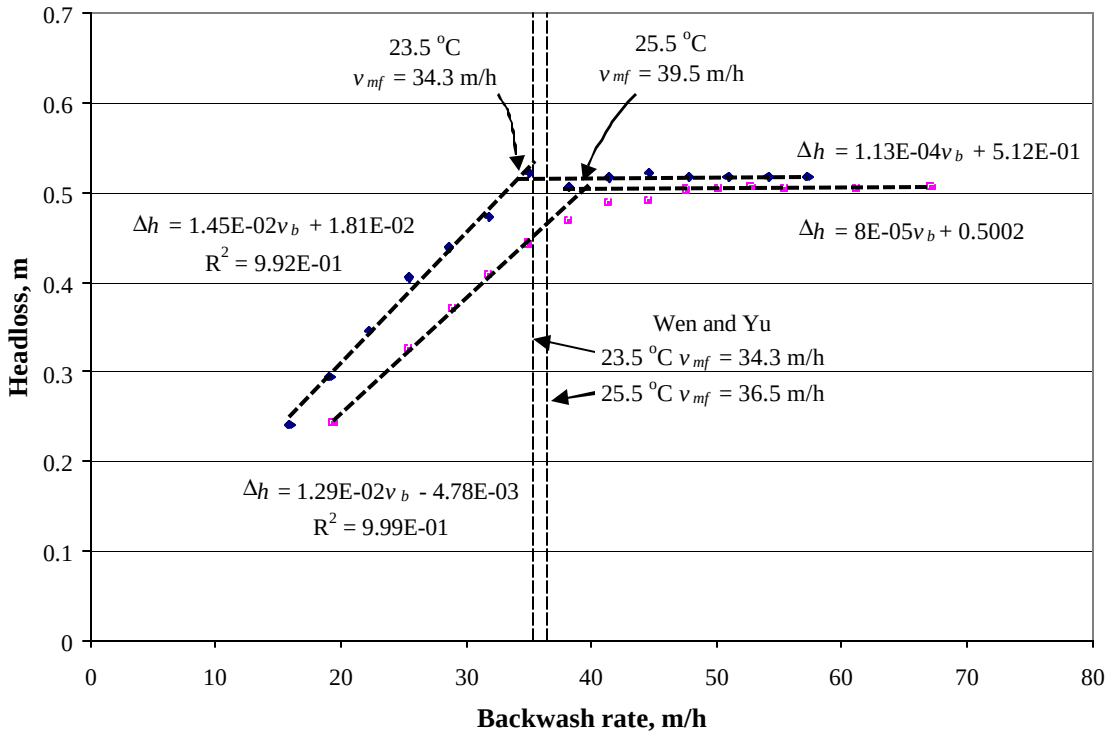

Figure 4.2 (a) Determining the minimum fluidization velocity for 0.7 mm sand

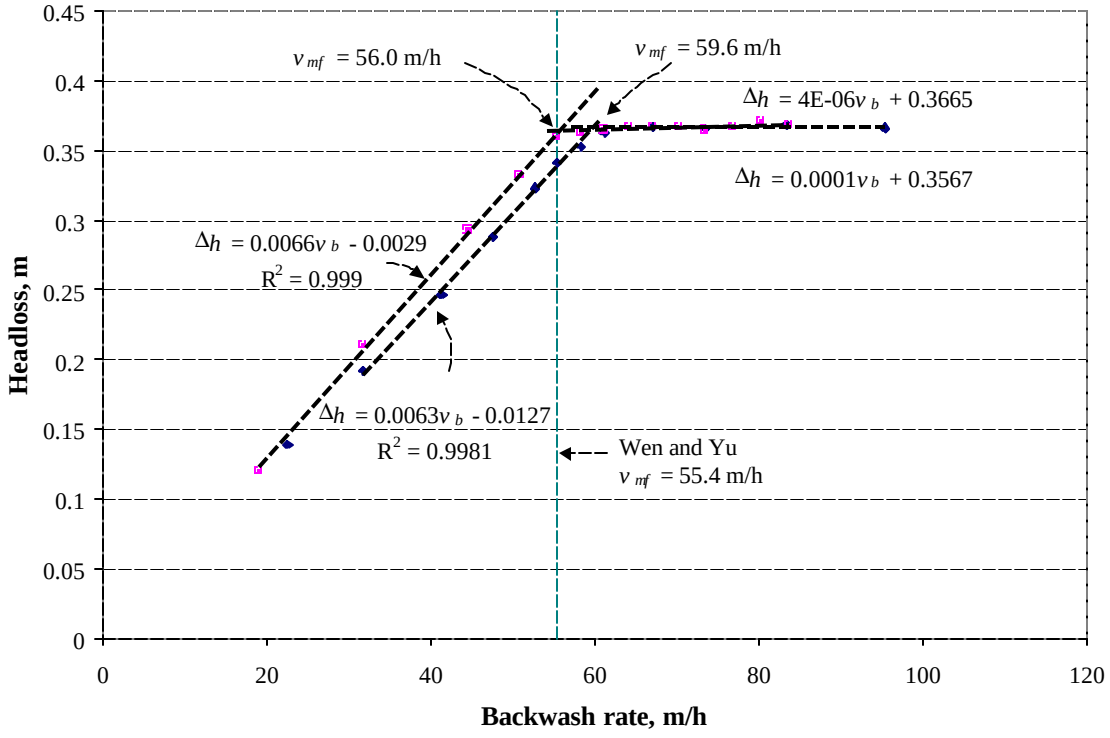

Figure 4.2 (b) Determining the minimum fluidization velocity for 1-1.4 mm sand

There was a good agreement between the measured values and the values predicted by Wen and Yu (within the reproducibility of the measurements). It was therefore assumed that Wen and Yu's model would provide accurate predictions of v_{mf} for each filter bed at temperatures other than those at which it was measured. Figure 4.3 shows the minimum fluidization velocity for each bed calculated as a function of temperature using Wen and Yu's equation for the range of temperatures encountered in this investigation.

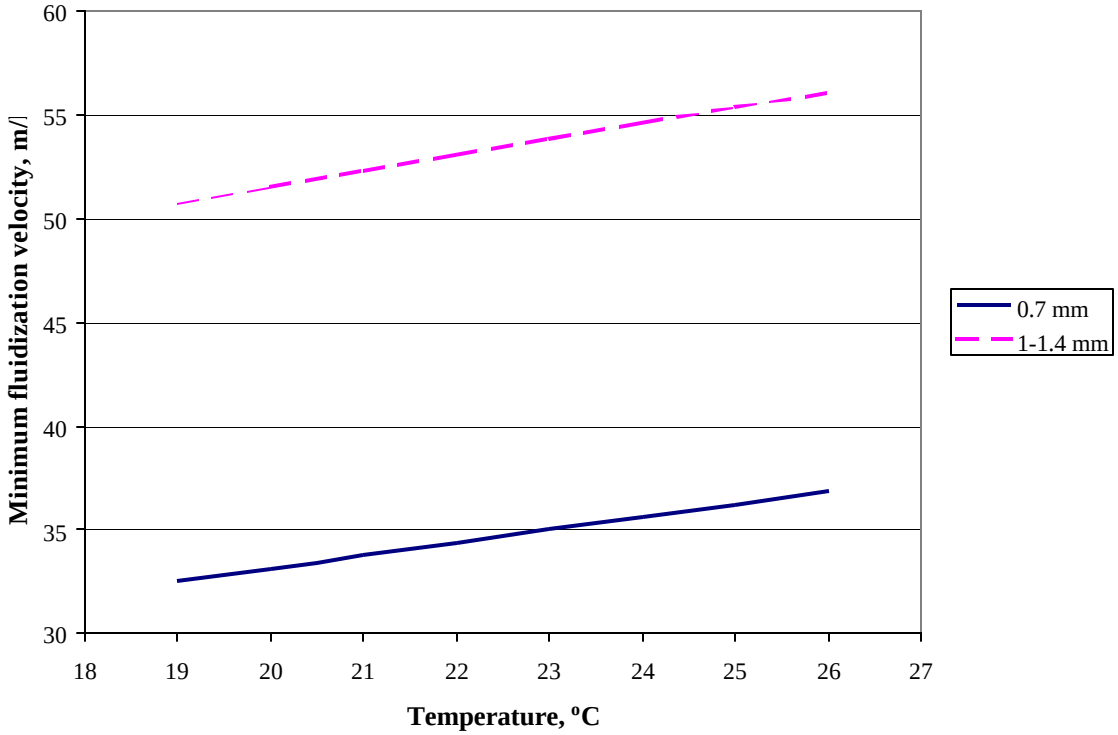

Figure 4.3 Predicted minimum fluidization velocity as a function of temperature (Equation 4.10)

In the current study, backwash rates in the 1 – 1.4mm sand bed ranged from 61 to 95 m/h, or 1.1 v_{mf} to 1.8 v_{mf} . The backwash rate for the 0.7 mm sand bed was always 53 m/h and the temperatures ranged from 21 to 26 ^{0}C, corresponding to 1.4v_{mf} to 1.6v_{mf}.

4.4.2. Fluidized bed expansion

In this study, Dharmarajah and Cleasby's (1986) correlation for predicting fluidized bed expansion as a function of media properties was used to estimate the porosity for each size fraction in each filter bed. If the backwash velocity in a particular layer was less than the minimum fluidization velocity for that layer then the porosity was assumed to be e_{mf} .The expanded height of each layer was calculated and the results summed to obtain the total bed height. The average porosity was then calculated from the overall height.

The model was initially set up in a Microsoft Excel spreadsheet that calculated the bed expansion corresponding to the conditions at which each experimental measurement was made. The model results were then compared to measurements of the actual bed expansions at various temperatures and backwash rates. The surface area sphericities presented in Table 4.2 were used as initial estimates in the spreadsheet model. Figure 4.4 shows the agreement between model and measurements for the 1-1.4 mm filter sand using y = 0.81, the value obtained from Equation 4.2. The dates refer to fluidization experiments carried out between January and November 2001. The average e_{mf} was assumed to be 0.5 (+/-0.005) based on the results of the fluidization tests (See Figure 4.2).

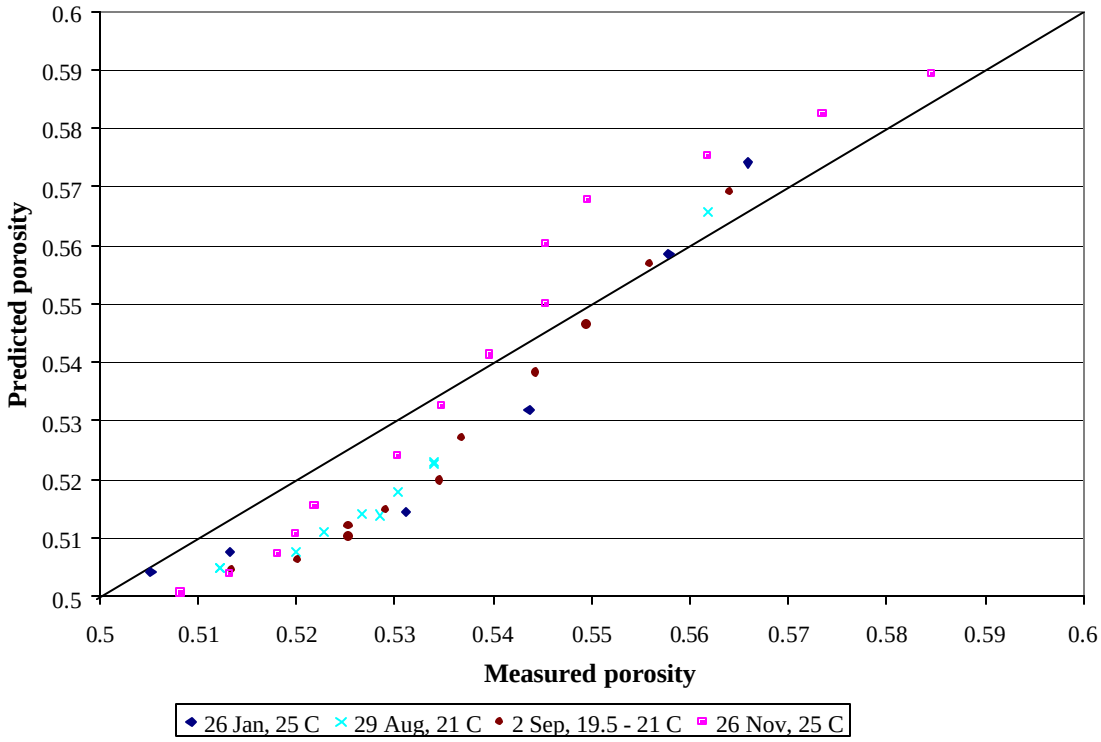

Figure 4.4 Predicted vs measured porosity for 1-1.4 mm sand, y = 0.805, v_b = 61 - 108 m/h

Overall, the measured and predicted porosities agreed fairly well for the 1-1.4 mm sand although the model tended to over-predict at higher porosities and under-predict at lower porosities. Results presented in Dharmarajah and Cleasby (1986) (Figure 16) show the same the tendency.

In the case of the 0.7 mm sand, using y = 0.86 resulted in the over-prediction of porosity for all the flowrates considered. However, adjusting the sphericity down to y = 0.81 resulted in the smallest sum of square errors for porosities from 0.51 to 0.62. The results are shown below.

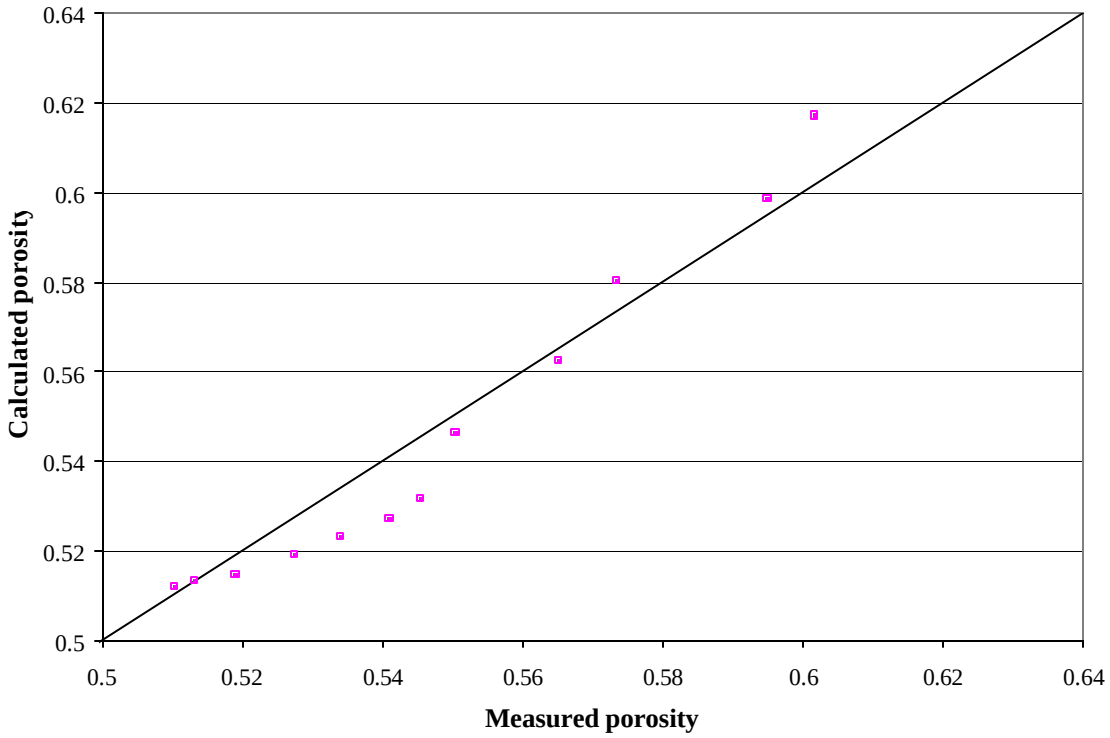

Figure 4.5 Predicted vs measured porosity at 25.5 ^{o}C, 0.7 mm sand, y = 0.81, v_b = 38 - 87 m/h

Once a reasonable fit between the model and measured porosities had been established, a Mathcad 8.0 worksheet was set up to calculate the expanded bed porosity as a function of average mesh size, d_i, backwash rate, v_b and temperature and then fit the results to the power law form of the porosity – backwash velocity relationship (Equation 4.2).

Expressing the results of Equation 4.13 in the form of Equation 4.9 facilitated the calculation of the dissipation function (Equation 4.3) and theoretical optimum backwash rates for the filter sand used in the current study. Figures 4.6 and 4.7 show values of k_{iTy}, and n_{iTy} at 20 and 25^{0}C. The sensitivity of the expansion coefficients to y is also shown. The solids lines

were calculated using y = 0.81 while the dotted lines show the effect of varying y between 0.7 and 0.9. k_{iTy}, increases with grain size, temperature and sphericity (greater velocities are required to achieve a given expanded bed porosity). n_{iTy} shows the opposite trend. The range n = 3.1 – 3.5 corresponds to the size range 0.4 to 0.8 mm, which is approximately the range of sand sizes that Amirtharajah (1971, 1978) worked with. Once the values of k_{iTy}, and n_{iTy} had been calculated, the optimum backwash rate and porosity corresponding to each media size could be calculated (Equations 4.1 and 4.2). In addition, the dissipation function (Equation 4.3 for each grain size could be calculated as a function of backwash rate.

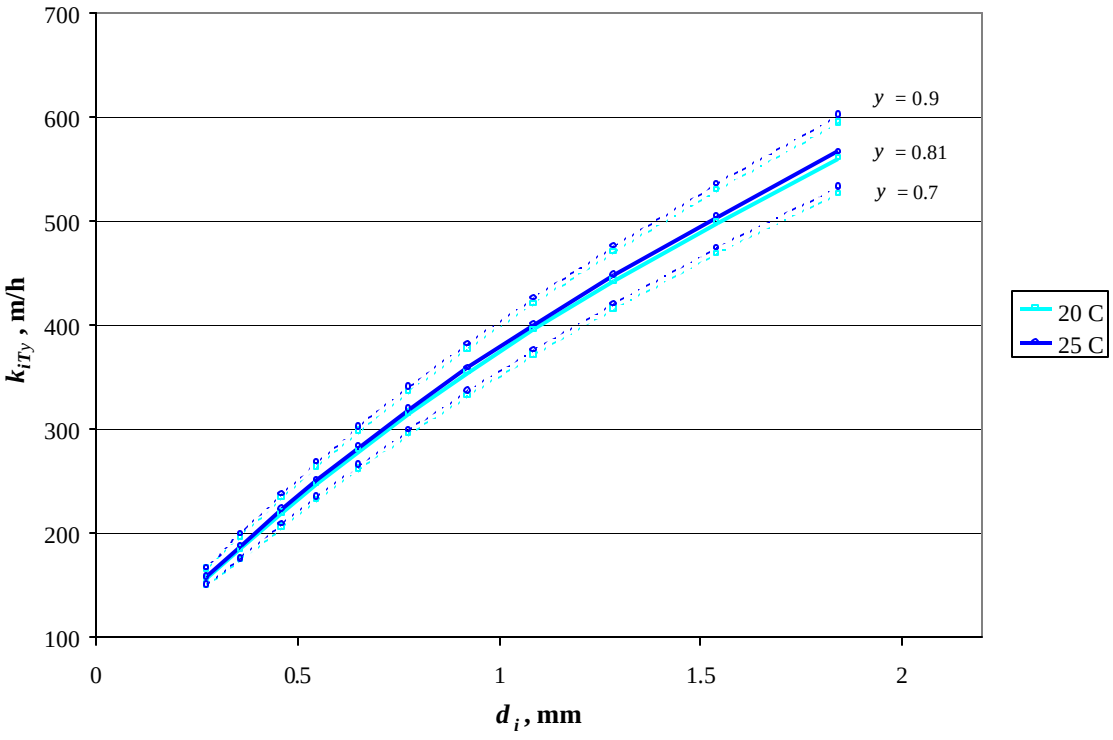

Figure 4.6 k_{iTy} as a function of grain size

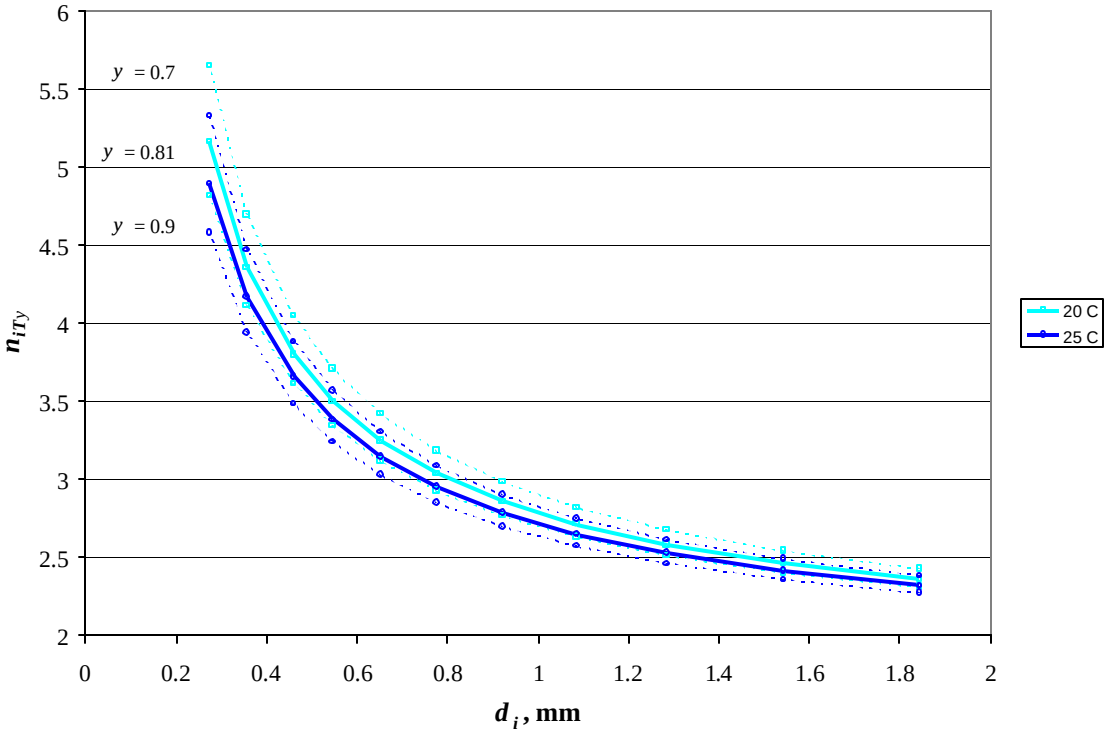

Figure 4.7 n_{iTy} as a function of grain size

4.5. Predicting the optimum backwash conditions and the rate of power dissipation

The optimum porosity and backwash rate for a given media size can be estimated using Equations 4.1 and 4.2 respectively. The results are plotted in Figure 4.8 and 4.9 and show the same dependency on grain size, temperature and sphericity as k_{iTy}, and n_{iTy} . The theoretical optimum backwash rate increases with grain size but it is important to note that the theoretical optimum porosity decreases with grain size. Therefore the optimum cleaning efficiency at e = 0.7 reported by Amirtharajah (1978) does not necessarily apply for backwashing of coarser media.

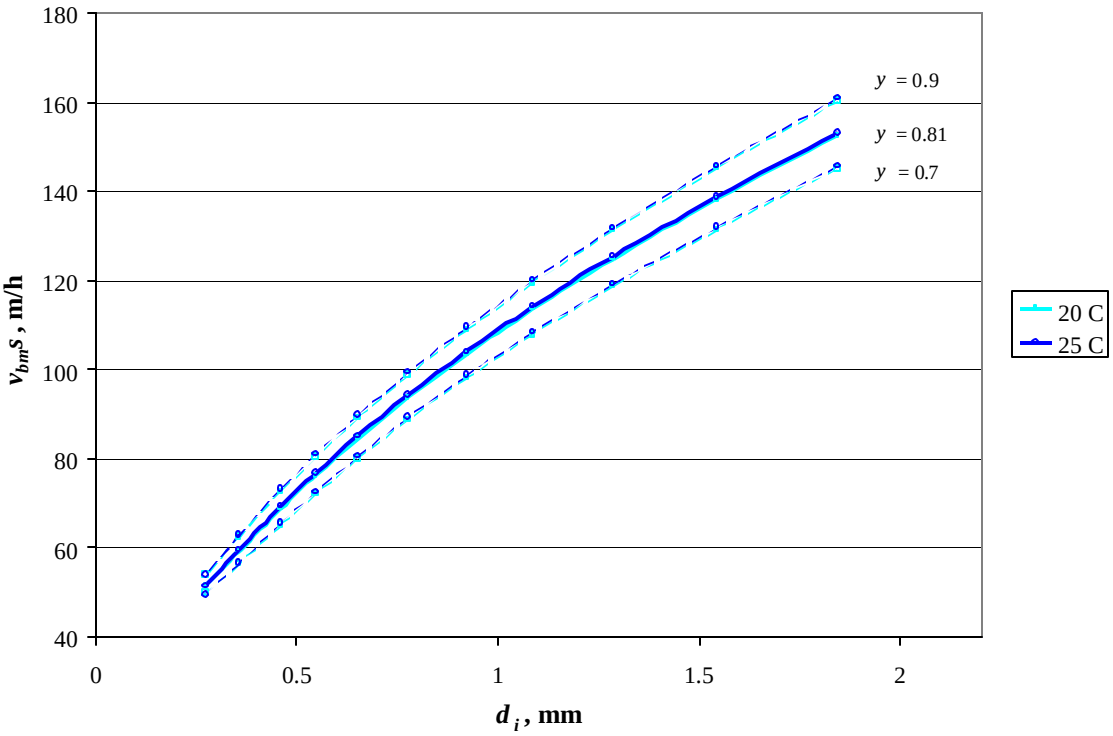

Figure 4.8 Optimum backwash rate as a function of grain size

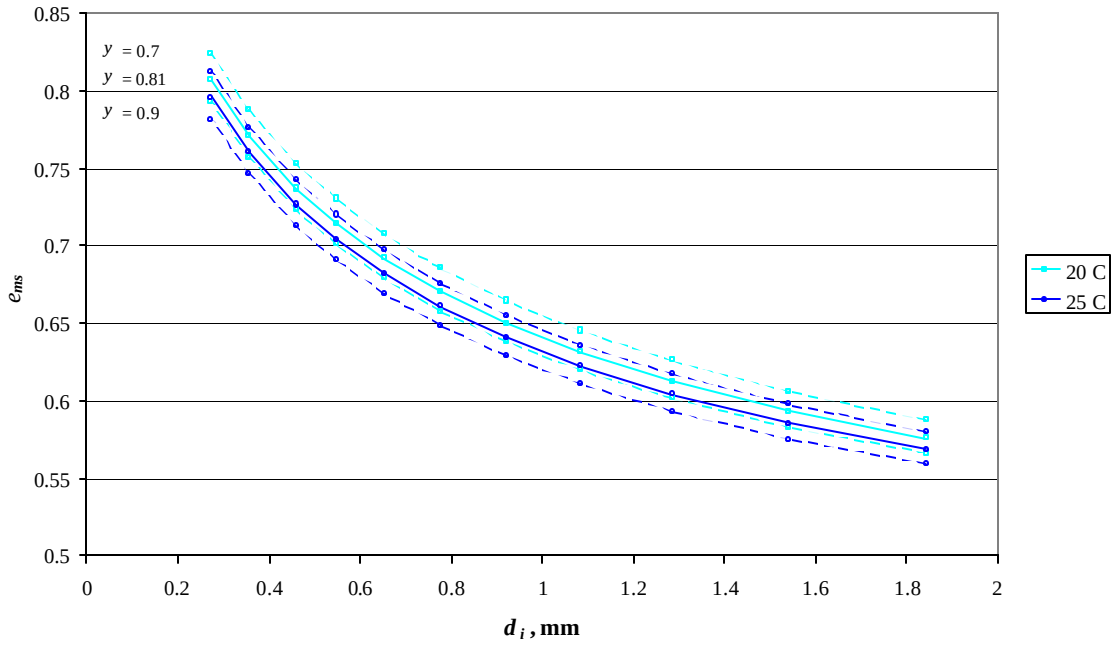

Figure 4.9 Optimum backwash porosity as a function of grain size

When trying to determine the theoretical backwash velocity for a filter bed containing a range of grain sizes, it is necessary to select an appropriate media size to represent the characteristics of the filter in terms of backwash cleaning efficiency. Kawamura (1975b) based his model of the optimum backwash rate on the d_{60} media size. However, as discussed in Chapter 2 (Section 2.2.4), in a stratified filter bed, the bulk of deposits will be attached to the finer media sizes so the d_{60} size is not representative of the sections of the bed in which cleaning is most required.

Amirtharajah (1978) presented experimental evidence that detachment efficiency in a graded filter bed was maximized when the porosity in the top 3 inches (76 mm) of the fluidized bed was close to the theoretical optimum. However, the implications of this observation for the selection of the optimum backwash rate for graded media was not discussed in any detail.

Figure 4.10 shows the mean dissipation function as a function of velocity and grain size d_i. For $v_b > v_{mfi}$, Φ_i was calculated using Equation 4.3. For $v_b < v_{mfi}$, it was assumed that the headloss gradient within a layer of media d_i was given by

$$\left(\frac{\Delta h}{l}\right)_i = \frac{v_b}{v_{mfi}} g \left(\frac{r_s - r}{r}\right)\left(1 - e_{mf}\right) \qquad 4.18$$

$\left(\frac{\Delta h}{l}\right)_i$ = Headloss gradient for media size d_i at backwash rate $v_b < v_{mfi}$

The dissipation function at sub-fluidized velocities then becomes

$$\Phi_i' = m\left[\frac{\frac{v_b}{v_{mf}} g(r_s - r)(1-e_{mf})}{me}\right] \qquad 4.19$$

Φ_i' = Dissipation function for grain size d_i at $v_b < v_{mfi}$,, J/m^3/s

For the sake of consistency, v_{mf} was assumed to be

$$v_{mfi} = k_{iTy} e_{mf}^{\,n_{iTy}} \qquad 4.20$$

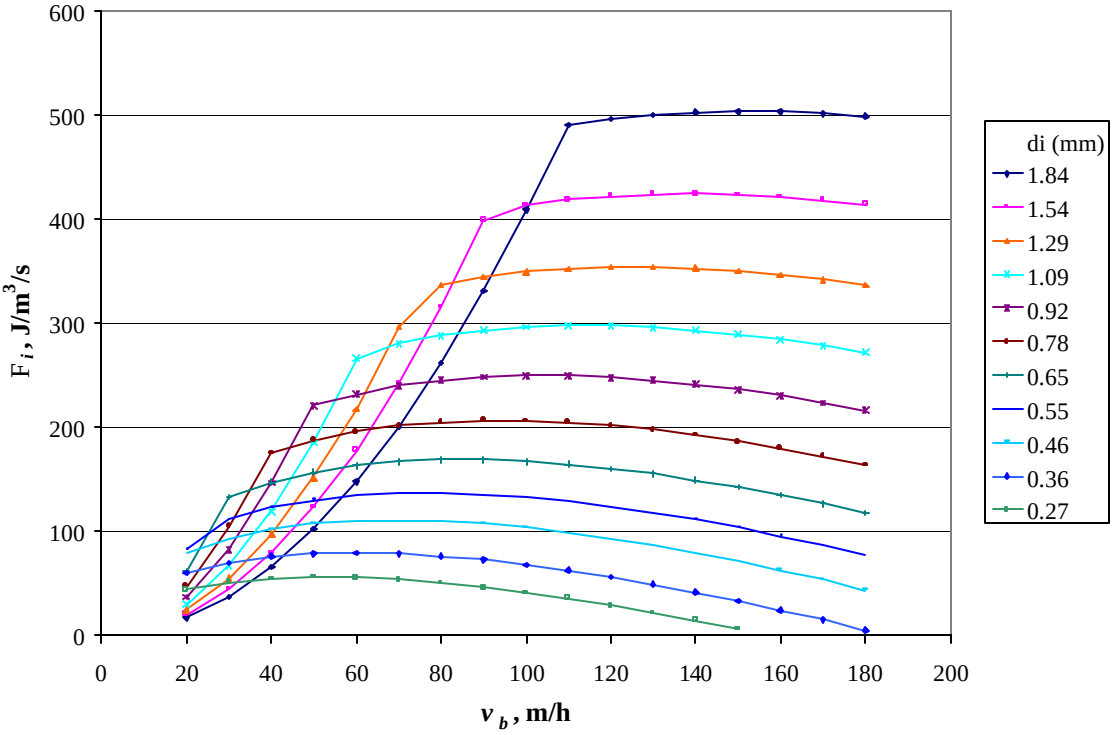

Figure 4.10 Power dissipated per unit volume fluid at 20 °C

From Figure 4.10 it is evident that the finest grains pass their optimum backwash rate before the coarser grains are fluidized. However, at lower backwash rates, the power dissipation for sub-fluidized coarse grains can be higher than the power dissipation for fine fluidized grains. This reinforces the view that backwash should be optimized in terms of the finer fraction of the media but the question of how to identify the characteristic fine fraction of a given bed remains.

Amirtharajah (1978) found that backwash was optimized when the porosity of the top 76 mm of a 0.455 mm graded sand bed was at 0.74, corresponding to 50 % expansion. The fixed bed height was 0.547 m so the expanded height was 0.686 m therefore the top 76 mm constituted 11 % of the total fluidized bed height. Based on this example, one possible strategy for optimizing backwash in graded beds would be to try to attain the theoretical optimum porosity in the top 10 % of the fluidized bed. However, this procedure would have to be tested against actual measurements of backwash efficiency over a range of realistic situations.

The grain size distribution of the top 10 % (by height) of the fluidized bed depends on the expansion of each layer of the media and degree of intermixing of different grain sizes. The porosity in each layer of the fluidized bed can be inferred from the headloss profile since $h \propto (1-e)$ (Equation 2.10).

Figure 4.11 shows measured and calculated backwash headloss profiles in the 0.7 mm sand bed where h is the headloss between $z = z$ and $z = 0$ and z is the height from the base of

the filter. The predicted headloss profiles were calculated by assuming the fluidized bed was perfectly stratified into layers corresponding to the size distribution analysis results (Table 4.1). The headloss across each layer was then calculated using either Equation 2.10 or Equation 4.18, and the volume of media in each layer. The data points on the dashed curves indicate the upper and lower limits of each size fraction. For the 0.7 mm sand, the bulk of the media in the top 10 % of the bed was the size fraction 0.6 to 0.71 mm with mean mesh size, d_i = 0.65 mm.

Measured headlosses tended to be lower than the calculated headlosses but the curves show the same trend. The headloss gradient decreased towards the top of the bed indicating an increase in porosity as a result of media stratification.

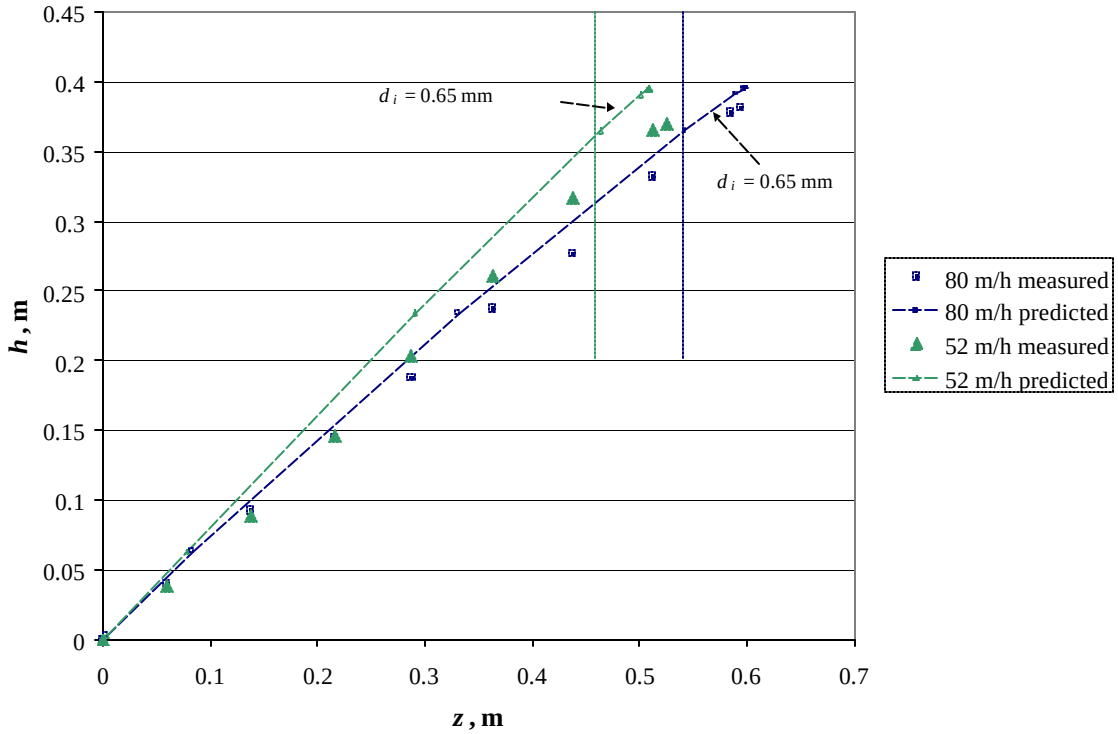

Figure 4.11 Headloss profiles for 0.7 mm sand at 25.5 °C

The vertical dotted lines indicate the top 10 % of the measured bed height. In this region, the average mesh size was 0.65 mm. The optimum backwash rate for d_i = 0.65 mm was estimated to be 85 m/h and the optimum porosity was 0.69. The next smallest fraction, 0.55 mm contributed only 0.9 % to the total mass of the bed, however, experience has shown that grains finer than the d_{10} may play a significant role in the formation of mudballs (Kawamura, 1975b). From Figure 4.8, the optimum backwash velocities for the 0.55 and 0.65 mm sizes are sufficiently close that optimizing for the one size should not significantly influence the efficiency of cleaning of the other.

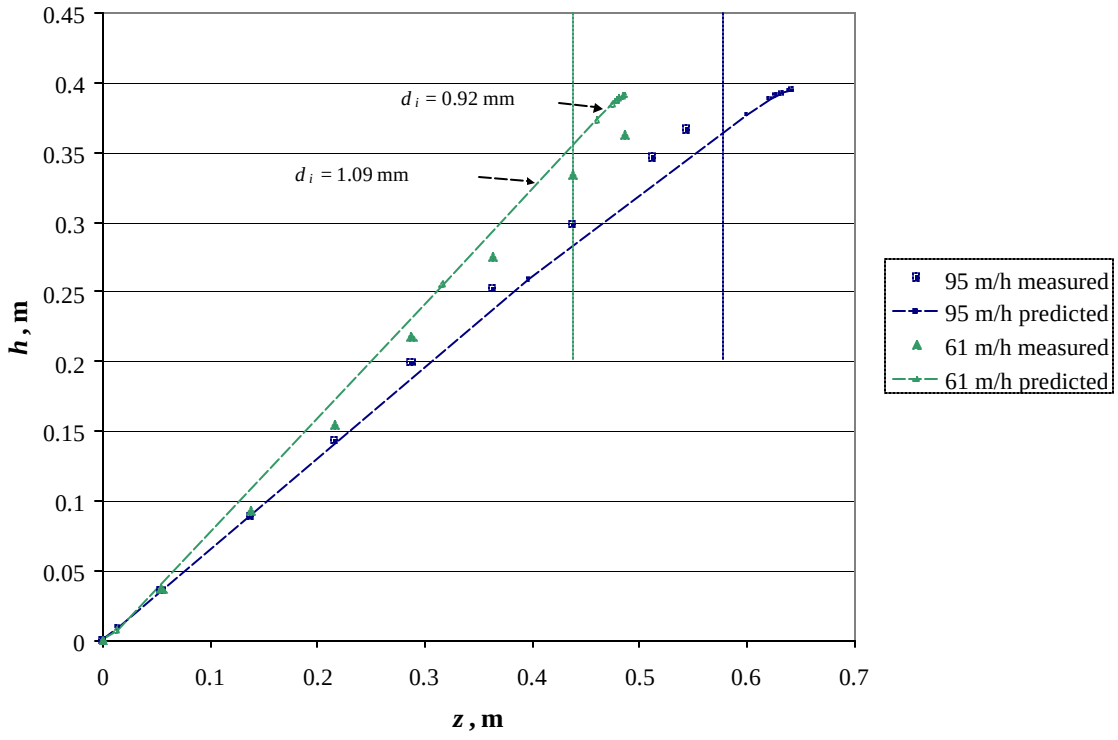

Figure 4.12 Backwash headloss profiles for 1 – 1.4 mm sand at 25.5 ^{o}C

Figure 4.12 shows the headloss profiles for the 1 – 1.4 mm sand bed. 61 and 95 m/h were the minimum and maximum backwash rates used in clogged bed experiments in the current study. The top 10 % of the bed consisted primarily of the 0.92 and 1.09 mm size fractions with the smaller sizes (d_i = 0.36 to 0.78 mm) making up 1.6 % of the total weight of the bed. The theoretical optimum backwash rate at 25 ^{o}C based on the 0.92 and 1.09 mm sand were 104 to 114 m/h and the optimum porosities were 0.64 and 0.62 respectively.

The theoretical optimum backwash conditions and dissipation functions calculated in this chapter are compared to trends in measurements of backwash efficiency in Chapter 9.

CHAPTER 5

MATERIAL BALANCE CALCULATIONS

5.1. Introduction

In order to assess the effect of various factors on backwash efficiency, one first needs to be able to determine what the efficiency is. This chapter describes the material balance calculations carried out to determine the mass of floc deposited in the filters and efficiency of backwash for each backwash experiment in this study.

The most direct measure of efficiency is the amount of material retained in the filter after backwashing. In this study, the mass retained after water only backwash was determined by dislodging the remaining deposits using a violent combined air and water wash regime as described in Section 3.5.2. Material balance calculations for this procedure are presented in Section 5.2.

When several consecutive filter runs were conducted with water only backwash, it was not possible to obtain a direct measurement of the mass retained after each individual run. Section 5.3 presents two methods that were developed to estimate the backwash efficiency for individual filter runs where no air scour was used.

Section 5.4 presents material balance calculations used to check the overall accuracy of the opacity meter described in Section 3.4.2. In general, accurate on-line measurement of high turbidities in flocculated suspensions is difficult (Hall and Fitzpatrick, 2000) and in this study, data from the opacity meter was used only to calculate the rate of detachment of floc during backwashing and not to determine the overall backwash efficiency. However, material balance calculations were a useful tool for evaluating the performance and limitations of the instrument.

5.2. Calculating the backwash material balance

In this study the mass of solids detached during water only backwash was determined by collecting the backwash effluent in 120 L drums and analyzing the contents for suspended solids concentration as described in Section 3.5.2. The mass of solids detached by combined air and water wash was determined in the same way. The total mass of floc recovered from a filter by backwashing (expressed as mass per unit filter area) was

$$M_{TB} = M_D + M_{CB} \qquad 5.1$$

M_{TB} = Total mass of floc detached from filter, g/m^2

M_D = Mass of floc detached during water backwash, g/m^2

M_{CB} = Mass of floc detached during combined air and water backwash, g/m^2

In this study, it was assumed that all the floc retained in the filters after water only backwash could be detached by sustained and vigorous combined air and water wash. The recommended method for determining the amount of floc remaining in a filter bed is to conduct an abrasion test on representative samples of the media (Amirtharajah, 1978; Kawamura, 1991; Logsdon et al, 2002). This involves shaking or mixing up media samples in successive volumes of water and determining the concentration of floc released. In this study, the combined air and water backwash regime used was more violent than would be possible in a full-scale filter without damaging the underdrain. Furthermore, combined air and water wash was continued until there was essentially no more floc being detached from the filter. Therefore, it seemed reasonable to consider this backwash step to be equivalent to an *in situ* abrasion test and the total mass detached should theoretically equal the total mass deposited during filtration.

$$M_{TB} = M_{TF} \qquad 5.2$$

M_{TF} = Total mass of floc deposited during filtration, g/m^2

The efficiency of water only backwash is the fraction of total mass deposited detached by during this backwash step.

$$\% \text{ detachment} = \frac{M_D}{M_{TF}} \times 100\ \% \qquad 5.3$$

An alternate and probably more useful indicator of backwash efficiency was the mass retained in the filter after water backwash, M_R.

$$M_R = M_{CB} = M_{TF} - M_D \qquad 5.4$$

M_R = Mass of floc retained in filter after water only backwash, g/m^2

The mass detached in any backwash step was calculated as the sum of the products of the volume and mixed concentration of the backwash water collected in each drum used (more than one drum was often required to collect the backwash water from a single backwash step).

$$M_B = \frac{\sum_{i=1}^{N} c_i \times volb_i}{1000 \times A} \qquad 5.5$$

M_B = Mass detached during given backwash step (M_D or M_{CB}), g/m^2

N = Number of drums of backwash water collected

$volb_i$ = Volume of backwash water in the ith drum, L

c_i = Suspended solids concentration in the ith drum, mg/L

A = Filter area = 3.14 x 10^{-4} m^2

For a few of the more dilute samples, the suspended solids concentration was not measured directly and was instead estimated from the measured turbidity using the relationships between suspended solids and turbidity presented in Appendix 2.

The volume of water in each drum could be determined within approximately ± 0.9 L. Duplicate measurements of suspended solids typically agreed within 1.3 %. Therefore the maximum and minimum estimates of the mass recovered were calculated as follows:

$$M_{B,\max} = \frac{\sum_{i=1}^{N} (1.013 c_i) \times (volb_i + 0.9)}{1000 \times A} \quad 5.6$$

$$M_{B,\min} = \frac{\sum_{i=1}^{N} (0.987 c_i) \times (volb_i - 0.9)}{1000 \times A} \quad 5.7$$

$M_{B,max}$ = Maximum estimate of mass recovered during backwash, g/m^2

$M_{B,min}$ = Minimum estimate of mass recovered during backwash, g/m^2

Since the mass detached during water backwash, M_D, and the mass detached during combined air and water backwash M_{CB}, were independent measurements, the maximum and minimum estimates of the total mass deposited during a single filter run were

$$M_{TF,\max} = M_{D,\max} + M_{CB,\max} = M_{D,\max} + M_{R,\max} \quad 5.8$$

$$M_{TF,\min} = M_{D,\min} + M_{CB,\min} = M_{D,\min} + M_{R,\min} \quad 5.9$$

For n runs in series with combined air and water backwash after the n^{th} run, the solids balance can be expressed as

$$\sum_{i=1}^{n} M_{TF} = \sum_{i=1}^{n} M_D + M_{CB} = \sum_{i=1}^{n} M_D + \sum_{i=1}^{n} M_R \qquad 5.10$$

$\sum_{i=1}^{n} M_{TF}$ = Cumulative mass deposited, g/m^2

$\sum_{i=1}^{n} M_R$ = Cumulative mass retained, g/m^2

The maximum and minimum estimates of the cumulative total mass deposited are

$$\left(\sum_{i=1}^{n} M_{TF}\right)_{\max} = \sum_{i=1}^{n} M_{D,\max} + M_{CB,\max} = \sum_{i=1}^{n} M_{D,\max} + \left(\sum_{i=1}^{n} M_R\right)_{\max} \qquad 5.11$$

$$\left(\sum_{i=1}^{n} M_{TF}\right)_{\min} = \sum_{i=1}^{n} M_{D,\min} + M_{CB,\min} = \sum_{i=1}^{n} M_{D,\min} + \left(\sum_{i=1}^{n} M_R\right)_{\min} \qquad 5.12$$

For individual filter runs the maximum estimate of the detachment efficiency corresponds to the maximum estimate of M_D and minimum estimate of M_{CB}.

$$\max \,\%\, \text{detachment} = \left(\frac{M_{D,\max}}{M_{D,\max} + M_{CB,\min}}\right) \times 100\,\% \qquad 5.13$$

$$\min \,\%\, \text{detachment} = \left(\frac{M_{D,\min}}{M_{D,\min} + M_{CB,\max}}\right) \times 100\,\% \qquad 5.14$$

5.3. Estimating the total mass deposited and retained for consecutive filter runs

In this study, the efficiency of water only backwash for a single filter run was determined by detaching any remaining floc as described in Section 3.5.2. However, when several consecutive filter runs were conducted with water only backwash, it was not possible to obtain a direct measurement of M_R for each individual run. For these runs, only M_D could be measured directly. M_{TF} could theoretically be estimated as

$$M_{TF} = \int_0^{t_f} [c_{in}(t) - c_{out}(t)] Q(t) dt \qquad 5.15$$

t = Filter run time, h

t_F = Total run length, h

c_{in}, c_{out} = Filter influent and filtrate concentrations respectively, mg/L

Q = Flow rate, L/h

In practice, it is difficult to measure low concentrations of suspended solids (< 5 mg/L) accurately. According to Standard Methods (American Public Health Association, 1999), sample volume should be selected to ensure at least 10 mg of solids is retained on the filter paper in TSS analysis. In the multiple filter run (mud accumulation) experiments, coagulated water concentrations ranged from 1.2 to 2.6 mg/L, which meant that 4 to 8 L of sample would have to be filtered to get 10 mg. In general 2 – 3 L of sample was used for dilute samples.

Filtrate samples would have required 5 to 10 times the sample volume to achieve useful results and this was deemed impractical with the available equipment.

The concentrations in Equation 5.15 could be estimated using correlations between suspended solids and turbidity (Appendix 2). However, calculating M_{TF} using this procedure was found to result in large relative errors in the estimation of M_R.

Sections 5.3.1 and 5.3.2 describe two alternate methods for predicting M_{TF} and M_R that appeared to be more accurate than Equation 5.15. Multiple filter run experiments all used alum as the coagulant. The first method (Section 5.3.1) assumed that the floc consisted primarily of aluminum hydroxide precipitate. The amount of precipitate formed as a result of coagulation with alum was calculated based on the filtrate pH and temperature and volume of coagulant consumed. The second method (Section 5.3.2) was based on the observation that the fixed bed height after backwashing tended to increase as the amount of retained mud increased. In Section 5.3.3, the two sets of estimates of compared and a set of “optimum” estimates of the mass balnce terms for individual filter runs is constructed.

5.3.1. Estimating the total mass deposited from total mass of aluminium hydroxide precipitated

When alum is added to water, aluminium cations react with hydroxyl ions to form several different hydroxide species including amorphous aluminium hydroxide precipitate, $Al(OH)_3(a)$.

$$Al_4(SO_4)_3.14.3H_2O \rightarrow 4Al^{3+} + 3SO_4^{3-} + 14.3H_2O$$

$$Al^{3+} + 3OH^- \Leftrightarrow Al(OH)_3(a)$$

Aluminium has a minimum solubility in water at around pH 6. The solubility of $Al(OH)_3$ for the average operating conditions (temperature and filtrate pH) for each filter run was calculated using the U.S. EPA 's chemical speciation package Minteqa2 (Version 3.11 USEPA, 1991). The amount of precipitate formed was then calculated from the amount of coagulant consumed during the experiment. The efficiency of precipitate removal in the filter was assumed to be the same as the efficiency of turbidity removal. The total mass deposited during a given filter run was therefore estimated to be

$$M_{ppt} = dose \times volf \times \frac{M_{Al(OH)_3}}{M_{alum}} \times \left(1 - \frac{[Al]_{S,avg}}{[Al]_T}\right) \times \left(1 - \frac{filt}{coag}\right) \qquad 5.16$$

M_{ppt} = Mass precipitate deposited in filter, g/m^2

dose = Average alum dose during filter run, mg/L

volf = Volume of water filtered, m^3/m^2

$M_{Al(OH)3}$ = Molecular mass of $Al(OH)_3$ = 78.00

M_{alum} = Formula weight of alum ($Al_2(SO_4)_3.14.3H_2O$) = 599.77

$[Al]_{S,avg}$ = Solubility of aluminum based on average operating conditions, mol/L

$[Al]_T$ = Total aluminum added, mol/L

filt = Average filtrate turbidity for run, NTU

coag = Average influent turbidity for run, NTU

More details on the solubility calculations are provided in Appendix 3. The variations in temperature, filtrate pH and alum dose for all the experiments carried out in the 0.7 mm sand filter are shown in Figure 5.1. M0 to M66 were experiments consisting of a single filter run and backwash where the backwash was delayed 0 to 66 hours after filtration stopped. The purpose of these experiments was to determine the effect of floc age on backwash efficiency. M1R1, M2R1-M2R2, M4R1-M4R4, M6R1-M6R6 and M9R1-M9R9 were series of 1, 2, 4, 6, and 9 consecutive filter runs with water only backwash.

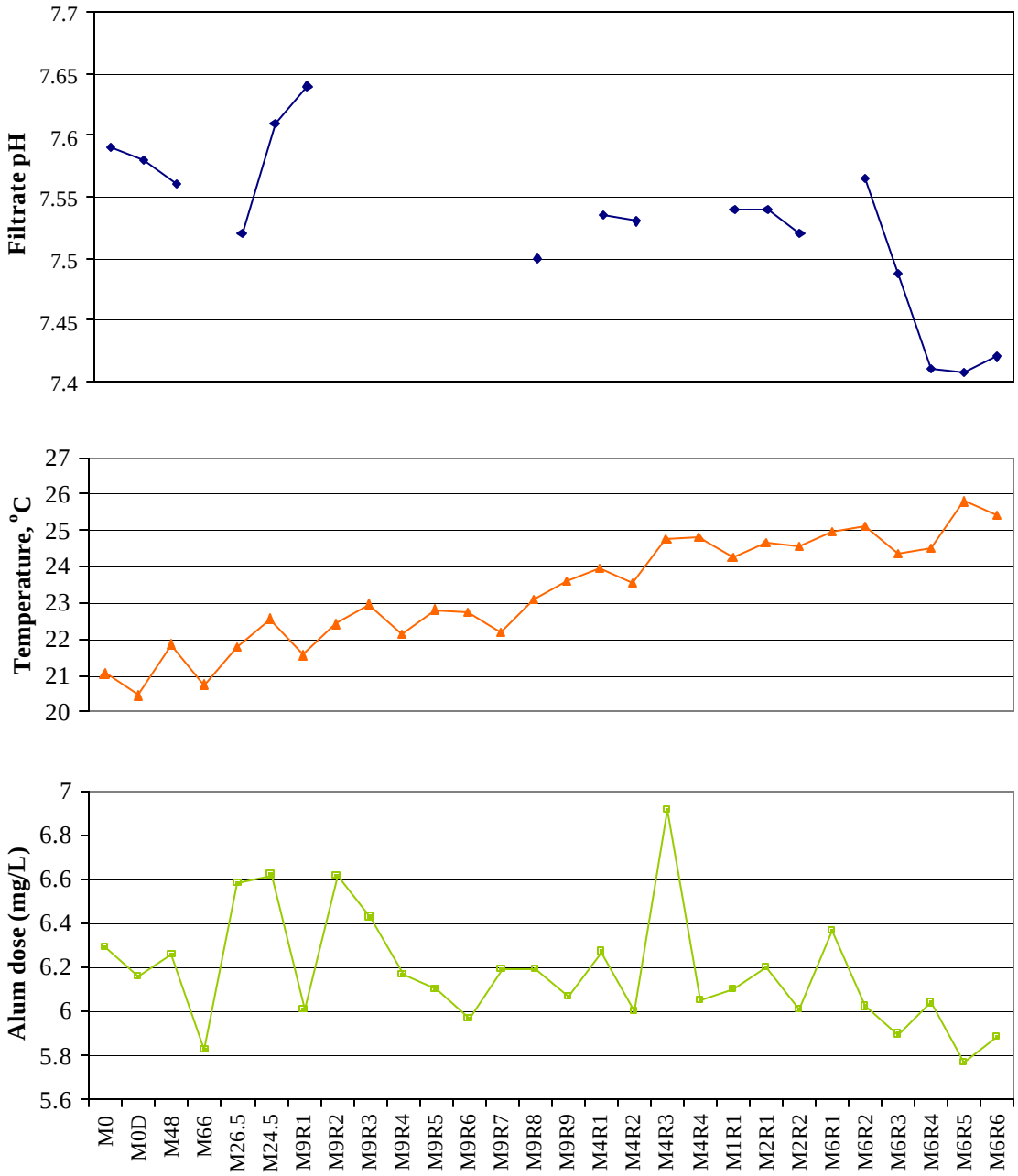

Figure 5.1 Variability in alum dose, temperature and pH

The reasons for the variability in filtrate pH were not clear. During this period, the raw water pH recorded at Wiggins varied from 7.3 to 8.4 (Table 3.2), however, fluctuations in filtrate pH did not necessarily correlate with fluctuations in raw pH. No filtrate pH data was obtained for experiments M9R2-M9R7 due to problems with the pH electrode. Estimates of the missing pH data points were obtained by assuming a linear variation in pH between the measured values.

The sum of estimates of deposited precipitate for a given series of filter runs, ΣM_{ppt}, was found to agree quite well with total mass of solids recovered during backwashing, ΣM_{TF} as shown in Figure 5.2 below.

Upper and lower estimates for ΣM_{ppt} were calculated based on the assumption that there were two main sources of uncertainty in the calculation of the mass of precipitate. The first was in the measurement of the volume of alum dosing solution. Each filter run consumed about 10 L of solution and the volume remaining in the reservoir could be determined within an accuracy of approximately ± 0.5 L. For each series of consecutive filter runs, errors in the estimation of coagulant consumed for individual runs cancelled out in the cumulative total volume consumed. For example, for a series of nine consecutive filter runs (M9R1-M9R9), the total volume of dosing solution consumed was 86.5 ± 0.5 L.

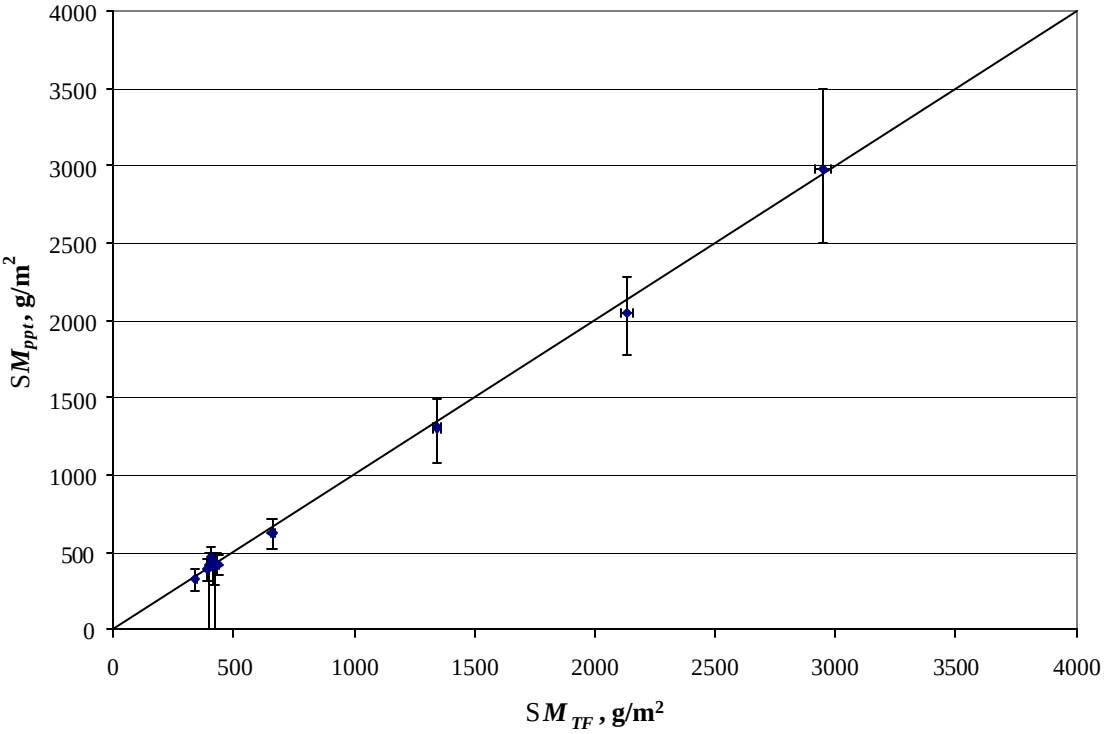

Figure 5.2 Calculated mass of $Al(OH)_3$ precipitate deposited vs total mass recovered during water and air scour backwashing

The second major source of uncertainty in the mass of precipitate was the measurement of pH. The solubility of $Al(OH)_3(a)$ is strong function of pH as shown in Figure 5.3. The assumptions about the pH measurements used to calculate the margins of uncertainty are discussed in Appendix 3.

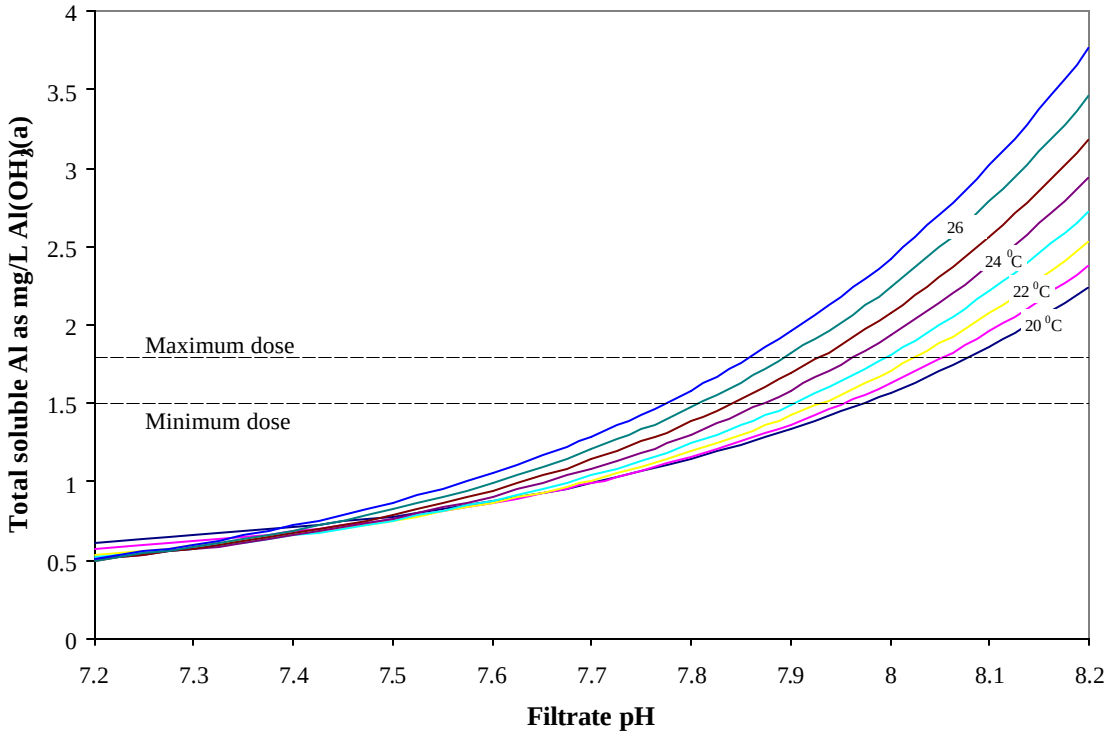

Figure 5.3 Solubility of amorphous $Al(OH)_3$ at filter operating conditions

Figure 5.3 was generated using Minteqa2 for the temperatures and pH's spanning the ranges measured during both the backwash delay and multiple run experiments (See Figure 5.1). The maximum and minimum dose lines correspond to alum doses of 6.9 and 5.8 mg/L respectively as alum. Problems with the pH electrode were experienced during some of the earlier experiments resulting in pH either not being measured or the results obtained being considered unreliable. This led to uncertainties in the estimates of aluminium solubility for some of the experiments. Uncertainties in pH measurements for a given series of experiments were additive; however, the generally good agreement between calculated and measured values in Figure 5.2 suggests that the pH values used were reasonably accurate.

If M_{ppt} can be used as a reasonable estimate of M_{TF}, then M_R can be estimated as

$$M'_R = M_{ppt} - M_D \tag{5.17}$$

M'_R = estimated mass remaining M_R based on M_{ppt}, g/m^2

M_{ppt} = Estimated mass of $Al(OH)_3(a)$ precipitate deposited in filter, g/m^2

M_D = mass detached during water backwash, g/m^2

From Equation 5.10, the estimated cumulative mass retained after *n* runs is

$$\sum_{i=1}^{n} M'_R = \sum_{i=1}^{n} M_{ppt} - \sum_{i=1}^{n} M_D \tag{5.18}$$

5.3.2. Estimating cumulative mass retained based on increase in initial bed height

Brouckaert et al. (2003) observed that the settled filter bed height after fluidized backwash tended to increase with the accumulation of mudballs in an autonomous valveless filter (AVF) and in pilot scale simulations of the AVF. This trend was apparently independent of changes in temperature, which can also affect settled bed height. In a clogged filter bed, expansion occurs at very low sub-fluidisation backwash rates because of the restriction of flow area in the bed. Therefore it seems reasonable that sludge and mudballs remaining in a filter bed

after backwashing would cause the bed to settle out to a larger volume than a clean bed. This phenomenon may have been enhanced by the slow reduction of backwash flow in the AVF.

In the current study, backwash flow was reduced from a maximum of 54 to 16 m/h over a period of 60 s. The increase in settled bed height with number of filter runs is shown in Figure 5.4.

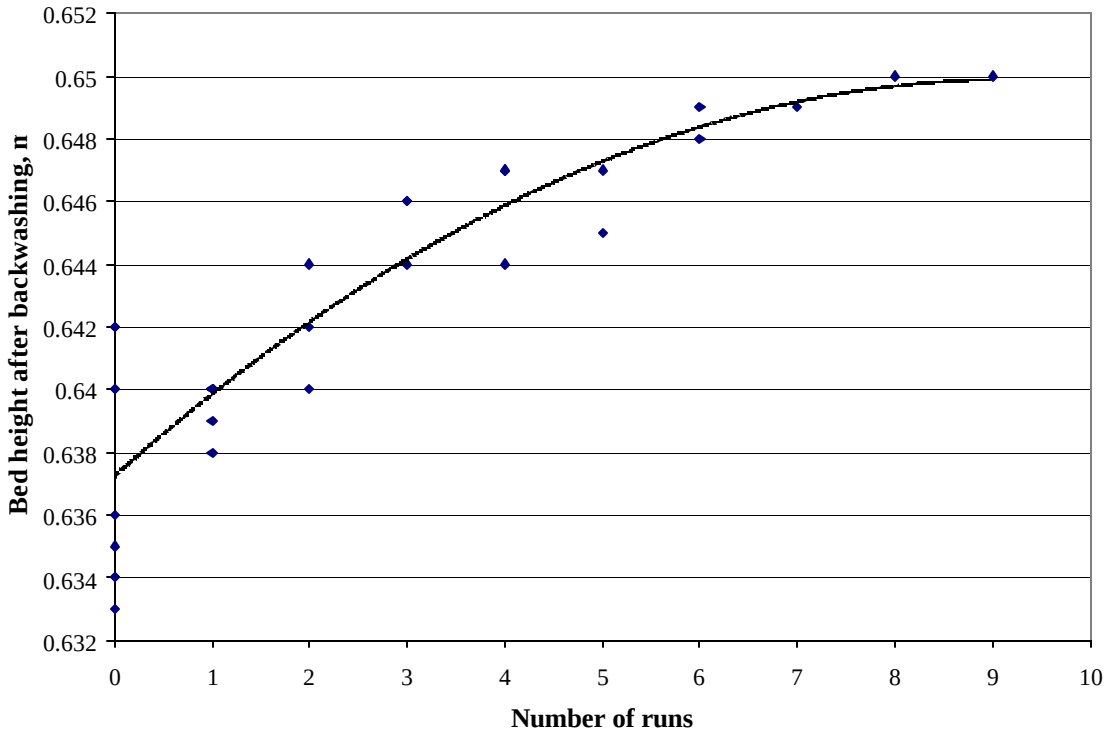

Figure 5.4 Increase in settled bed height after backwash

This raised the possibility that the initial bed height, which could be measured for any filter run, might be useful for calculating the cumulative mass retained in the filter after

backwashing. Based on Figure 5.4, an exponential relationship between settled bed height after backwash, Z_s, and cumulative mass retained was proposed.

$$\sum M_R = C_4 \exp\left(A_4 \Delta Z_s\right) \qquad 5.19$$

SM_R = Cumulative mass retained, g/m^2

ΔZ_s = Change in settled bed height, m

A_4, C_4 = Regression coefficients

ΔZ_s is the increase in settled bed height relative to the clean bed height. In this study, the settled filter bed height was usually only measured after the filter had been started up again. Experience with laboratory filters had shown that the settled bed height of a clean filter depended on a number of factors including the temperature at which the filter bed had settled out and whether the filtrate valve was opened smoothly or abruptly. This complicated the calculation of ΔZ_s.

Figure 5.5 shows the clean filter bed height Z_0 as a function of temperature. These measurements were taken at the beginning of the first run in each series. The average of these measurements was $Z_{0,ave}$ = 0.6348 m.

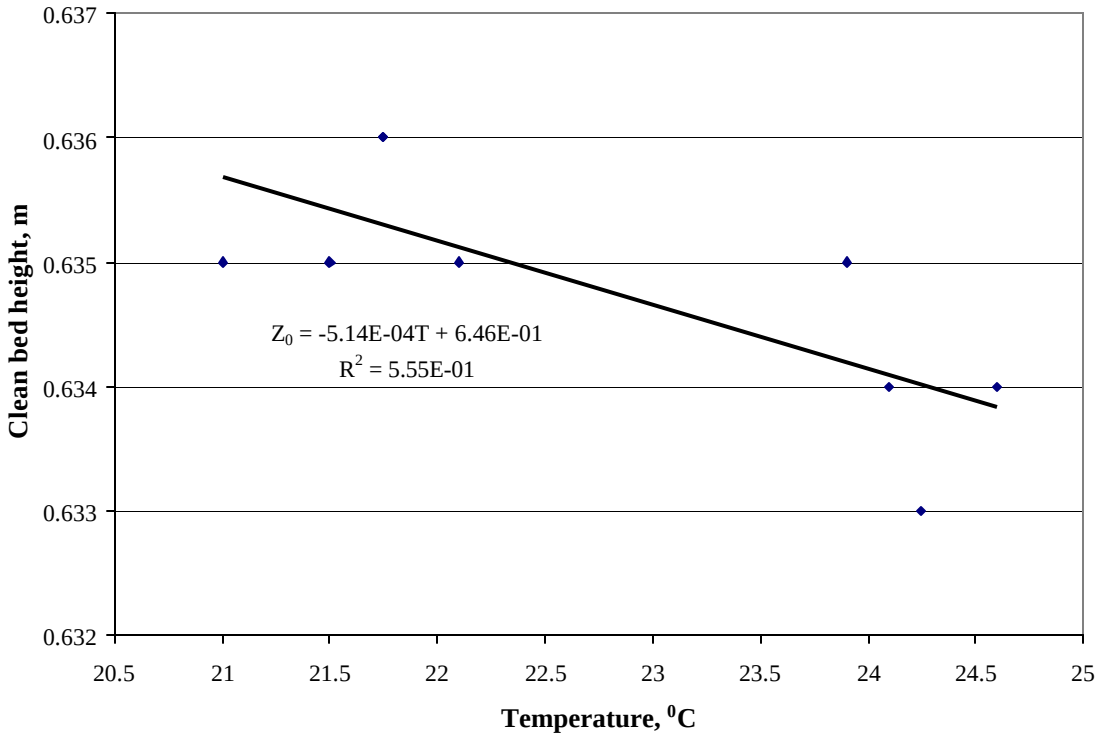

Figure 5.5 Temperature dependence of settled clean bed height, Z_0

Figure 5.6 shows ΣM_R plotted against ΔZ_s calculated using either Equation 5.19 or 5.20

$$\Delta Z_s = Z_s - Z_{0,ave} \qquad 5.20$$

$$\Delta Z_s = Z_s - Z_{0,T} \qquad 5.21$$

Where

$$Z_{0,T} = -5.14 \times 10^{-4} T + 0.646 \qquad 5.22$$

$Z_{0,T}$ = Temperature corrected clean bed height, m

T = Water temperature at which bed height determine, ^{0}C

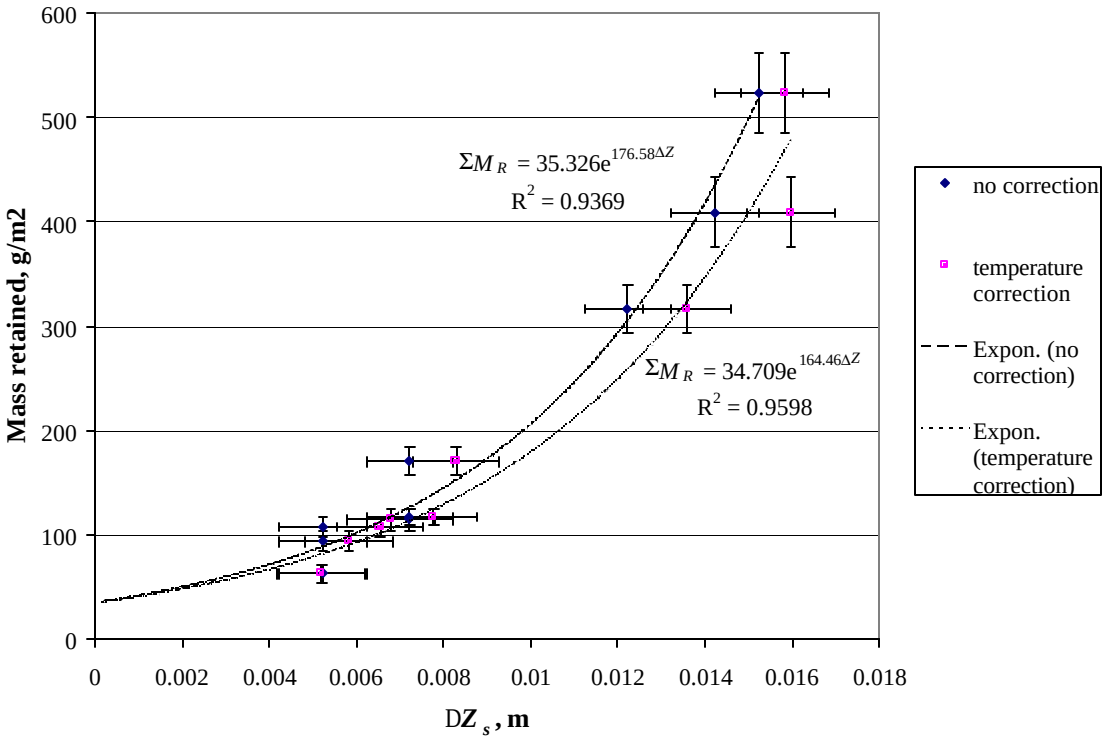

Figure 5.6 Relationship between cumulative mass retained and change in initial bed height with and without temperature correction

The uncertainty in ΔZ_s was assumed to be ± 1 mm. The curves in Figure 5.6 are exponential trendlines calculated by Excel. When ΔZ_s is calculated using Equation 5.20, the agreement of the regression model predictions with the data is relatively good at high values of ΔZ_s, but less good at lower values. Conversely, when Equation 5.21 is used, there is better agreement between model and data at low ΔZ_s than at high ΔZ_s. This suggests that the cleaner

the filter bed, the more sensitive the settled bed height is to factors such as temperature, whereas the dirtier the bed, the less important factors other than the mass of floc retained become.

In Figure 5.7, ΔZ_s is calculated using Equation 5.21 for $\Delta Z_s < 0.009$ m and Equation 5.20 for $\Delta Z_s > 0.009$m. This results in better agreement between model and data over the entire range of ΔZ_s.

The vertical bars are the 95 % confidence intervals on the estimates based on the data set and regression statistics. Further details on the calculation of these confidence intervals are provided in Appendix 3.

The final result of the regression analysis is

$$\sum M_R'' = 29.158 \exp(191.04 \Delta Z_s) \qquad 5.23$$

$\sum M_R''$ = Cumulative mass retained estimated from settled bed height, g/m^2

ΔZ_s = $\Delta Z_s = Z_s - Z_{0,ave}$ for $DZ_s > 0.009$ m

ΔZ_s = $\Delta Z_s = Z_s - Z_{0,T}$ for $DZ_s > 0.009$ m

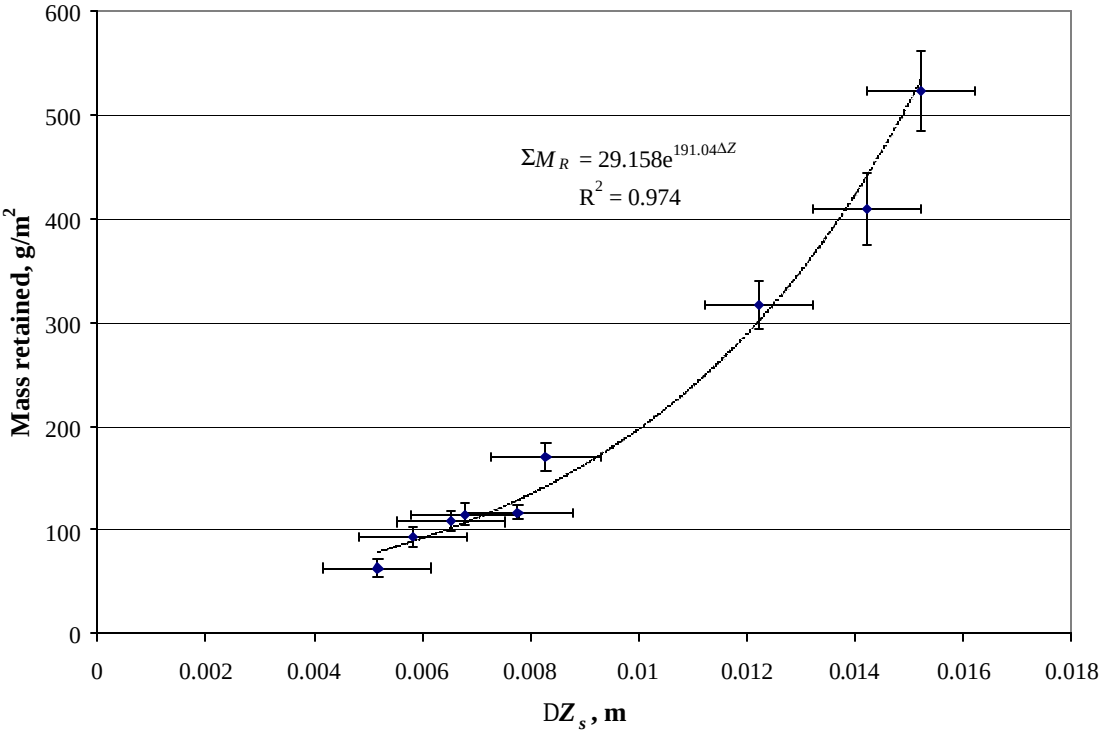

Figure 5.7 Relationship between cumulative mass retained and change in settled bed height

5.3.3. Determining the optimum set of estimates

In Figure 5.8, $\sum M'_R$ and $\sum M''_R$ are plotted against measured values of ΣM_R. The upper and lower limits on the estimates of $\sum M'_R$ (dashed lines) represent the sources of uncertainty discussed in Section 5.3.1 and may be excessively conservative. Figure 5.8 shows that $\sum M''_R$ (based on settled bed height) is a better estimator of ΣM_R than $\sum M'_R$. (based on precipitate formed). However, neither M'_R nor M''_R is necessarily a good estimator of M_R, the incremental increase in mass retained for a given run. M''_R is calculated as

$$\left(M_R''\right)_k = \sum_{i=1}^{k} M_R'' - \sum_{i=1}^{k-1} M_R'' \qquad 5.24$$

$(M_R'')_k$ = Incremental increase in mass retained after k^{th} run, g/m^2

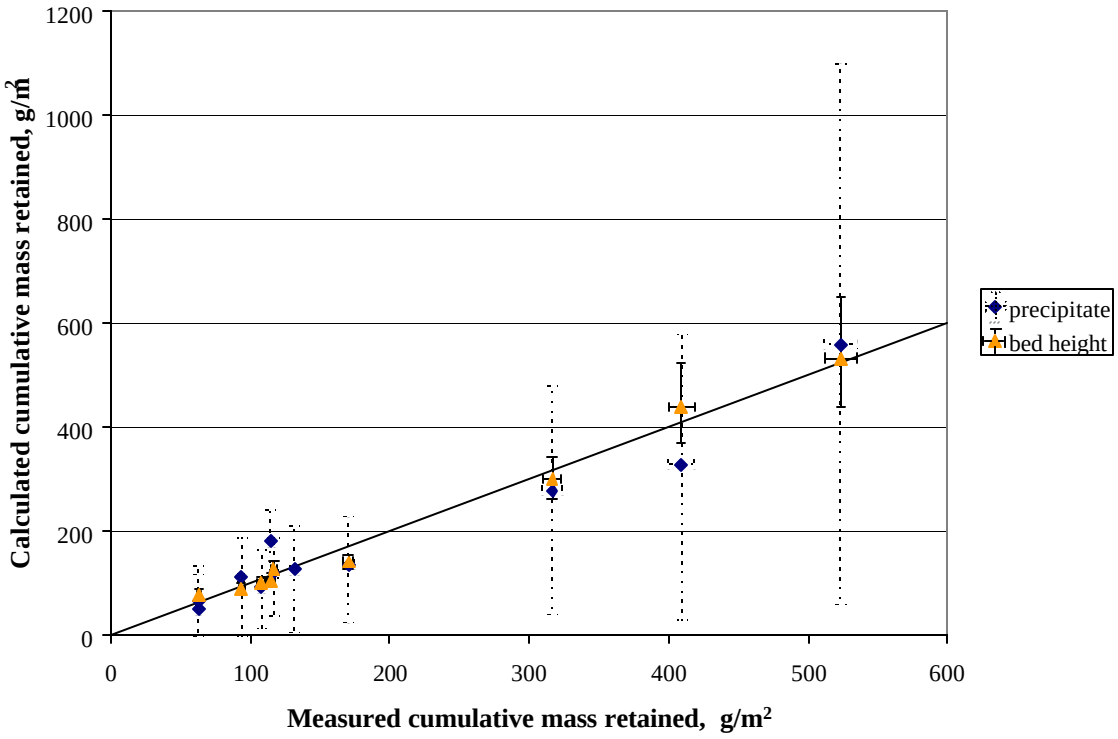

Figure 5.8 Estimates cumulative mass retained vs measured cumulative mass retained

Uncertainties in the estimates of $\sum_{i=1}^{k-1} M_R''$ and $\sum_{i=1}^{k} M_R''$ tend to be amplified in their difference. Similarly, large volumes of dosing solution consumed are measured more accurately than small volumes so that relative errors tend to be greater in the estimation of M_R' compared to $\sum M_R'$. Figures 5.9 and 5.10 show the estimates of $\sum M_R'$, $\sum M_R''$, M_R' and M_R'' and

their averages with margins of uncertainty for series M2R1-M2R2, M4R1-M4R4, M6R1-M6R6 and M9R1-M9R9. The estimation of these margins of uncertainty is discussed in Appendix 3. For series M2R1-M2R2, M1R1-M4R4 and M9R1-M9R9, the estimators $\sum M_R'$ and $\sum M_R''$ are fairly close, however, they diverge sharply for Series M6R1-M6R6. One of the possibilities considered was that the average of $\sum M_R'$ and $\sum M_R''$ might be a better estimator of the true value of ΣM_R than either estimator on its own. However, it is evident from Figure 5.6 that the average value would be a worse estimator of the measured value of ΣM_R than $\sum M_R''$ for all series except for M6R1-M6R6. Furthermore, there was no obvious explanation for the sharp increase in mass retained estimated by $\sum M_R'$ for run M6R6. It therefore seemed reasonable to assume that for M6R1-M6R6, the average of $\sum M_R'$ and $\sum M_R''$ was the best available estimator of ΣM_R although $\sum M_R''$ was the best estimator for all other series.

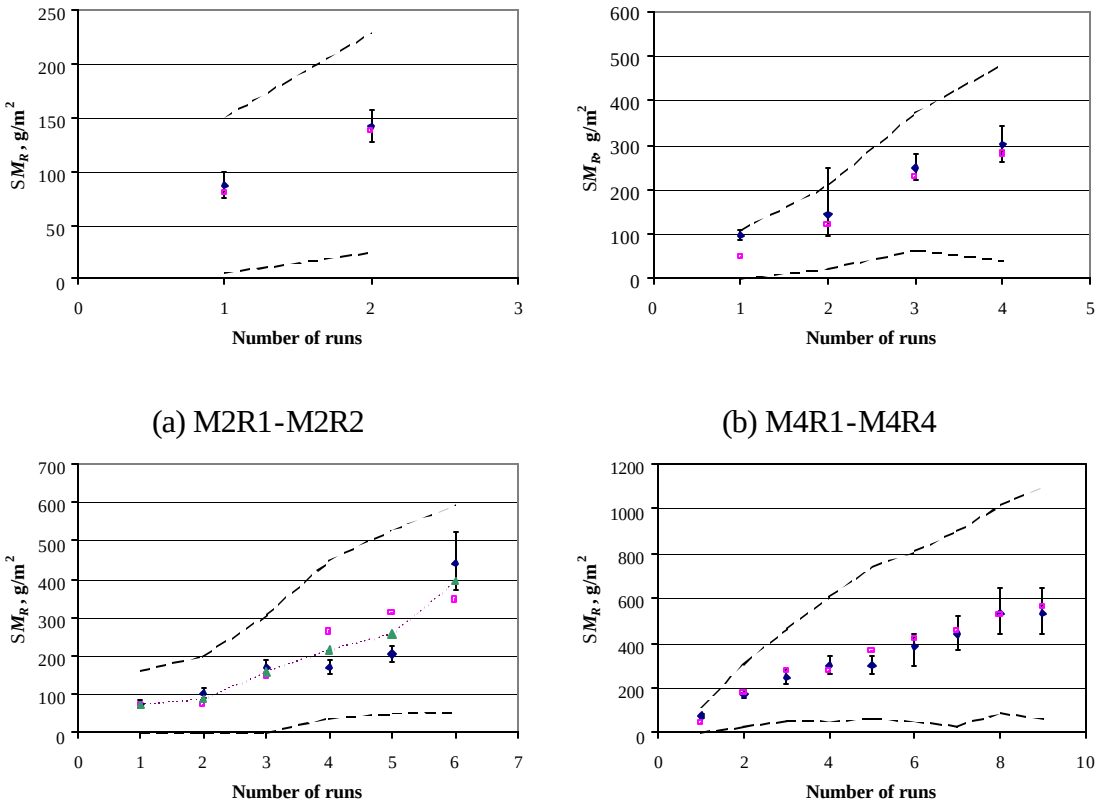

(a) M2R1-M2R2

(b) M4R1-M4R4

(c) M6R1-M6R6

(d) M9R1-M9R9

Figure 5.9 Estimated values of cumulative mass retained ΣM_R

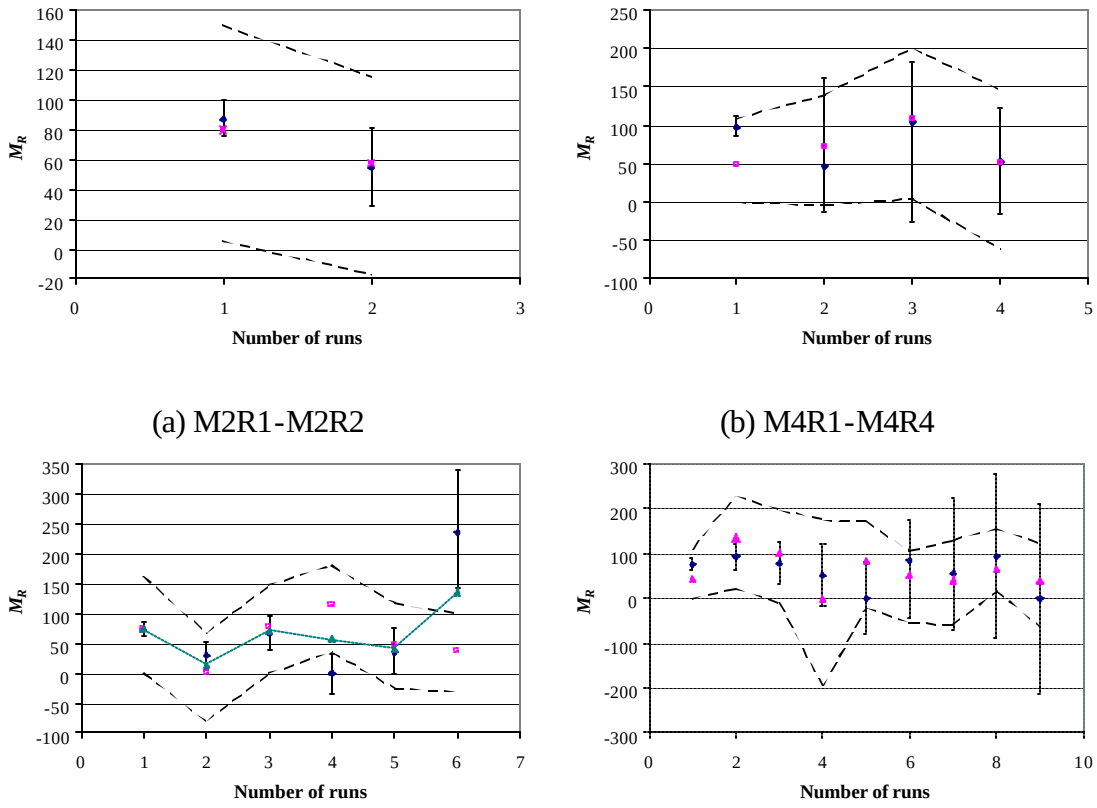

(a) M2R1-M2R2

(b) M4R1-M4R4

(c) M6R1-M6R6

(c) M9R1-M9R9

Figure 5.10 Estimated values of mass retained, M_R

The optimum estimator of M_R was then defined as follows. For M6R1-M6R6

$$M_{R,opt} = \frac{M'_R + M''_R}{2} \qquad 5.25$$

$M_{R,opt}$ = Best estimator of M_R, g/m^2

For all other runs with the exception of M4R2, M0, M0D and M1R1

$$M_{R,opt} = M''_R \qquad 5.26$$

The bed height after backwashing was not measured for M4R2 so in this case M'_R was used instead of M''_R. The measured values of M_R were obviously the best estimates for the single run experiments M0, M0D and M1R1. The cumulative mass retained was calculated as

$$\left(\sum M_{R,opt}\right)_k = \sum_{i=1}^{k} \left(M_{R,opt}\right)_i \qquad 5.27$$

$(\Sigma M_{R,opt})_k$ = Best estimate of cumulative mass retained after k runs, g/m^2

The margins of uncertainty for $M_{R,opt}$ were estimated to be the intersection of the margins of uncertainty for M'_R and M''_R except for runs M6R4 and M6R6. Here the upper and lower limits of the estimate of $M_{R,opt}$ were taken to be M'_R and M''_R. Figure 5.11 shows $M_{R,opt}$ plotted against run number.

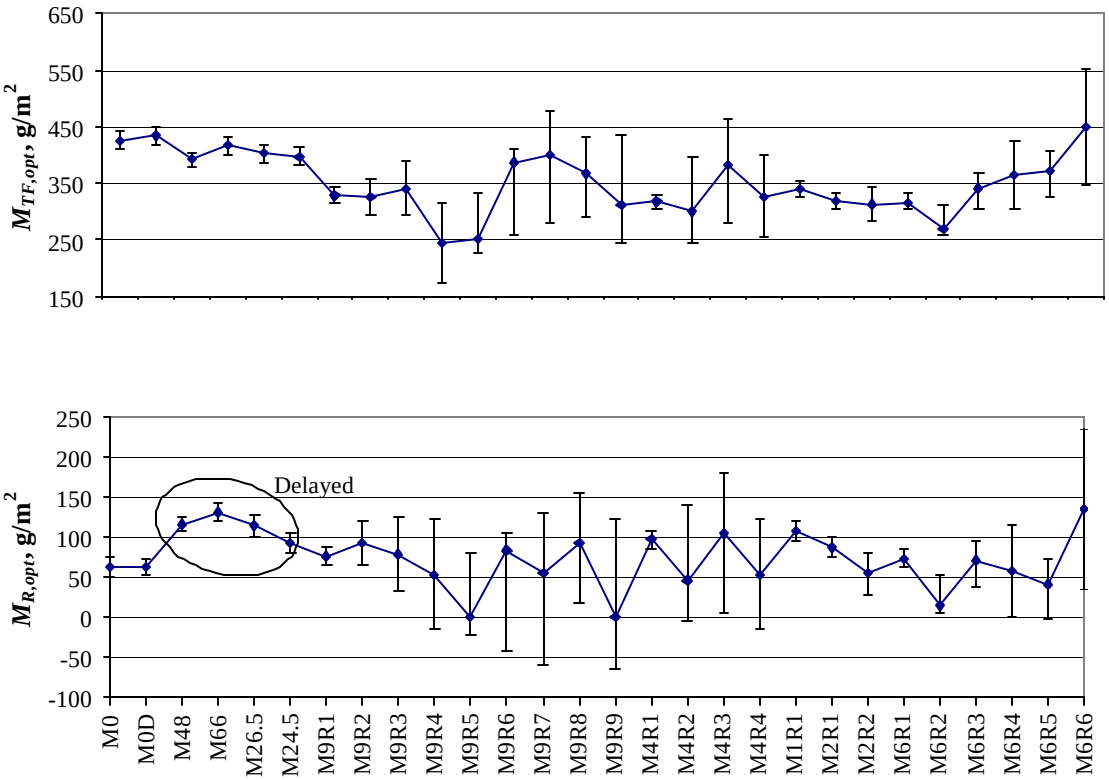

Figure 5.11 Best estimates of incremental mass retained and total mass deposited for individual filter runs

The $M_{R,opt}$ estimates are used in Chapter 9 to look for correlations between backwash efficiency and various parameters relating to filter operation and performance. Unfortunately, there was a large degree of uncertainty in even the best estimates of M_R obtained. This arose in part because the quantitative relationships between mass deposited and hydroxide solubility, and the association between mass retained and filter bed height were only discovered after the experimental work was complete. It is probable that there would have been less uncertainty and scatter in the estimates of M_R had there been more focus on obtaining accurate and reproducible

measurements of bed height and pH during the experimental phase. These procedures for estimating the mass retained in a filter could be useful in future experimental work and could potentially be adapted for estimating mud accumulation in full scale filters.

5.4. Accuracy checks on the opacity meter

In this study, the concentration profile during backwash was measured on-line using the opacity meter described in Chapter 3. Sample for the opacity meter was drawn from above the surface of the backwashing filter through a 22 mm diameter sampling probe located below the backwash trough. The accuracy with which the meter was able to capture the backwash concentration depended on two factors: (i) how representative the sample flowing through the meter was of the mass of floc detaching from the filter, and (ii) the accuracy and stability of the calibration during backwash.

The opacity meter drew sample from only 1.2 % of the filter area and the concentration of the backwash effluent was not necessarily uniform across the filter cross section. This was especially true near the beginning of backwash when violent mixing of the top sections of the bed occurred. Furthermore, the sensitivity of the calibration to temperature at low turbidity made the accurate measurement of low concentrations (< 10 mg/L) difficult.

The overall accuracy of the meter (combined effect of sample representativeness and meter accuracy) could be checked by comparing the mass detached calculated from the

concentration profile and independent measurements of the total mass of solids in the backwash effluent. The overall recovery was defined as

$$\% \text{ recovery } = \frac{\sum_i c_i Q_i \Delta t}{1000 M_D A} \times 100\% \qquad 5.28$$

c_i = ith concentration measurement from opacity meter signal, mg/L

Q_i = flowrate at ith measurement, L/s

Δt = sample interval = 0.25 s

M_D = mass detached during (water only) backwash, g/m^2 filter area

A = filter area = 0.0314 m^2

The sampling recovery was defined as:

$$\% \text{ sampling recovery } = \frac{M_{OM} \times Q_b}{M_D A \times sample\,rate \times 3600} \times 100\% \qquad 5.29$$

M_{OM} = Total mass of solids in opacity meter sample, mg

Q_b = Backwash flowrate, L/h

$M_D A$ = Total mass detached during backwashing, *mg*

sample rate = Measured sampling rate, L/s

The meter accuracy could be checked by comparing the average concentration measured during backwash to the concentration of the sample collected. However, in practice,

the sample port had to be opened before the backwash pump was started and closed after the pump was stopped. This resulted in some dilution of the sample corresponding to the backwash duration. The additional water collected should have made a negligible contribution to the total solids in the sample. Consequently, the actual solids concentration measured from the opacity meter sample could be corrected by dividing the total mass by the volume actually collected during backwash.

The expected opacity meter sample volume was the measured sampling rate multiplied by the duration of the backwash. It was assumed that the sampling rate remained constant throughout backwash because the water level in the filter column could not change very much.

$$c'_{OM} = \frac{c_{OM} \times V_{OM}}{V_{OM}^{<\exp>}} = \frac{c_{OM} \times V_{OM}}{sample\,rate \times t_{bw}} \qquad 5.30$$

c'_{OM} = Corrected opacity meter sample concentration, mg/L

V_{OM} = Actual volume of opacity meter sample, L

$V_{OM}^{<\exp>}$ = Expected volume of opacity meter sample, L

t_{bw} = Duration of backwash, s

The average concentration from the meter output was simply the arithmetic mean of all the instantaneous concentrations recorded during the backwash. This value was then expressed as a percentage of the corrected measured concentration.

$$\%\ \text{meter recovery} = \frac{c_{PD,avg}}{c'_{OM}} \times 100\,\% \qquad 5.31$$

$c_{PD,avg}$ = Average concentration calculated from the photodiode output voltage, mg/L

Factors affecting the accuracy of the opacity meter and its impact on the measurement and analysis of the backwash concentration profile with time are discussed further in Section 7.3.

CHAPTER 6

BEHAVIOR OF REAL FILTERS DURING BACKWASHING

6.1. Introduction

Chapter 2 Section 2.4 reviewed several models of filter backwash which have attempted to relate the concentration of detached floc in the backwash effluent to the rate of detachment of deposits from individual media grains. For any model to be useful for the interpretation of experimental data and/or as a tool for the design and optimization of filter backwash, it must capture all of the critical features of the process. One of the objectives of the current study was to evaluate existing backwash models according to this criterion and to either propose improvements or alternate modeling approaches. Chapter 6 presents the experimental findings of the current investigation regarding the behavior of real clogged filter beds during backwashing, including video footage of some of the backwash experiments. Chapter 7 discusses the quantitative modeling and analysis of the backwash effluent concentration profile with time, drawing on the findings presented in Chapter 6.

The backwash models reviewed in Chapter 2 all assumed that a filter can be represented as a fluidized bed for most or all of the duration of backwash. These models essentially described backwash as mass transfer from a fluidized bed at hydrodynamic steady state. The transition of the bed from the fixed to the fluidized state was implicitly or explicitly

assumed to be smooth and complete even for the most clogged and compacted regions at the top of the bed. Only Hall and Fitzpatrick (1998) accounted for some dislodgement of floc from the media during the expansion of the bed and recognized that the mechanism involved would be different from detachment of deposits from fluidized grains.

As discussed in Section 2.4.5, the expansion and disintegration of a clogged fixed bed structure is neither smooth nor uniform. Hall and Fitzpatrick (2000) reported that the top most clogged sections of their laboratory filter beds tended to collapse into the lower fluidized sections during expansion, resulting in substantial mixing of the flow that in turn affected the backwash concentration profile. A similar phenomenon was observed in the current study. Since a large fraction of the total floc is detached from the media during the transitional phase, the mechanisms involved in the break down of the clogged regions may affect the overall efficiency of backwash and certainly do affect the backwash concentration profile.

Section 6.2 outlines the experimental work discussed in this Chapter. Section 6.3 provides a detailed description and analysis of the behavior of the filter bed from the time that the backwash pump was started to the time that the bulk of the floc had been flushed from the bed. Section 6.4 discusses the implications of the phenomena observed in this study for modeling real filters.

6.2. Experimental work

The experiments discussed in this Chapter were all carried out in the 1 – 1.4 mm sand bed described in Chapter 4. The laboratory filter set up was described in Section 3.2. and 3.4. Experiments were recorded video as described in Section 3.5.3.

The first set of experiments took place in January and February 2001 (midsummer in South Africa) and used alum as the coagulant in the filter run (AU series). These experiments looked at the effect of varying the backwash rate from 61 to 77 m/h while keeping the terminal headloss constant at ~ 1.4 m (AU70 to AU61_29h) and varying the terminal headloss between 0.3 and 1.4 m while keeping the backwash rate constant at 61 m/h (AU61_8h to AU61_26h).

The second set of experiments was carried out in October and November 2001 (late Spring) and used Z464N as the coagulant (ZU series). In these experiments, the filter was run to a terminal headloss of ~ 1.6 to 1.7 m and the backwash rate was varied from 61 to 95 m/h (ZU61 – ZU95).

Note: the code used for each experiment here identifies the coagulant used (A = alum and Z = Z464N) and the backwash rate. For example, AU70 refers to an experiment carried out using alum as the coagulant and a backwash rate of 70 m/h. Since several AU experiments were carried out at 61 m/h, the codes for these experiments also include the filter run times. AU61_8h indicates a filter a run time of 8 hours.

The experimental conditions for the AU experiments are summarized in Table 6.1. The coagulant dose was increased from 5 to 8 mg/L midway through experiment AU77, the first experiment in the series. The experimental conditions for the ZU experiments are listed in Table 6.2.

In addition, a number of experiments were carried out to investigate the response of clogged filter beds to very low (sub-fluidized) backwash rates in order to gain a better understanding of mechanisms involved in the disintegration of the clogged bed structure. These experiments are described separately in Section 6.3.3.2.

Table 6.1(a) Experiments with alum coagulation – filtration conditions

Alum dose:	8 mg/L*
Filtration rate:	6.2 – 6.7 m/h
Influent turbidity (coagulated)	2.1 – 2.8 NTU
Filtrate turbidity	0.22 – 0.29 NTU
Raw pH	7.6 – 8.1
Filtrate pH	7.2 – 7.9

Table 6.1(b) Experiments with alum coagulation – backwash conditions

Experiment	Backwash rate and temperature	Filter run time and terminal headloss	Total mass of floc deposited, g/m^2 (M_{TF})
AU77*	77 m/h, 24 ^{o}C 141 % v_{mf}	46 h 1.53 m	-
AU70	70.3 m/h, 24.75 ^{o}C 127 % v_{mf}	32 h 1.39 m	881
AU68	67.5 m/h, 26 ^{o}C 121 % v_{mf}	27.8 h 1.42 m	731
AU64	63.8 m/h, 25 ^{o}C 116 % v_{mf}	27.4 h 1.43 m	767
AU61_29h	61.2 m/h, 24.5 ^{o}C 111 % v_{mf}	29.2 h 1.42 m	830
AU61_26h	61.2 m/h, 25.5 ^{o}C 109 % v_{mf}	25.8 h 0.98 m	633
AU61_17h	61.2 m/h, 25.5 ^{o}C 109 % v_{mf}	17.2 h 0.70 m	430
AU61_7h	61 m/h, 25.5 ^{o}C 109 % v_{mf}	7.8 h 0.30 m	183

Table 6.2(a) Experiments with Z464N coagulation – filtration conditions

Z464N dose:	2.5 – 2.8 mg/L
Filtration rate:	6.2 – 6.6 m/h
Influent turbidity (coagulated)	0.9 – 1.3 NTU
Filtrate turbidity	0.10 – 0.13 NTU
Raw pH	7.7 – 8.4
Filtrate pH	7.7 – 8.4

Table 6.2(b) Experiments with Z464N coagulation – backwash conditions

Experiment	Backwash rate and temperature	Filter run time and terminal headloss	Total mass of floc deposited, g/m^2 (M_{TF})
ZU95	95 m/h, 23.5 ^oC 175 % v_{mf}	49.6 h 1.66 m	576
ZU94	94 m/h, 21 ^oC 180 % v_{mf}	46.8 h 1.64 m	569
ZU84	84 m/h 24 ^oC, 154 % v_{mf}	40.8 h 1.68 m	597

Table 6.2(b) cont.

ZU81	81 m/h, 23 °C 150 % v_{mf}	40.9 h 1.64 m	577
ZU78	78 m/h, 24.75 °C 141 % v_{mf}	39.7 h 1.75 m	583
ZU74	74 m/h, 22.75 °C 138 % v_{mf}	41.4 h 1.72 m	667
ZU70	70 m/h, 22.75 °C 130 % v_{mf}	42.6 h 1.64 m	545
ZU67	67 m/h, 21.4 °C 127 % v_{mf}	46.9 h 1.64 m	576
ZU64	64 m/h, 23 °C 119 % v_{mf}	44.5 h 1.68 m	603
ZU61	61 m/h, 23 °C 113 % v_{mf}	47.1 h 1.60	616

6.3. Backwash behavior of experimental filters

6.3.1. General description of backwash behavior

After the backwash pump was started, it took several seconds for the media to become fully fluidized. Fluidization proceeded from the bottom of the bed upwards until the whole bed

was fluidized. The un-fluidized media at the top of the bed was pushed up in a plug as the layers beneath it expanded. Backwash could therefore be divided into two phases. Phase 1 was the transition from a fixed to a fluidized bed. Part of the bed was fluidized and the other part retained some of the structure of the fixed bed. In Phase 2, the bed was fully fluidized.

This was true for both clean and clogged filter beds. However, clean filter beds expanded smoothly and monotonically to their steady state height whereas the behavior of clogged beds was somewhat more complicated.

In a clogged filter, the media in the upper layers of the filter was cemented together with floc and was relatively impermeable to flow. During Phase 1 of backwashing, the height of clogged beds always increased more rapidly than clean beds and overshot the steady state height of the fully fluidized bed by several centimeters. Furthermore, although the bed expansion initially proceeded in a smooth linear fashion, the top section eventually began to tilt and buckle until its surface broke open. The videos of the backwash experiments showed that, in most cases, the surface of the bed began tilting up at the opposite side to the camera while the front edge slowed down. At the same time, it was typical to see a gap between the fluidized and fixed sections develop at the front of the filter (facing the camera). This is shown in Figure 6.1 (a). It appeared that, unlike the lower sections, the top, most clogged section of the bed did not expand when the media below it became fluidized. Instead the flow started to force its way around the plug of sand and floc, causing the bed surface to buckle and eventually break open.

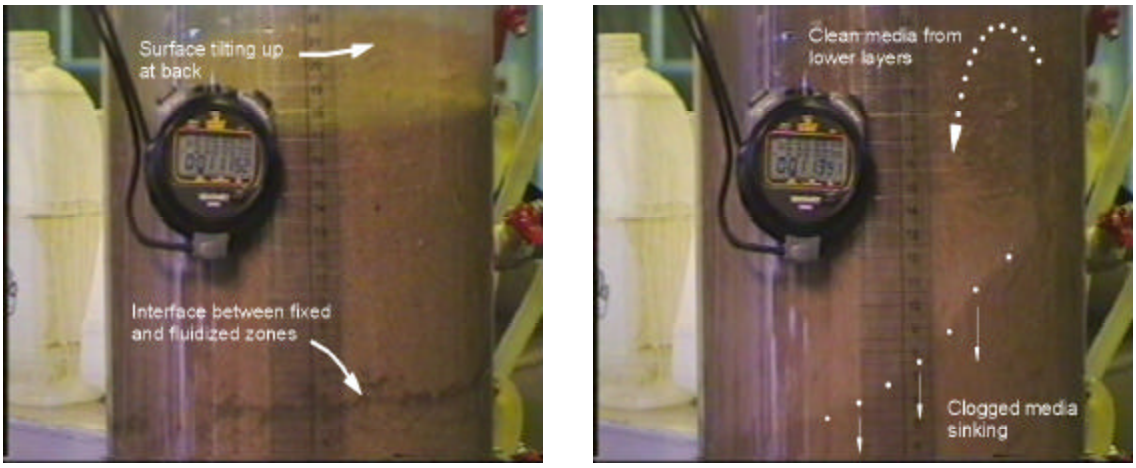

(a) buckling of fixed layer before disintegration (b) Mixing of upper layers of the filter

Figure 6.1 Clogged filter bed just before and just after flow breaks through bed surface

Once the backwash flow broke through the surface of the bed at the back edge, the rest of the residual structure collapsed into the filter and was rapidly eroded away. In the process, clean sand (either sucked from the lower fluidized layers or eroded from the disintegrating fixed section) could be observed piling up on top of the sinking clogged layer. This is shown in Figure 6.1 (b). These observations agree with those reported by Hall and Fitzpatrick (2000), and to some extent, support Huang and Basagoiti's (1989) assumption that complete mixing of the filter media occurs at the beginning of backwash.

Once the disintegration of the clogged bed was complete, the behavior of the fully fluidized bed was also different for dirty filters compared to initially clean beds. The dirty filter media took up to a minute and in some cases longer to settle back to its steady state height and this tended to be greater than the steady state height of the clean bed at the same backwash rate. Figure 6.2 shows the expanded bed height and headloss between manometer ports "f" and

"j" for experiment AU70. One bed volume is the volume of fluid in the steady state fluidized bed. Both headloss and bed height increased smoothly in the first few seconds of backwash. The sharp spikes and drops in both curves between 5 and 10 seconds corresponded to the rapid disintegration of the top section of the bed. Once disintegration was complete, both headloss and bed height settled slowly to their steady state values, which in this case were reached around 85 s or approximately 3.5 bed volumes into the backwash.

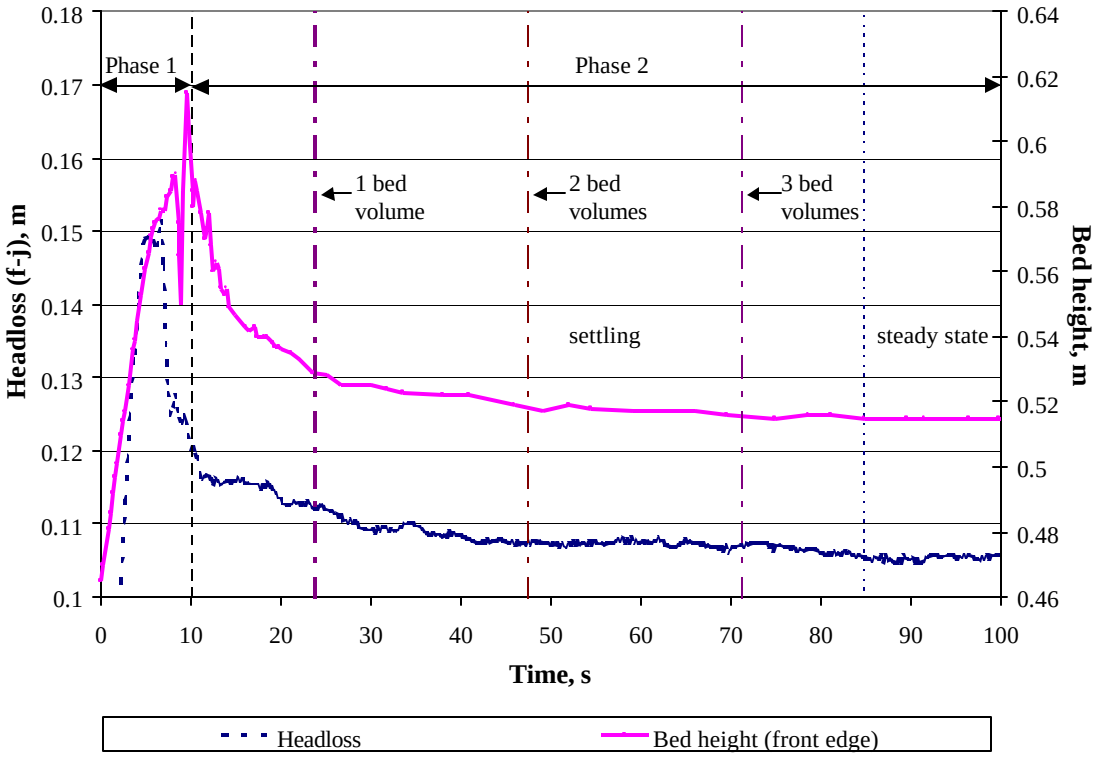

Figure 6.2 First 100 seconds of backwash – Experiment AU70

6.3.2. Interpreting the headloss measurements

During the first part of Phase 1, the bed surface moved up at a constant velocity that was found to be approximately equal to the superficial backwash velocity. This suggested that the top section of the bed was initially impermeable to the backwash flow. During this period, the headloss between ports f and j increased linearly up to some point (5 s in Figure 6.2) and then leveled off. This always occurred before the linear expansion of the bed ended. During the linear expansion phase, the headloss should have been approximately proportional to the mass of media between the two measurement ports. If the bed height continued to increase but the headloss leveled off, then it is likely that the zone of fluidization had reached the lower port (f), i.e. media was no longer moving into the section f-j. (See Table 3.1 for the locations of the ports).

Once the surface of the bed began to tilt, the system could no longer be considered linear. In this experimental set up, the backwash flow tended to be diverted to the back of the filter column where the manometer ports were located, resulting in a spike in measured headloss. While the pressure probe signal could no longer be considered proportional to the media mass, it did provide an indication of the intensity of mixing in the filter. The disintegration of the top section of the filter produced a sharp oscillation in the signal that died down as the surface of the fluidized bed began to stabilize.

During Phase 2, the fact that the headloss h_{fj} followed a decreasing trend parallel to the bed height indicated that at least some of the media below port "f" (z = 0.363 m) had expanded beyond its steady state porosity. (A decrease in bed height with constant headloss would have indicated that only the media above "f" had over expanded).

The phenomena observed during dirty filter backwashing, possible mechanisms involved and implications for backwash modeling are presented in detail next.

6.3.3. Expansion and disintegration phase

6.3.3.1. Mechanisms involved in disintegration

The disintegration of the clogged filter bed typically produced brief but violent churning in the top sections of the filter at the same time as the bulk of the floc was detaching from the media. This would obviously have an impact on any attempt to extract information about the intrinsic rate of detachment from the backwash concentration profile, as has been attempted by several of the authors discussed in Chapter 2. Understanding how and why the clogged bed structure disintegrates in the way it does, is important in any attempt to interpret backwash turbidity data for the early stages of backwash. Furthermore, the mechanisms involved in the disintegration and the length of time the clogged bed structure persists may yield information about the strength of the floc bonds that is relevant to the efficiency of backwash and the formation of mudballs.

Video recordings of the backwash experiments revealed that the timing of the buckling and disintegration of the top of the clogged bed was related to its interaction with the manometer ports. The manometer ports were attached to sides of the filter column by 29 mm diameter welds. The welds projected no more than 2 mm into the column but this appeared to be sufficient to disrupt the smooth expansion of the filter bed. Figures 6.3 and 6.4 show the first 10 s of backwash for experiments AU70 and ZU70. The horizontal dashed lines show the upper and lower edges of the manometer port welds and the vertical dotted line indicates the point at which the surface of the bed broke open. The corresponding video clips is "Phase 1 – 70 m/h". A better view of the ports and the response of the bed surface can be seen in the clip "Interaction with Manometers".

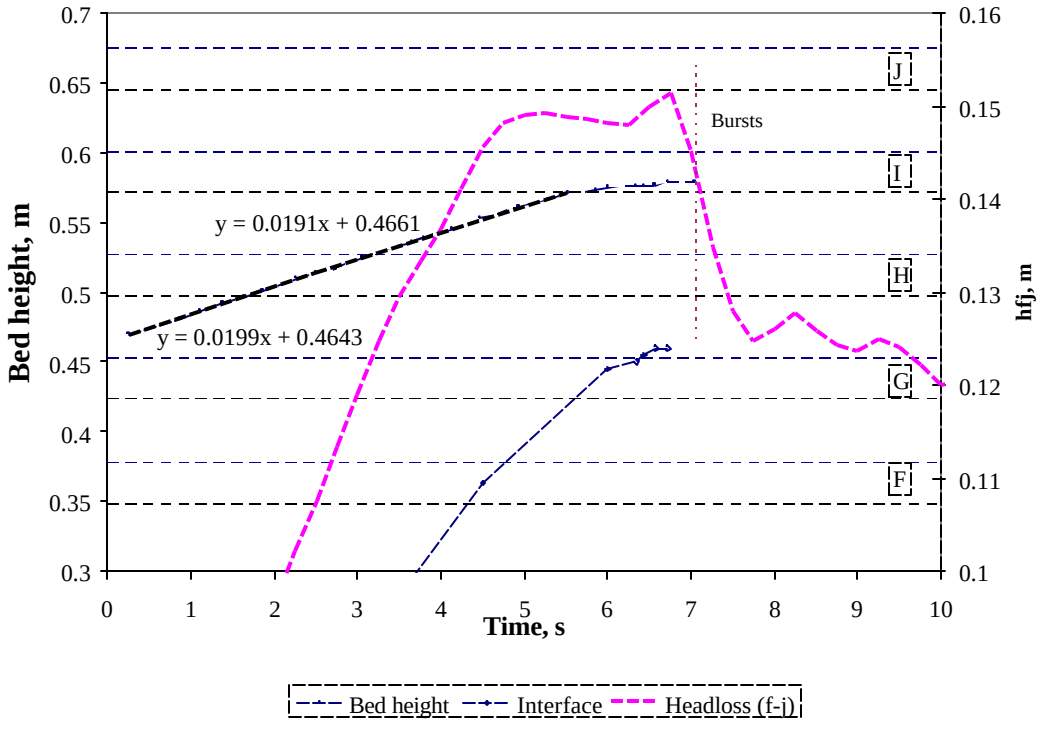

Figure 6.3 First 10 s of backwash – Experiment AU70

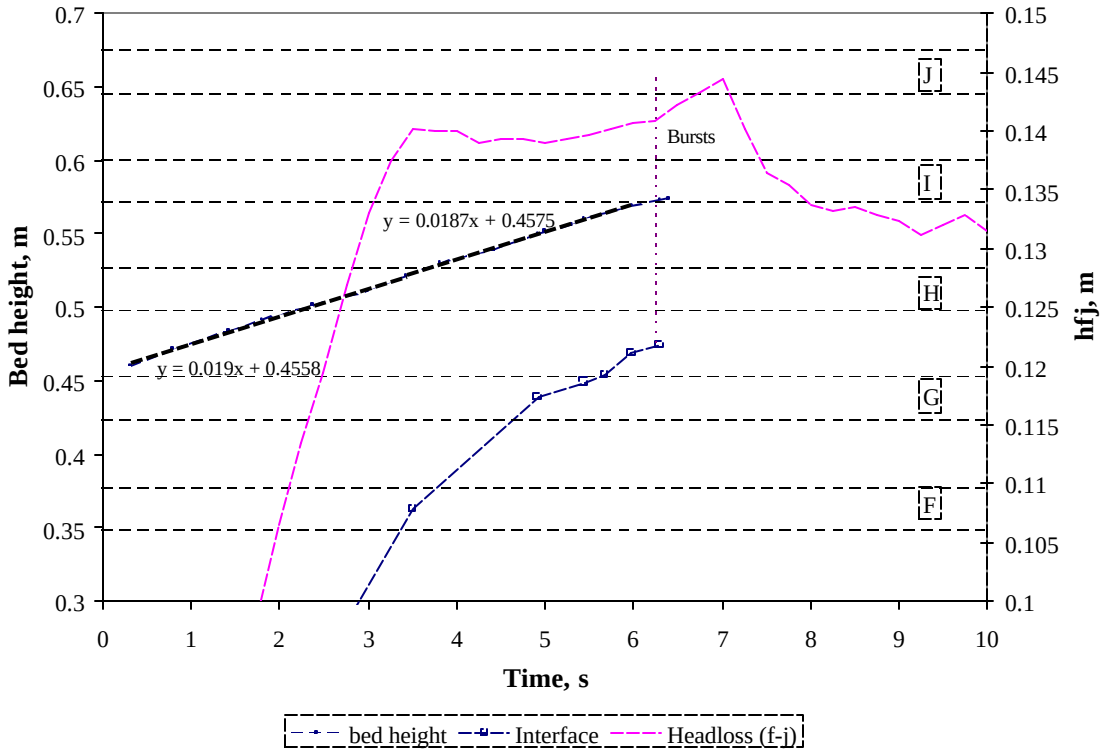

Figure 6.4 First 10 s of backwash –Experiment ZU70

Figures 6.3 and 6.4 show that for both experiments, the linear expansion of the bed ended as the surface reached manometer port "i". Close examination of the linear expansion phase indicated that the velocity of the bed surface also decreased slightly after the bed expanded past "h". In the videos, a puff of turbidity was generally observed adjacent to port "h" as the bed surface passed by, indicating that the flow through the bed may have increased. The regression line equations on the figures correspond to the bed height before and after it passes the midpoint of "h". In both cases the slope of the line and therefore the velocity of the bed decreased above "h".

When the bed surface reached port "i" in experiment AU70, the front edge slowed down while the back edge began tilting up, clearly indicating that the flow was being diverted towards the back of the filter. For ZU70, much less tilting occurred and the flow broke through the surface about 0.5 s earlier than in AU70.

Analysis of the pressure probe signals also indicated differences in the final disintegration of the top of the bed in the two experiments. For experiment AU70, the pressure peaked just before the bed broke open, suggesting that this was due to the diversion of the flow to the back of the filter. For ZU70, the pressure peaked after the bed broke, suggesting the flow distribution was relatively even up until this point and that the diversion to the back of the column was as a result of the surface breaking open.

There also appeared to be differences in the way the fixed bed structure disintegrated at the interface between the fixed and fluidized sections. The alum bed appeared to crumble grain by grain or in small chunks whereas the Z464N bed crumbled in larger chunks and layers and the gap between the fluidized and clogged media was larger. The upward propagation of the fluidized zone appeared to slow down as the alum bed surface began to tilt whereas it continued right up to the point that the Z464N surface burst open. This is consistent with the greater degree of tilting observed in the case of the alum bed – most of the backwash flow was being diverted up the side of the filter column.

Figures 6.3 and 6.4 show the approximate position of the interface between the fixed and fluidized sections as a function time. The first point corresponded to the time that the headloss (f-j) first leveled off (assumption l_{fl} = 0.363 m = height of fluidized section) while the remainder of the points were obtained from the video footage. The rate of fluidization in ZU70 appeared higher in AU70. h_{fj} leveled off 1 s earlier in ZU70 compared to AU70 indicating an earlier arrival of the interface between the fixed and fluidized sections. Since the rate of overall bed expansion was approximately the same in both cases, this implies that the clogged section disintegrated more rapidly in the case of ZU70. The thickness of the plug of clogged media as seen from the front of the filter at the time that filter broke open was ~11 cm for AU70 as opposed to ~10 cm for ZU70.

For experiment ZU70, the terminal headloss was greater and the efficiency of floc removal was less than for experiment AU70 (1.64 m and 73 % respectively compared to 1.40 m and 93 %). Intuitively, one might expect that the stronger floc bonds in the Z464N clogged bed would have held the clogged bed structure together better than the alum floc bonds, but the opposite appeared to be true. Some insights into the differences in the way that the two beds disintegrated were found by studying the behavior of the beds under conditions of very low backwash flow.

6.3.3.2. Response of the clogged bed structure to very low backwash flows

During backwashing, the maximum shear that can be applied to any part of the filter bed, whether clogged or fluidized, is limited by the weight of the filter grains. If the drag force exceeds the buoyant of the mass of the solid particles, then it will either expand or move as a plug to relieve the stress. Consequently, the average shear stress on media grains during backwashing is in general substantially less than that during the later stages of filtration.

Three experiments were carried out to investigate the effect of very low backwash rates on the structural integrity of the clogged 1 - 1.4 mm sand filter bed. Alum was used as the coagulant in the first two experiments and Z464N was used in the last. The experimental conditions are summarized in Table 6.3. The alum dose used in Experiments 1 and 2 was 6 mg/L as opposed to 8 mg/L in the AU experiments, consequently the rate of headloss development during filtration and the terminal headlosses were lower.

In each experiment, the backwash flow was increased in small increments and the headloss profile at each flowrate measured. The bed height and total headloss at each flowrate are shown in Figures 6.5 and 6.6.

Table 6.3 Filter conditions for very low backwash

	Experiment 1	Experiment 2	Experiment 3
Dose	6 mg/L alum	6 mg/L alum	2.5 mg/L Z464N
Influent turbidity	1.8 – 1.9 NTU	1.3 – 1.5 NTU	0.9 – 1.3 NTU
Run time	26 h	34 h	45 h
Terminal headloss	0.88 m	1.08 m	1.57 m
Backwash temperature	20.75 °C	21 °C	21.5 °C

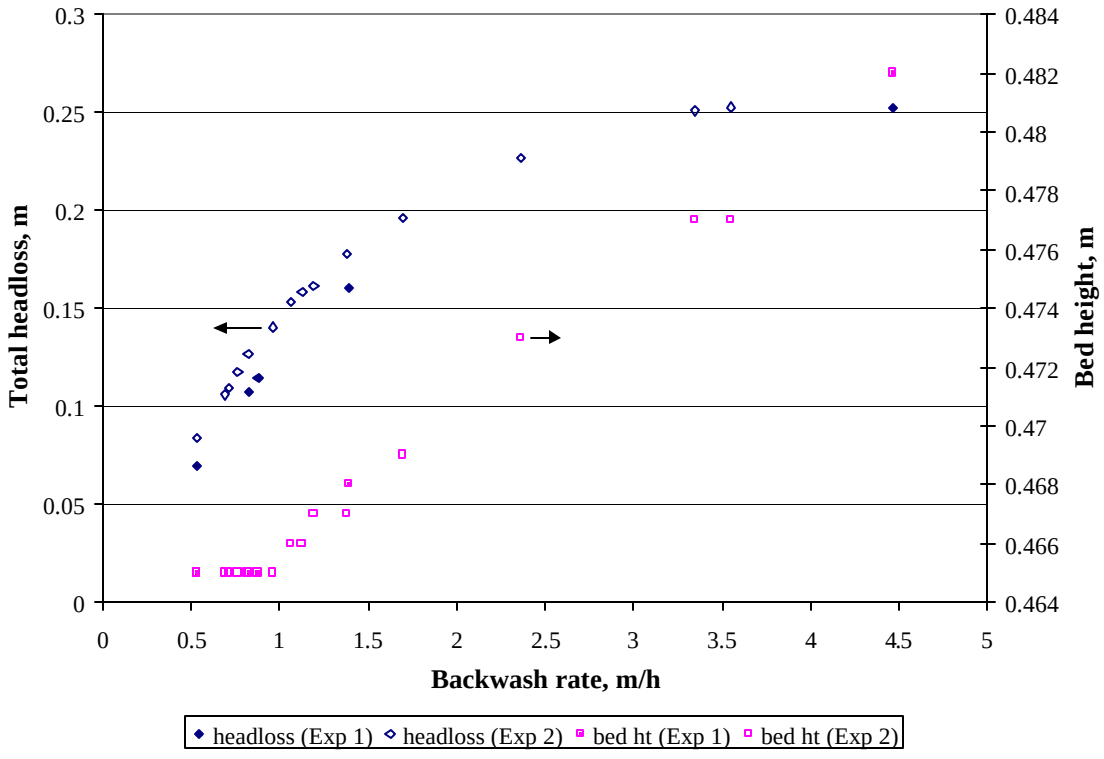

Figure 6.5 Low flowrate backwash in filter clogged with alum floc

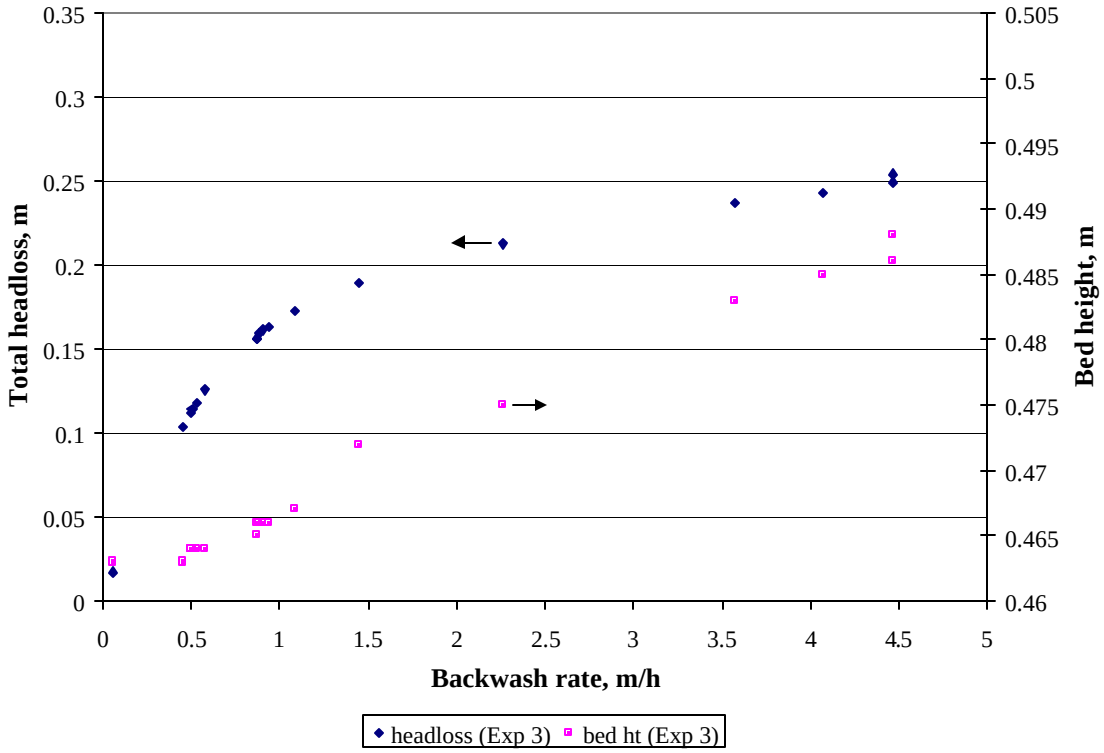

Figure 6.6 Low flowrate backwash in filter clogged with Z464N floc

Note that the minimum fluidization velocity for this bed at 21 °C was 52 m/h so the backwash rates in Figures 6.5 and 6.6 ranged from 0 to 10 % v_{mf}.

The headloss across the bed increased linearly with backwash rate up to the point that the bed began to expand and thereafter gradually leveled off. Expansion started at about 1 m/h (2 % v_{mf}) for the alum clogged bed and 0.5 m/h (1 % v_{mf}) for the Z464N bed. Channeling became evident in the Z464N at 4.5 m/h. Although the bed height had not reached port "h", channeling was first noticed on the side of the bed adjacent to the ports. The alum experiments were discontinued before any channeling was observed.

Horizontal cracks in the bed were observed from before the point of incipient expansion and extended deeper into the bed as the flow increased. The cracks often seemed to start at the pressure ports, suggesting that the welds were acting as stress raisers.

The headloss profile at each backwash flow was measured and compared to the terminal headloss profile at the end of the filter run. The terminal headloss profile (change of headloss with depth) could be approximated by a fourth order polynomial.

$$h_t(z) = Az^4 + Bz^3 + Cz^2 + Dz \qquad 6.1$$

z = Distance from bottom of bed, m

$h_t(z)$ = Headloss between bottom of bed and z, m

A,B,C,D = Polynomial regression coefficients

One would not necessarily expect the hydraulic resistance of the bed to be the same for both up-flow and down-flow. However, for the lowest flowrates (before any bed expansion was observed), it was found that the headloss between any two manometer ports was approximately equal to

$$\Delta h_{bw} = \Delta h_t \left(\frac{Q_{bw}}{Q_t} \right) \qquad 6.2$$

Δh_{bw} = Difference between two points in the backwash headloss profile, m

Δh_t = Difference between two points in the terminal headloss profile, m

Q_{bw} = Backwash flowrate, L/h

Q_t = Flowrate at which terminal downflow headloss profile was measured, L/h

Therefore at very low backwash rate the headloss profile had the same polynomial shape as the terminal headloss profile. However, as the flowrate increased and the bed began to expand, the headloss gradient at the top of the bed became constant. Figure 6.7 shows backwash headloss profiles from Experiment 2 at 0.5 m/h (before expansion), 1.06 m/h (critical backwash rate), 1.7 m/h and 4.1 m/h (after expansion). The dashed lines show the headloss estimated form Equation 6.2 while the dotted lines indicate the region in which Equation 6.2 no longer applied.

The maximum headloss gradient which is expected to develop in the bed is equivalent to the weight of the media per unit volume at the lowest porosity. This can be estimated by dividing the total fluidized bed headloss by the fixed bed height. The measured fluidized bed headloss for this filter was 0.373 m while the headloss calculated from Equation 2.10 (headloss across a fluidized bed) was 0.395 m.

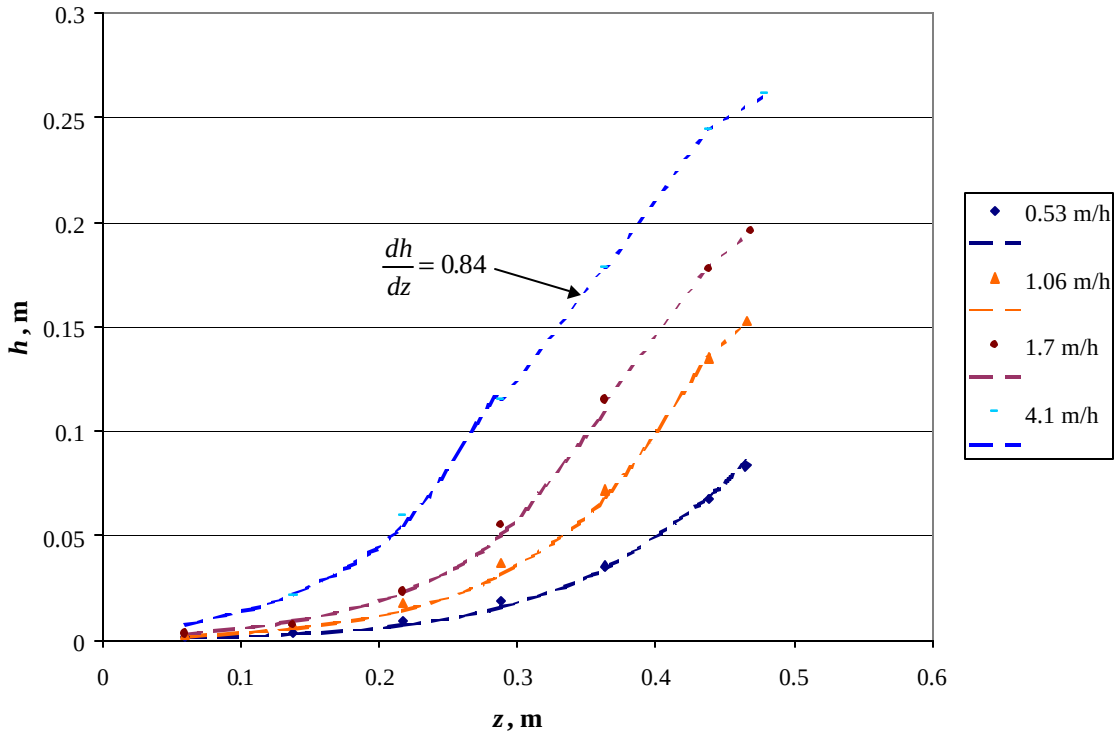

Figure 6.7 Low rate backwash headloss profiles in filter clogged with Z464N floc

The fixed bed height in this experiment was 0.465 m so the maximum gradient was expected to fall in the range 0.802 to 0.849 m/m. The slopes of the constant gradient sections of the curves in Figure 6.7 ranged from 0.82 to 0.84, except for the top most sections where the gradient was slightly lower. This may have been due to measurement errors (the slope is very sensitive to the length of the segment), higher porosity near the top of the bed or greater disruption of the bed structure.

The overall conclusion from this exercise was that the flexural strength of the clogged bed was insufficient to support its weight. The bed structure and hydraulic resistance appeared to be preserved up to the point that the critical headloss gradient was achieved and then the

structure began to fracture and expand to accommodate the additional flow. The welds on the manometer ports appeared to play a role here too. The flowrates at which fracture and expansion occurred were extremely low: 0.5 m/h for the Z464N bed and 1 m/h for the alum beds.

It was not possible to determine the actual flow through the clogged section of the bed during normal backwash to this degree of accuracy, however, it can be said with certainty that a small amount of stress on the structure induced by through flow and/or the manometer welds would cause the structure to fail. Once the media below any section of the bed fluidized, its weight would no longer be supported and it would begin to disintegrate. In the case of the alum beds, the grains may have been held more loosely in the floc matrix and therefore tended to break way individually or in small clusters. The lower permeability of the Z464N bed may have made it more susceptible to fracture so that the structure tended to break apart in layers. The disintegration of the bed from the bottom up presumably proceeded until the remaining plug of media became thin enough to be disrupted by an increase in flow adjacent to the manometer ports.

6.3.3.3. Effect of solids loading and backwash rate on the disintegration of the bed during Phase1

In addition to the differences in behavior between the alum and Z464N filter beds, the disintegration of the clogged zone also appeared to be affected by backwash rate and degree of

solids loading. Figures 6.8 and 6.9 show the first 10 seconds of backwash for Z464N clogged beds at 95 and 61 m/h, the highest and lowest rates used in this study. In these figures, only the position of the front edge of the bed surface and the interface between the fixed and fluidized sections are shown. The corresponding video file is "ZU - Effect of Rate".

.

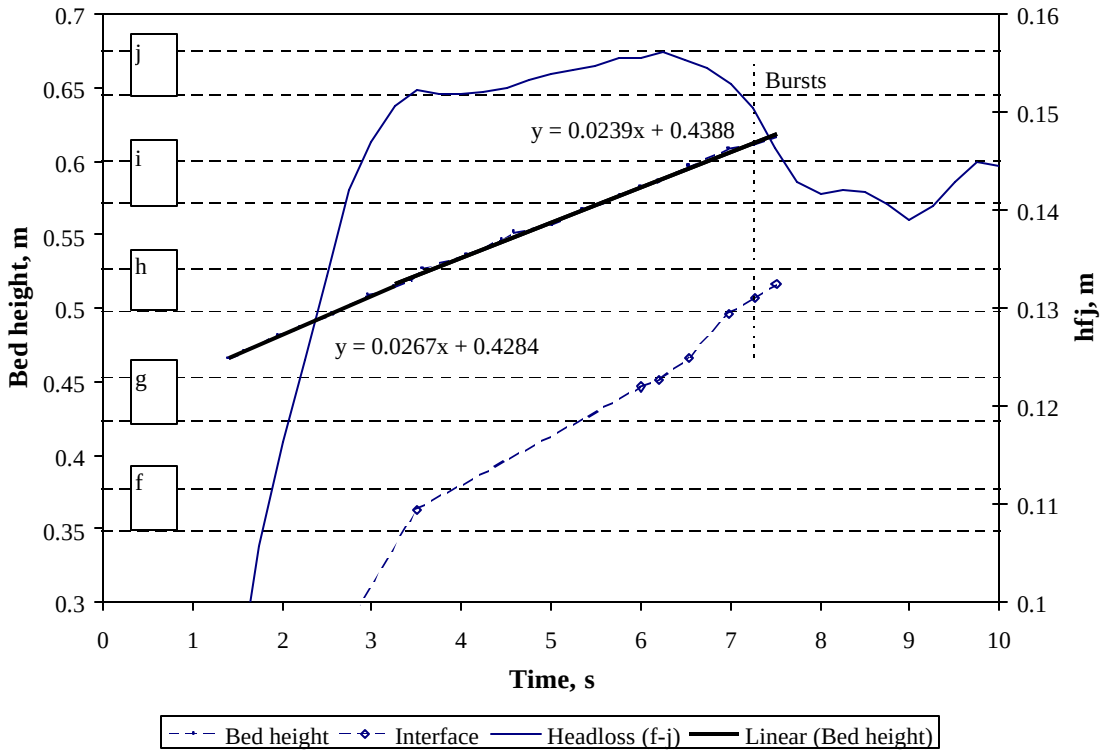

Figure 6.8 First 10 s of backwash – Experiment ZU95 (175 % v_{mf})

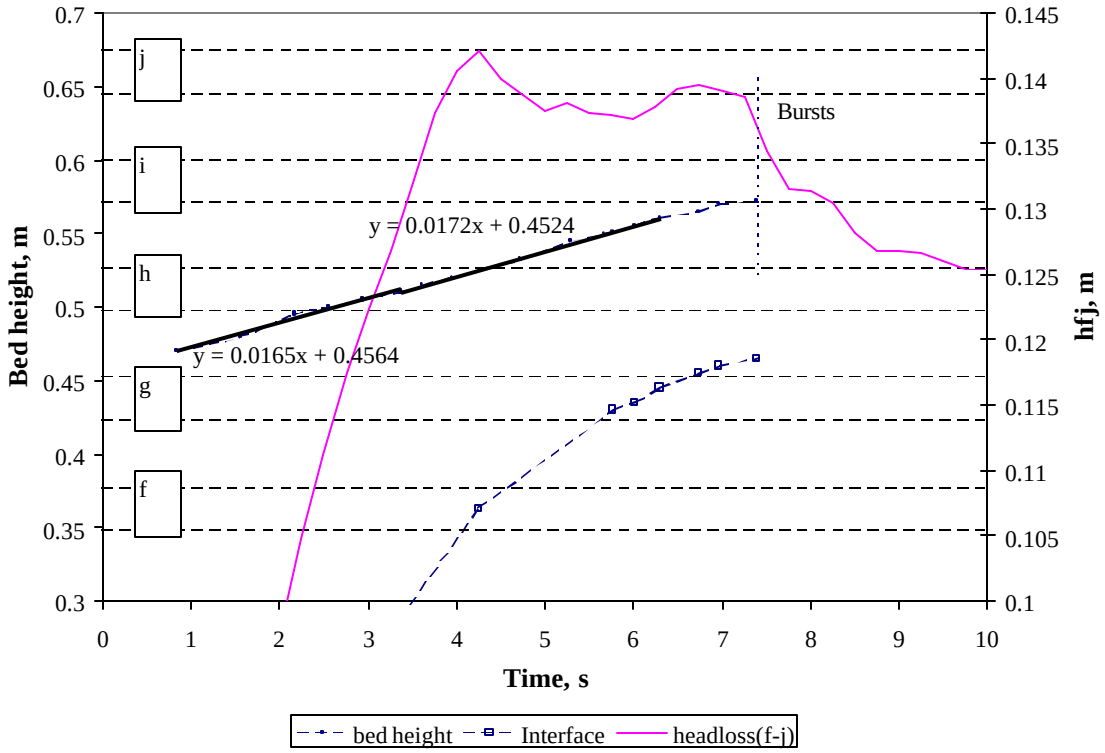

Figure 6.9 First 10 s of backwash – Experiment ZU61 (113 % v_{mf})

At 95 m/h the front edge of the expanding bed overshot port "i" before breaking up whereas at 61 m/h the front edge stopped just below "i" while the back edge was pushed past the weld. At 70 m/h (Figure 6.4) the front edge reached half way past "i". Therefore, while the position of the manometer ports appeared to have been the major factor determining how far the bed expanded before breaking apart, the momentum of the top section also appeared to play a role.

Figures 6.10, 6.11, 6.12 and 6.13 show the first 10 seconds of backwash for experiments AU61_8, AU61_17, AU61_26 and AU61_29. These experiments were carried

out to determine the effect of filter run time and solids loading on the backwash. The corresponding video clips can be found in "Effect of Loading".

For the lowest degree of clogging (8 hour run time) the separation of the bed into a clogged and a fluidized section was barely discernible and the flow broke through at several points around the perimeter as the bed surface reached port "h". It appears that there had been insufficient time and floc deposition for the media to be cemented together except perhaps in the top few millimeters of the bed. The datalogger file for this experiment was corrupted so there was no record of the headloss.

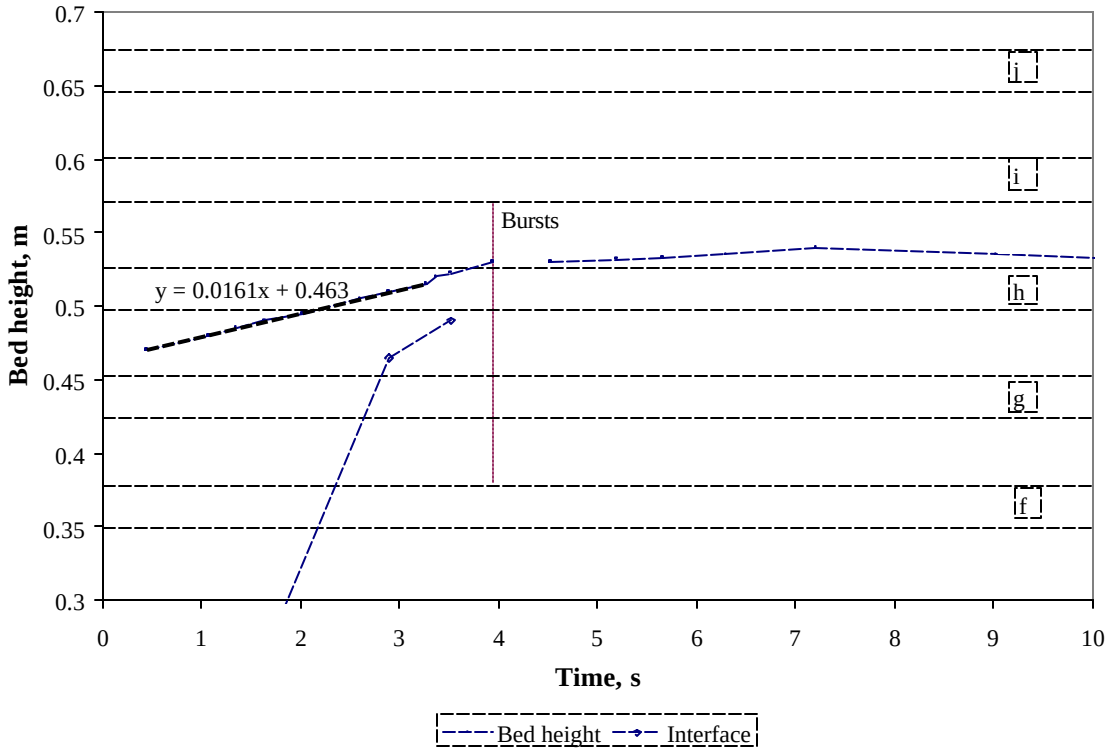

Figure 6.10 First 10 s of backwash – Experiment AU61_8h (109 % v_{mf})

In the next clip, the filter had been run overnight (17 hour run time) and the clogged section was much easier to see. Furthermore, the back edge of the bed reached as far as port "i" before breaking open. Disintegration and flow breakthrough occurred most rapidly adjacent to the manometer ports but flow breakthrough also occurred at the front of the filter before the view was obscured by the turbidity.

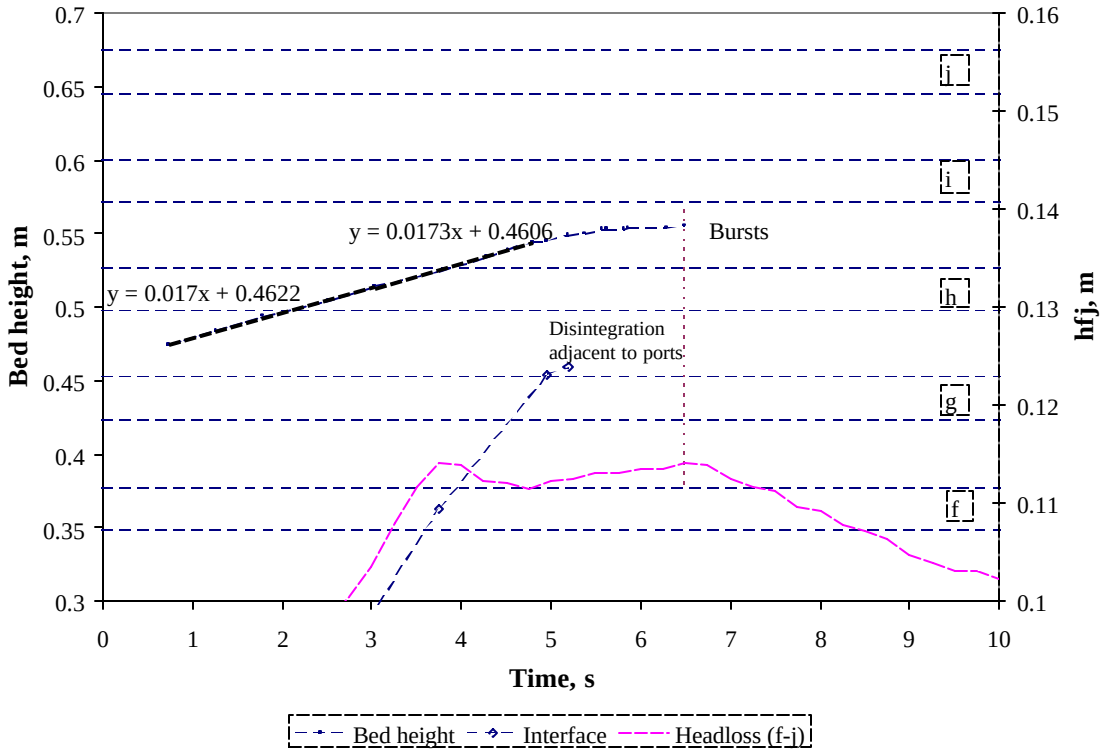

Figure 6.11 First 10 s of backwash – Experiment AU61_17h (109 % v_{mf})

For the 26 hour run time, the horizontal fissure in the bed appeared later than for the 17 h run, but again, it can be seen that disintegration proceeded most rapidly adjacent to the manometer ports. In the 29 hour run, the interface did not come into view until after the bed broke.

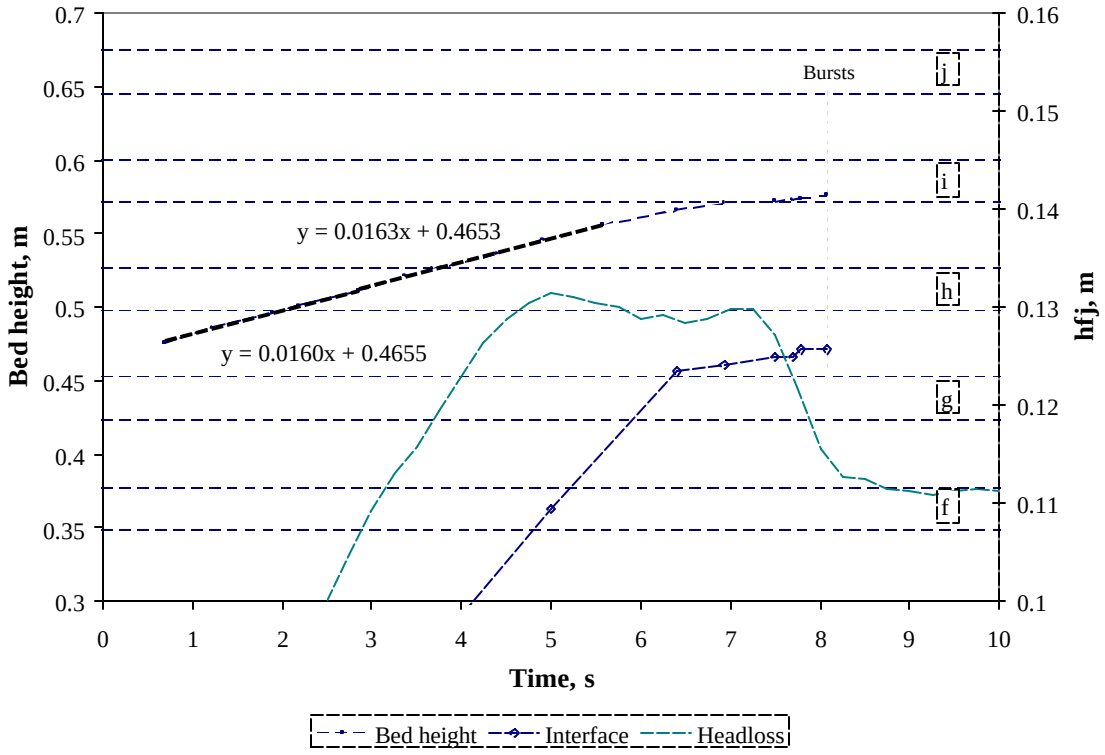

Figure 6.12 First 10 s of backwash –AU61_26h (109 % v_{mf})

The velocity of the top surface of the bed was more or less the same for all experiments at 61 m/h (59.7 – 60.5 m/h). It appeared that the more clogged the bed, the slower the disintegration of the residual zone and the later buckling started. The difference in the headloss peaks for run times 17 to 29 hours was also striking. The greater the degree of clogging, the greater the mass of media pushed above port "f" appeared to be. This is consistent with a slower rate of disintegration.

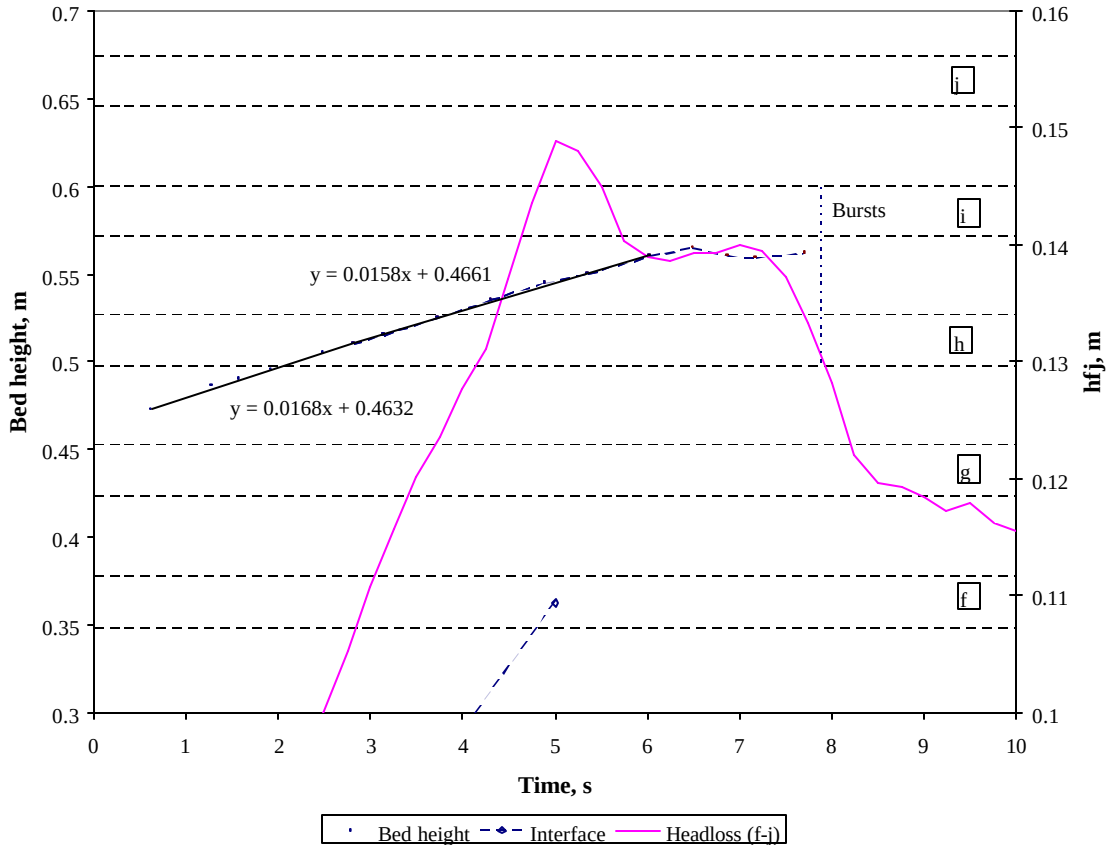

Figure 6.13 First 10 s of backwash – Experiment AU61_29h (111 % v_{mf})

The rate at which the fluidized zone was propagated up through the filter in the first few seconds of backwash can be estimated from the time at which the headloss levels off.

$$\frac{dl_f}{dt} = \frac{0.363}{t_p} \qquad 6.3$$

l_f = Height of the fluidized zone, m

t_p = Time at which measured headloss between "f" and "j" levels off, s

Assuming that the flow through the surface of the filter is initially negligible, the corresponding rate of disintegration of the fixed bed section can be estimated as

$$-\frac{dl_{fx}}{dt} = -\left(v_b - \frac{dl_f}{dt}\right) \qquad 6.4$$

l_{fx} = Height of the fluidized zone, m

Note this only applies to period $t < t_p$. Figure 6.14 shows the estimated rate of disintegration $-\frac{dl_{fx}}{dt}$ plotted against the backwash rate. The rate of disintegration for experiment AU61_8h was estimated from the video footage since there was no pressure drop data. Disintegration was more rapid for the Z464N beds and the less clogged alum beds (AU61_8h and AU61_17 h) than for the heavily clogged alum beds but there was no trend with respect to backwash rate.

The differences in the rate of disintegration can be explained by comparing the terminal headloss profiles for the different experiments. Figure 6.15 shows the terminal headloss profiles for experiments AU70, ZU70 and AU61_17h. Although ZU60 had the highest terminal headloss of the three experiments, the headloss profile in the lower sections of the bed was more similar to the profile for AU61_17 than the more heavily clogged AU70.

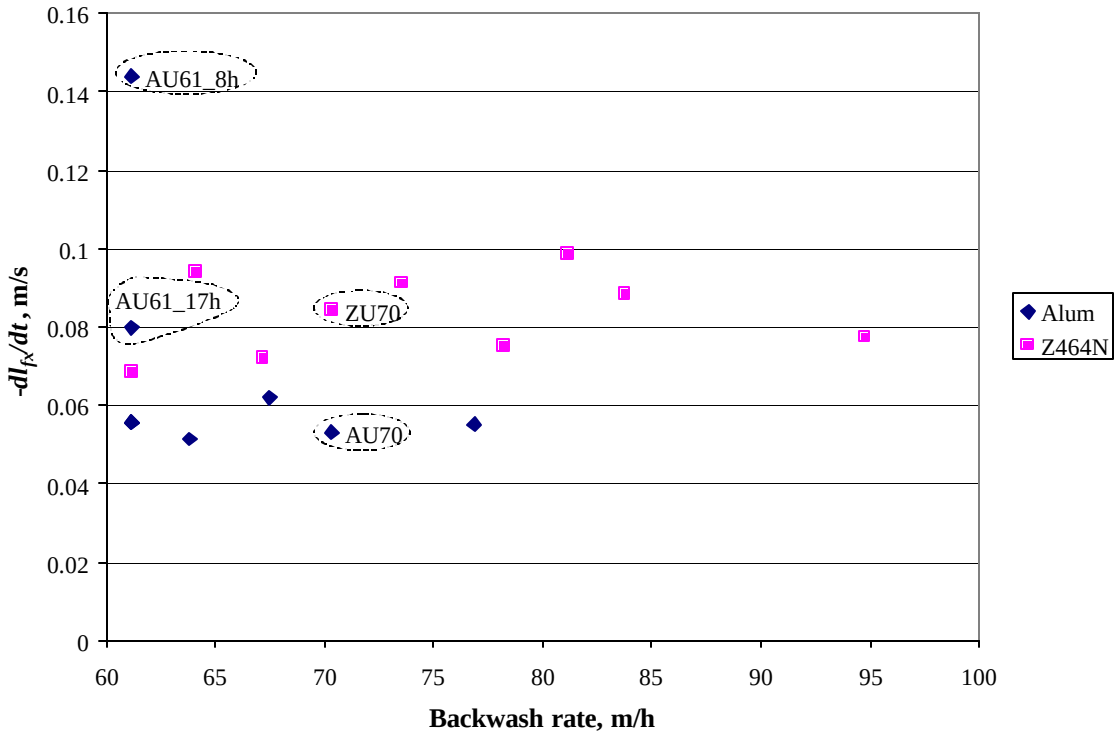

Figure 6.14 Backwash rate and rate of disintegration

Recall that the rate of disintegration $-\frac{dl_{fx}}{dt}$ is based on the time t_p required for l_f to reach z = 0.363 m. The fixed bed height of the media in the fluidized zone at t_p can be estimated by subtracting $l_{fx}(t_p)$ from the total fixed bed height at terminal headloss. For AU70, ZU70 and AU61_17h, l_f = 0.363 m corresponded to z = 0.295 m and z = 0.305 m respectively in the fixed bed. In Figure 6.15, the terminal headloss profiles for AU61_17h and ZU70 were very similar up to z = 0.3 m whereas the headlosses in this region were significantly higher for AU70. Consequently, the rate of disintegration within a given region of the filter appears to be related to the degree of clogging in that region.

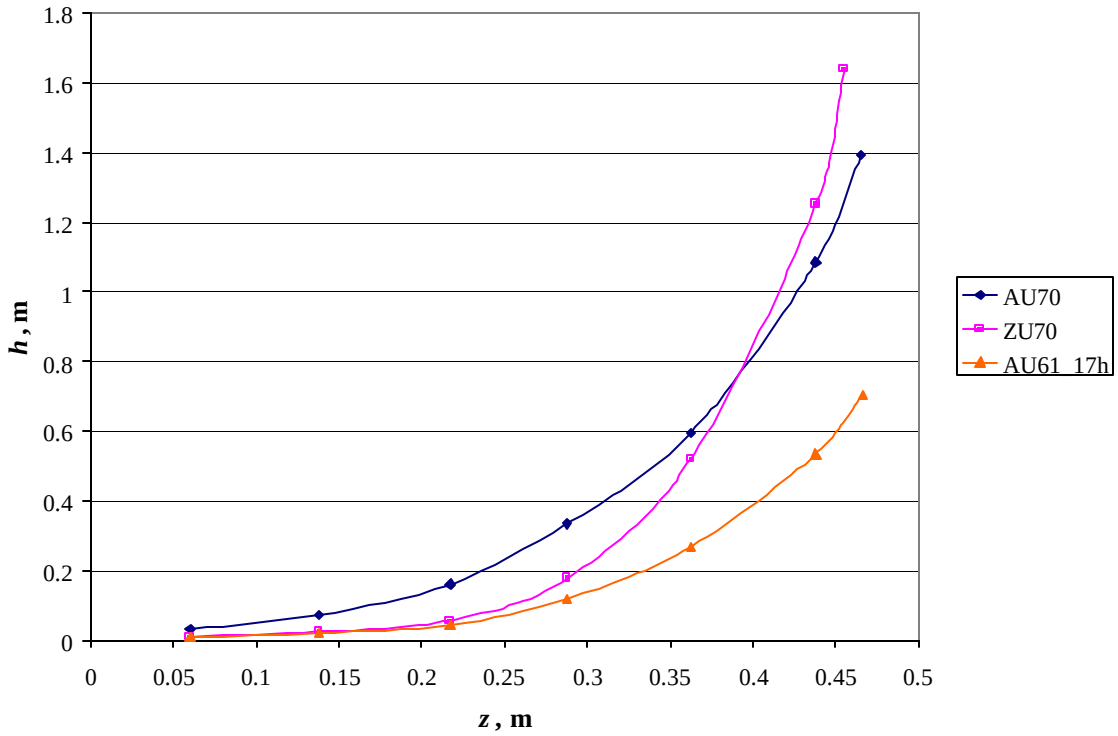

Figure 6.15 Terminal headloss profiles for AU70, ZU70 and AU61_17h

Figure 6.16 shows $-\frac{dl_{fx}}{dt}$ plotted against the total mass deposited in the filter. The data points for AU70, ZU70 and AU61_17h are marked. The overall trend seems to be that greater masses of floc (and hence greater floc volumes) correspond to slower rates of disintegration.

In this case (and in general when filters are run to a particular terminal headloss) greater masses of deposited floc corresponded to deeper penetration of the floc into the bed. There are two possible explanations for the apparent effect on the rate of disintegration. The first is that although the floc matrix was not strong enough to keep the bed structure together, it did slow down its disintegration. An alternate possibility is that as the media expanded and the floc

detached, the viscosity of the suspending fluid increased causing the media in the lower sections to over expand. Viscosity effects are discussed further in Section 6.3.4.

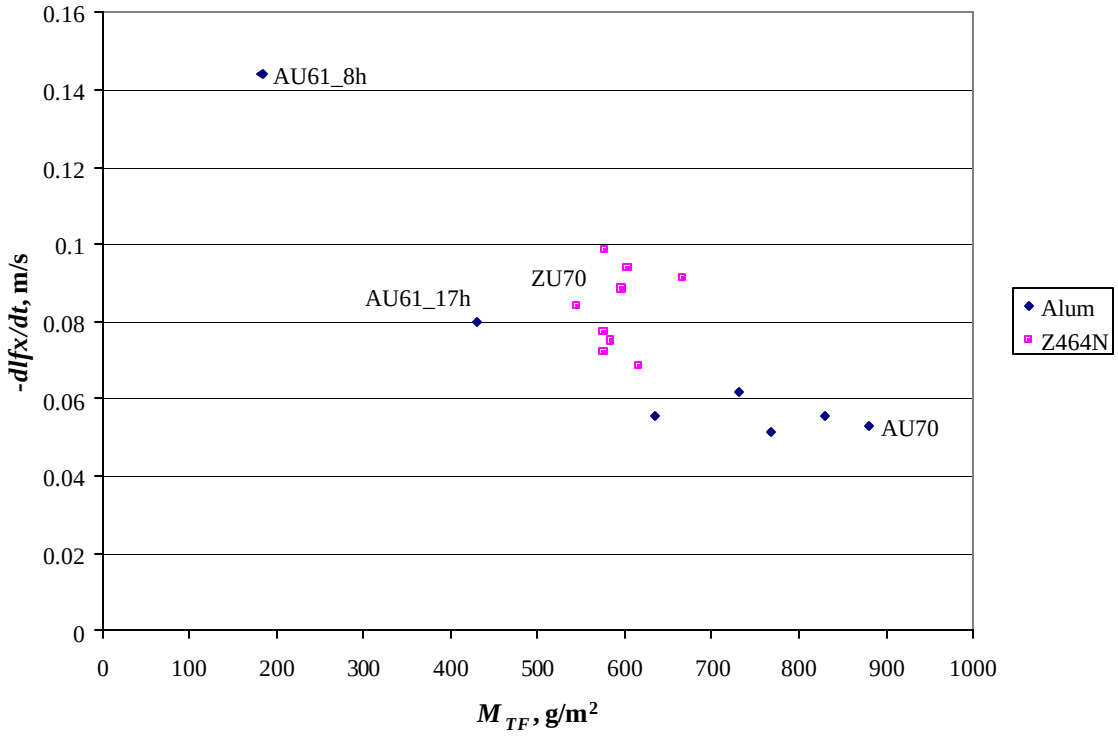

Figure 6.16 Rate of disintegration as a function of total mass deposited

6.3.4. Over expansion of the fully fluidized filter bed

During the expansion and disintegration phase the dirty filter bed always overshot its steady state height by several centimeters. Once all the media had fluidized the bed began to settle back down to its steady state height. The settling process tended to take up to a minute or more.

By contrast, clean fluidized beds that were subjected to a sudden drop in backwash rate settled out to their new bed height in matter of seconds. Examples of flow reduction experiments can be seen in the video "Flow Reduction".

The difference between the settling behavior of the filter bed in the Z464N and alum experiments for uniform sand was also notable. In the alum experiments, the filter bed tended to shoot up higher and break up more violently than in the Z464N experiments, but then it also settled back more rapidly. Furthermore, the alum floc tended to wash out more quickly with a clear band of fluid developing above the bed surface fairly soon after the violent agitation of the bed subsided. The video clip "Phase 2 – 70 m/h" shows the behavior of the fluidized bed in experiments AU70 and ZU70. The headloss (f-j), bed height and backwash concentration as functions of time for experiments AU70 and ZU70 are shown in Figure 6.17. Note that the time in Figures 6.17 (c) and (d) refer to the time that the floc arrived at the entrance to the sampling probe.

The presence of floc attached to the media and in the suspending fluid could have affected the expansion characteristics of the fluidized bed in several ways. Suspended floc would tend to increase the viscosity of the flow and hence the bed expansion, while floc deposits may have increased the volume of the media grains and/or affected the drag forces they were subjected to, since friction is a function of surface properties.

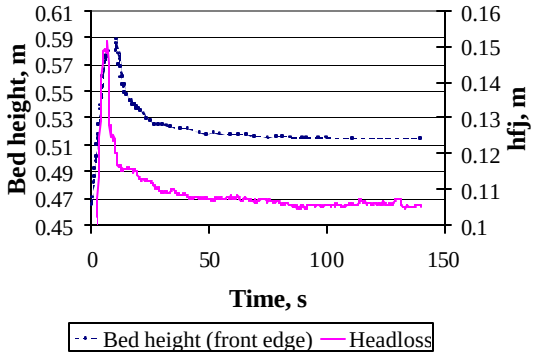

(a) Bed height and headloss (f-j) – AU70

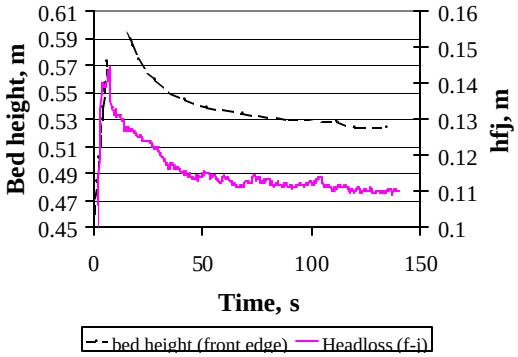

(b) Bed height and headloss (f-j) – ZU70

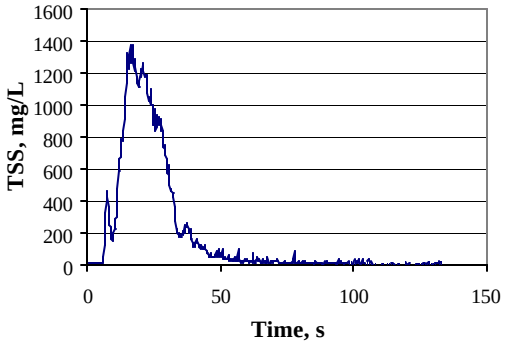

(c) Backwash concentration – AU70

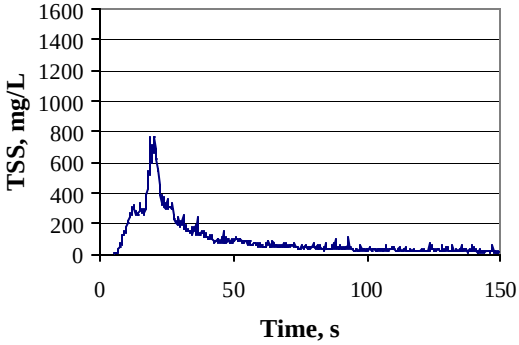

(d) Backwash concentration – ZU70

Figure 6.17 Bed height, headloss and backwash concentration for experiments AU70 and ZU70

Figures 6.18 and 6.19 show the steady state bed height and headloss for the AU and ZU series experiments compared to measurements made in clean beds at the same backwash rates. The mass retained at the end of backwash, M_R is also shown.

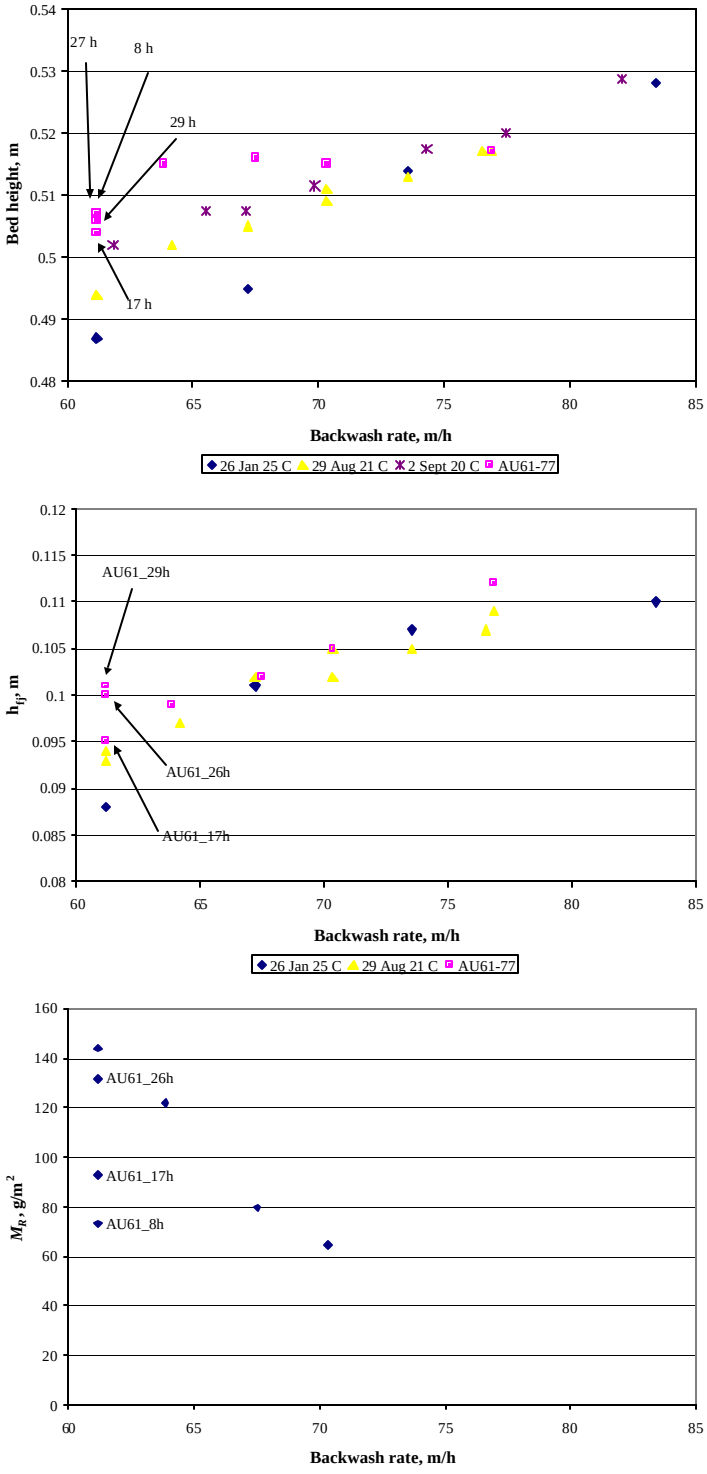

Figure 6.18 Expanded bed height, headloss (f-j) and mass retained after backwash for AU61 to AU70

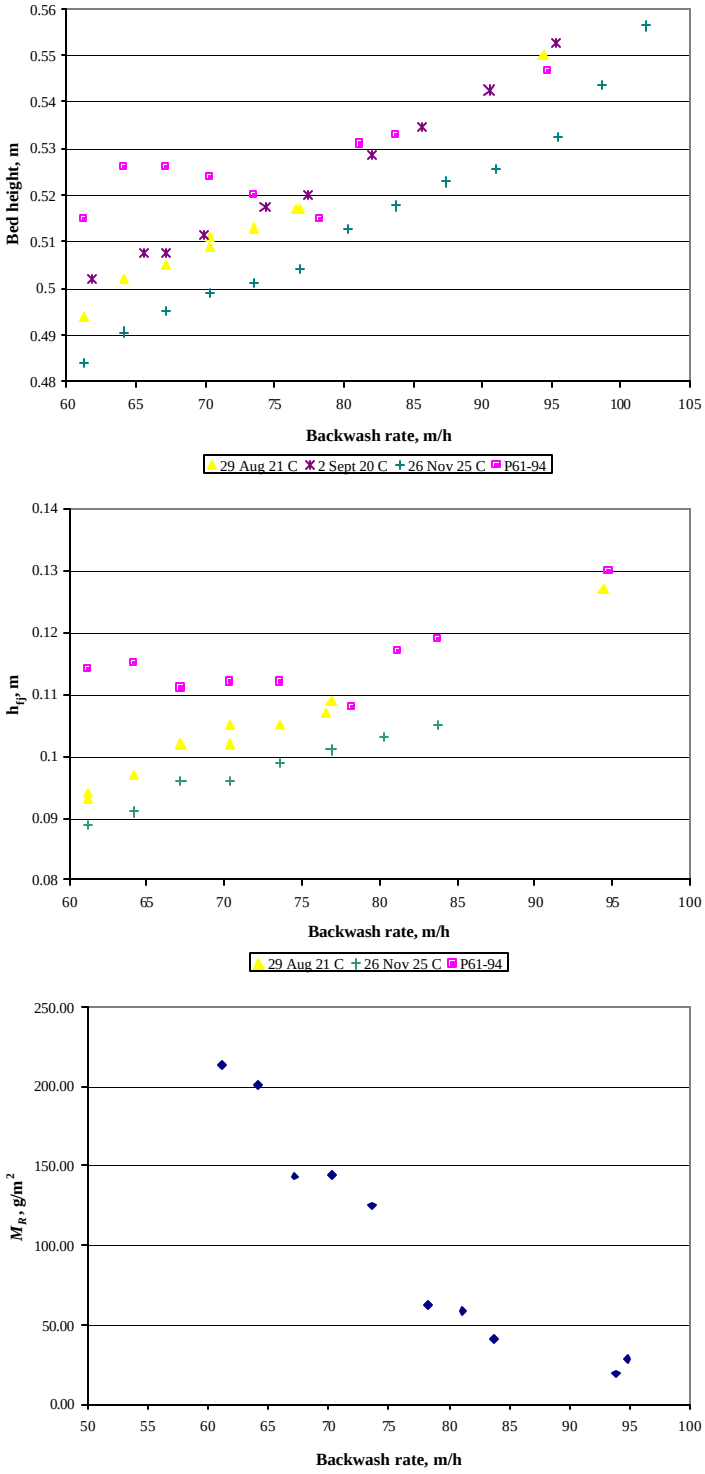

Figure 6.19 Expanded bed height, headloss (f-j) and mass retained after backwash for ZU61 to ZU95

The backwash temperature varied from 24 to 26 C for the alum experiments and from 21 to 24.75 ^{o}C for the Z464N experiments. Variations in temperature and hence in water viscosity may have caused some variability in measured bed heights at a given backwash rate. Bed expansion is expected to be higher at lower temperatures. However, for the clogged bed backwash experiments, both bed height and h_{fj} were always greater than the clean bed measurements at 21 ^{0}C, the lowest temperature at which measurements were made.

For backwash rates < 78 m/h, the magnitude of the deviation increased with the mass of floc retained in the filter. For backwash rates > 78 m/h, turbulence effects at steady state (both clean and dirty filters) made it increasingly difficult to obtain accurate bed height and headloss measurements. For the highest backwash rate shown (94 m/h), the bed did not appear to reach steady state expansion before the flow was reduced.

The maximum mass retained was 213 g/m^2 filter area whereas the mass of sand in the zone f-j varied from 175 to 229 kg/m^2 so the increase in mass of the media due to the mass of the floc would have had a negligible effect on the headloss. The volume of floc retained in each experiment was estimated assuming a floc density of 1030 kg/m3 (Huang and Basagoiti, 1989) and it was found that the increase in media volume would contribute less than 0.2 mm to the bed height. Since neither volume nor mass increase can explain the increase in bed height, it is assumed that the presence of the floc deposits must have increased the drag force on grains. The increase in headloss, h_{fj} in dirty beds indicate that floc deposits persisted below 0.363 m in the expanded bed.

Figure 6. 20 shows the relationship between the concentration of floc leaving the filter bed and the porosity in the top section (f-j). The porosity was estimated using Fair and Hatch's relationship. (Equation 2.10). The concentration corresponding to porosity at time *t* was estimated by calculating the lag time *t'* between water leaving the bed and reaching the sampling probe and then finding the concentration at the probe at time *t + t'*.

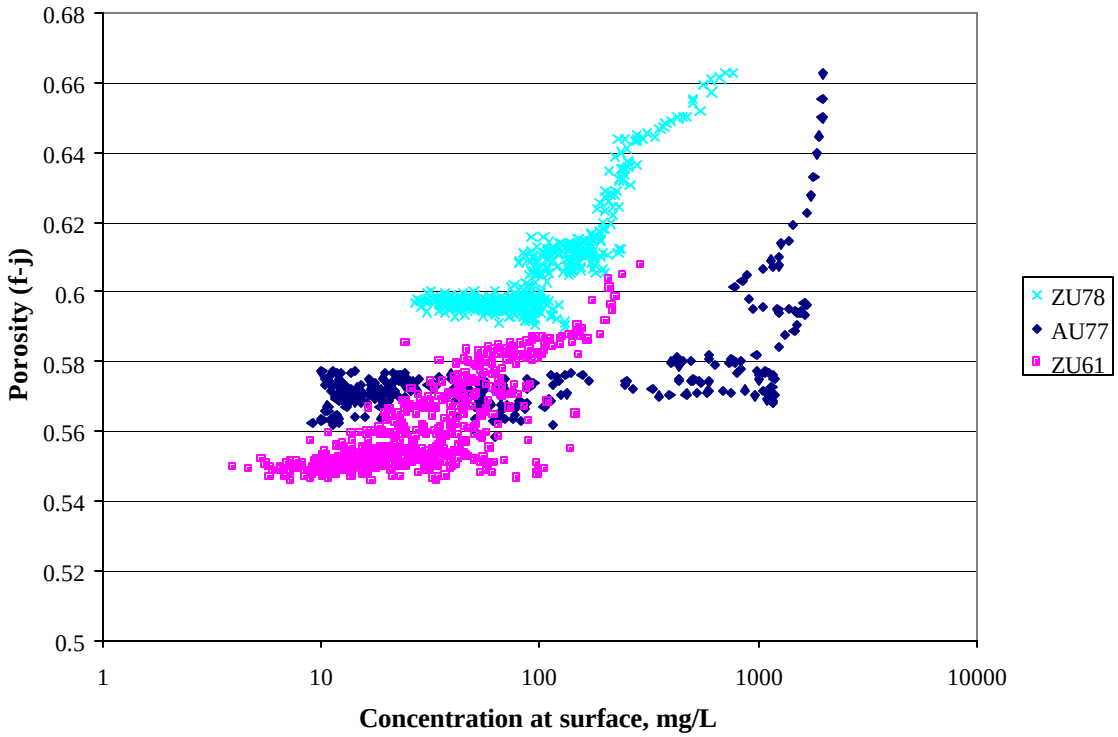

Figure 6.20 Relationship between porosity and backwash concentration

For experiments ZU61 and ZU78, the increase in porosity above its steady state value appeared to be approximately proportional to the log of concentration above 100 mg/L. There did not appear to be any relationship between porosity and measured concentration for AU77 but this may have been due to dispersion effects. The concentration leaving the filter in the alum

experiments typically changed much more quickly than in the Z464N experiments and consequently the estimated concentration at t + t' would have been more sensitive to mixing conditions between the filter bed and the sampling probe.

6.4. Implications for backwash modeling

6.4.1. Deviations from steady state fluidization and one-dimensional expansion

The most significant deviation of real filters from the idealized behavior assumed in existing backwash models, is the expansion and disintegration of clogged bed at the beginning of the backwash. Since the bulk of the floc probably is detaches during the disintegration phase, the way in which this part of the process is handled will have a major impact on the ability of any model to predict the backwash concentration profile.

Amirtharajah (1985) noted that the model relating detachment kinetics to the concentration profile did not apply to the beginning of backwash. Huang and Basagoiti (1989) assumed that the filter media was fully fluidized at time zero and that there was instantaneous mixing throughout the bed at $t = 0$ such that there was a uniform initial deposit concentration profile. The assumption of media mixing in the early stages of backwash appears to be partially correct. However, these authors also assumed that the intrinsic rate of detachment (the parameter k_3 in Equations 2.35 and 2.36) was constant for the entire duration of the backwash.

This seems unlikely since the mechanisms involved in the disintegration of the bed are quite different to the mechanisms involved in detachment from fluidized grains.

Hall and Fitzpatrick (2000) assumed that a fraction a of the initial deposits detached instantaneously as each layer expanded but did not account for mixing between the layers. Since the fraction detached during expansion was a fitting parameter, its value would end up including both the initial rate of detachment and mixing effects. However, it would only be valid for the system in which it was measured.

The increase in fluidized bed porosity during Phase 2 is a less important deviation from ideality than the mixing in Phase 1, however, it will have some effect on the prediction of the concentration profile (See Equations 2.35 to 2.37). A higher porosity will result in greater dilution of the detached floc that could in turn affect the estimation of the rate of detachment.

The magnitude of the effect will depend in part on the filtration step. Large volumes of easily detached floc would be expected to result in a greater degree of over-expansion. For example, Hall and Fitzpatrick (2000) and Huang and Basagoiti (1989) reported substantially higher backwash peak concentrations than were recorded in the current study (10,000 – 15,000 mg L and 3,000 – 46,000 mg/L respectively compared to < 2,500 mg/L in this study). This is because they used high concentration filter influent solutions (200 mg/L and 6 – 85 mg/L respectively compared to < 4 mg/L) to clog their experimental filters Consequently, the over-

expansion effect in these studies may have significantly greater than was observed in this investigation.

6.4.2. Equipment specific and scale-up effects

The experimental evidence presented in this chapter indicates that the timing, scale and intensity of the mixing associated with disintegration are a function of the equipment, the degree of clogging of the media and the backwash velocity. Most laboratory and full-scale filters have irregularities in their walls that will destabilize the expansion of the bed at some point. For example, Hall and Fitzpatrick (2000) had both pressure taps and sampling probes at various heights within their filter bed. Huang and Basagoiti's (1989) laboratory filters had backwash effluent outlets at various heights above the bed, which may have affected experiments at higher backwash rates. The effect of such irregularities on experimental results should be taken into consideration in the design of laboratory scale filters for backwash studies.

Of probably greater importance is the effect of filter diameter on the disintegration of the clogged media plug and the resultant mixing. It was beyond the scope of the current study to investigate the effect of filter dimensions and geometry on backwash, but it was evident from the types of phenomena observed that they would have significantly affected the backwash behavior.

A common problem encountered in experimental filters using lighter media such as anthracite and GAC is that during backwash, the media tends to move up as a piston instead of fluidizing and may wash out of the filter unless the operator takes steps to break the plug up. Lang et al. (1993) found that fluidization of the media became increasing difficult with decreasing ratio of filter diameter to media size. These authors attributed difficulties in fluidizing media in small filters to particle bridging. It was not clear whether they were referring to clean or clogged beds or both, but is likely that cementation effects due to the presence of deposited floc would be much more effective than particle bridging in holding the media plug together.

In the current study, the clogged layers at the top of the bed broke up and collapsed into the filter as a result as flow localization adjacent to the walls. The resistance of the clogged layers to flexural stresses was undoubtedly a function of the ratio of plug thickness to filter diameter, among other factors. The larger the diameter of the filter, the sooner the collapse and disintegration of the top layers would be expected to occur. In general, the number and spatial arrangement of filter nozzles or orifices may also affect the distribution of flow during this period and hence also the disintegration of the media plug, as suggested by Hall and Fitzpatrick (2000).

6.4.3. Modeling Phase 1 of backwash

In theory, it would be possible to investigate the effect of filter dimensions and irregularities on backwash behavior using a range of experimental filter designs in order to develop a model that could be scaled up to any size filter. In practice, this would not be a

particularly useful exercise if its was focused on fluidized backwash without auxiliary wash. This is because there are few applications outside of the laboratory where this backwash regime is still used. Modeling the disintegration of the clogged bed during auxiliary backwash would be relatively straightforward because the energy dissipated in the top layers of the bed is more predictable and uniformly distributed. For this reason, filter scale up effects would probably be less important than in fluidized water only backwash.

However, fluidization without auxiliary wash is likely to remain the backwash regime of choice for fundamental studies of particle detachment because of the relatively simple equipment required. When interpreting the results of these studies, it is important to not overlook the effects of mixing on the peak of the backwash concentration profile with time.

Chapter 7 discusses the impact of mixing effects on the backwash concentration profile measured in the current study and the quantitative analysis of detachment kinetics in Phase 2. A possible approach to modeling Phase 1 for backwash with and without auxiliary wash is also proposed.

CHAPTER 7

THE BACKWASH CONCENTRATION PROFILE AND THE KINETICS OF DETACHMENT

7.1. Introduction

One of the objectives of this study was to investigate the effect of various parameters on the mechanisms and rate of floc detachment during backwash. Since the kinetics of detachment are a function of the mechanisms involved, experimental data on the rate of detachment could potentially be used to test models of the detachment process at both the microscale (detachment from individual grains) and the macroscale (erosion of clogged regions). However, fluidized beds are particularly challenging systems in which to study detachment since it not possible to obtain direct measurements of the rate of detachment from individual fluidized grains.

Several authors (See Section 2.3) have suggested that the intrinsic rate of detachment (rate of detachment at the grain scale) can be related to the backwash concentration profile. The rate of detachment at any point in the bed is typically defined a to be

$$\frac{\partial s_t(z)}{\partial t} = -k s_t(z) \qquad 7.1$$

$s_t(z)$ = Specific deposit at time t and depth z, volume or mass of deposit per unit volume bed

k = Detachment rate constant, 1/s

z = Filter depth measured from top of bed, m

k is assumed to be a function of both the hydrodynamic detachment forces and the adhesive forces which resist detachment. Equation 7.1 applies to the detachment of deposits from individual filter grains and does not apply the disintegration and erosion of clogged regions in the bed. In practice, one needs to have a model of the backwash flow characteristics and of the distribution of filter deposits with bed depth to be able to isolate the effect of the detachment kinetics on the backwash profile. Existing models have assumed a plug flow regime during backwash and either a uniform distribution of filter deposits (Amirtharajah, 1985; Huang and Basagoiti, 1989) or no intermixing of the layers of the original clogged bed during expansion and fluidization (Bhargava and Ojha, 1989, Hall and Fitzpatrick, 1998).

In Chapter 6 it was shown that the characteristics of flow vary with backwash time, backwash rate and the degree of clogging of the filter bed, making it extremely difficult to define a realistic flow model. Furthermore, even if the initial distribution of deposits in the fixed bed is known, violent mixing and subsequent settling of the filter media means that the distribution of remaining deposits varies due to the motion of the grains as well as the detachment process. The

widely reported characteristic exponential decay in backwash concentration may simply be a characteristic of the mixing in the filter and might not provide any information about the intrinsic rate of detachment (except that the time constant of detachment is much faster than the time constant of mixing).

However, it was also clear from the backwash videos presented in Chapter 6 that the violent mixing at the beginning of backwash subsided very rapidly and the bed approached steady state fluidization before all the floc was flushed out. Therefore it is possible that the plug flow models presented in Chapter 2 might be reasonable approximations of the detachment behavior some time after disintegration was complete.

A model which only applies to the tail of the concentration profile, while less useful than a model of the entire backwash process, can be used to predict the impact of backwash remnants on filter ripening in the subsequent filter run. Amirtharajah and Wetstein (1980) showed that concentration of the filter ripening peak could be related to backwash effluent concentration towards the end of backwash while Amburgey et al. (2003) showed that the amount of backwash remnants passing into the filtrate could be reduced by reducing the backwash rate for a period at the end of backwash.

Depending on whether the concentration of newly detached floc is of greater or lesser magnitude than remnants of the floc detached in the initial stages of backwash, it may or not or

may not be possible to extract information about the rate of detachment from the concentration profile.

Section 7.2 discusses the impact of mixing effects on the backwash concentration profiles measured in the current study. Section 7.3 presents the analysis of backwash kinetics in the later stages of backwash. Section 7.4 discusses the implications of the results for backwash modeling and proposes a simple model of mixing and detachment during the initial stages of backwash.

7.2. Impact of mixing effects

Hall and Fitzpatrick (2000) observed that mixing of adjacent layers in the filter bed typically resulted in dual peaks in the concentration profile with the effect being most pronounced at higher backwash rates. In the current study, multiple peaks in the concentration profile were more evident at low backwash rates and for higher masses of deposited floc, M_{TF}. Figure 7.1 shows the profiles for backwash at 61 m/h. Figure 7.2 compares the profiles for alum and Z464N experiments for backwash rates 64 to 78 m/h. Figure 7.3 shows the profiles for the Z464N experiments with the highest backwash rates. M_{TF} is the total mass of solids deposited during filtration (Chapter 5).

Multiple peaks were typical of the alum concentration profiles. The peaks were most distinct for the lowest backwash rate (61 m/h Figure 7.1 (a), (c)) and the highest loading

(AU77, M_{TF} not measured, run time = 46 h). In experiments AU64 to AU70 (Figure 7.2) the peaks tended to merge together but were still distinguishable. In the Z464N experiments, the backwash turbidity peak became more jagged at lower backwash rates and smoother at higher rates but was always smoother than the alum peaks.

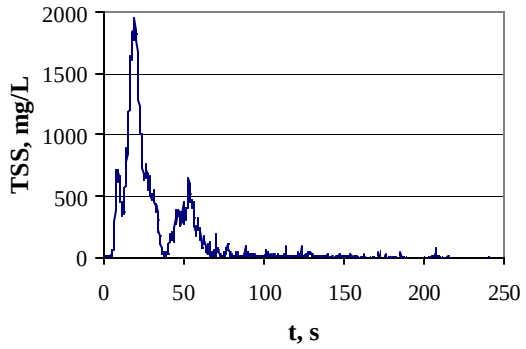

(a) AU61_29h - M_{TF} = 830 g/m^2

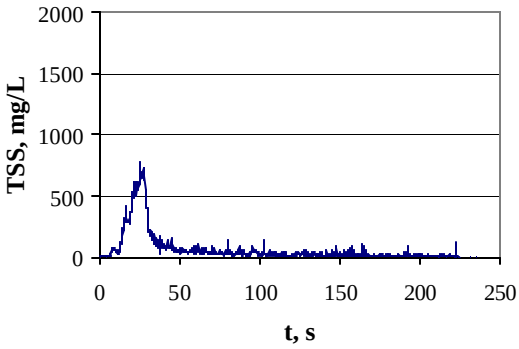

(b) ZU61 - M_{TF} = 661 g/m^2

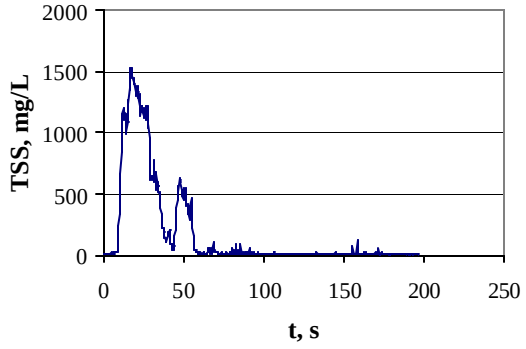

(c) AU61_26h - M_{TF} = 633 g/m^2

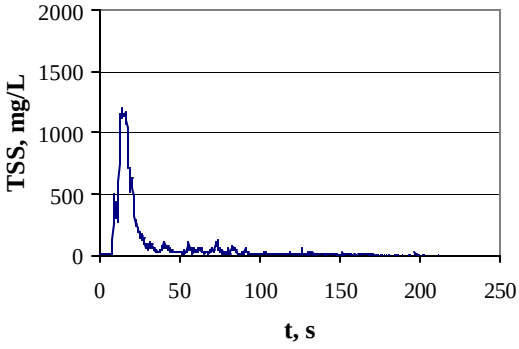

(d) AU61_17h - M_{TF} = 430 g/m^2

Figure 7.1 Concentration profiles for backwash at 61 m/h

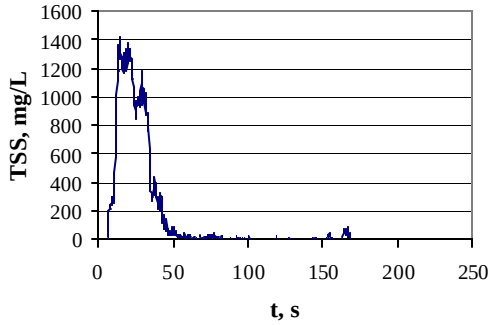

(a) AU64 - M_{TF} = 767 g/m^2

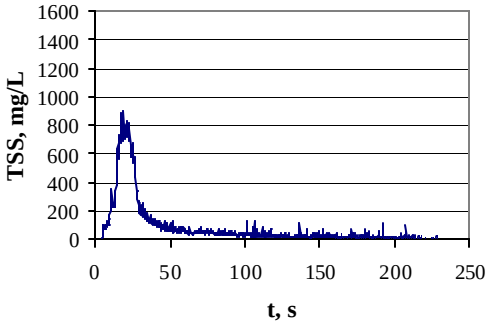

(b) ZU64 - M_{TF} = 603 g/m^2

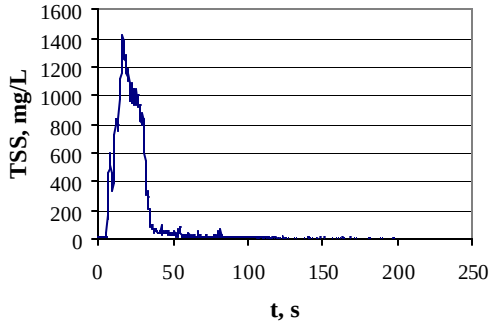

(c) AU68 - M_{TF} = 731 g/m^2

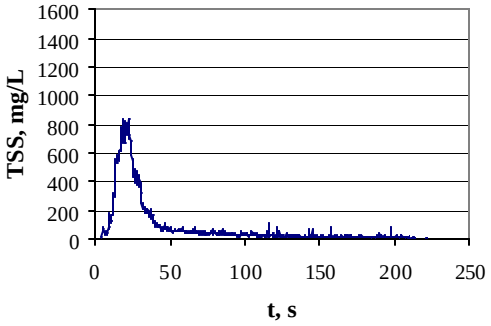

(d) ZU67 - M_{TF} = 576 g/m^2

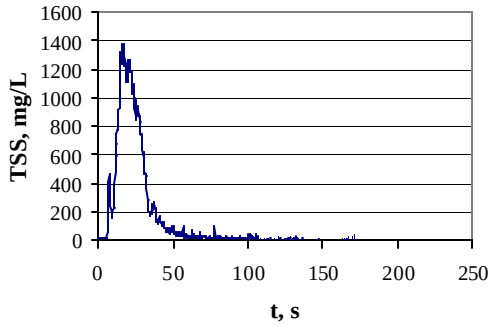

(e) AU70 - M_{TF} = 881 g/m^2

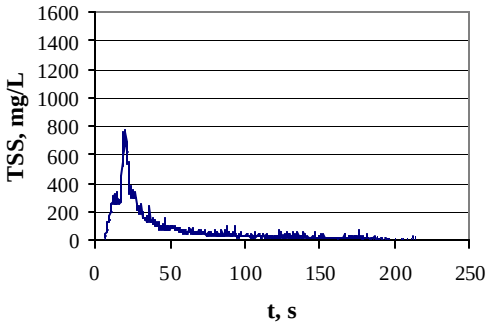

(f) ZU70 - M_{TF} = 545 g/m^2

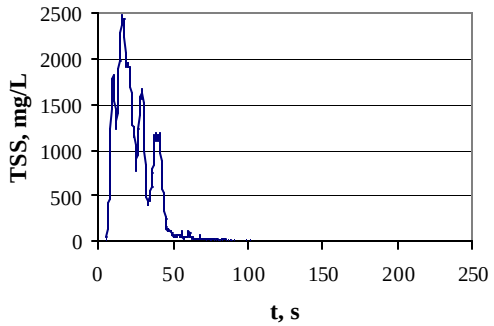

(g) AU77 - M_{TF} = not measured

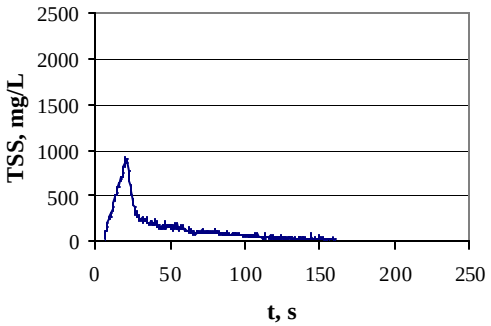

(h) ZU78 - M_{TF} = 583 g/m^2

Figure 7.2 Backwash concentration profiles for backwash rates 64 to 78 m/h

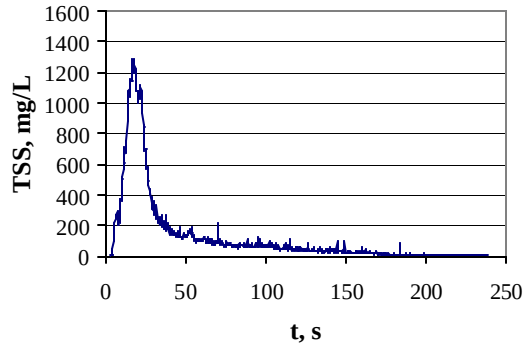

(a) ZU74 - M_{TF} = 667 g/m^2

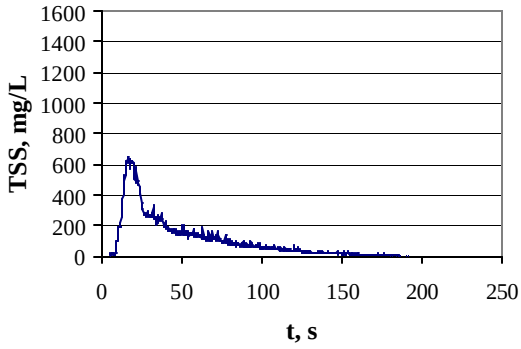

(b) ZU81 - M_{TF} = 577 g/m^2

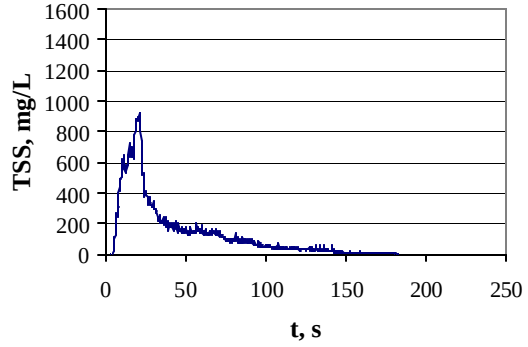

(c) ZU84 - M_{TF} = 597 g/m^2

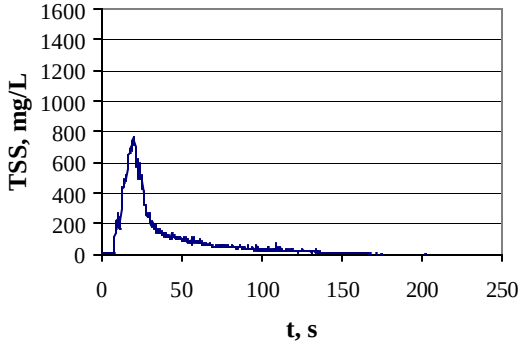

(d) ZU94 - M_{TF} = 569 g/m^2

Figure 7.3 Concentration profiles for backwash rates 74 to 94 m/h

Pulses in backwash concentration could also be observed in the video clips for AU61_17h to AU68. (See video file "Multiple concentration peaks"). For backwash rates up to 68 m/h, it was typical to see the turbidity above the bed clearing rapidly and then to have an additional cloud of floc emerge. The video clip for 78 m/h was less clear: no distinct breaks in the turbidity emerging from the bed were observed but a dense, turbulent cloud of large floc could be observed at the top the screen (just below the sampling probe) and it is possible that the observed peaks were due to mixing above the bed. By contrast, in the Z464N videos, there tended to be gradual and smooth transitions from high to low concentration above the bed

surface and little evidence of a cloud of floc lingering above the bed (See "ZU – Backwash turbidity"). This may have been due to lower concentrations of smaller, lighter floc.

When the video clips for alum experiments with backwash rate 61 m/h and various degrees of loading are compared ("Multiple concentration peaks"), it appears that the pulses in backwash turbidity are related to the intensity of mixing in the top sections of the bed when it breaks up. The greater the amount of floc in the bed, the more violent its break-up. Chunks of clogged media could be seen breaking off and sinking into the media below. Furthermore, it is probable that some of the suspended floc was also sucked back into the bed to emerge later as additional peaks in the profile.

At higher backwash rates, (68 and 70 m/h), the break up of the bed was even more violent, but the higher fluid velocities and possibly more rapid and complete disintegration of all clogged sections resulted in more complete blending of the detached material before it was flushed out of the filter.

In the Z464N experiments, the break-up of the clogged media generally appeared to be less violent than the alum experiments at the same backwash rate. This may have been due to the lower mass of deposited floc. The headloss fluctuations perhaps provide a clearer indication of the relative intensity of mixing for the two series of experiments. Figure 7.4 shows the variation of headloss in the first 20 s of backwash for experiments AU70 and ZU70.

Backwashing of a clean filter bed at 70 m/h and 24 °C is also shown. The fluctuation in headloss as the AU70 bed breaks up is almost double that for ZU70.

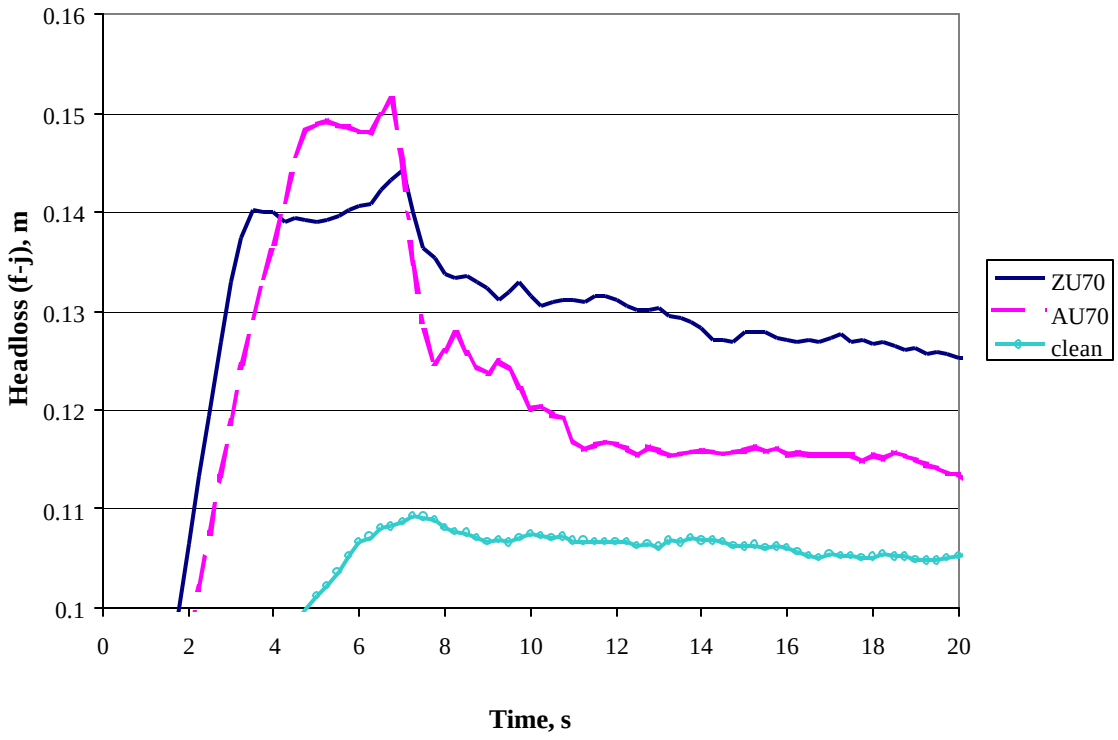

Figure 7.4 Headloss as an indicator of intensity of mixing – 70 m/h

Floc also appeared to be released from the bed more slowly and steadily in the Z464N experiment compared to the alum experiments (no clear layer is observed until much later). This can be seen from the backwash concentration profiles. The Z464N peaks were lower but the tail concentrations were typically higher than for alum. (This is even more obvious when the turbidity profile is plotted on a log-linear plot. Log-linear plots are presented in the Section 7.3. The lower peaks for Z464N were partly because the total mass deposited was generally lower.

However, when values of M_{TF} were comparable (ZU61 - M_{TF} = 661 g/m^2, AU61_26h - M_{TF} = 633 g/m^2), the alum peak was still higher.

According to Kawamura (1991) a low peak and long tail on the backwash concentration profile indicates a less efficient backwash than a higher peak and a lower tail. This seems to be true when comparing alum and Z464N curves at the same backwash rate. However, interestingly, in the case of the Z464N experiments, the higher the backwash rate (and hence the higher the removal efficiency) the higher the concentrations in the tail tend to be. This could be either due to greater dispersion effects (dispersivity coefficient rather than macroscopic mixing) at higher flows and/or due to the detachment of larger amounts of floc at higher backwash efficiency.

These results suggest that in the case of alum experiments, the detachment of the floc from the media was extremely rapid and the features of the backwash concentration profile were primarily determined by dispersion and mixing effects both within and above the media. Detachment of at least some part of the deposited floc in the Z464N experiments appears to have proceeded more slowly. Furthermore, smaller initial masses of deposited floc (M_{TF}) appeared to result in less violent mixing when the bed disintegrated, so that the impact of the intrinsic detachment rate was not necessarily swamped by dispersion effects.

The quantitative analysis of the backwash concentration profile is discussed next.

7.3. Accuracy of the on-line backwash concentration data

The amount of information that can be extracted from the backwash concentration profile depends on the accuracy and frequency of the concentration measurements. Backwash concentration may be determined as a function of time using grab samples of the effluent or, if available, some kind of on-line meter that is able to measure suspended solids. On-line meters can provide greater resolution of the backwash concentration profile than grab samples but it is often difficult to obtain accurate and reproducible real time measurements of suspended solids concentration as a result of variations in particle size distribution. For example, Hall and Fitzpatrick (2000) did not use coagulant in their experiments because flocculation interfered with the calibration of their on-line solids meter.

The measured backwash concentration profile is also affected by the choice of sampling point. Samples collected from the backwash effluent pipe will be affected by mixing above the fluidized bed, at the inlet to and within the pipe itself. However, using probes to draw sample from points close to or within the filter bed is also not ideal because there is some variation in concentration across the filter cross section.

In this study, the concentration profile during backwash was measured on-line using the opacity meter described in Chapter 3. Sample for the opacity meter was drawn from above the surface of the backwashing filter through a 22 mm diameter sampling probe located below the backwash trough. Preliminary tests carried out when the opacity meter was first set up

suggested that the sample drawn from this point was reasonably representative of the total backwash effluent but more detailed analysis of the mass recovery in the AU and ZU experiments indicated that this was not always the case. Overall recoveries of total solids detached based on the opacity meter signal (defined in Equation 5.28) ranged from 60 to 119 % for the AU experiments and 62 to 107 % for the ZU experiments.

Possible sources of error were by-passing of the sampling probe, poor sensitivity at low turbidity, base-line drift due to temperature effects (discussed in Section 3.4.2) and particle size effects. Identifying the source of the error would be helpful in determining its probable impact on the calculation of detachment rates in the later stages of backwash. For example, by-passing effects during the initial stages of backwash would have little impact on the analysis of the tail of the concentration profile, while base-line drift could be a more serious problem.

For the AU and ZU experiments, the effluent from water only backwash was collected in two separate drums. Therefore, it was possible to compare the accuracy of the meter at the beginning and end of backwash by calculating the expected concentration in each drum separately and comparing it to the measured value. Table 7.1 shows the mass recovery for the first and second drums as well as the overall recovery for each experiment. M_D was not measured in experiment AU77 and the opacity meter output for experiment ZU95 was not recorded.

Overall recoveries ranged from 60 to 119 % for the AU experiments and 62 to 107 % for the ZU experiments. The recovery for the first drum was usually better than the recovery for the second drum.

The % recovery for each drum is plotted against the measured concentration in the drum (c_{D1} and c_{D2}) in Figures 7.5 (a) and (b). For alum, the % recovery for drum 1 decreased with increasing concentration c_{D1} while the recovery for drum 2 showed the opposite trends. This suggested that the opacity meter tended to under-predict higher concentrations in drum 1. The predicted concentration for drum 2 tended to be more accurate for higher concentrations. For Z464N, the recovery for both drums increased with increasing concentration.

For experiments ZU61 to ZU84, the sample that passed through the meter was collected and analyzed separately for suspended solids. This made it possible to check two different aspects of the device's performance. First, the total mass in the opacity meter sample could be compared to the total mass in the backwash water to check how representative the sample was of the backwash. Secondly, the measured concentration in the opacity meter sample could be compared directly to the concentration calculated from the signal output to check the accuracy of the meter.

Table 7.1(a) Opacity meter recoveries for AU61 to AU70

Experiment	Volume 1	Recovery	Volume 2	Recovery	M_D, g/m^2	Overall recovery
AU70	91 L	62 %	40 L	31 %	817	60 %
AU68	94 L	76 %	38 L	39 %	652	70 %
AU64	95 L	85 %	38 L	70 %	645	80 %
AU61_29h	92 L	80 %	38 L	61 %	686	76 %
AU61_26h	24 L	117 %	115 L	126 %	502	119 %
AU61_17h	75 L	73 %	55 L	101 %	338	74 %

Table 7.1(b) Opacity meter recoveries for ZU61 to ZU94

Experiment	Volume 1	Recovery	Volume 2	Recovery	M_D, g/m^2	Overall recovery
ZU94	70 L	81 %	66 L	64 %	550	79 %
ZU84	81 L	104 %	56 L	93 %	556	102 %
ZU81	83 L	82 %	45 L	129 %	518	86 %
ZU78	77 L	98 %	59 L	82 %	521	96 %
ZU74	75 L	109 %	59 L	88 %	542	107 %
ZU70	72 L	73 %	65 L	72 %	401	73 %
ZU67	106 L	78 %	35 L	58 %	433	77 %
ZU64	66 L	85 %	72 L	77 %	403	84 %
ZU61	62 L	61 %	69 L	76 %	403	62 %

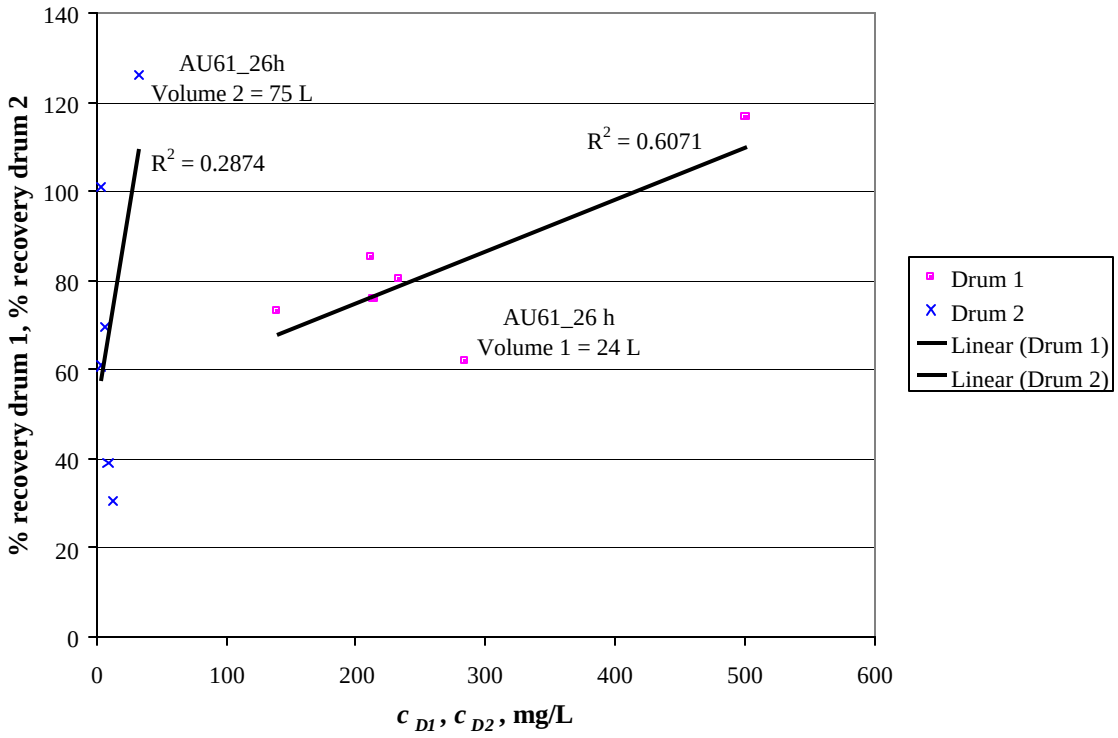

Figure 7.5(a) % recovery for each drum – AU61_17h to AU70

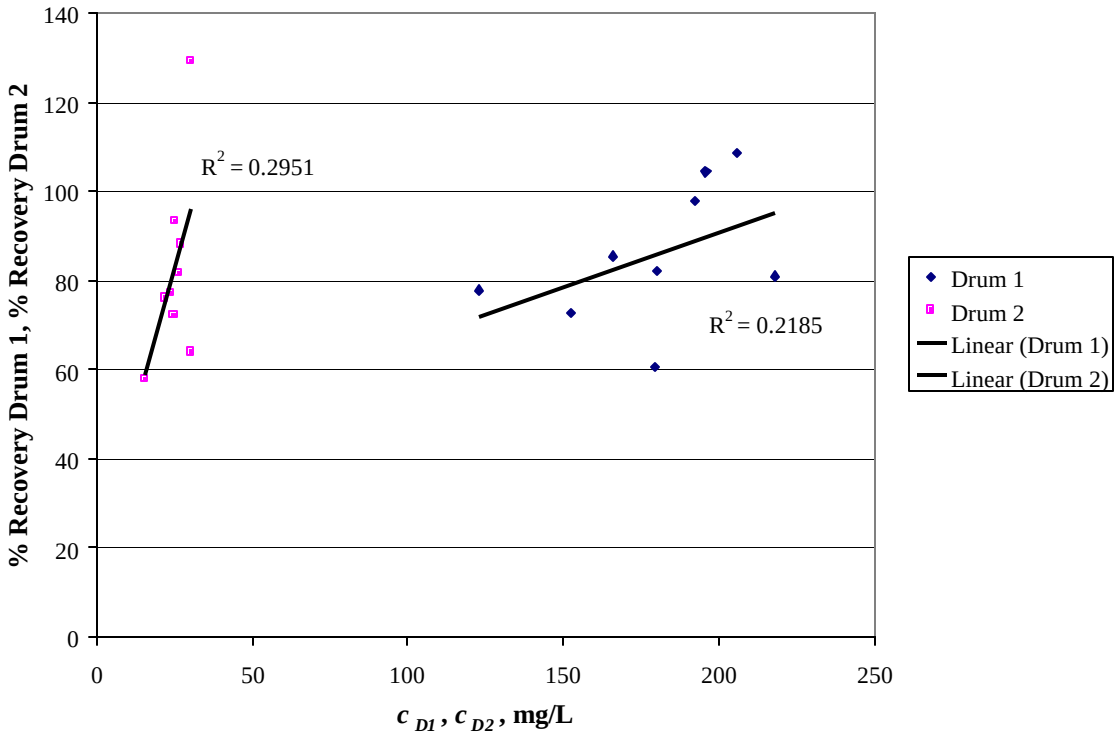

Figure 7.5(b) % recovery for each drum – ZU61 to ZU94

Table 7.2 summarizes the results for sample recovery (Equation 5.29), meter recovery (5.31) and overall agreement between the measured results and calculated solids detached (5.28). The meter accuracy was better than the overall accuracy in 5 out of 9 cases but the variability was greater (69 to 155 % compared to 62 to 100 %). Figure 7.6 (a) and (b) show the meter, sampling and overall recovery plotted against M_{TF} and M_D for the ZU experiments. There was no correlation between sampling recovery and mass detached but both the meter and overall recovery increased with increasing M_D. However, the sampling recovery decreased with increasing M_{TF}.

Table 7.2 Sampling, meter and overall recoveries for ZU61 to ZU84

Experiment	Overall recovery $\frac{M_{PD}}{M_D}\times 100\%$	% sampling recovery	% meter recovery
ZU84	102 %	90 %	136 %
ZU81	86 %	90 %	98 %
ZU78	96 %	96 %	101 %
ZU74	107 %	77 %	155 %
ZU70	73 %	113 %	69 %
ZU67	77 %	90 %	85 %
ZU64	84 %	82 %	101 %
ZU61	62 %	69 %	92 %

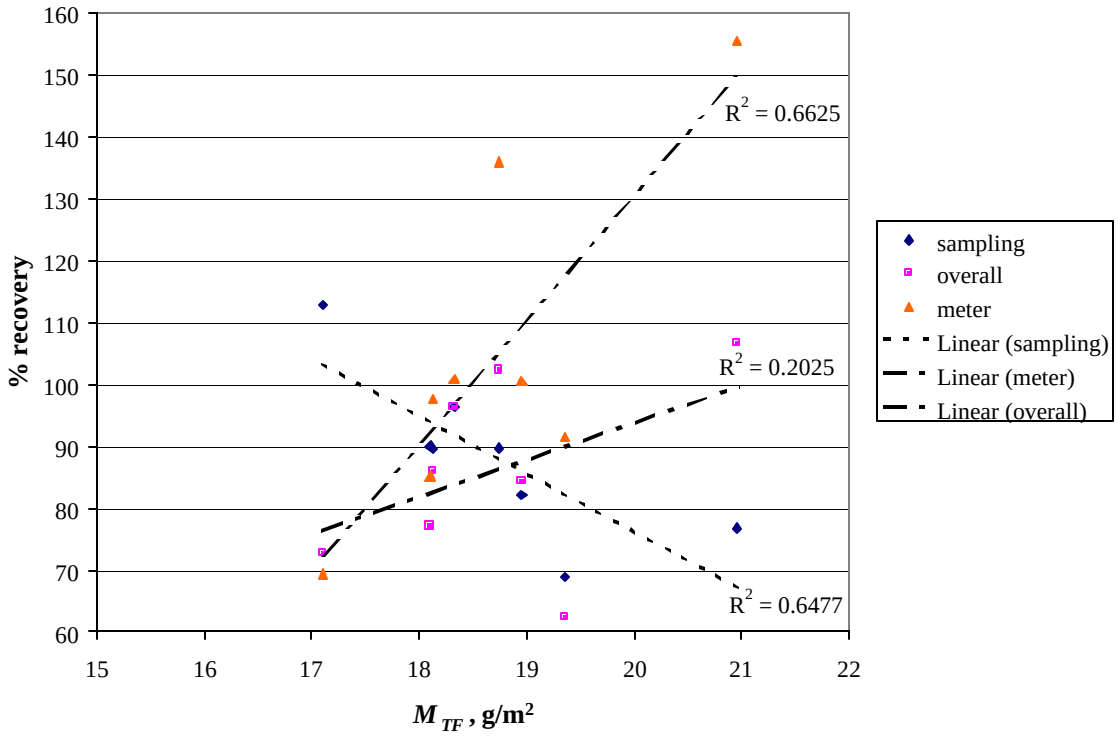

Figure 7.6 (a) % recovery vs M_{TF} – ZU experiments

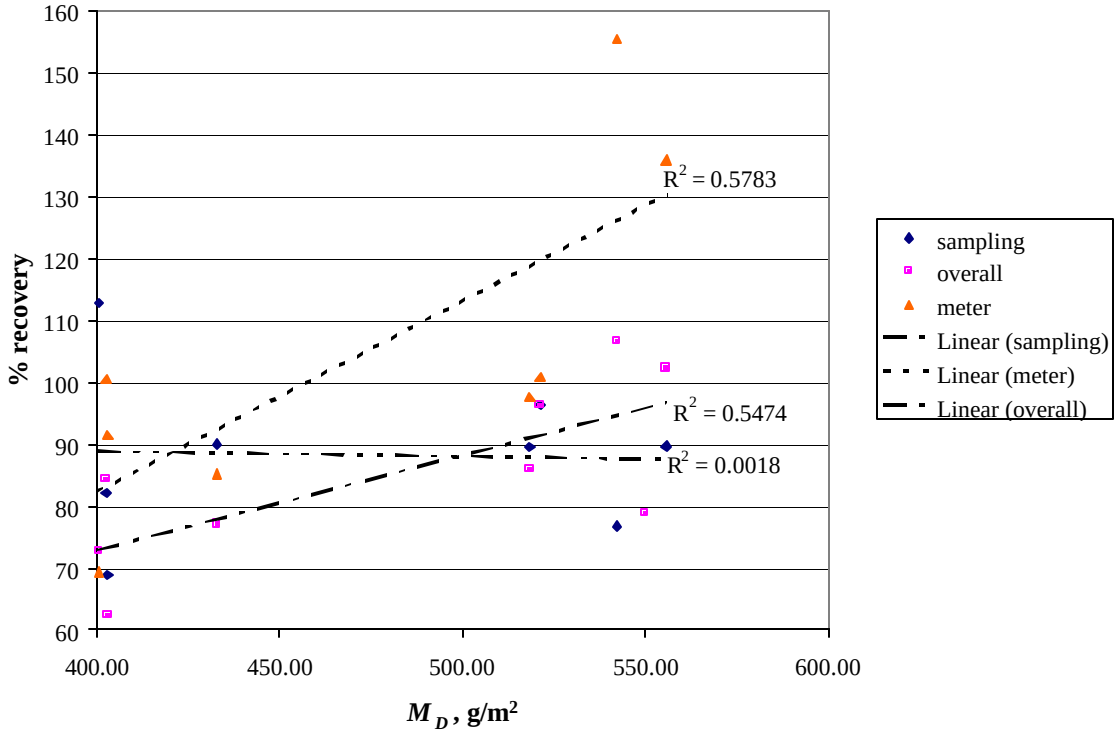

Figure 7.6 (b) % recovery vs M_D – ZU experiments

Low sampling recoveries would result from high local concentrations of detached floc bypassing the sampling probe. This would be most likely to occur as the surface of the bed broke open at the edge of the filter. Since the lop-sidedness of the disintegration process increased with increased loading of the filter, it makes sense that greater values of M_{TF} would be associated with greater variability of the concentration across the filter cross-section and greater potential for bypassing. It can also be inferred that the sampling recovery was worse for the alum than the Z464N experiments. The overall recoveries for the AU experiments are plotted against M_{TF} and M_D in Figure 7.7. The overall recovery decreases with increasing M_{TF} and M_D, which is consistent with low sampling recoveries due to bypassing.

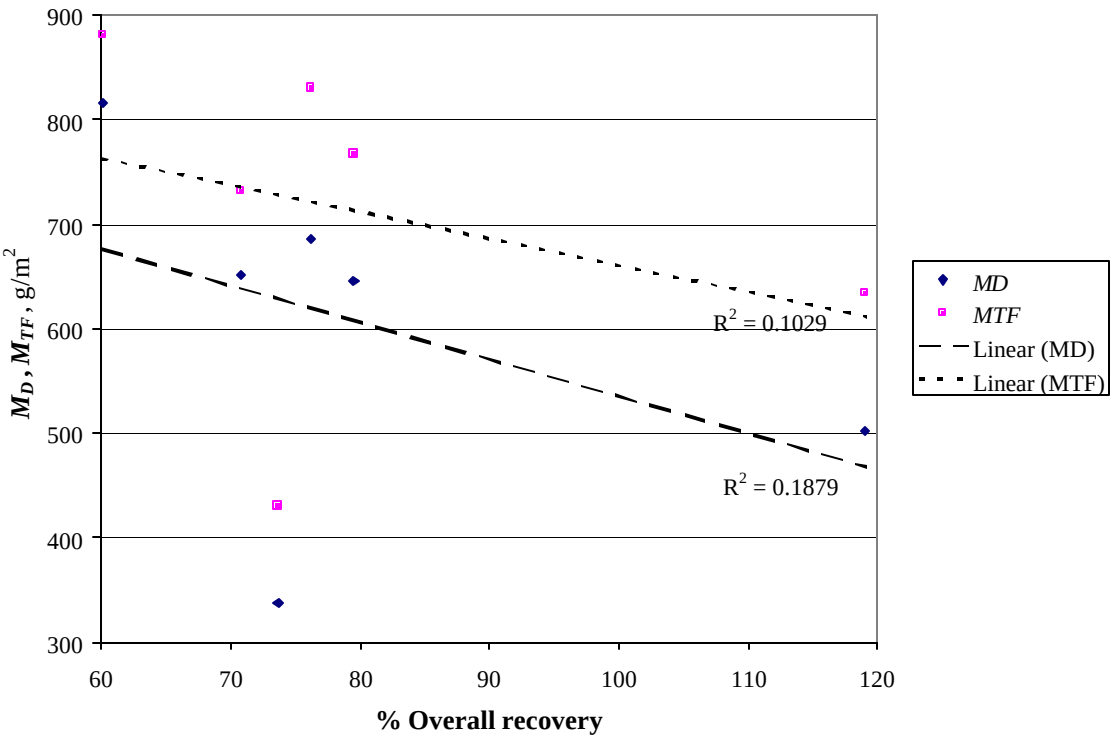

Figure 7.7 M_D and M_{TF} vs overall recovery for AU experiments

Overall it can be concluded that the opacity meter was generally not able to capture the peak concentration very accurately due to bypassing effects, particularly for the alum experiments. The meter was also not accurate at low concentrations at the end of backwash due to the inherent limitations of the detector. However, the overall recoveries were reasonable (60 to 119 % for alum and 62 to 107 % for Z64N) and it is probable that the measurement of concentration in the intermediate region was sufficiently accurate to yield information about the kinetics of detachment.

7.4. Experimental determination of the detachment rate constant from the backwash concentration profile

According to Huang and Basagoiti (1989) and Amirtharajah (1985), the backwash concentration should be related to the rate of detachment by a function of the form

$$c = b \exp\left(-k_3 t\right) \tag{7.2}$$

k_3 = Rate of detachment constant, 1/s

b = A function of the porosity and specific deposit

For Equation 7.2 to be valid, the specific deposit must be uniform throughout the zone in which detachment is occurring and that zone must have been flushed at least once (so each element of fluid leaving the bed has had the same contact time with the dirty media). The deposits in the fixed bed are not uniformly distributed but, based on the backwash videos, the

media does get mixed up to some extent at the beginning of backwash. However, as the media settles out, it presumably also re-stratifies. Since the heaviest floc deposits and lowest rates of energy dissipation are associated with the finest media grains, the residual floc deposits would tend to once again become concentrated in the top layers.

Equation 7.2 can still be held to valid if it is assumed that, while the total residual deposits are concentrated near the surface, the detachable fraction of the deposits is more uniformly distributed and/or the zone in which detachment is occurring is sufficiently thin that the distribution of deposits within the zone has little impact on the predicted concentration profile. It is not necessary to assume that the deposits are uniformly distributed throughout the depth of the bed.

In the current study, it was assumed that once the disintegration of the clogged bed was completed and the resulting turbulence had died down, the bed would have to be flushed at least once before the effect of the intrinsic detachment rate could be determined. The time at which the disintegration was complete was estimated using the fluctuations in the pressure signal. Figure 7.8 shows dh as a function of time for several different experiments with different backwash rates and degrees of clogging. dh was calculated as

$$dh_i = h_i - h_{i-1} \tag{7.3}$$

h_i = headloss measurement at time t_i

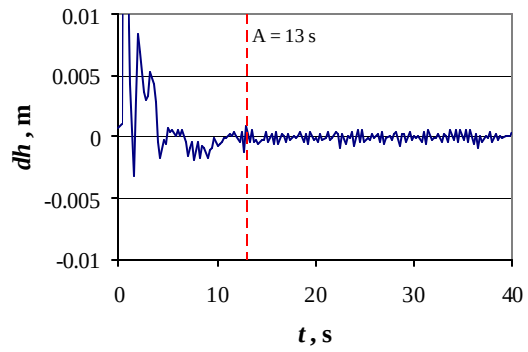

(a) AU61_17 h

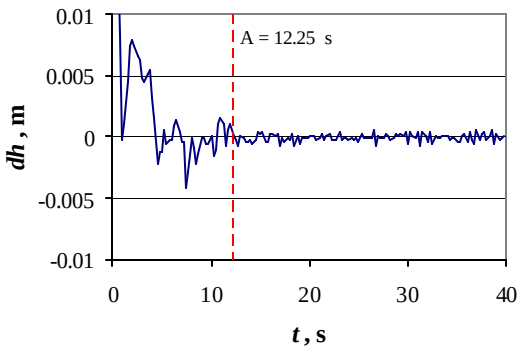

(b) ZU61

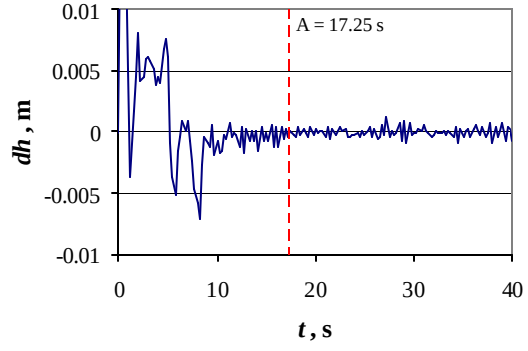

(c) AU61_29 h

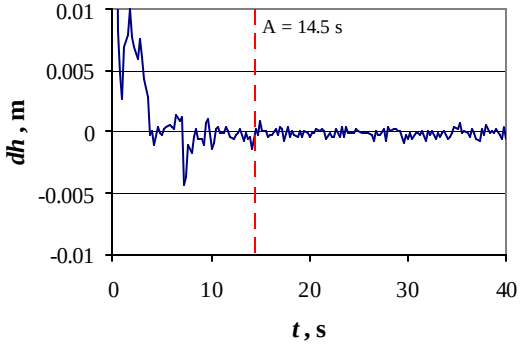

(d) ZU70

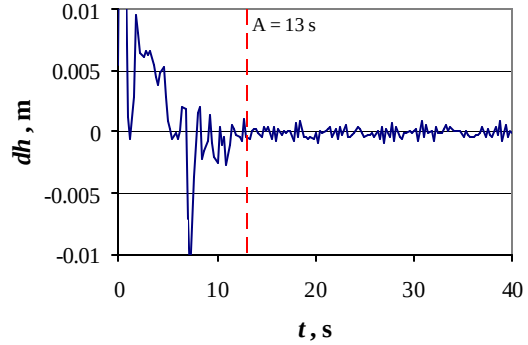

(e) AU70

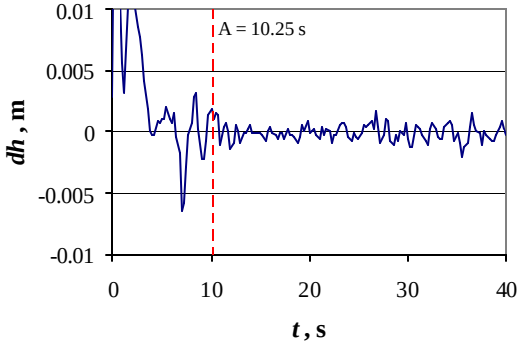

(f) ZU94

Figure 7.8 Headloss fluctuations

The oscillation in the headloss signal decayed rapidly over the first 10 s. Thereafter, the behavior of the signal was slightly different in each case but in all cases, mixing was clearly over after 20 s. The only trend observed was that the magnitude of the oscillations after 10 s increased with increasing backwash rate. When each signal was inspected more closely, it was not always easy to define an exact point at which the oscillation due to mixing disappeared. For the sake of consistency, the time at which the intense mixing was assumed to be over was one interval (0.25 s) after the last peak (positive or negative) that was larger than any oscillation measured after 20 s. This is indicated by the vertical line A on the headloss fluctuation plot for each experiment in Figure 7.8. The procedure for selecting A is illustrated in Figure 7.9, which shows the plot for AU70 on expanded axes.

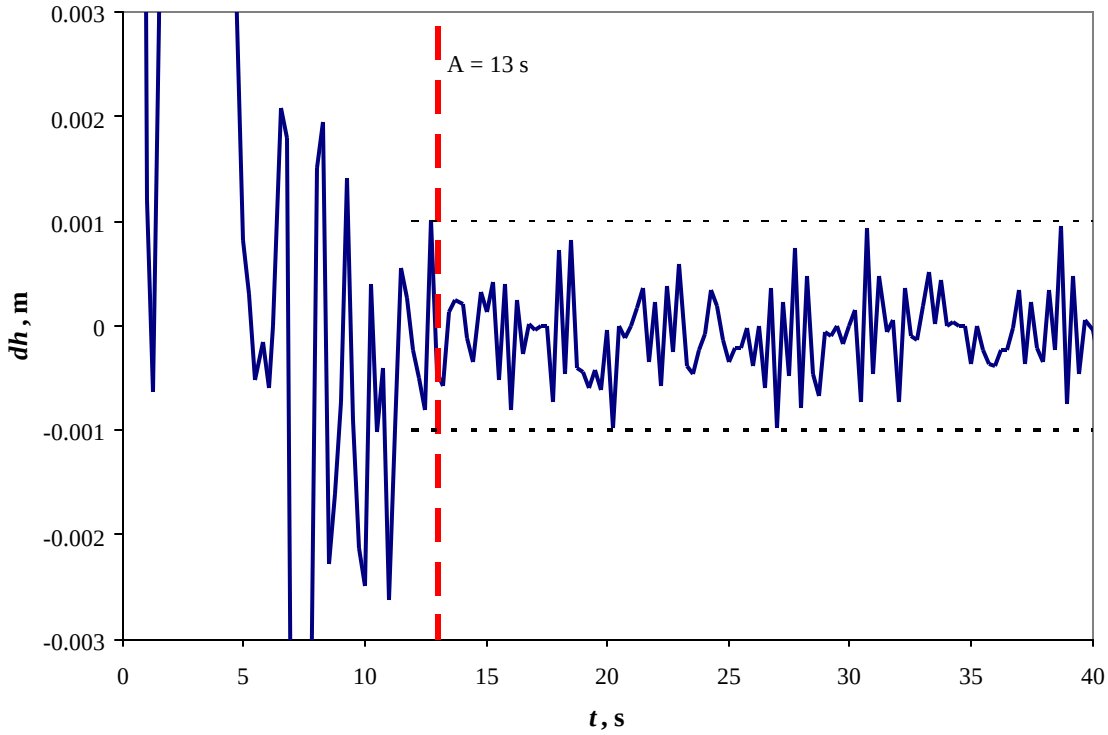

Figure 7.9 Estimating the time at which initial mixing ends – Experiment AU70

If Equation 7.2 is valid then the later part of the concentration profile should approximate a straight line when plotted on a log-linear scale. The concentration profiles from Section 7.2 are reproduced in Figures 7.10. to 7.12 as log-linear plots. Only the constant backwash velocity portion of the concentration profile was considered in determining the detachment rate so data corresponding to the turn down period of each experiment are not shown.

The four lines in addition to A (time at which pressure oscillations die down) in Figures 7.10 to 7.12 indicate the times required to flush the bed to remove the remnants of the disintegration process. These are

B: The time for one fluid volume (base of the filter to sampling probe) to pass through the filter.

C: The time for the pressure drop fluctuations to die down and for the filter to then be flushed with one fluid volume (A+B)

D: The time for two fluid volumes to pass through the filter (2 x B)

E: The time for the pressure drop fluctuations to die down and for the filter to then be flushed with two fluid volumes (A+D).

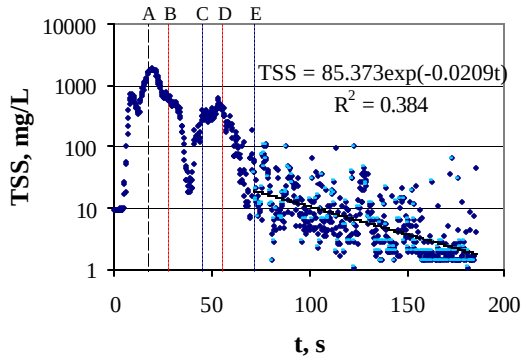

(a) AU61_29h - M_{TF} = 830 g/m^2

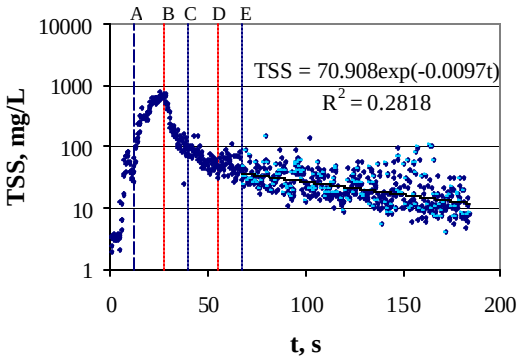

(b) ZU61 - M_{TF} = 661 g/m^2

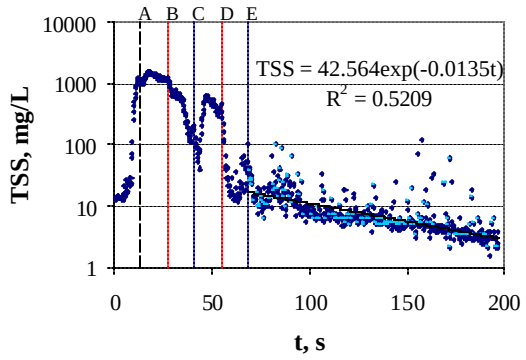

(c) AU61_26h - M_{TF} = 633 g/m^2

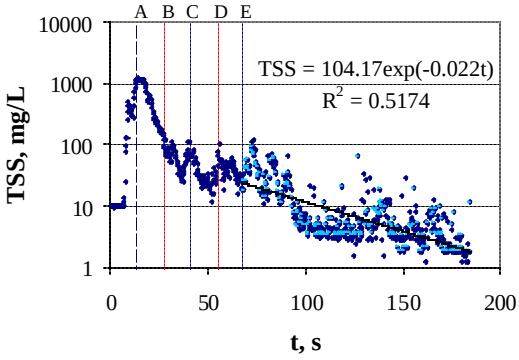

(d) AU61_17h - M_{TF} = 430 g/m^2

Figure 7.10 Log-linear backwash concentration profiles for 61 m/h

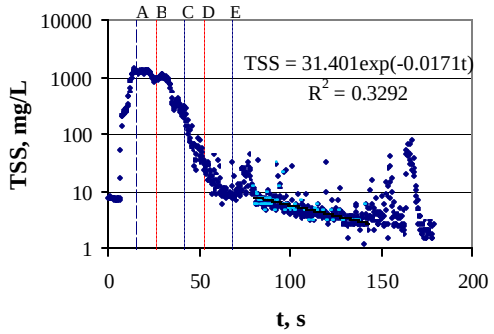

(a) AU64 - M_{TF} = 767 g/m^2

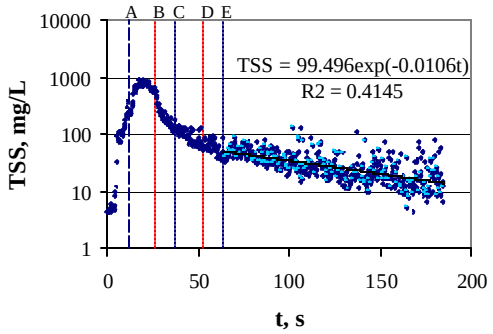

(b) ZU64 - M_{TF} = 603 g/m^2

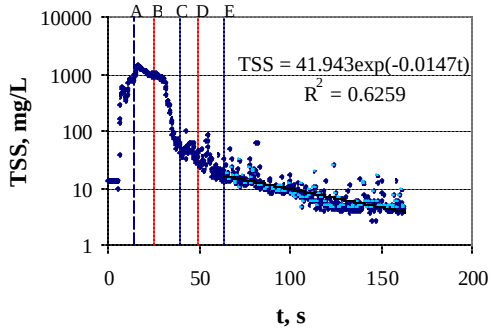

(c) AU68 - M_{TF} = 731 g/m^2

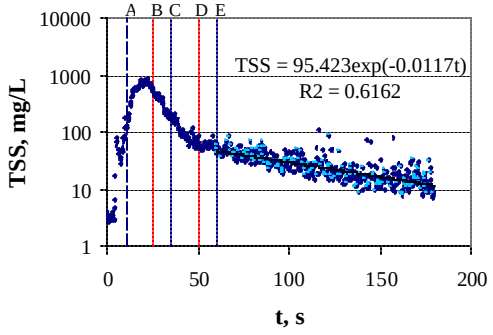

(d) ZU67 - M_{TF} = 576 g/m^2

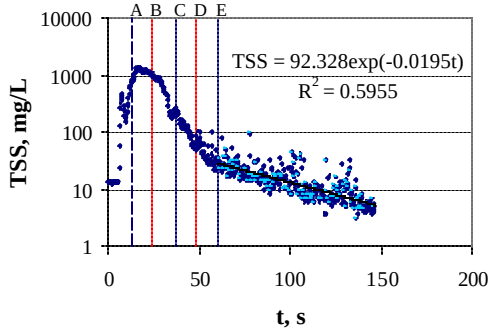

(e) AU70 - M_{TF} = 881 g/m^2

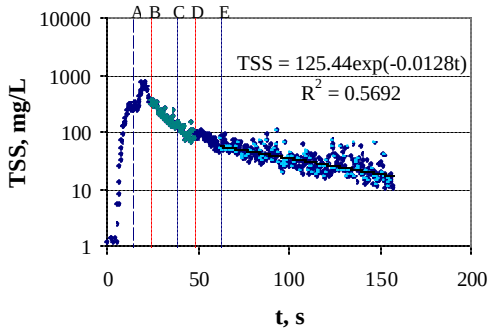

(f) ZU70 - M_{TF} = 545 g/m^2

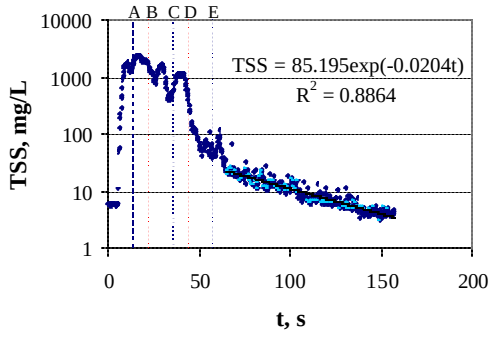

(g) AU77 - M_{TF} = not measured

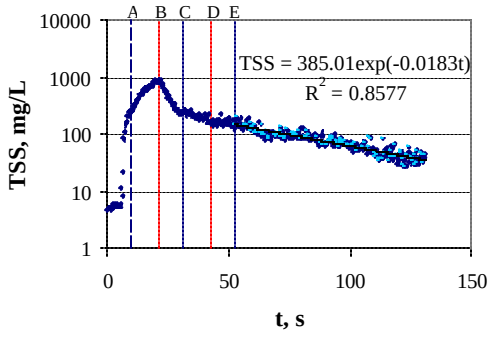

(h) ZU78 - M_{TF} = 583 g/m^2

Figure 7.11 Log-linear concentration profiles for 64 to 77 m/h

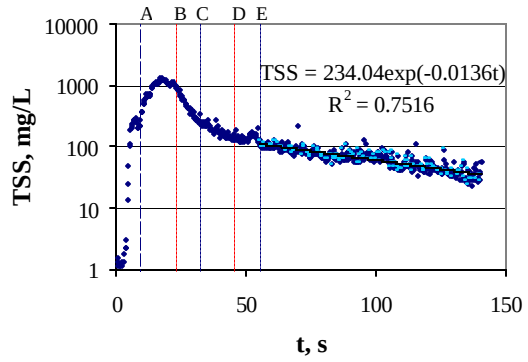

(a) ZU74 - M_{TF} = 667 g/m^2

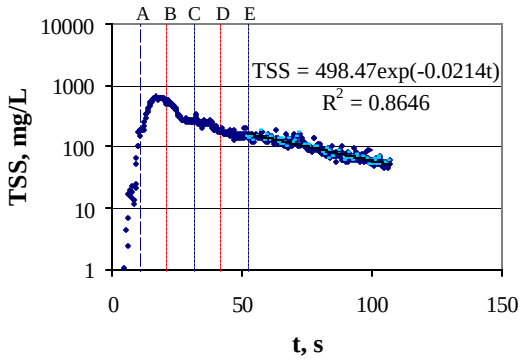

(b) ZU81 - M_{TF} = 577 g/m^2

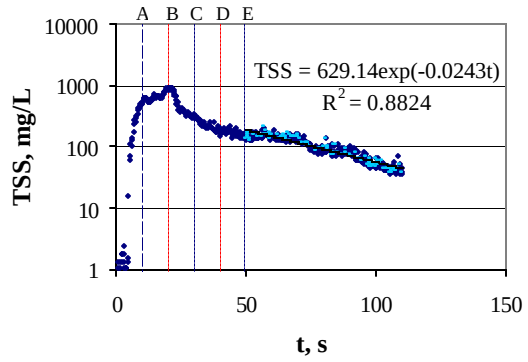

(c) ZU84 - M_{TF} = 597 g/m^2

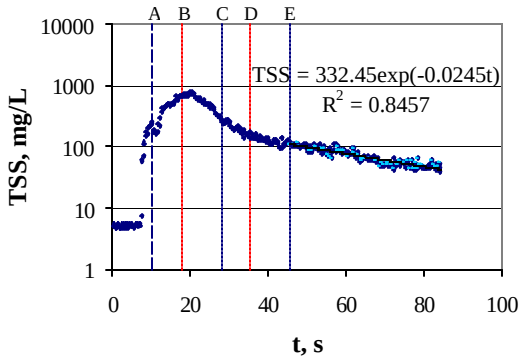

(d) ZU94 - M_{TF} = 569 g/m^2

Figure 7.12 Log-linear concentration profiles for ZU74 to ZU94

The log-linear scale tended to emphasize the scatter in the measurements in the range < 100 mg/L. Increased scatter was associated with lower backwash rates and higher degrees of clogging and may have been the result of mixing and/or flocculation effects in the vicinity of the sampling probe. Spikes in turbidity would have resulted from larger flocs being drawn into the sampler. Since the floc leaving the filter bed was not uniformly mixed across the cross section, it was not clear whether the scatter was representative of the variability in the backwash effluent concentration or not. Furthermore, since overall recoveries through the meter tended to be less

than 100 % (Tables 7.1 and 7.2) there was no clear justification for filtering out the larger peaks. Therefore no attempt was made to smooth the data.

For most of the alum experiments, the log-linear section of the concentration profile appeared to start around E, that is two fluid volumes after the pressure oscillations died down. For the Z464N experiments, the log-linear portion appeared to start a little earlier, at D at lower backwash rates and C at backwash rates greater than 70 m/h. This may have been due to less intense mixing at the beginning of backwash. For the sake of consistency, the section from E to the start of the backwash rate turn down was used to estimate the intrinsic detachment rate constant, k_3, in Equation 7.2 for both alum and Z464N experiments. The exponential trendline for the log-linear section of the profile is shown on each plot.

If the empirically determined rate parameters actually reflected the intrinsic rate of detachment then they might be expected to be correlated with the efficiency of backwash. If on the other hand, they were merely artifacts of mixing processes then they might be better correlated with other factors such total mass deposited and/or detached.

Figures 7.13 to 7.16 show the regression coefficient k_3 plotted against backwash rate, mass retained, mass detached and total mass deposited. The upper and lower estimates of the total mass deposited, mass detached and mass retained were discussed in Chapter 5. 95 % confidence intervals for k_3 were calculated in the regression analysis (Microsoft Excel Regression tool).

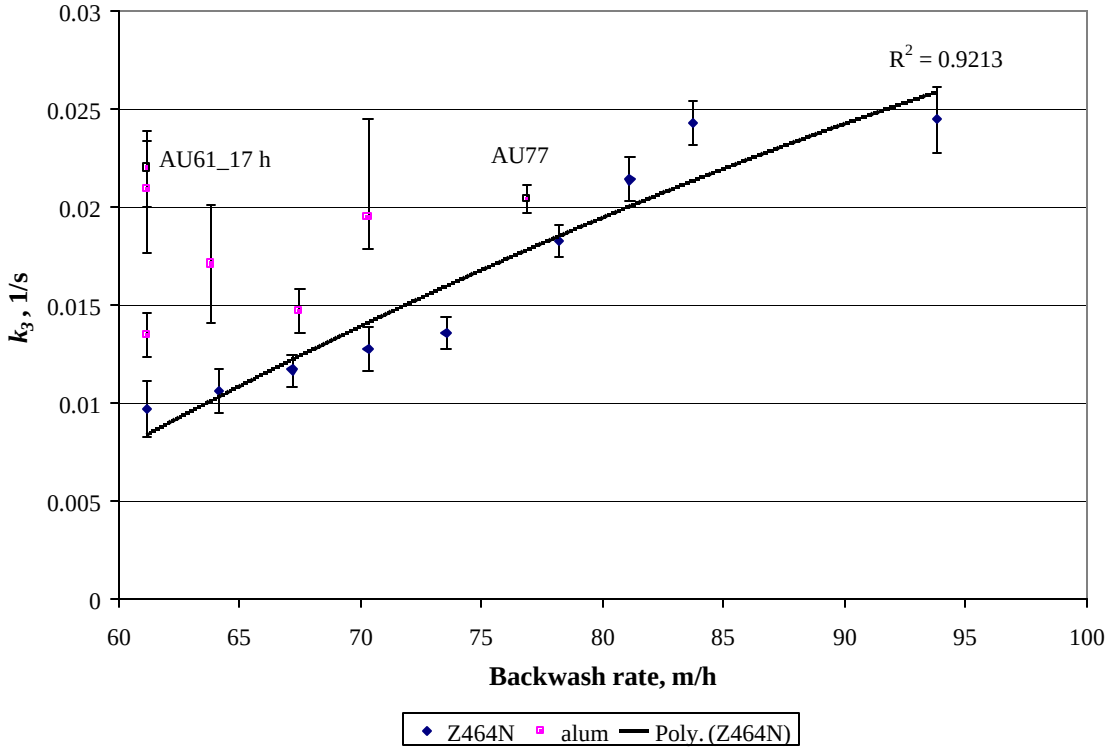

Figure 7.13 k_3 vs backwash rate

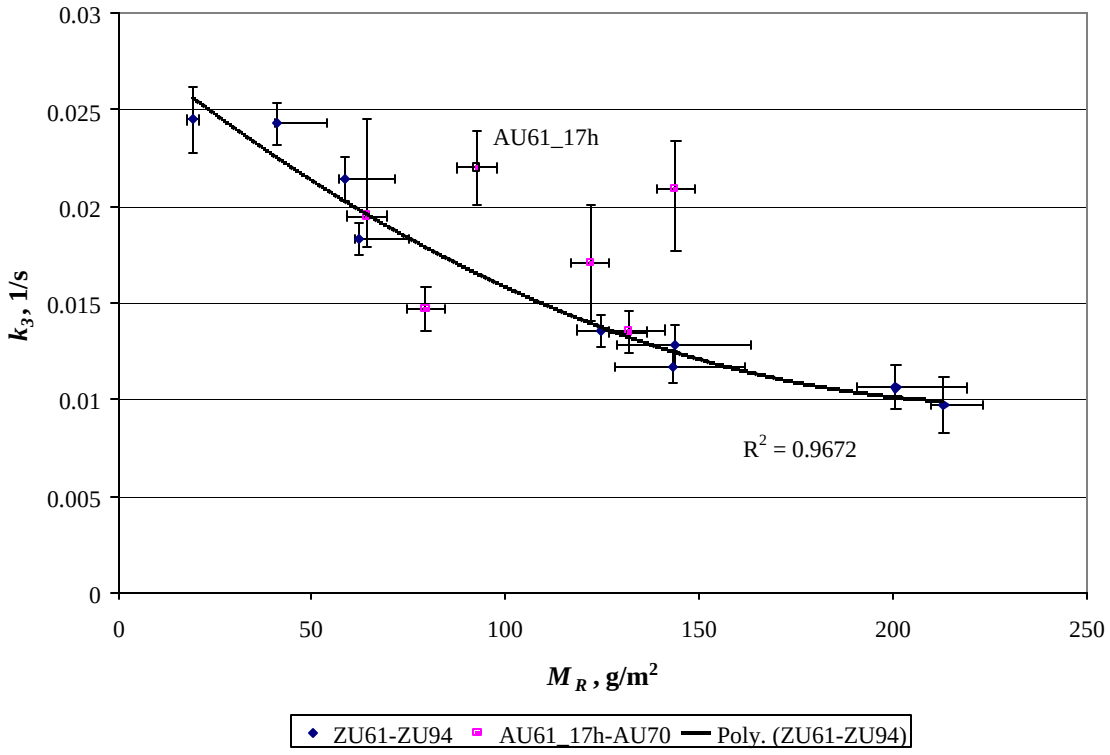

Figure 7.14 k_3 vs mass retained

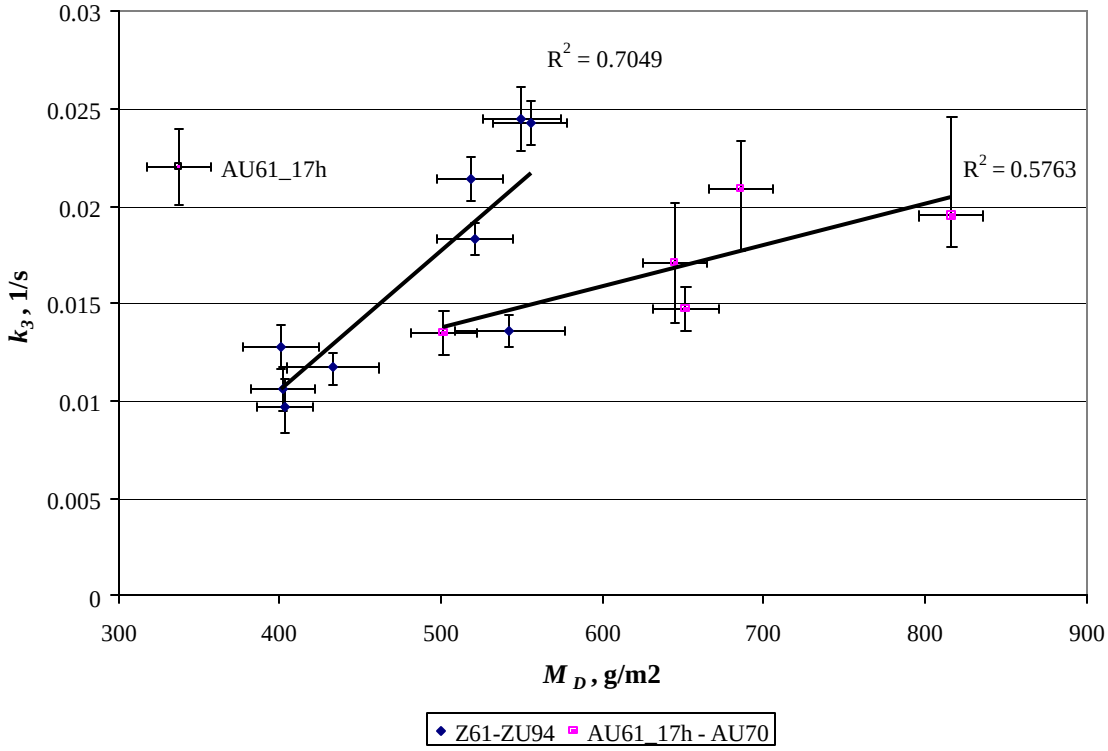

Figure 7.15 k_3 vs mass detached

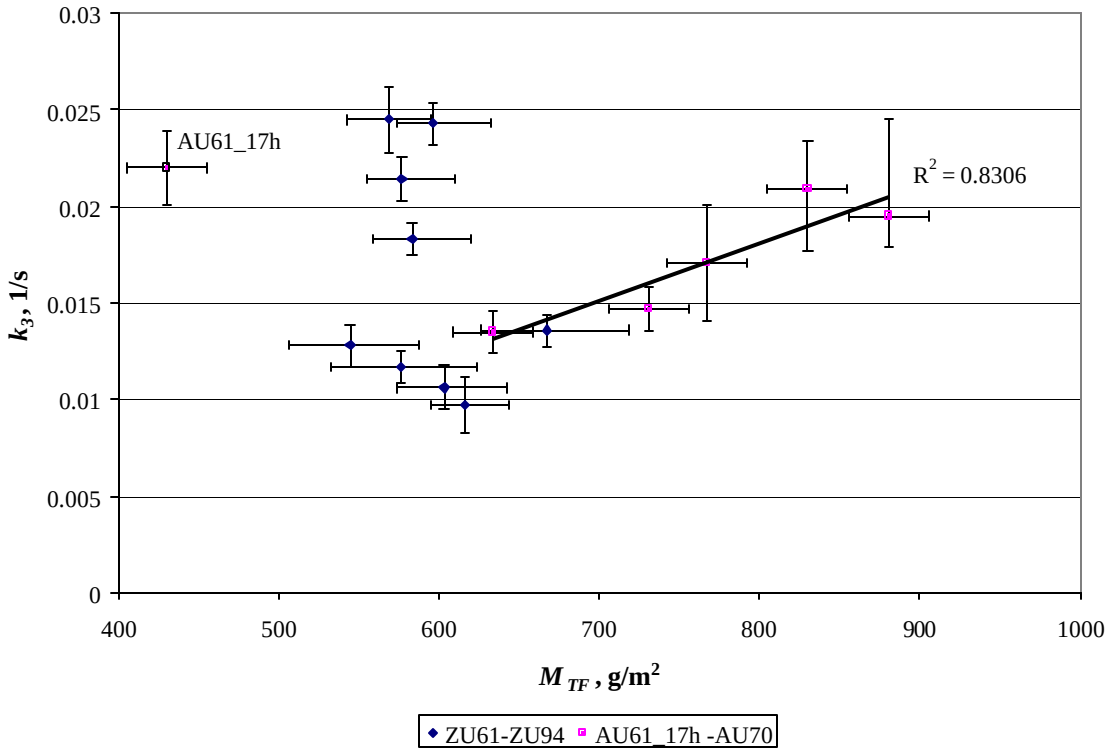

Figure 7.16 k_3 vs total mass deposited

For the Z464N experiments there is a strong correlation between k_3 and both backwash rate and mass retained. There was no correlation between k_3 and total mass deposited. The correlation between k_3 and mass detached (water only backwash) is weaker then the correlation with mass retained and simply reflects the fact that mass detached is negatively correlated with mass retained.

By contrast, for the alum experiments, k_3 was most strongly correlated with total mass deposited and showed little correlation with either mass retained or backwash rate. Furthermore, the k_3's were higher for alum than Z464N at the same backwash rates. However, it was interesting to note that the k_3 values for alum were most comparable to the values of Z464N when plotted against mass retained.

These results support the view that the alum deposits were detached more or less instantaneously and that the slope of the tail of the turbidity profile was determined mainly by mixing effects. However, for Z464N, a significant fraction of the deposits detached more slowly at a rate related to the efficiency of backwash. Furthermore, mixing near the beginning of backwash appeared to be less intense making it easier to distinguish the detachment rate from the effect of mixing.

It therefore appears that for weaker floc deposits, the slope of the backwash concentration profile will not yield the intrinsic rate of detachment, whereas for stronger deposits that detach more slowly, Equation 7.2 can be applied to the tail end of backwash.

7.5. Modeling the backwash concentration profile

In this study, two distinct phases of the backwash process were identified. The first phase is the transition from the fixed to the fluidized bed. In the second phase, the media is fully fluidized. Three of the four models reviewed in the study strictly speaking only applied to the second, fluidized stage. Only Hall and Fitzpatrick (1998) accounted for some dislodgement of floc during the expansion stage. However, these authors assumed the expansion process was smooth and orderly whereas experimental observations clearly demonstrate it is actually quite chaotic. The grains in the top section of the bed remain cemented together until the whole structure erodes and disintegrates starting at weak points at the filter wall. The disintegration and collapse of the top of the filter results in short term flow localization and violent mixing.

Not only is a large amount of floc released during the disintegration, but the intense initial mixing means that remnants of the disintegration process remain in the filter for some time after the mixing subsides. The influence of the two phases of backwash on the concentration profile are illustrated in Figure 7.17.

Modeling the disintegration phase of the backwash process would be difficult. As discussed previously, the scale, timing and violence of the associated mixing is a function of several factors including the clogged state of the filter bed and the equipment in which the experiment is being carried out.

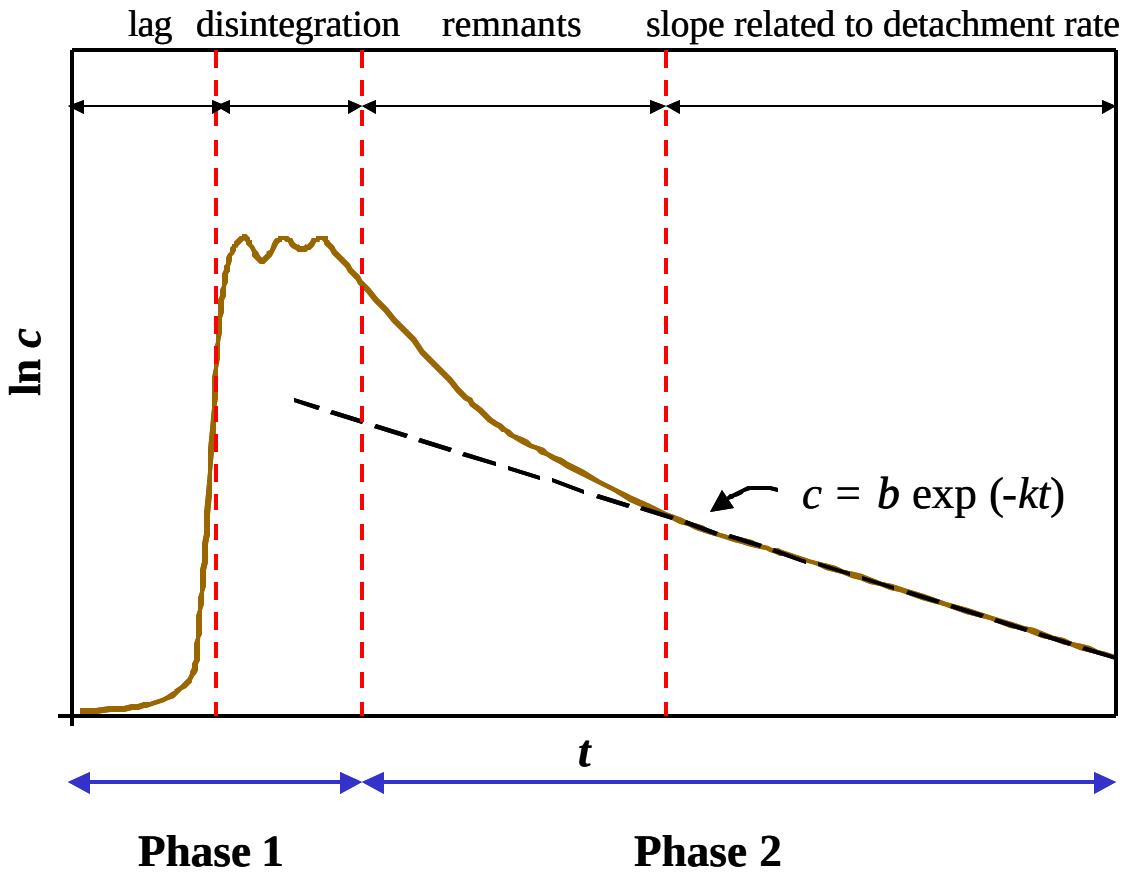

Figure 7.17 Effect of backwash phases on the effluent concentration profile

The simplest possible model of this phase would be to assume that, for a limited period of time, the top section of the filter bed could be modeled as a completely mixed flow reactor as shown in Figure 7.18. During this period, the concentration of suspended solids and remaining media deposits would be assumed to be uniform throughout the mixing zone. The average rate of detachment could either be assumed to be constant or proportional to the mass of deposit remaining ($M_R(t)$). The rate constant k_{mix} would a be fitting parameter in the resulting model of the concentration profile. The period of mixing, t_{mix}, could for example be assumed to last from

the time that the surface of the clogged bed breaks open to the time that the pressure fluctuations die down, or it could be treated as a fitting parameter. Similarly, the volume V_{mix} could be estimated from visual observations of the filter bed or treated as a fitting parameter in a model of the backwash concentration profile.

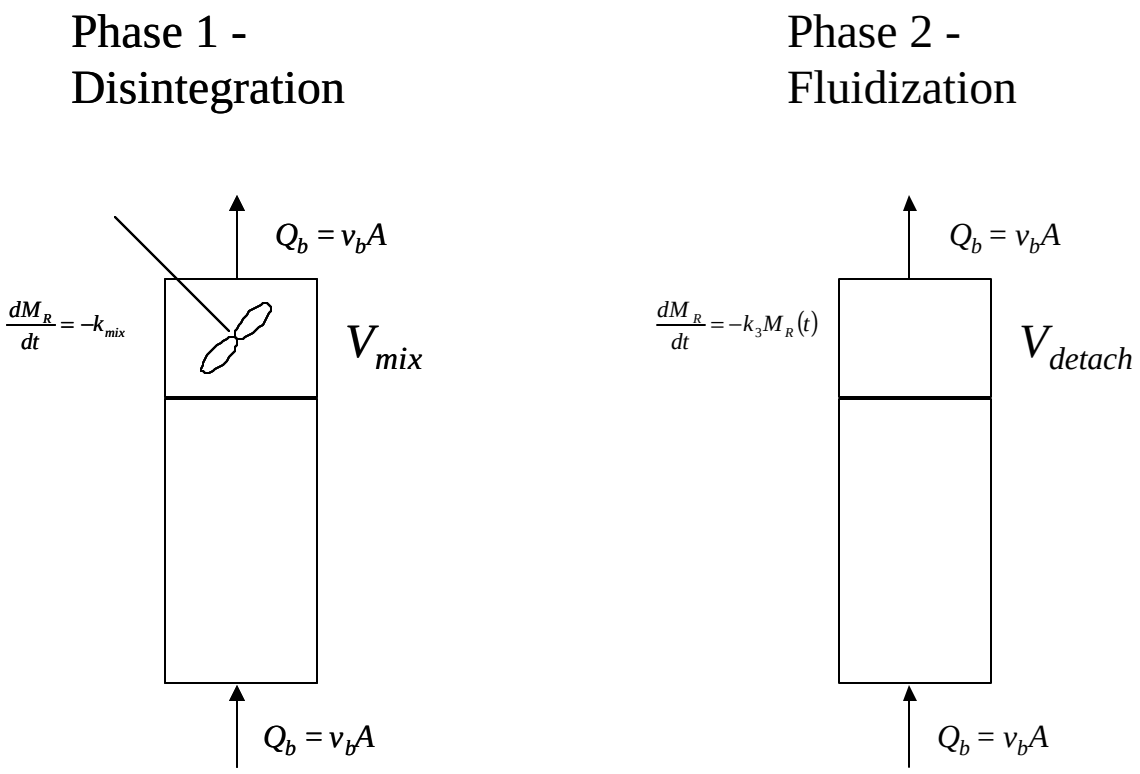

Figure 7.18 Conceptual model of phases of backwash

Once the mixing period was over, the filter would be assumed to return to a plug flow situation. In this case, the model of Huang and Basagoiti (1989) discussed in Section 2.3.3. could reasonably be applied, except that it would be assumed that the residual floc deposits

were confined to the top section of the filter rather than distributed through the entire filter depth. The volume V_{detach} would be a fitting parameter which might be different in value to V_{mix}.

There are two points to note about this modeling approach. The first is that the parameters V_{mix}, t_{mix}, k_{mix} and V_{detach} would be specific to the experimental conditions and equipment in which they were measured so that the results could not be scaled up. However, if it was demonstrated that the proposed model captured the essential features of the backwash process at laboratory scale, then it could theoretically also be calibrated with data from full-scale filters.

The second and more important point is that the same approach would be applicable to systems using auxiliary backwash and in fact, it would probably be easier to apply. When either air or surface wash is used, energy dissipation is more uniformly distributed through the clogged regions of the bed, than when up-flow wash alone is used. Furthermore, the intensity of the agitation of the media can be varied by adjusting the air or surface wash rates, making it easier to study the effect of energy dissipation on the detachment rates.

When an auxiliary wash is used, the mixing period would probably have two characteristic detachment rates: one for the disintegration of the clogged layers and another for detachment from fluidized grains while the auxiliary system is still in operation. The mixing volume would be easier to estimate than in the up-flow wash only case since the mixing action would be sustained for a longer period of time.

Overall, it can be concluded that given the complexity of the disintegration process in up-flow water only backwash, there is no advantage in terms of simplicity in trying to model this backwash regime instead of the more technologically relevant case of backwash with auxiliary wash. There are however, still a few applications for water only backwash, such as the autonomous valveless filters discussed in Chapter 1 and Chapter 8.

CHAPTER 8

MASS ACCUMULATION AND THE GROWTH OF MUDBALLS IN FILTERS

8.1. Introduction

Chapters 5 and 6 focused on the phenomena observed in filters within the timescale of a single backwash. Of greater importance is how backwash conditions impact the filter in the long term. Failure to adequately clean filters during backwashing results in the deterioration of the state of the filter bed, which can eventually negatively impact the performance of the filter. Filters with inefficient backwash tend to accumulate aggregates of dirt, media and coagulant known as "mudballs" (Logsdon et al., 2002). These can grow into inactive sub-surface masses of clogged material, which increase local velocities in the filter with a potentially negative impact on filtrate turbidity and filter run time (Cleasby, 1990). Clogged regions of the filter also tend to contract as the headloss increases, causing the development of cracks in the bed, which result in short circuiting of the filter influent and a subsequent decline in filtered water quality.

Filter cracking and mudballing problems are essentially inevitable in filters which do not employ auxiliary backwash (Baylis, 1959) and recognition of this fact has led to the widespread use of either air scour or surface wash systems in filtration plants throughout the world. However, there has been very little research that quantifies the rate of accumulation of mud in

filters as a function of backwash conditions. Such information could be useful for designing filtration processes to be more robust when optimal backwash conditions cannot be guaranteed, for example in rural areas with a shortage of skilled operators and maintenance staff.

This chapter discusses the phenomenon of filter mudballing and presents a possible approach to modeling the deterioration of the filter media in order to be able to predict the useful life of a filter bed. Section 8.2 discusses the mechanisms of mudball formation and Section 8.3 presents experimental data on the rate of mud accumulation. Section 8.4 presents some preliminary ideas on the quantitative modeling of mudball accumulation and discusses how experimental data could be incorporated into such a model.

8.2. Mechanisms of mudball formation

Mudballing has been a major concern in the management of rapid filters in water treatment for as long as they have been used in the industry. Several theories on how mudballs form and accumulate have been advanced.

Baylis (1954) suggested that compaction of floc deposits at high filter headlosses (2.5 to 3 m) resulted in the formation of mud particles that did not break down during water only fluidization backwash and were too heavy to flush out of the filter without using excessively high flow rates which would lead to media losses. With each subsequent filter run, the mud particles would become more compacted and would grow in size as additional material deposited on

them and smaller particles became fused into larger masses. Newly formed mudballs would tend to remain close to the surface of the bed after washing but eventually become heavy enough to cause them to sink deeper into the filter during fluidization. Mudballs could also become clumped together within the filter bed, forming large solidified masses at the bottom of the bed or adjacent to the walls

Baylis (1954) went on to note that the rate of growth of the mudballs within the media is reduced by abrasion of the filter sand during backwash. When the rate of abrasion equals the rate of growth the volume of clogged areas in the filter does not change. In some cases, especially in the colder months, the clogged volume may even decrease.

Baylis (1954) was ambiguous about the role of the filter media in the formation of mudballs. He commented that some sand is usually incorporated into the mudballs, increasing their weight. However, later texts have defined mudballs as aggregates of filter media and mud (dirt and coagulant) (Cleasby, 1990; Logsdon, et al. 2002). Cleasby (1990) suggested that mudballs are formed when the heaviest solids deposits near the surface of the bed break into pieces during backwash (i.e. when the disintegration of the bed described in Chapter 6 is not complete).

Kawamura (1975a) analyzed the size of sand encapsulated in mudballs found in the upper portions of a sand filter from the Amagasaki Filtration Plant in Japan and found that most of the sand was of much smaller size than the effective size of the bed (d_{10} = 0.33 mm vs. d_{10} =

0.55 mm) and of very uniform size (UC = 1.2 vs UC = 1.5). He also quoted a study by the City of Kyoto which found that 0.45 mm filters accumulated ten times more mud than 0.7 mm sand filters over a period of 4years with backwash at the same rate (Water Dept., City of Kyoto, 1956). Kawamura concluded that a small fraction of the sand formed the core of individual small mudballs, which grew rapidly into large mudballs or lumps in the absence of auxiliary wash. He therefore recommended (a) skimming off the top 2.5 to 5 cm of the stratified filter media every time a new layer is added to a filter and (b) using coarser and more uniformly sized media in filters without auxiliary wash.

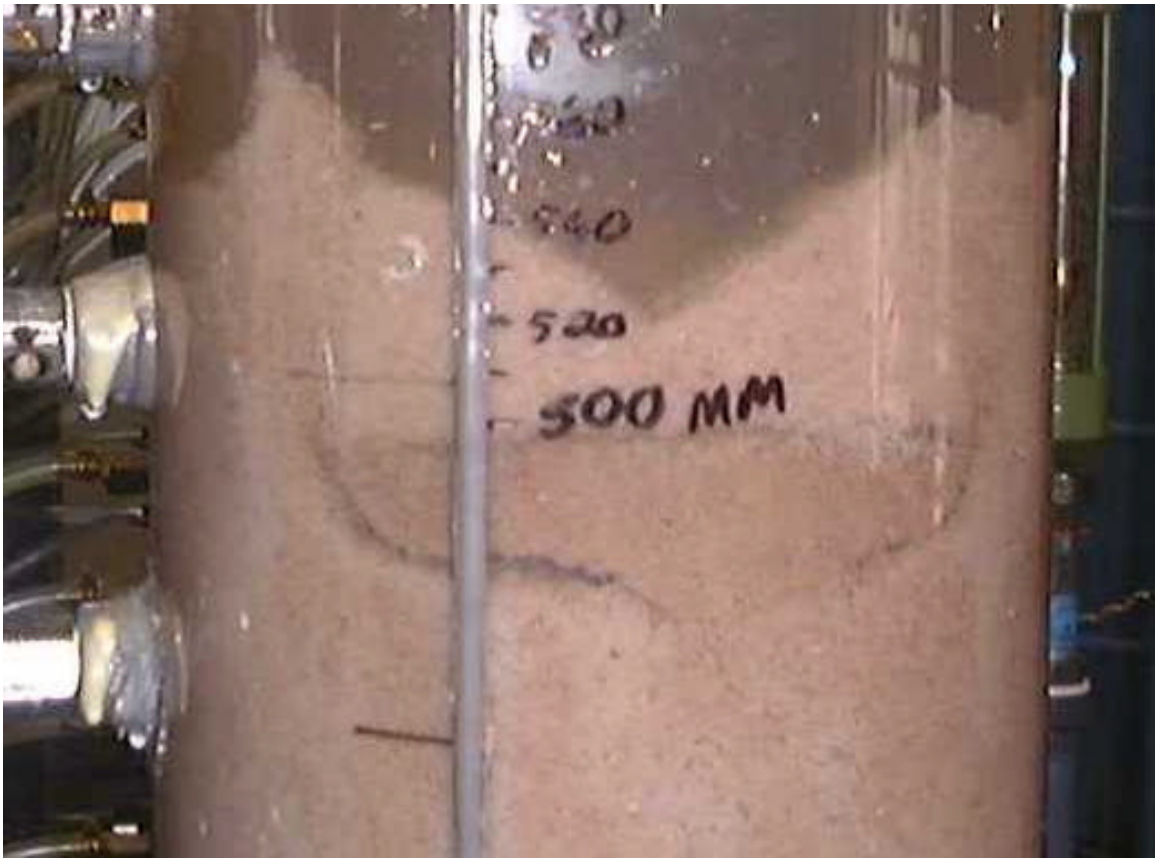

Figure 8.1 Residual clogged bed structure at sub-fluidization backwash velocities – 0.8 mm sand

Brouckaert et al. (2003) observed several different types of phenomena involving the accumulation of mud in filters. For alum doses of 15 – 20 mg/L and backwash rates close to the minimum fluidization velocity, the disintegration of the upper clogged layers of 0.7 mm and 0.8 mm sand beds was not always complete. Irregularly shaped chunks of clogged media up to 10 cm across were observed sinking into the bed as the top sections began to expand. This is shown in Figure 8.1. The chunks of media were slowly eroded away as the backwash progressed but residue from the original structures was visible through subsequent filter runs.

This did not appear to occur at lower alum doses and in media with lower fluidization velocities (anthracite and 0.5 mm sand) backwashed at the same rates (i.e. at higher $\%v_{mf}$). However, water only backwash always left a thin coating of sludge on the surface of the bed. This was most evident for dual media filters where the light brown alum floc contrasted with the black anthracite grains. In fact, while the media was still fluidized, it was possible to see that the top layer of the filter was primarily made up of fine grains with coatings of floc that the shear forces in this layer appeared unable to remove. After a few runs without auxiliary wash, clusters of pebble like mudballs began to appear below the surface of the bed. Figure 8.2 shows an example of mudball clusters in a 0.7 mm sand bed after six consecutive filter runs with water only backwash. The sludge layer on the surface of the media can also be seen. Figure 8.3 shows the surface sludge layer after nine consecutive runs without auxiliary wash.

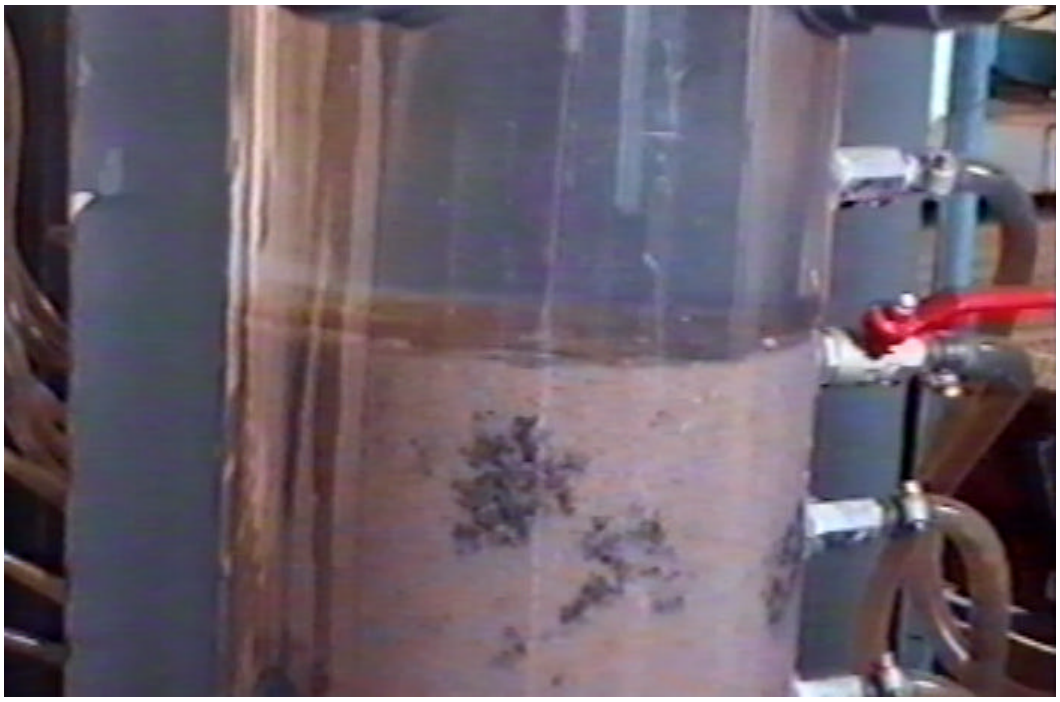

Figure 8.2 Mudball clusters and sludgy surface for 0.7 mm sand bed after six consecutive runs without air scour

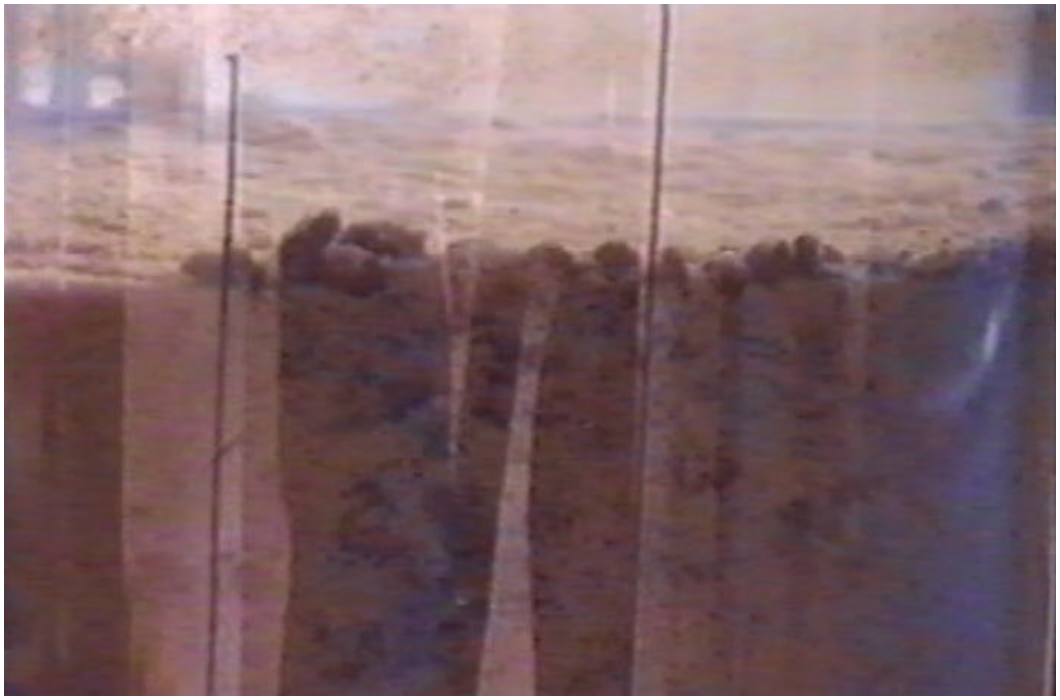

Figure 8.3 Mudballs and sludge on the surface of a 0.7 mm sand filter after nine consecutive runs without air scour

Brouckaert et al. (2003) ran a 0.7 mm sand and a dual media (0.9 mm anthracite and 0.5 mm sand) filter for a total cumulative run time of one month without auxiliary wash to observe the development of mudballs and assess their impact on filter performance. The experimental conditions are summarized in Table 8.1. Note that these experiments were simulating the operation of valveless filters, the design of which results in the backwash rate decreasing over the course of a normal backwash.

At the end of the monitoring period, the filter media were removed from the laboratory filters and the structure and distribution of mudballs as well the general state of the media examined further. Apart from the mudballs, the 0.7 mm sand was relatively clean below the first 1 cm from the bed surface. The top surface of the bed was however coated with a thin layer of sludge. In contrast, the entire anthracite layer was impregnated with sludge. Near the top of the bed, small clusters of anthracite were loosely glued together by patches of relatively soft floc. Deeper in the anthracite, the mudballs became larger, harder and contained increasing amounts of relatively coarse sand. It is thought that this sand may have been carried into the anthracite layer by high velocity channels that developed during backwashing due to mudballing at the interface. Mudballs at the interface were entirely coated with sand but their sand content decreased towards their centres where the material was similar to the mudballs found near the bed surface. The sand below the interface was remarkably clean and no evidence of mudballing was found.

Table 8.1(a) Media properties and design for the laboratory scale simulation and full -scale operation of the autonomous valveless filter (Brouckaert et. al, 2003)

MEDIA PROPERITIES			
	Silica sand		Anthracite
	0.5 mm	0.7 mm	
d_{10}	0.52 mm	0.72 mm	0.91 mm
d_{90}	0.91 mm	1.04 mm	1.60 mm
UC	1.42	1.36	1.48
Density	2642 kg/m^3		1545 kg/m^3
MEDIA DESIGN			
	Laboratory Filters		Full Scale AVF
	0.7 mm sand	Dual media	Dual Media
Sand size Sand depth	0.7 mm 0.52 m	0.5 mm 0.41 m	0.5 mm 0.39 m
Anthracite size Anthracite depth	_	0.9 mm 0.12 m	0.9 mm 0.12 m

Table 8.1(b) Operating conditions for the laboratory scale simulation and full -scale operation of the autonomous valveless filter (Brouckaert et. al, 2003)

FILTRATION CONDITIONS					
	Filtration Rate, m/h	Water Temperature, ^{o}C	Alum Dose, mg/L	Coagulated Water	
				Turbidity, NTU	pH
Parallel operation of the laboratory filters and the AVF (1 month)	6.0 – 6.9	21 – 26	5.5 – 6.5	1.5 – 6	7.5
Extended operation of the AVF (14 months)	5.8 – 6.4	18 – 26	0 – 8	1 – 40	7.3 – 7.8

BACKWASH CONDITIONS			
	Laboratory Filters		Full Scale AVF
	0.7 mm sand	Dual media	Dual Media
Backwash volume, m^3/m^2	3.2	3.2	2.2
Backwash rates, m/h	55 – 25	55 – 25	46 – 25

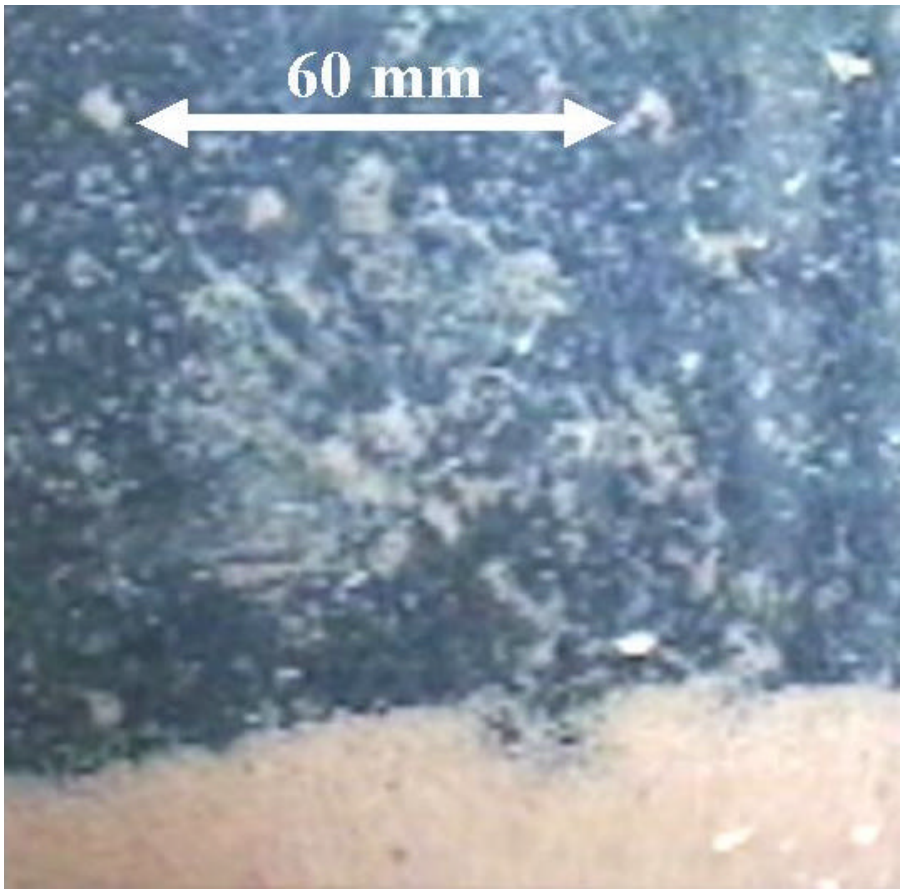

Figure 8.4 Mudballing at the sand-anthracite interface of a dual media filter

Similar observations were made when the anthracite layer was excavated from a full-scale valveless filter. The state of deterioration of the anthracite was more advanced than in the dual media laboratory filter since the AVF had been running for a longer period with lower backwash rates and backwash volume (See Table 8.1). The interface between the sand and anthracite was entirely composed of mudballs of various sizes and relatively coarse sand was found throughout the anthracite layer. However, the sand below the interface was clean and free of mudballs. Figure 8.5 shows mud accumulation and mudballs found in the AVF.

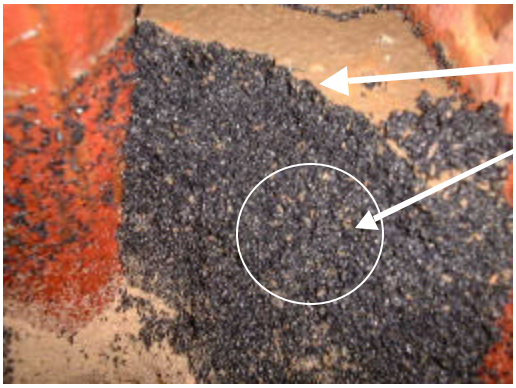

1. Incomplete removal of floc from top layer of fluidised media

2. Developing mudballs (anthracite grains cemented together by patches of floc)

3. Large mudball from the sand-anthracite interface

Figure 8.5 Mudballing in the AVF

One striking aspect about the mudballs shown in Figures 8.2 to 8.5 is that they are completely different in appearance to the clogged structure formed during a single filter run (Figure 8.1). The mudball floc appears to be very much denser. Also it is clear that the larger mudballs are agglomerate structures, which implies that they were formed over multiple filter runs. Based on these observations, the following mechanism for mudball formation was proposed:

Mudballing probably starts off in the top-most layer of filter grains, which are not completely cleaned during backwash. These grains start off with the highest concentration of

deposits and are subjected to the lowest shear forces during backwashing because of their small size. The partially cleaned grains settle back after backwashing and adjacent floc coated grains are squeezed together during the subsequent filter run. As in the case of initially clean filter grains, the coated grains become cemented together during the subsequent filter run. However, the cementation process has a head start and consequently, the grains are more likely to remain bonded together during the following backwash. Once grains have become irreversibly bonded together, the crevices between them tend to fill up with floc resulting in smooth, spherical, pebble-like mudballs.

Eventually, small individual mudballs become bonded together into larger structures that sink into the filter. In dual media filters, intermixing, which results in lower porosities at the sand-anthracite interface, can result in heavier clogging in these regions, which could lead to mudballing. However, mudballs found in this region may also have originated in the top layers filter and have accumulated at the interface because of bulk density effects. The mechanism of mudball formation is illustrated in Figure 8.6.

If this proposed mechanism is correct, it has several important implications: The first is that a very small amount of floc retained in the filter after each backwash can potentially lead to the formation and growth of mudballs.

The second implication is that for the size of individual mudballs and clusters to increase, the matrix of floc holding the media grains together must increase in strength over time. This is because the larger a structure, the greater the eroding forces it is subjected to during backwash.

Baylis (1954) described mudball formation as resulting from the compaction of mud deposits but did not discuss the mechanisms involved in mud compaction. He presumably meant that water is squeezed out of floc deposits by the high shear stresses that develop in the clogged regions of the bed during filtration, resulting in a denser deposit structure.

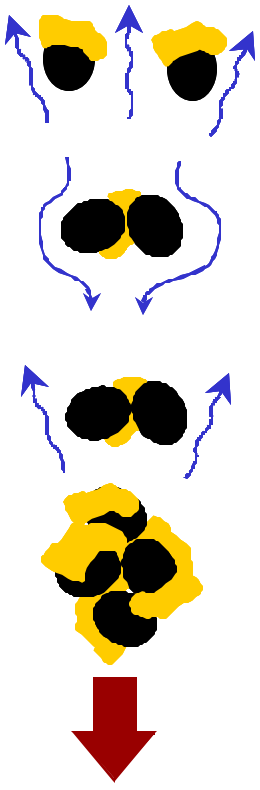

1. Water only backwash insufficient to remove floc deposits from top layer of fluidised media
2. Floc coated media become cemented together during next run
3. Bond strength increases with time – clusters of grains remain intact through subsequent backwashes.
4. Clusters grow and develop into mudballs
5. Mudballs sink into filter as density/weight increases

Figure 8.6 Proposed mechanism for mudball formation

The shear stresses that develop during gravity filtration are however not all that high. Camp (1965) estimated that a hydraulic gradient of 1.3 m/m near the top of a clogged filter bed correspond to an average shear stress in the pores of 0.125 N/m^2. The maximum headloss across the top few centimeters of a clogged filter is expected to be less than 1 m (See for example, Figure 6.15). Furthermore an increase in deposit density, if this actually occurs, does not explain how the mudballs could increase in size. This suggests that there are other mechanisms involved.

Floc is by nature both cohesive and adhesive. There is also evidence to suggest that floc particles become more difficult to detach the longer they remain in the filter even within the time scale of single filter run. For example, Camp (1965) noted that velocity gradients within the clogged filter media are much higher than they are during flocculation and yet the floc deposits remain intact.

There are a number of possible explanations for the apparent increase in deposit strength with time. First, the mechanisms by which floc attach to filter grains should be considered. Floc particles are typically an order of magnitude or smaller than the pores in a clean filter bed. Floc particles become attached to the surface of the media and to each other as result of physicochemical interaction forces such as van der Waals attraction. The magnitude and direction of the interaction force is a function of the separation distance between the floc particle and the surface or structure it is attaching to. The maximum attractive force typically occurs at a separation distance of less than 1 nm. However, it takes a finite amount of time for

any two structures to approach this closely since water molecules in the intervening space first have to be squeezed out of the way. Therefore it is reasonable to expect individual interfacial bonds to increase in strength over time up to some maximum.

At a larger scale, the first coating of floc laid down on a filter grain would be expected to be a loosely attached highly porous structure. As the shear stress in the filter pores gradually increase, individual flocs or clusters of flocs will either break away or be squashed into a denser more compact structure with more interparticle and interfacial contacts and hence greater cohesive strength.

In the case of water treatment floc there may be other time dependent physical, chemical and even biological processes that affect the cohesive and adhesive properties of deposits. For example, adjacent flocs in which ferric or aluminum hydroxide precipitates are a major component may tend to fuse together as a result of solubility effects.

Whatever, the mechanisms involved, there is empirical evidence that floc deposits become siginifcantly more difficult to remove with age. Experience has shown that running filters for 36 h without backwashing can lead to an irreversible deterioration of the state of the filter media even when the rate of solids loading is low and auxiliary backwash is used (Monk and Willis, 1987). Experimental evidence of an increase in floc strength with age is presented in Section 8.3 and in Chapter 9.

If the mechanical strength and possibly also the density of the mud component of any given mudball increases over each filter run, a structure which survives one backwash is most likely to survive the next backwash. Conversely, the most recently formed bonds and floc deposits are the most likely to fail. The video clip "Mudball clusters" shows small mudballs breaking off larger structures in the 0.7 mm and dual media beds.

For a given set of hydraulic conditions and cohesive strength of the mud encapsulating filter grains, there is presumably a critical size of structure that will survive backwash. Baylis (1954) indicated as much when he observed that the rate of growth of clogged regions in a filter can reach an equilibrium with the rate of abrasion.

Auxiliary backwash increases the intensity of the hydraulic forces that destroy the clogged bed structure and strip away filter deposits (Cleasby, 1990). This probably helps to eliminate or limit mudball formation by both decreasing the amount of freshly deposited floc retained in the filter after each run and limiting the maximum size of structures that can develop over multiple runs. However, for surface wash and sequential air and water wash, increased agitation of the filter media occurs only in top part of the filter bed and mudballs which sink below this zone will not be broken up (Cleasby, 1990). Maximum energy dissipation and cleaning efficiency throughout the filter bed is achieved by simultaneous air and sub-fluidization water wash (Amirtharajah, 1993). Cleaning of dual media filters can be improved by using a sub-surface wash system to target the interface between the sand and anthracite layers (Kawamura, 1975b).

8.3. Investigation into the rate of accumulation of mass in the filter over multiple runs and the effect of the aging of floc deposits on backwash efficiency

8.3.1. Experimental objectives

Observations of mudballing in the AVF study suggested that what happens to residual floc deposits in a filter between one backwash and the next may be as or more important as what happens during a single backwash. This section discusses a set of experiments carried out to address this issue. The specific experimental objectives were to

1. Prove that the strength of floc deposits increases with time

2. Quantify the accumulation of mud in a filter over multiple runs with water only backwash.

8.3.2. Experimental methodology

Two sets of experiments were undertaken. In the first set, water backwash after individual runs was delayed by various amounts of time to determine the impact of the delay time on the backwash efficiency. The second set of experiments consisted of several series of consecutive filter runs with water only backwash. At the end of each series, the cumulative mass of mud retained after water only backwash was determined. The experimental set up for both

sets of experiments is summarized in Table 8.2. These experiments were carried out in the same 0.7 mm sand bed used in the AVF study discussed in Section 8.2.

Table 8.2 Experimental conditions for delayed backwash and mudball accumulation experiments

Filter	0.7 mm sand
Coagulant	Alum
Dose	5.8 to 6.9 mg/L
Filtration Rate	5.8 to 6.8 m/h
Backwash Rate	54 m/h
Backwash Volume	3.8 m^3/m^2

8.3.2.1. Delayed backwash

In this set of experiments, each filter run started with a clean filter bed. The filter was run to 1.6 – 1.7 m of headloss (26 – 29 h) and then shut off. The clogged filter was left offline for a period of time and then backwashed as described in Chapter 3 to determine the efficiency of detachment by water backwash. The delay times for each experiment are listed in Table 8.3.

Table 8.3 Backwash delay times

Experiment	Delay Time (h)	Order of experiments
M0	0	1
M0D	0	2
M24.5	24.5	6
M26.5	26.5	5
M48	48	3
M66	66	4

8.3.2.2. Accumulation of mud in the filter over multiple filter runs

Five series of experiments consisting of one to nine consecutive filter runs with water only backwash were conducted. At the end of each series, after the final water backwash, the accumulated mud remaining in the filter was removed by air scour as described in Chapter 3. The multiple filter run experiments are summarized in Table 8.4.

It was originally intended that each filter run should last approximately 24 hours, however, most of the filter runs had to be terminated earlier because the maximum filter headloss had been reached. Run times varied from 19 to 24 h.

Table 8.4 Mud accumulation experiments

Series	Number of consecutive filter runs with water only backwash	Order of experiments
M1R1	1	3
M2R1 – M2R2	2	4
M4R1 – M4R4	4	2
M6R1 – M6R6	6	5
M9R1 – M9R9	9	1

8.3.3. Experimental Results

8.3.3.1. Effect of delaying backwash on backwash efficiency

In this set of experiments, a normal filter run was carried out and then the clogged filter bed was left to stand for various amounts of time before backwashing. This was to test the hypothesis that floc bonds increase in strength with time and that the longer that floc remains in the filter, the harder it becomes to remove. The impact of backwash delay time on detachment efficiency is shown in Figures 8.7 and 8.8. The confidence intervals reflect uncertainty in the measurement of the masses of floc detached during water only and air scour backwash. Details of the calculation of uncertainties were given in Chapter 5.

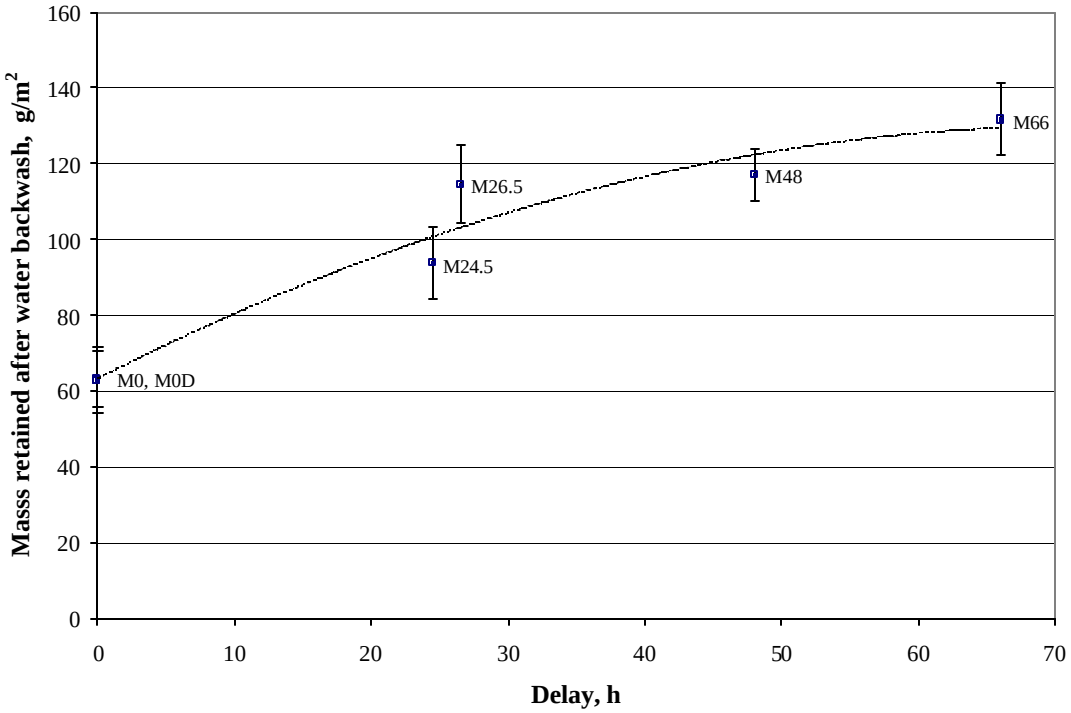

Figure 8.7. Mass retained in filter after water backwash as a function of delay time

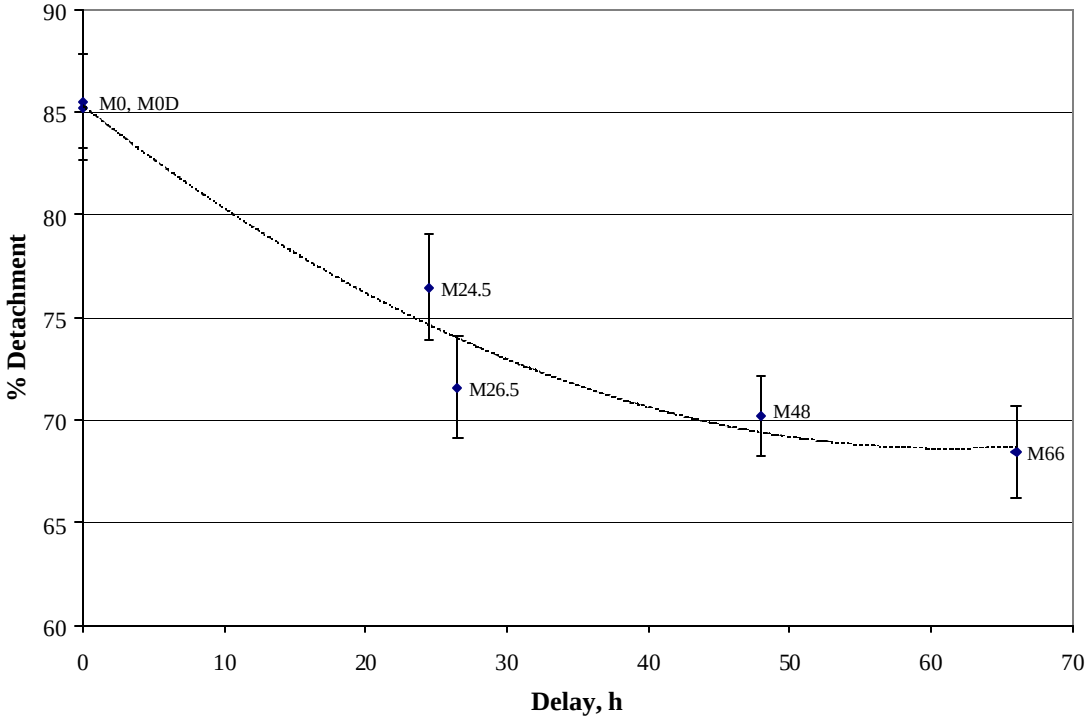

Figure 8.8. Efficiency of water backwash as a function of delay time

In Figures 8.7 and 8.8, the efficiency of detachment is shown as levelling off, however, more data would be required to confirm this trend. The maximum increase in deposit strength appeared to occur in the first 24 hours. This is important because under normal conditions, most filters run for 24 hours or more between backwashes. This means that floc retained in the filter after the last backwash could become significantly more difficult to remove by the time the next backwash occurs. Another practical implication of these results is that it is important to backwash filters as soon as possible after the end of the filter run to avoid a decrease in cleaning efficiency.

8.3.3.2. Accumulation of floc in the filter over multiple filter runs

Figures 8.9 and 8.10 show the accumulation of deposit not removed by water backwashing over consecutive filter runs without air scour backwash. Each point represents the mass retained after the final water only backwash at the end of each series, as determined by backwashing the filter bed with air and water combined.

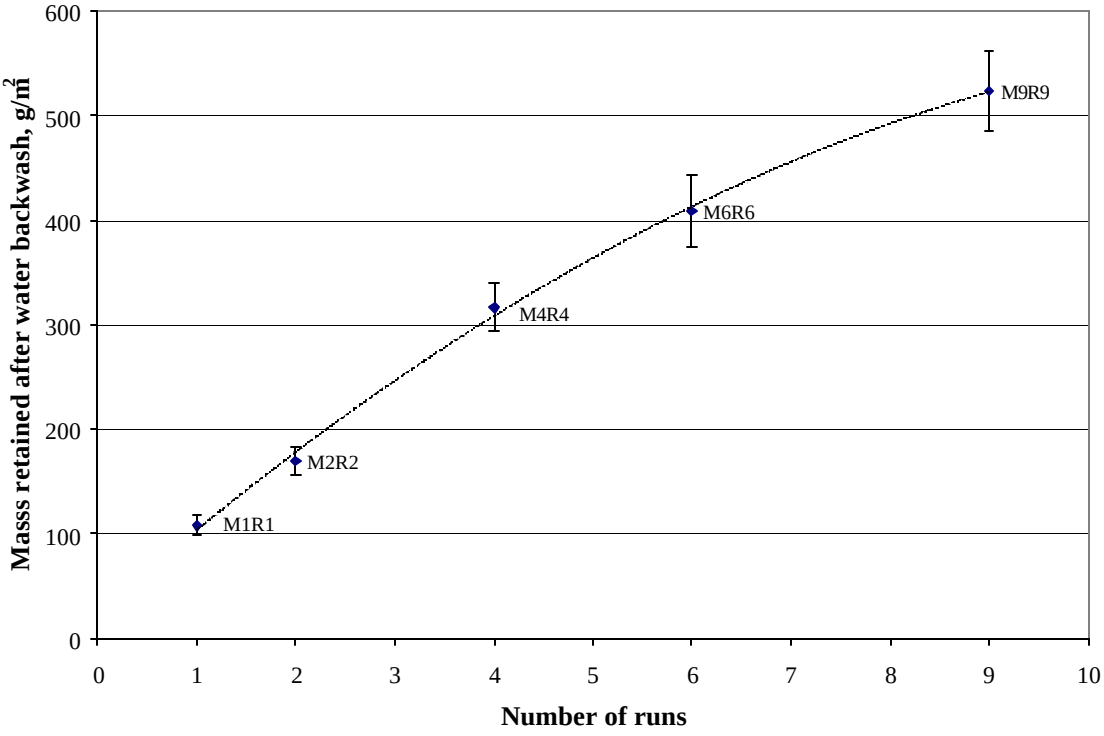

Figure 8.9 Mass retained in the filter after water backwash as a function of run number

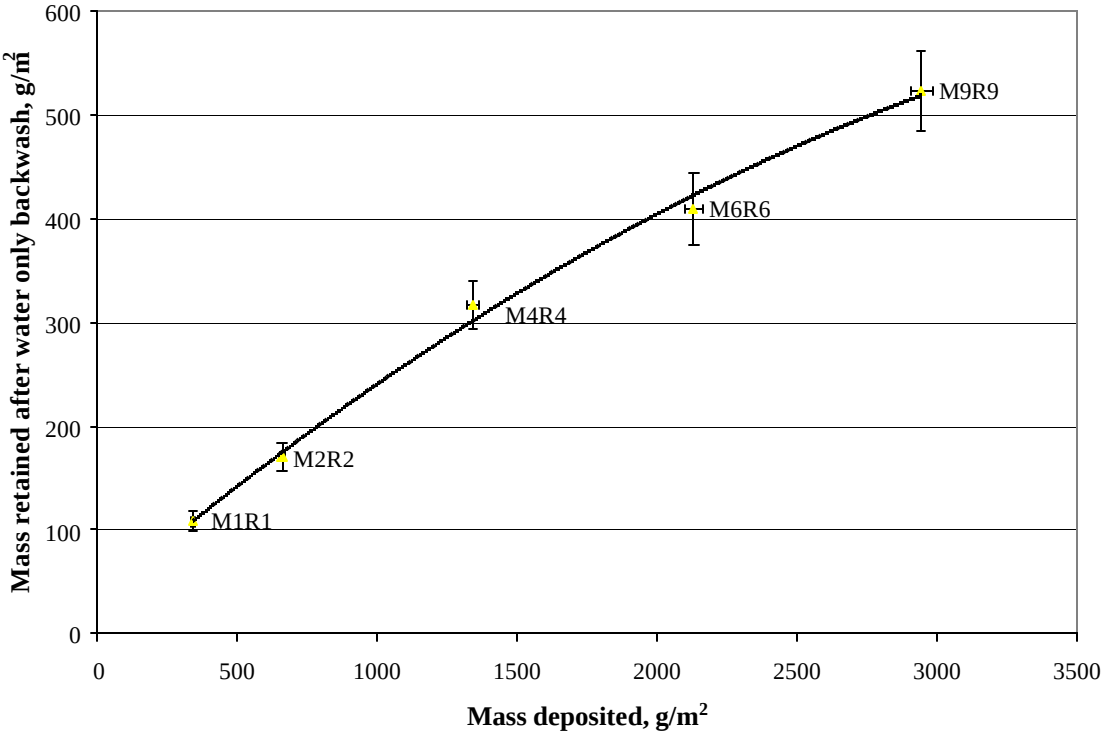

Figure 8.10 Mass retained in filter after water backwash as a function of cumulative mass deposited

Both figures suggest that the rate of accumulation of retained deposit may decrease as the number of runs increase. Possible physical explanations include:

- Floc retention is accelerated by the presence of fine sand grains, as suggested by Kawamura (1975a), which become bound up in mudballs. As the supply of fine grains decrease, the rate of accumulation of floc after backwashing decreases.

- The formation of mudballs results in increased local velocities during backwashing which results in more efficient detachment of freshly deposited floc.

- The increase in size in the mudballs increases the hydrodynamic forces they are subjected to during backwash. Consequently, the rate of abrasion of mudballs tends to limit their rate of growth, as suggested by Baylis (1954).

The apparent decrease in rate of accumulation becomes more obvious when the average mass retained per run, $\frac{\sum M_R}{n}$, is plotted against the number of runs.

There appears to be a power law relationship between the mass retained per run and the number of runs. The power law relationship was calculated by regressing $\ln\left(\frac{\sum M_R}{n}\right)$ against ln (n) where n is the number of runs. However, this result must be treated with caution. Figure 8.11 shows that the results for experiments M0 and M0D do not fit the trendline for experiments M1R1-M9R9. This indicates that number of runs, n, cannot be the only factor affecting mass retained. This raises the possibility that the apparent relationship between ΣM_R and n was fortuitous. The possible effect of factors other than run number on the mass retained after each run is discussed in Chapter 9.

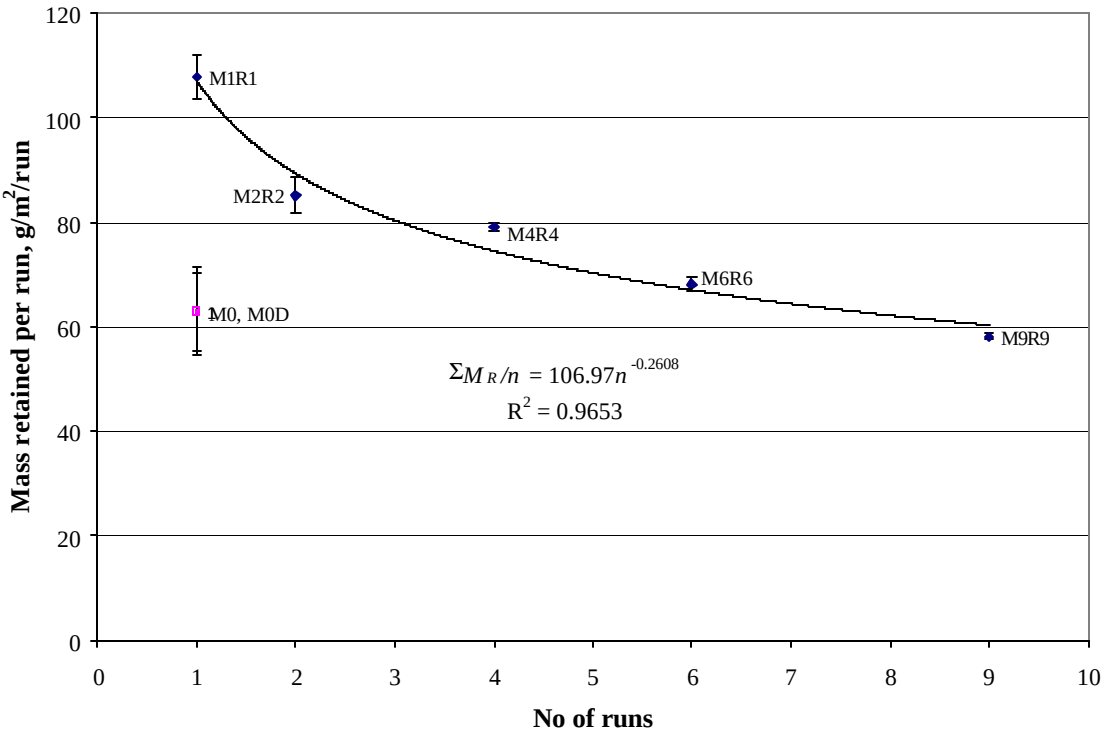

Figure 8.11. Mass retained per run

Figures 8.12 and 8.13 show that there was no apparent relationship between run number and mass deposited per run, $\frac{\sum M_{TF}}{n}$, or fraction of mass deposited retained, $\frac{\sum M_R}{\sum M_{TF}}$, and run number so it would seem that the relationship indicated in Figure 8.11 did not arise from differences in total mass deposited for the different experimental series. Note that the mass deposited in experiments M0 and M0D was greater than in the other experiments shown because lower rates of headloss development meant that these experiments were run for longer periods to achieve the same terminal headloss.

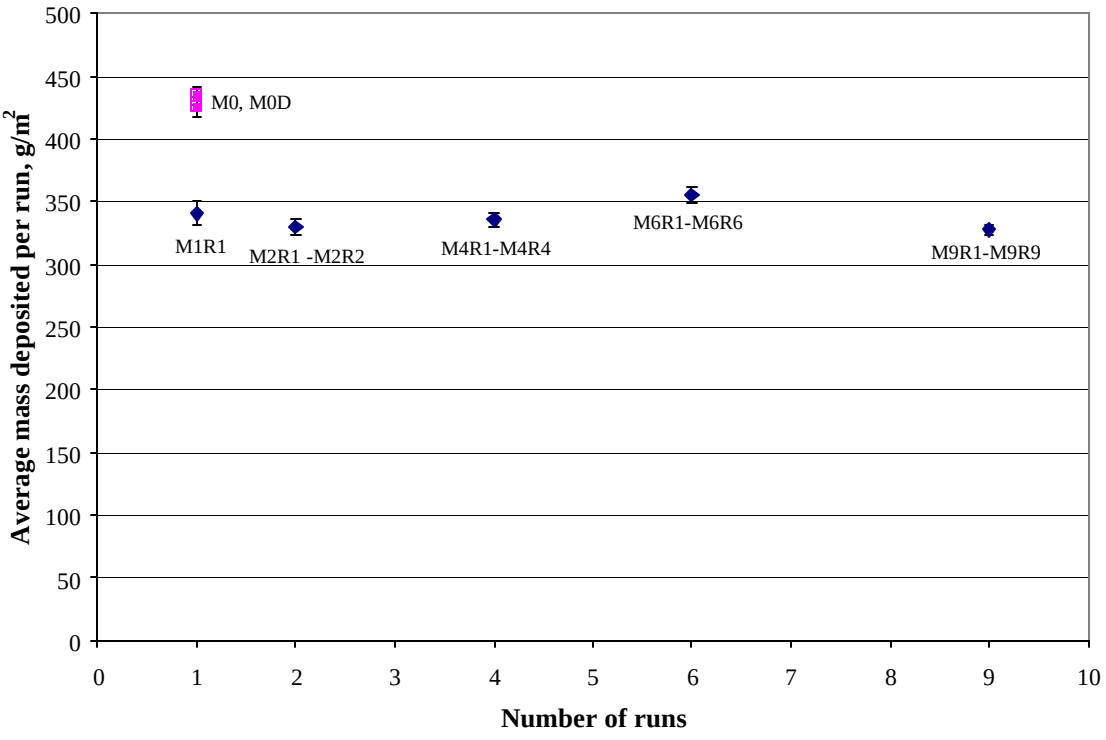

Figure 8.12 Average mass deposited per run

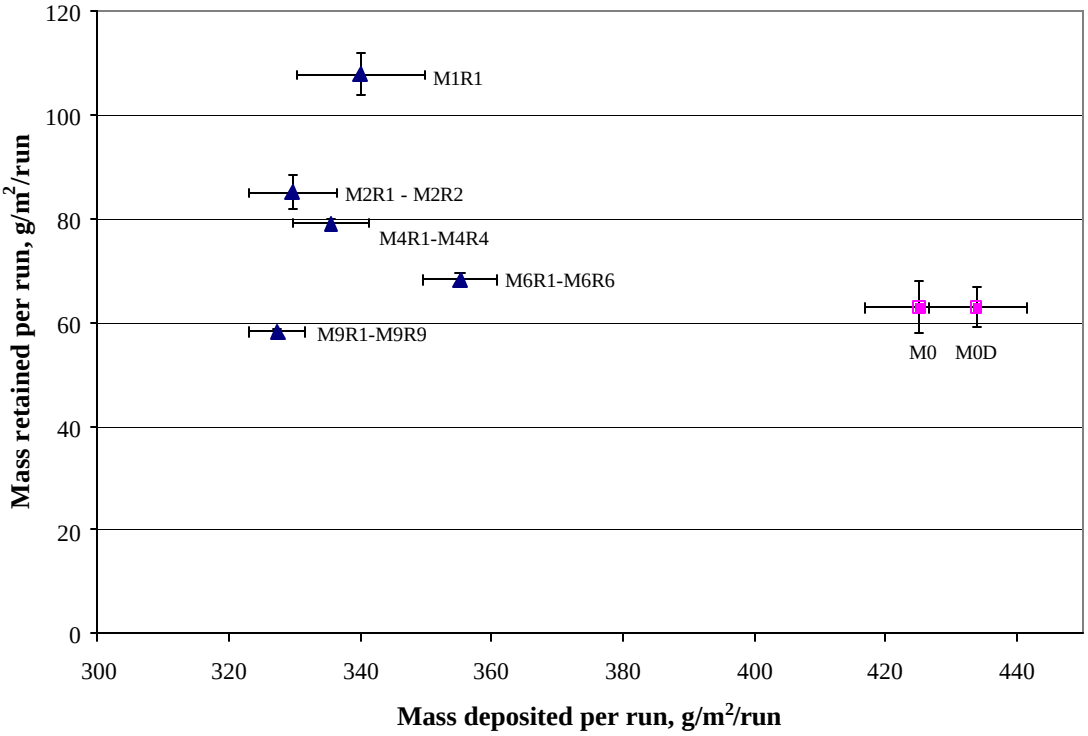

Figure 8.13 Mass retained per run vs mass deposited per run

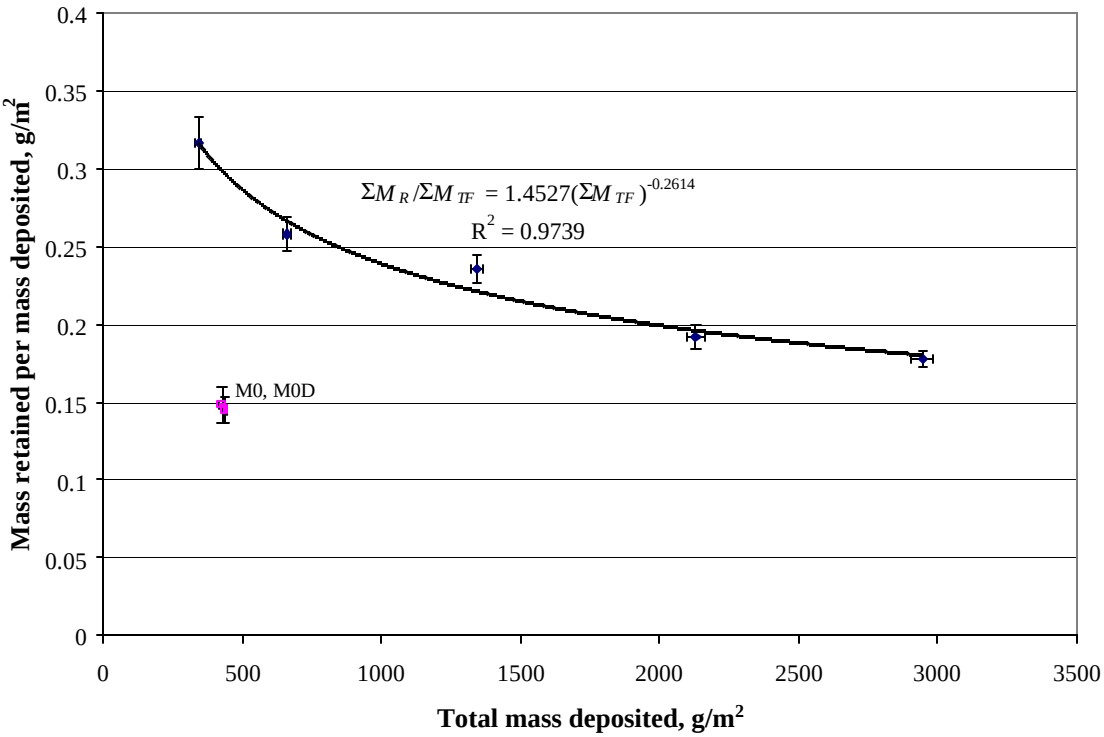

Figure 8.14 Mass retained per mass deposited vs total mass deposited

Figure 8.14 shows that there was a slightly better exponential correlation between $\frac{\sum M_R}{\sum M_{TF}}$ and ΣM_{TF} as compared to n. This suggests that the mass deposited in a given run did have some effect on the mass retained after backwash, although it was less important than the accumulated effects of previous runs.

If the mass increment retained after backwash generally decreases with increasing run number, then this trend should be reflected in the data for individual series. There were no direct measurements of total mass deposited or retained for individual runs (with the exception of M1R1) and the estimates of M_R presented in Chapter 5 did not show a consistent trend with respect to run number. If there was a trend however, it may have been obscured by errors in the estimates since the relative margins of uncertainty were fairly large. The only mass measurement for individual runs was the mass detached by water backwashing, M_D. Figure 8.15 shows mass detached for individual runs as a function of run number.

Figure 8.15 shows that mass detached tends to increase with run number for individual series and the combined data set as a whole. M9R4 appears to be an outlier (however, it was included in the regression) and there were independent observations to suggest that the mass deposited during this run was significantly less than in other runs. (the terminal headloss was significantly lower than in other filter runs). Therefore, if it can be assumed that the total mass deposited, M_{TF}, did not tend to increase with run number, then the detachment data supports

the idea that the incremental increase in mass retained, M_R, decreases with increasing number of runs.

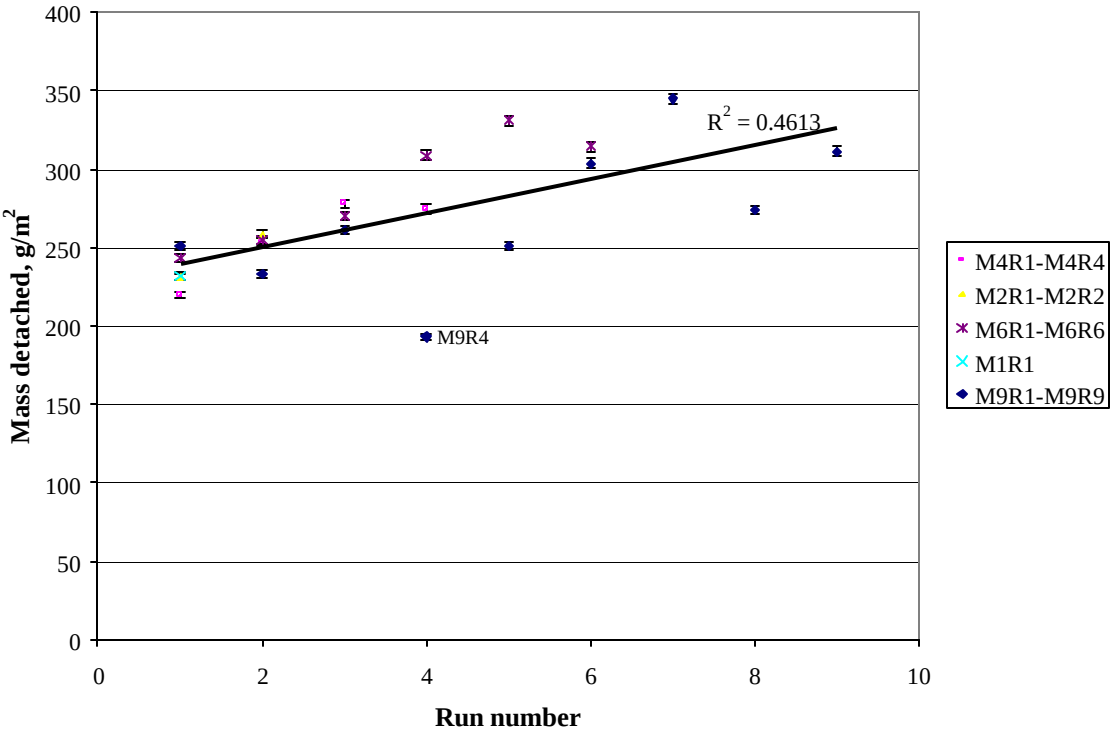

Figure 8.15 Mass detached by water backwash as a function of run number

Based on the results presented so far, the following observations can be made. Assuming that backwash conditions remain constant (specifically duration and magnitude of detachment forces), the mass of freshly deposited floc retained after backwash is a function of the following factors:

1. The strength of cohesive and adhesive forces between floc particles and media grains. These would depend on factors such as coagulant type and dose. Other factors relating to the operating conditions and nature of the influent particles must also play a role. For example, it is not immediately obvious why experiments M0 and M0D should have produced substantially different results to experiments M1R1 to M9R9.

2. The number of consecutive runs with water only backwash, or possibly more specifically the mass of floc retained from previous runs.

3. The mass of floc deposited in the last filter run may play a role, although it appears to be less significant than either of the previous types of effects.

The dependence of backwash efficiency on filtration conditions is discussed further in Chapter 9.

8.4. Modeling the accumulation of mud in a filter over multiple runs

If the rate of accumulation of retained mud $\frac{\Delta M_R}{\Delta n}$ could be predicted based on the filtration and backwash conditions, then it might be possible to predict how long a filter could be

run for until mudballing became a critical problem. Kawamura (1991) suggested that the state of a filter bed could be assessed in terms of the % volume of mudballs. Less than 0.1 % indicates a clean bed, 0.1 – 0.5 % indicates the media is in good condition, 0.5 - 1.0 % may be considered fairly clean, 1 – 5 % indicates the filter is in bad condition and if greater than 5 % of the volume is made up of mudballs then the filter media should be replaced.

A crude estimate of the volume of mudballs in the experiments M1R1 to M9R9 can be obtained by making assumptions about the composition of the mudballs and the mud density. The clean fixed bed porosity in these experiments was approximately 0.48, therefore it was assumed that mudballs would consist of 52 % by volume of sand and 48 % of mud. The density of the mud deposits was assumed to be r_d = 1030 kg/m^3 (Huang and Basagoiti, 1989). The estimated volume of deposits corresponding to a given value of M_R is

$$V_{dr} = \frac{\sum M_R}{1000\, r_d} \qquad 8.1$$

V_{dr} = Volume of filter deposits per unit filter area, m^3/m^2

ΣM_R = Cumulative mass retained, g/m^2

r_d = Deposit density, kg/m^3

The corresponding volume of mudballs is

$$V_{mb} = \frac{V_{dr}}{e_0} \tag{8.2}$$

V_{mb} = Volume of mudballs per unit filter area, m^3/m^2

e_0 = Fixed bed porosity

The % volume of mudballs is

$$\% \text{ volume} = \frac{V_{mb}}{l_{fx}} \times 100\,\% \tag{8.3}$$

l_{fx} = Fixed bed height, m

The rate of increase in mudball volume is

$$\frac{\Delta V_{mb}}{\Delta n} = \left(\frac{1}{1000\, r_d e_0} \right) \frac{\Delta\left(\sum M_R\right)}{\Delta n} \tag{8.4}$$

The % volume of mudballs, rate of increase of mudball volume and number of runs to reach 5 % volume based on the average rates of accumulation for experiments M0, M0D, M1R1 and M9R1 – M9R9 are presented in Table 8.5. The fixed bed height l_{fx} was assumed to be 0.6345 m.

Table 8.5 Estimated rates of mudball accumulation

Experiment	% Volume of mudballs	$\frac{\Delta V_{mb}}{\Delta n}$, m^3/m^3/run	Number of runs to reach 5 % volume
M0	0.020	0.00013	250
M0D	0.020	0.00013	250
M1R1	0.034	0.00022	145
M9R1-M9R9	0.17	0.00012	270

According to the estimates in Table 8.5, the media would have to be replaced after less than a year of operation assuming an average run time of approximately one day. However, as discussed in the previous section, Figures 8.9 and 8.11 suggest that the rate of mass accumulation decreased with the number of runs. One possible explanation given for this was that the rate of accumulation depended on the media size distribution and decreased as the finest grains are encapsulated in mudballs.

Based on the sieve analysis for this media (See Chapter 4 for details), 0.04 % of the media fell in the range 0.25 to 0.30 mm. Mudballing of this size fraction would produce 0.00027 m^3/m^2 of mudballs or 0.044 % of the filter volume. According to these crude estimates, it appears 50 to 75 % of the finest media fraction could theoretically be mudballed within a single filter run. Therefore it is not unreasonable to expect a decrease in the rate of accumulation of mudballs to occur within the first few filter runs. This is consistent with results of

Kawamura (1975a) and the calculated rates of power dissipation as a function of grain size in Chapter 4.

If the media size distribution needs to be taken into account, then the following model of mass accumulation can be proposed:

$$\frac{\Delta\left(\sum M_R\right)}{\Delta n} = f\left(p_{f1}, p_{f2}, p_{f3},..., p_{b1}, p_{b2}, p_{b3},..., (x_i d_i)_n\right) \qquad 8.5$$

p_{f1}, p_{f2}, p_{f3} = Parameters relating to the filter run which affect the strength of deposits e.g. coagulant used, run duration, etc.

p_{b1}, p_{b2}, pb_3 = Backwash parameters which affect the hydrodynamic detachment forces e.g. backwash rate and temperature, etc.

$(x_i d_i)_n$ = Size distribution of media not incorporated in mudballs after n filter runs

As the volume of mudballs in filter V_{mb} increases, this would tend to also impact the hydrodynamics of backwash. This effect might also need to be included in the model for $n >> 1$.

This modeling approach could be useful in designing filters such as valveless filters to operate for as long as possible with sub-optimal backwash conditions. Ideally the model could be calibrated for any filtration plant at any location using data from a few representative pilot filter runs and the size distribution of the filter media. Scale up issues would have to be

considered, however. The model could also be calibrated for situations where auxiliary wash is used and with full-scale plant data. The mud accumulation profile in a full-scale filter bed can be determined using a core sampling technique described by Kawamura (1991). This involves extracting core samples from the bed and using the abrasion test (Described in Section 5.2) to determine the amount of mud retention at different points and depths in the filter bed. Core sampling is a recommended part of routine filter inspection (Logsdon et al., 2002).

More experimental work on different backwash conditions, media size distributions and the backwash behavior of more severely mudballed filters is required to check the model assumptions and develop a practical calibration procedure. A full investigation of all these parameters was beyond the scope of this study. However, Chapter 9 looks at the effect of various filtration and backwash parameters on the mass retained after a single filtration and backwash cycle.

CHAPTER 9

FACTORS AFFECTING THE EFFICIENCY OF BACKWASH

9.1. Introduction

The efficiency of floc detachment during backwash is known to be dependent on a number of factors. Several of these factors have been discussed in earlier chapters. Amirtharajah (1978) and others have found that detachment efficiency correlated with expanded bed porosity and related this to the theoretical average velocity gradient in the fluidized bed (Chapter 2). Kawamura (1975a) indicated that backwash efficiency decreases with decreasing grain size (discussed in Chapter 8), which is consistent with calculations of the mean velocity gradient as a function of grain size (Chapter 4). Chapter 8 provided experimental evidence of a decrease in backwash efficiency with the age of the floc deposits. It is also well established that floc containing polymeric coagulants is more difficult to detach than alum or ferric floc (Kawamura, 1975b; Martin, 1998).

At the scale of a single floc coated filter grain, the probability of some or all of the floc deposit detaching depends on the relative magnitudes of the detachment and attachment forces as well the duration of the backwash. Conceptually, this can be expressed as

$$-\int_0^t \frac{\partial s}{\partial t}\,dt = \int_0^t f_1(s)\cdot f_2\left(\frac{F_D}{F_A}\right)dt \qquad 8.1$$

s = Specific deposit

t = Backwash time

F_D = Characteristic detachment force

F_A = Characteristic attachment force

$f_2\left(\frac{F_D}{F_A}\right)$ is the probability that at any given floc aggregate will be detached at time t. Both the attachment and detachment forces vary with time and depend on the structure of floc deposits and media-floc composites.

Although there is a considerable body of theory on the detachment of particles in model system, predictions of the fundamental hydrodynamic and physicochemical forces in real filter backwash systems are at very best order of magnitude estimates. Furthermore, no existing fundamental force models adequately represent the complexity of the hydrodynamics and floc deposit structures in fluidized beds and therefore are incapable of making quantitative predictions of the rate of detachment or efficiency of backwash.

A more practical approach to modeling the detachment process might be to attempt to derive an empirical model of the backwash efficiency based on more easily measured parameters such as grain size, backwash rate and headloss development during filtration. This

chapter investigates the relationship between backwash and various parameters relating to conditions during both filtration and backwash. The first part of the chapter focuses on the hydrodynamic aspects of backwash and the second part attempts to identify the filtration parameters which predict the resistance of floc deposits to detachment.

9.2. Effect of hydrodynamic factors on backwash efficiency

9.2.1. Backwash rate and grain size

Mass retained in the filter after backwash is the most direct measurement of backwash efficiency (Amirtharajah, 1978). Figures 9.1 and 9.2 show the mass retained and % detachment for experiments ZU61 – 95, AU61_8h –AU70, M0, M0D and M1R1 as a function of backwash rate. (Of all the mass accumulations experiments discussed in Chapter 8, only the three experiments consisting of a single filter cycle with zero backwash lag time are considered at this point). The experimental conditions for AU and ZU experiments were listed in Tables 6.1 and 6.2 while the experimental conditions for M0, M0D and M1R1 were described in Section 8.3.

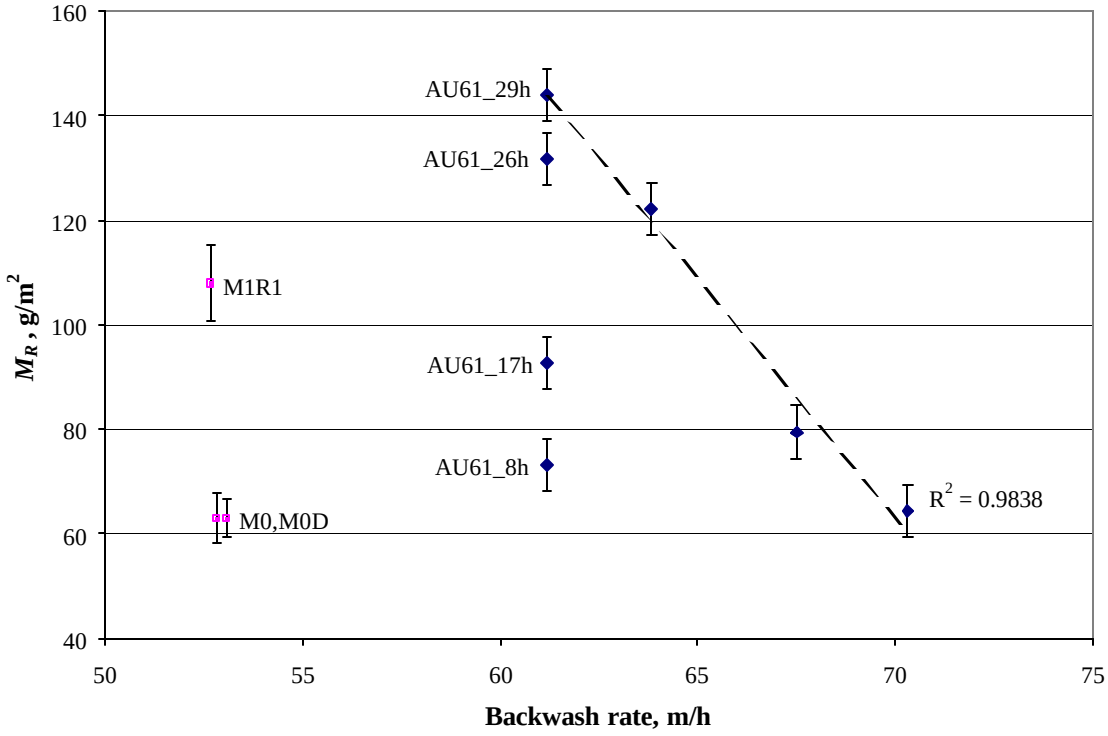

Figure 9.1 (a) Mass retained after backwash as a function of backwash rate – alum experiments

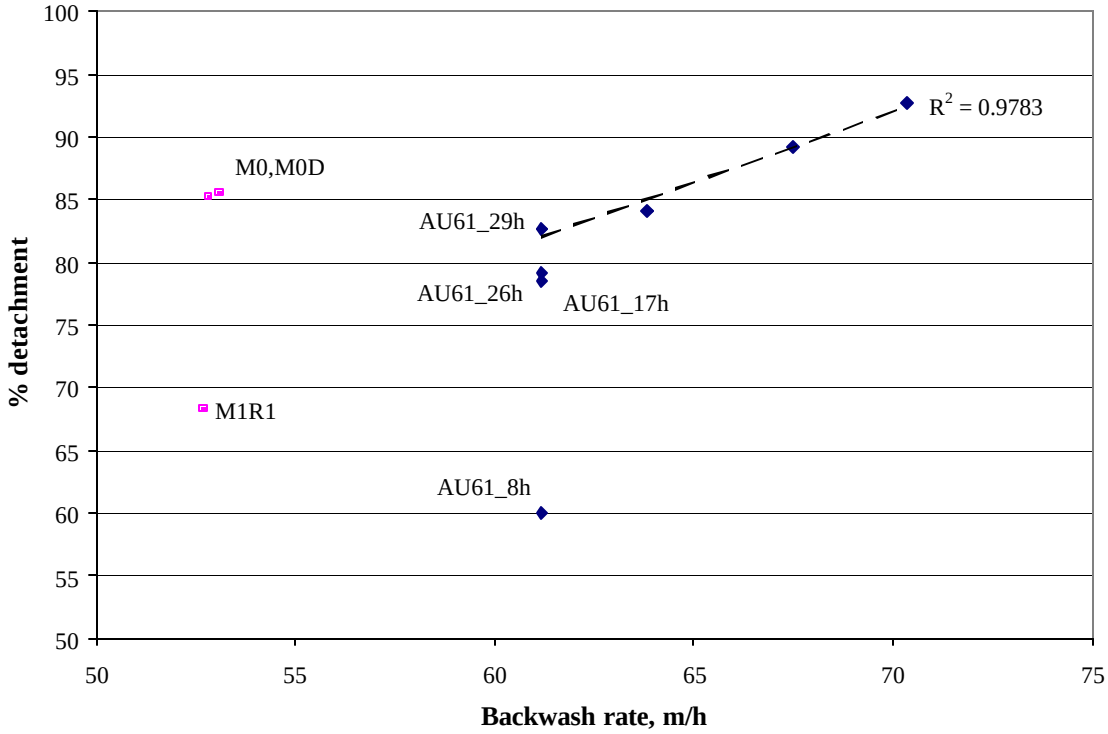

Figure 9.1 (b) % Detachment as a function of backwash rate – alum experiments

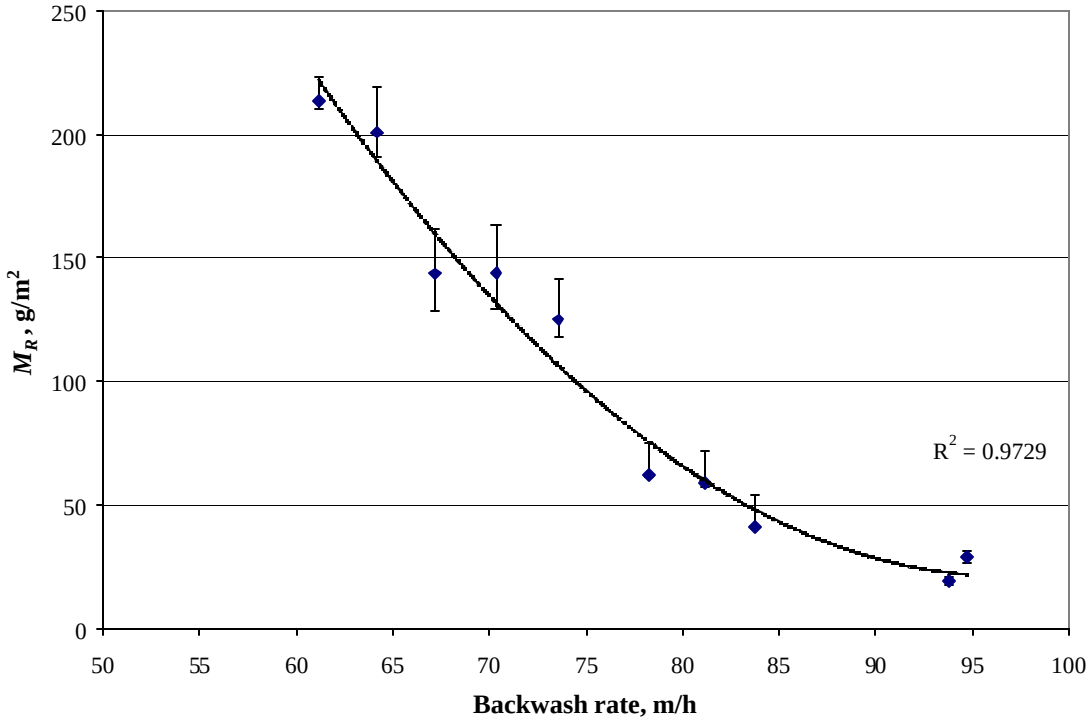

Figure 9.2 (a) Mass retained after backwash as a function of backwash rate – Z464N experiments

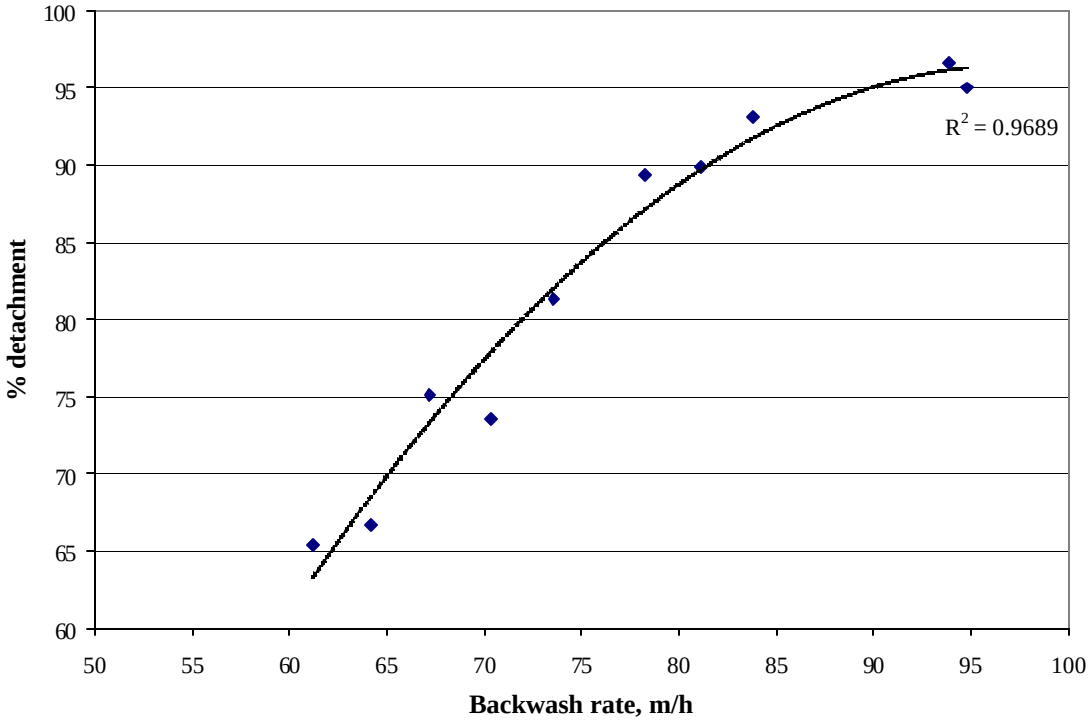

Figure 9.2 (b) % detachment as a function of backwash rate – Z464N experiments

There is a clear correlation between backwash rate and backwash efficiency for the ZU experiments. For the AU experiments, there was a greater variability in the filtration conditions (primarily filter run time and terminal headloss – see Table 6.1 (b)) and this appeared to have as much of an effect on the backwash efficiency as the backwash rate. For run times 27 to 32 hours (Au61_29h to AU70), the backwash efficiency increased with backwash rate. The mass retained in the 0.7 mm sand experiments tended to be less than in the AU experiments, but the % detachments were more comparable.

Section 4.4 discussed the estimation of the optimum backwash rates for a given filter bed based on the media size distribution. The effect of the finest fractions of the filter media on the optimum backwash rate was not entirely resolved. Using the methodology described in Section 8.4, it is possible to estimate the fraction of the media that retains floc deposits after backwash in each of the experiments in Figures 9.1 and 9.2. From Equations 8.1 and 8.2, the volume of media grains encapsulated in mudballs is

$$V_m = \frac{(1-e_0)}{e_0} V_{dr} = \frac{(1-e_0)}{e_0} \frac{M_R}{1000\, r_d} \qquad 9.2$$

V_m = Volume of media grains encapsulated in mudballs, m^3/m^2

e_0 = Fixed bed porosity

V_{dr} = Volume of filter deposits per unit filter area, m^3/m^2

M_R = Cumulative mass retained, g/m^2

Table 9.1 lists the maximum and minimum estimates of the volume fractions of filter grains encapsulated in each bed. Table 9.2 lists the finest size fractions in each bed and corresponding optimum backwash velocities. The optimum backwash velocities were calculated for y = 0.81 and 25^0C. In Figure 4.8, there is a negligible difference in optimum velocity between 20^0C and 25^0C. Assuming the density of the filter media is all the same, the volume fraction of grains of a particular size is the same as the mass fraction determined from the size distribution (Table 4.1).

When the estimated mudballed fractions in Table 9.1 are compared to the media size volume fractions in Table 9.2, they suggests that the retained deposits are restricted to the 0.27 mm size fraction for 0.7 mm and the 0.36 mm size fraction for the 1 – 1.4 mm sand (if the assumptions that went into the estimates in Table 9.1 are valid). The theoretical optimum backwash rate for 0.27 mm sand happens to coincide with the backwash rate for the 0.7 mm sand bed. However, the theoretical optimum backwash rate for the 0.36 mm size fraction is 60 m/h whereas the optimum backwash rate for the 1- 1.4 mm sand appears to be in the region of 95 to 100 m/h based on Figure 9.2. These backwash rates correspond to the optimum range for 0.78 and 0.94 mm sizes. Therefore, selecting the optimum backwash rate based on the mudballed size fraction does not appear to be helpful. Selecting the optimum backwash rate on the basis of the mean size of the top 10 % of the bed is probably a reasonable approach.

Table 9.1 Maximum and minimum volume fractions of grains encapsulated in mudballs after one filter run and water only backwash

	0.7 mm sand	1 – 1.4 mm sand
Total volume of grains	0.331 m^3/m^2	0.241 m^3/m^2
Maximum fraction mudballed	0.00018 (M1R1)	0.00048 (ZU61)
Minimum fraction mudballed	0.00010 (M0, M0D)	0.000044 (ZU94)

Table 9.2 Size fractions and optimum backwash velocities

Geometric mean size d_i, mm	Volume fraction x_i		v_{bms}, m/h
	0.7 mm sand	1 –1.4 mm sand	
0.92	0.4326	0.0285	104
0.78	0.3312	0.0051	94
0.65	0.0654	0.0023	85
0.55	0.0093	0.0025	77
0.46	0.0008	0.0045	69
0.36	0.0009	0.0011	60
0.27	0.0004		52

9.2.2. Power dissipation

Given that the optimum backwash rate theoretically coincides with the condition of power dissipation per volume, one might expect that the amount of filter deposit that survives backwash would be correlated with the rate of power dissipation in the upper sections of the filter bed. From Chapter 4, the average rate of power dissipation associated with size d_i is

$$\Phi_i = m\left[\frac{v_b g(r_s - r)(1-e_i)}{me_i}\right] \text{ for } v_b > v_{mfi} \qquad 9.3a$$

$$\Phi'_i = m\left[\frac{\frac{v_b}{v_{mf}} g(r_s - r)(1-e_{mf})}{me}\right] \text{ for } v_b < v_{mfi} \qquad 9.3b$$

Φ_i = Dissipation function for grain size d_i at $v_b > v_{mfi}$,, J/m^3/s

Φ'_i = Dissipation function for grain size d_i at $v_b < v_{mfi}$,, J/m^3/s

For the purposes of determining the optimum backwash rate for a graded media bed, it would be useful to know if backwash efficiency was strongly correlated with any particular media size. Figure 9.3 shows Φ_i for each of the mean mesh sizes in the top 10 % of the 1 – 1.4 mm bed plotted against the mass retained at the end of backwash.

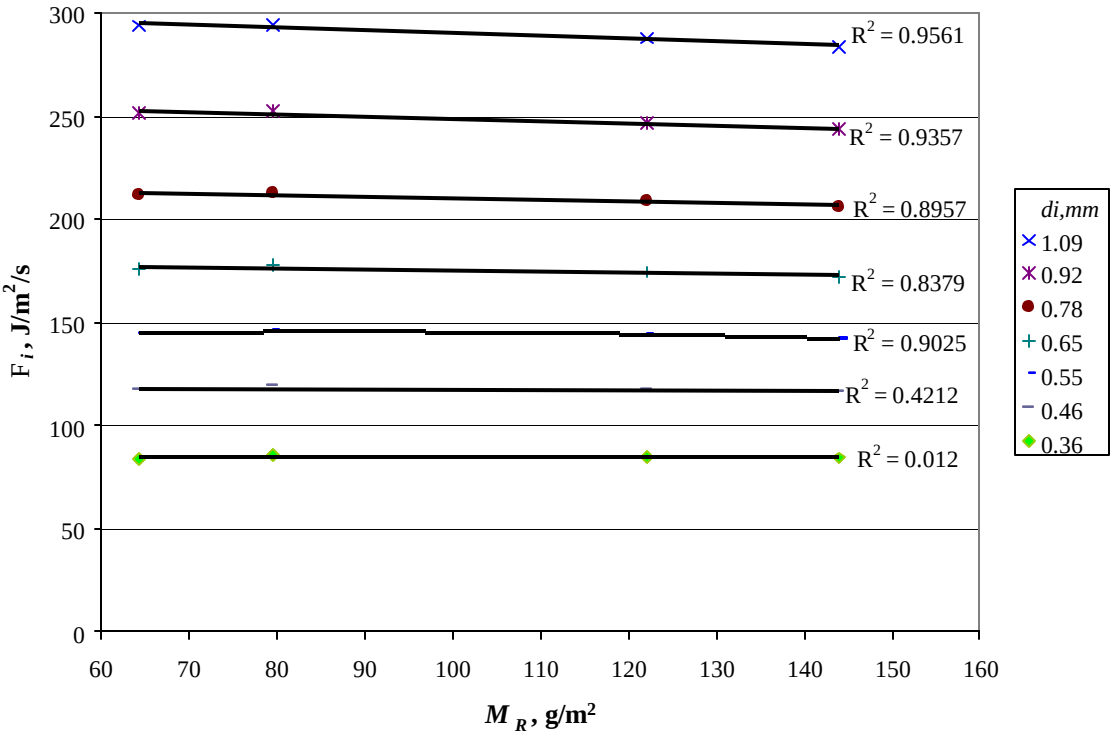

Figure 9.3 (a) Φ_i vs mass retained for experiments AU61_29h to AU70

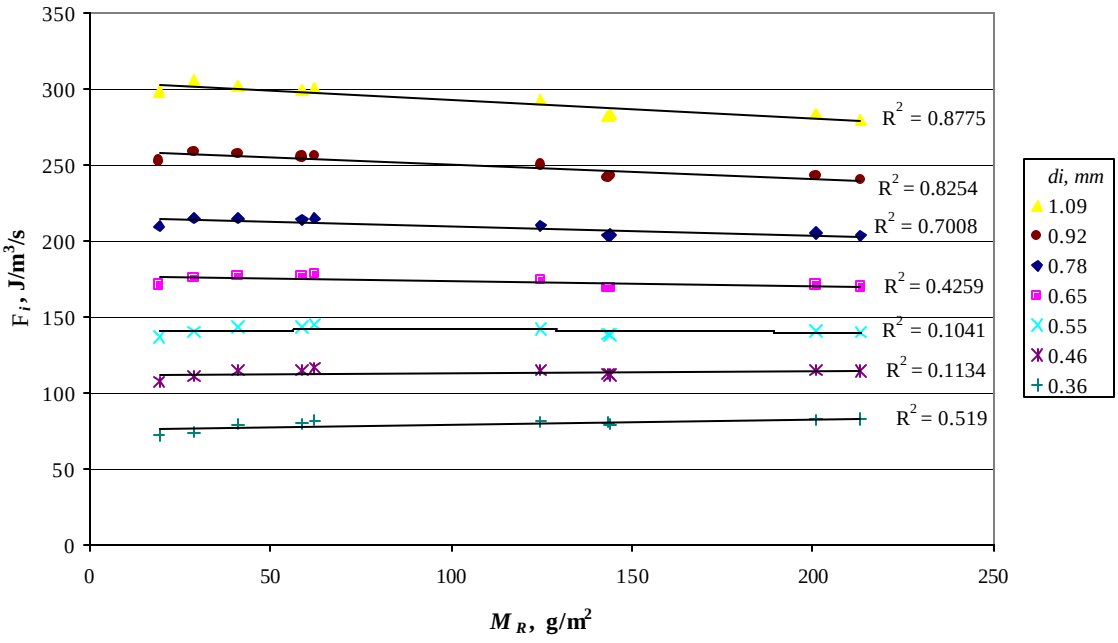

Figure 9.3 (b) Φ_i vs mass retained for experiments ZU61 to ZU95

The mass retained is most strongly correlated with Φ_i for the larger rather than smaller sizes. Furthermore, the mass retained actually increases (i.e. the efficiency decreases) as Φ_i for the finest size increases. The correlation between backwash rate and mass retained is better than the correlation between mass retained and Φ_i for all of the sizes in Figure 9.3. This suggests that the trends in Figure 9.3 merely reflect the relationship between Φ_i and backwash rate. Figure 9.4 shows the correlation between backwash rates and Φ_i for the ZU experiments.

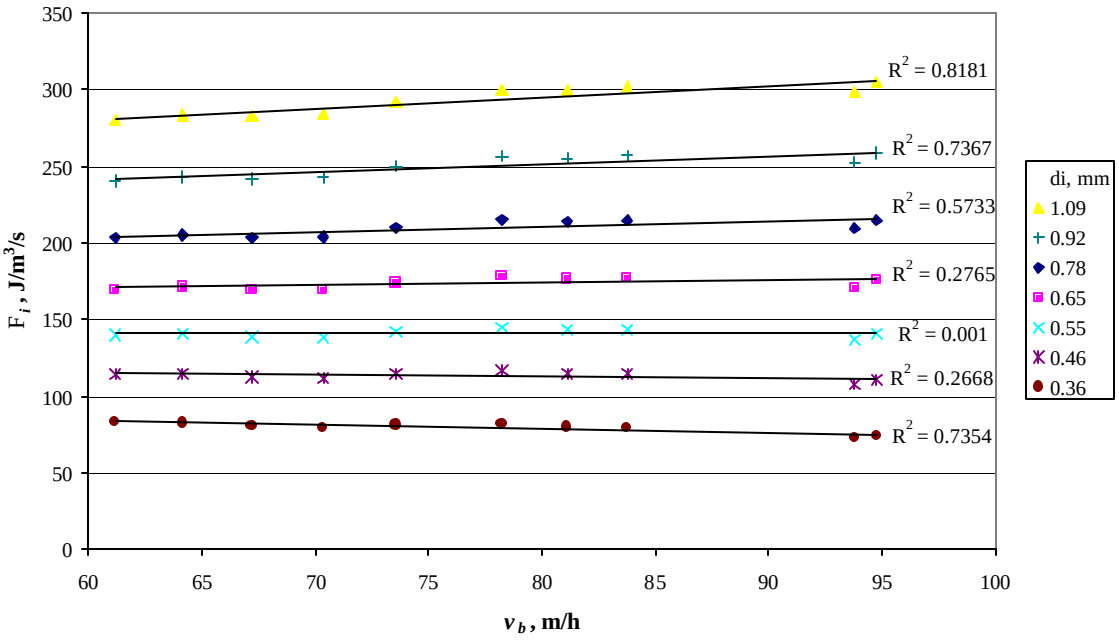

Figure 9.4 Φ_i as a function of backwash rate for experiments ZU61 to ZU95

From Figure 9.4, it is evident that the correlations between Φ_i and M_R are primarily reflections of the degree of correlation between backwash rate and Φ_i. Therefore, for this set of experiments, it appears that backwash rate is a better predictor of backwash efficiency than theoretical rate of power dissipation.

This will not necessarily hold true when comparing backwash efficiency for different size media, over wider temperature ranges and for greater than optimum backwash rates. In practice, real filters are very unlikely to be backwashed above the optimum rate since plants will opt for the lowest wash rate that gives satisfactory performance. Comparing backwash efficiency at different temperatures is complicated by the fact that floc strength is also a function of temperature (Bache et al, 1997). Therefore the best way to determine if Φ_i ever has any advantage over backwash rate for predicting backwash efficiency is to compare beds of different composition.

Ideally, the backwash efficiency for different filter beds should be compared at the same backwash rate as was done in the City of Tokyo (1956) study mentioned in Chapter 7. No comparison of the backwash efficiency for the 0.7 mm sand and 1 – 1.4 mm sand beds at the same backwash rate was made in the current study. However, the relationship between average Φ and backwash performance for the different beds at different backwash rates is shown by way of example.

The power dissipation per volume in the top 10 % of each bed was estimated as

$$\Phi_{10\%} = \sum_i c_i \Phi_i \qquad 9.4$$

c_i = Fraction of finest 10 % (by mass) made up of size d_i

Figure 9.5 shows the relationship between mass retained and $\Phi_{10\%}$ for the 0.7 mm and 1 – 1.4 mm sand beds. The theoretical power dissipation per volume in the top 10 % of the 0.7 mm sand bed was significantly lower than in the 1 – 1.4 mm bed, but the masses retained were similar to the AU experiments. This is contrary to the expectation that floc removal would tend to be less efficient in the finer sand. However, the parameters of the filtration steps of these experiments were different and so the differences in backwash performance were probably primarily due to differences in floc properties. This is discussed further in Section 9.3.

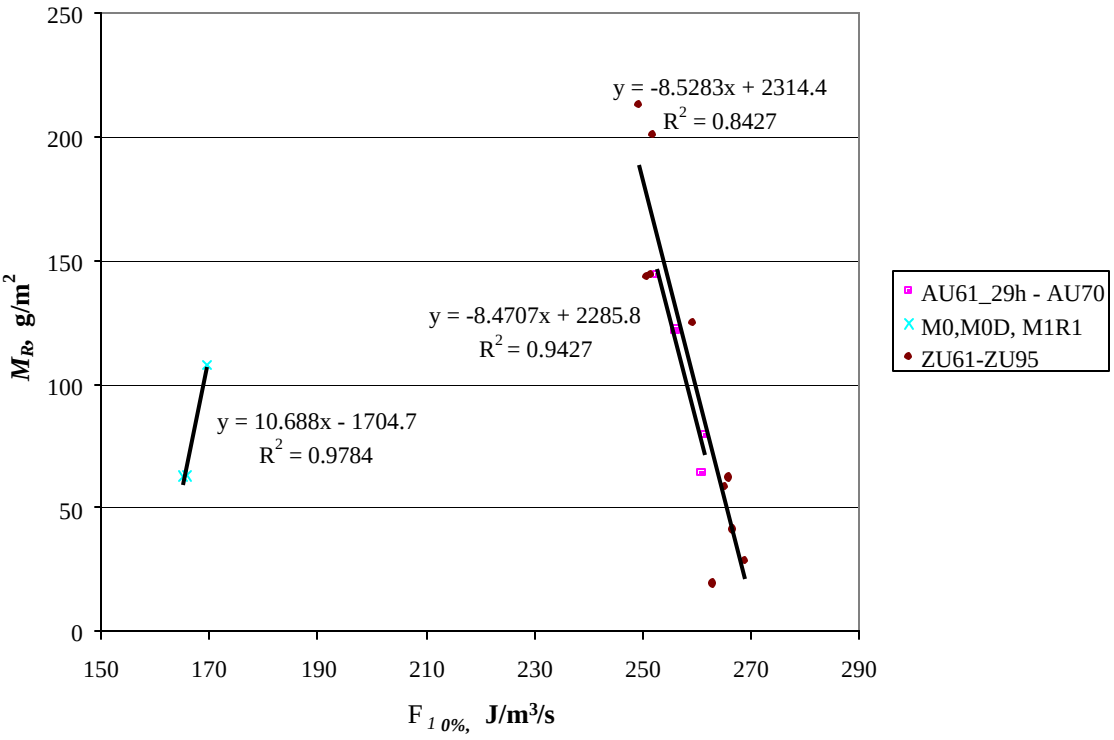

Figure 9.5 Mass retained as a function of $\Phi_{10\%}$

The data for the 1 – 1.4 mm bed showed the expected correlation between $\Phi_{10\%}$ and mass retained and that the trendlines for the two data sets are parallel. The three data points for

the 0.7 mm sand bed however showed an increase in mass retained with increasing power dissipation. This is assumed to be because the variation in backwash conditions was very small and that differences in floc conditions between the three experiments played the major role in determining backwash efficiency. Note that the differences in calculated shear stress for the 0.7 mm sand experiments were due to differences in temperature rather than backwash rate.

9.3. Factors affecting the cohesive and adhesive properties of floc deposits

With the exception of the AU61 experiments, where filter run time and terminal headloss were varied deliberately, the filtration parameters within each set of experiments were kept as consistent as possible. However, it was not possible to control the quality or temperature of the raw water coming into the plant. Within each of the three sets of experiments (AU, ZU and M experiments) there were variations in rate of headloss development and filtrate quality. These variations indicated changes in the quantity and characteristics of the influent floc that may also have impacted on backwash efficiency.

This section attempts to identify correlations between the mass retained after backwash and parameters relating to the filtration phase (i.e. p_{f1}, p_{f2}, p_{f3}… in Equation 8.5). First the experiments carried out in the 1 – 1.4 mm sand bed are analyzed then the results from the 0.7 mm sand bed are considered.

9.3.1. Variability in experimental conditions

Figures 9.6 to 9.8 show the variations in temperature, influent and filtrate turbidity, terminal headloss, rate of headloss development filter run time and total mass deposited for the AU, ZU and M (backwash delay and mass accumulation) experiments respectively. The experiments are listed in chronological order. The average influent (coagulated water) and filtered water turbidities were calculated by numerical integration of turbidity vs volume filtered, divided by the total volume filtered during the run.

$$coag = \frac{\sum_{i=0}^{N-1}\left[\left(V_{i+1}-V_i\right)\left(\frac{NTU_{in,i+1}-NTU_{in,i}}{2}\right)\right]}{volf} \quad 9.5$$

$$filt = \frac{\sum_{i=0}^{N-1}\left[b_i\left(V_{i+1}-V_i\right)\left(\frac{NTU_{out,i+1}-NTU_{out,i}}{2}\right)\right]}{volf} \quad 9.6$$

$coag$ = Average coagulated water turbidity, NTU

$filt$ = Average filtrate turbidity, NTU

V_i = Volume filtered at time of i^{th} turbidity measurement, m^3/m^2

$NTU_{in,i}$ = i^{th} coagulated water turbidity measurement, NTU

$NTU_{out,,i}$ = i^{th} filtrate turbidity measurement, NTU

b_i = weighting factor = 0.5, 0.75 or 1

$volf$ = Total volume of water filtered, m^3/m^2

The weighting factor b_i was used, where necessary, to compensate for low sampling resolution during the filter ripening stage. The rapid initial drop in filtrate turbidity could result in large errors in the result calculated using Equation 9.6 if the filter ripening curve was not well defined. The value assigned to b_i for each increment depended on how far filter ripening had progressed.

The average rate of headloss development was calculated as

$$\frac{dh_f}{dV_f} = \frac{term - h_0}{volf} \qquad 9.7$$

$\frac{dh_f}{dV_f}$ = rate of headloss development, mm/(m^3/m^2)

$term$ = terminal headloss, mm

h_0 = initial headloss, mm

Figure 9.6 shows a very slight overall increase in temperature (< 0.8 ^oC) and a 0.65 NTU drop in influent turbidity for the AU experiments. There was no trend in the filtrate turbidity. The alum dose was increased form 5.2 to 8 mg/L midway through experiment AU77 while it was maintained at 8.0 to 8.4 mg/L for the rest of the series. Therefore AU77 had the lowest average rate of headloss development. There was no systematic variation in the average dose (not shown) for the experiments after AU77 but the rate of headloss development for AU61_26h to AU61_8h was lower than for AU61_29h to AU68. This may have been due to the decrease in influent turbidity.

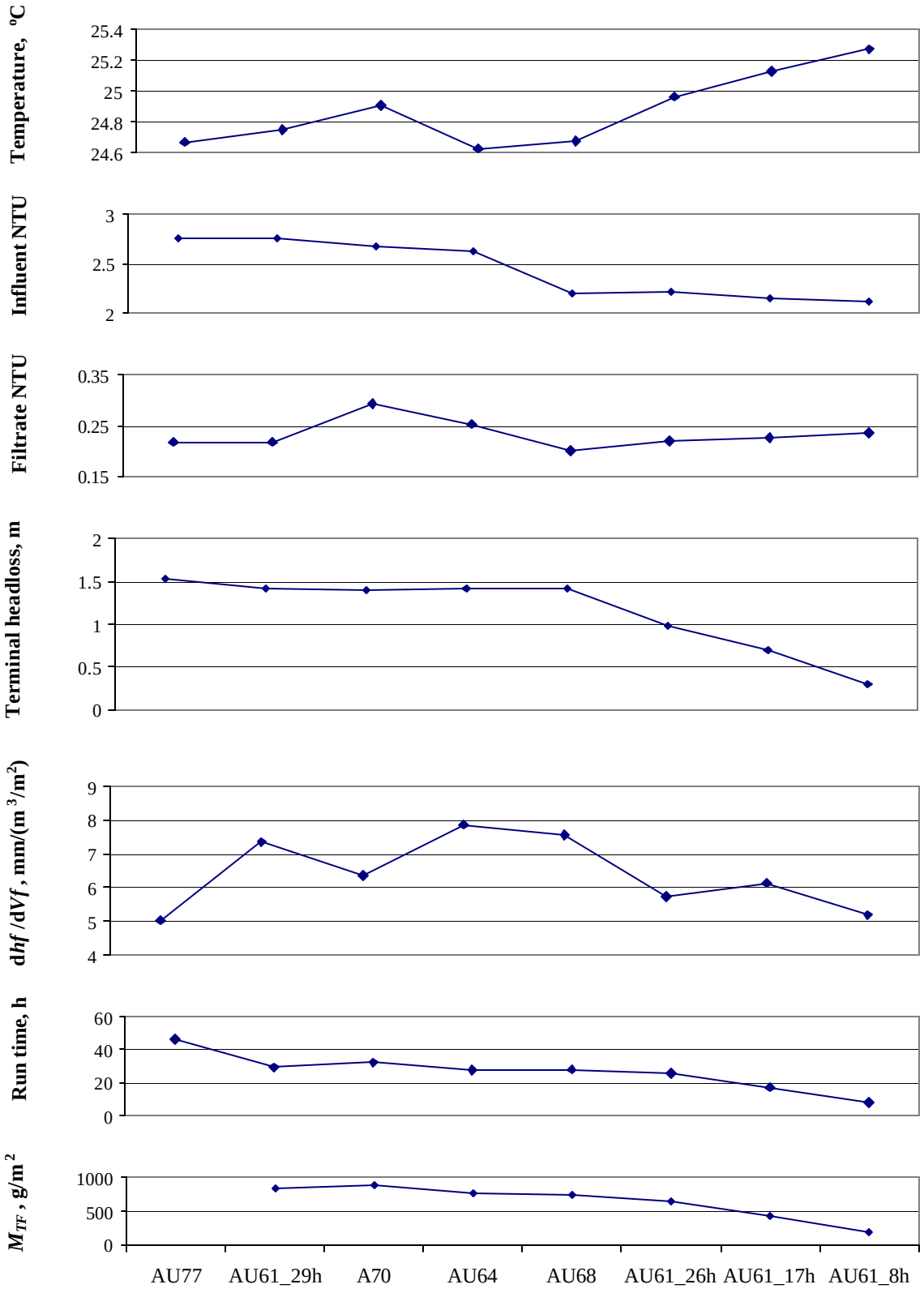

Figure 9.6 Variability in conditions for AU experiments

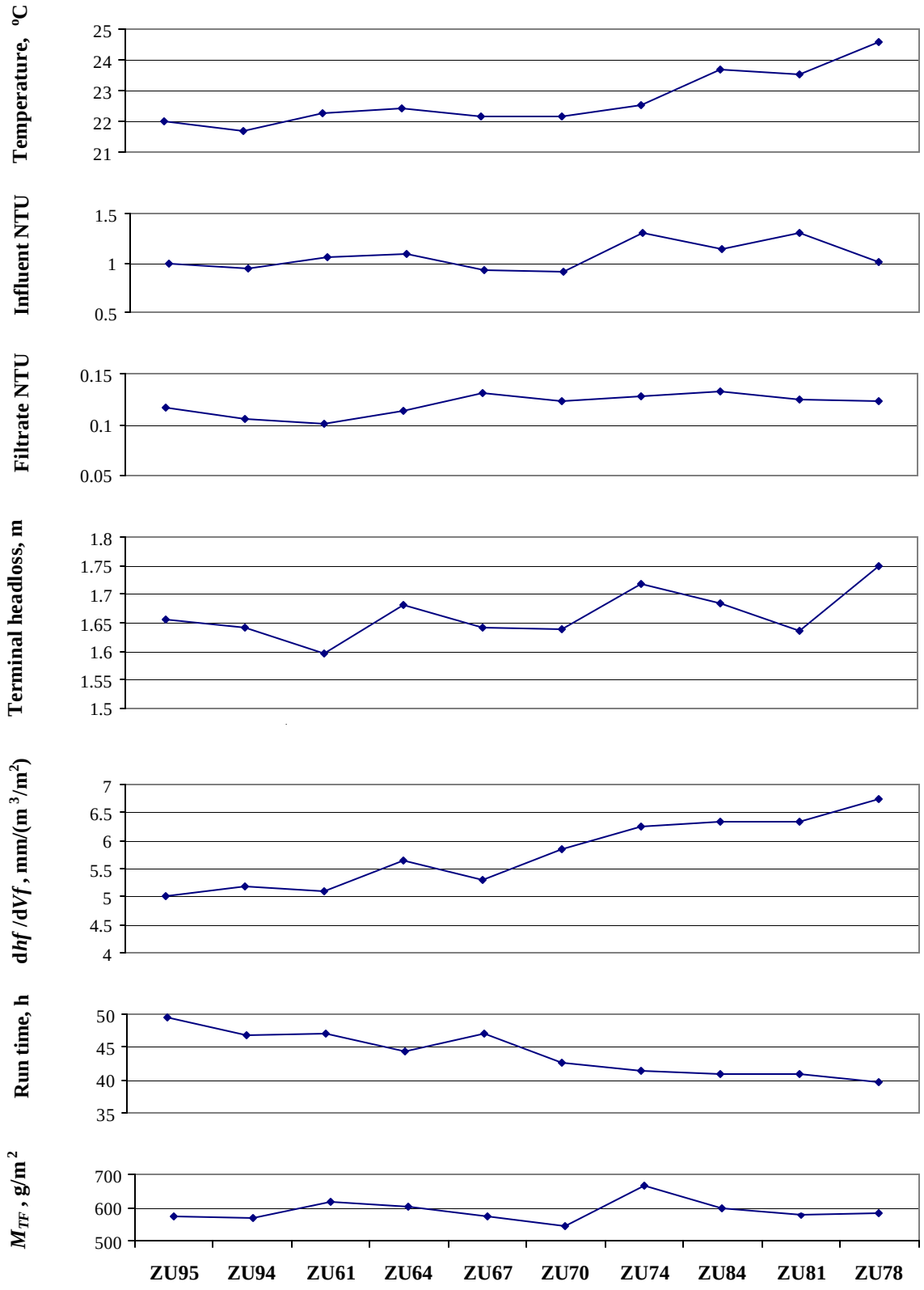

Figure 9.7 Variability of conditions in ZU experiments

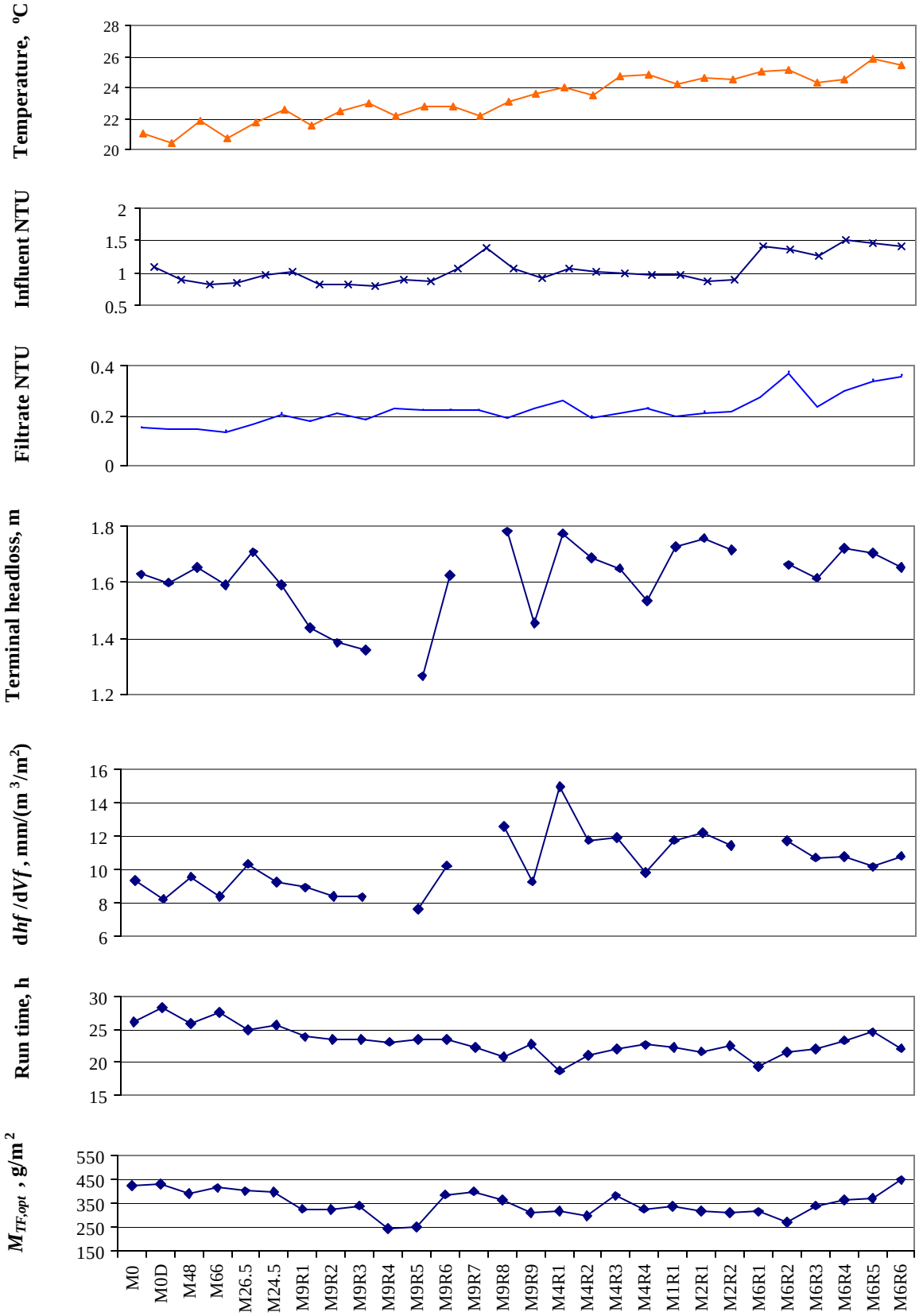

Figure 9.8 Variability of conditions in mass accumulation experiments

The total mass deposited was closely correlated with the filter run time but note that M_{TF} for AU61_26h was 24 % less than M_{TF} for AU61_29h although the decrease in run time was only 12 %. This was presumably also because of the decrease in influent turbidity.

For the ZU experiments, there was 2.5 ^{o}C overall increase in temperature. There was also a systematic increase in influent and filtrate turbidity and rate of headloss development. Run times decreased overall due to the higher rate of headloss development and but there did not seem to be any overall trend in the mass deposited. The average Z464N dose varied from 2.5 to 2.8 mg/L but did not show any systematic trends with time.

Experiments M0 to M6R6 started at around the same time as the ZU experiments (Spring 2001) but continued a few weeks longer into early summer. The average temperature increased by ~ 4.5 ^{0}C over the experimental period. The influent filtrate turbidities increased during the last series (M6R1-M6R) but the rate of headloss development increased earlier, towards the end of the first and longest series, M9R1-M9R9.

Filter run times were kept between 20 and 25 hours for must of the multiple cycle experiments and so the terminal headloss increased as the rate of headloss development increased. The delay experiments had run times of 25 to 29 hours and consequently tended to have higher values of $M_{TF,opt}$. Recall that $M_{TF,opt}$ is the best estimate of M_{TF} as defined in Chapter 5. The estimated mass deposited increased towards the end of the last series. There appeared to be a small drop in filtrate pH (7.6 to 7.4) during this period although there did not

appear to be any trend in the raw water pH (not shown). The alum dose and pH were shown in Figure 5.3. The increase in $M_{TF,opt}$ and decrease in pH were in fact related: the solubility of aluminium decreases with decreasing pH (above pH 6) and hence the lower measured pH led to a larger estimate of the mass of precipitate formed. This was consistent with the observed increase in influent turbidity.

The possible implications of these variations in filter operating parameters and performance are discussed next.

9.3.2. Potential impacts of filtration parameters on backwash efficiency

9.3.2.1. Total mass deposited (M_{TF})

The mass retained in the filter after backwash may or may not be influenced by the total mass deposited during filtration. On the one hand, if one assumes that on average any given unit of floc deposit has the same probability of surviving backwash as any other, then one would expect the mass retained in the filter to increase with increasing mass deposited. On the other hand, the volume of floc of a particular cohesive strength that can remain attached may be a function of the hydrodynamic situation and independent of the amount present at the beginning of backwash. In Figures 9.1 and 9.2, there was a slightly better correlation between mass retained and backwash rate than between mass retained and % detachment.

9.3.2.2. Filter run time

Experience has shown that allowing excessively long filter run times when influent turbidities are very low is detrimental to backwash performance (Monk and Willis, 1987). Furthermore, in Chapter 8 it was shown that backwash efficiency declined the longer a dirty filter was left standing before backwash. The greatest variability in filter run time occurred during the AU experiments when the terminal headloss was varied deliberately for the experiments at 61 m/h (Run time = 8 to 32 hours). However, there were also variations in run time for the ZU (39 to 49 hours), backwash delay and mass accumulation experiments as a result of changes in the rate of headloss development (19 to 28 hours). Run times were greatest for the ZU experiments because rates of headloss development were always lower than for the experiments with alum.

9.3.2.3. Rate of headloss development

For a given filter bed and filtration rate, the rate of headloss development should to some extent reflect the mechanical strength of the floc entering the bed and the deposits it forms on the media. This is because the weaker the floc is relative to the fluid shear forces during filtration, the deeper it will penetrate into the bed and the lower the rate of headloss development. Conversely, strong cohesive floc will tend to deposit closer to the surface of the bed resulting in rapid clogging. Consequently, there may be a relationship between headloss development and mass retained after backwashing. The mass retained would be expected to increase as the strength of the floc deposits and hence rate of headloss development increased.

The rate of headloss development is particularly attractive as an indicator of floc deposit strength for at least two reasons:

1. Rate of headloss development is an important indicator of filtration performance and is often monitored routinely.

2. Unlike direct measurements or theoretical calculations of interparticle interactions, which are necessarily based on several assumptions about floc structure and behaviour, rate of headloss development is related to the tendency of floc to remain attached to the same filter grains which are subjected to backwashing.

The disadvantage of rate of headloss development is that it is also a function of filtration rate and mass loading. These factors would have to be taken into account in developing a general model for the full range of typical filtration conditions. Furthermorer, higher rates of headloss development tend to result in shorter run times so these two factors may balance each other out.

In this study, the highest rates of headloss development occurred in the 0.7 mm sand filter (7.2 to 15 mm/(m^3/m^2)) because of the finer media size and the lowest rates occurred in the ZU experiments (5.0 to 6.7 mm/(m^3/m^2)) because the lower doses of coagulant required (~

2.5 mg/L of Z464N compared to 6 to 8 mg/L) produced less floc and hence less clogging of the media. Rates for the AU experiments varied from 5.2 to 7.9 mm/(m^3/m^2).

9.3.2.4. Turbidity removal efficiency

Another filtration performance parameter that may correlate with floc strength and cohesiveness is filtration removal efficiency. For a given filtration rate, a greater removal efficiency during filtration suggests a greater tendency of floc to adhere to the filter media which may also mean that it is more difficult to detach during backwash. For example, use of polymeric coagulants and filters aids can produce better filtrate quality but does require a more efficient backwash system to maintain the state of the filter bed than when alum or ferric chloride are used alone (Kawamura, 1975b). The turbidity removals for the AU and ZU experiments were all around 90 %. Average removal efficiencies varied from 80 to 86 % for the backwash delay experiments and from 75 to 81 % for the mass accumulation experiments.

The difference in turbidity removal efficiency does not explain the discrepancy between the backwash efficiencies for experiments M0, M0D and M1R1 in Figure 9.11 since in this case, M0 and M0D had the higher turbidity removal (84 % and 86 % for M0 and M0D compared to 79 % for M1R1) and higher backwash efficiency. However, it may explain the fact that the backwash efficiency was similar for 0.7 mm sand than for 1 to 1.4 mm sand in Figures 9.1 and 9.5 despite the lower backwash rates and average shear stess. In the 0.7 mm sand bed, the greater bed depth and finer media size would tend to produce better filtrate

quality than the relatively short, coarse 1 to 1.4 mm sand bed (Kau and Lawler, 1995). The fact that the turbidity removal efficiency was lower in the delay and mass accumulation experiments than the AU experiments indicated a weaker floc that would be more easily removed during backwash.

9.3.2.5. Temperature

Temperature could affect the efficiency of detachment in two ways. Viscosity increases with decreasing temperature, which increases shearing forces (although this would be offset to some extent by the increase in porosity). Floc strength is also known to increase with temperature (e.g. Bache et al, 1997). Both factors should tend to result in decreasing detachment efficiency with increasing temperature.

9.3.2.6. pH

The impact of pH on aluminum hydroxide solubility has already been discussed in Chapter 3. In addition, pH will affect the surface charges on particles. Amirtharajah and O'Melia (1990) present data from direct filtration with alum coagulation showing a local minimum in turbidity removal efficiency between pH 7 and 9.

9.3.2.7. Coagulant dose

The final factor considered here is coagulant dose. Both under and over dosing coagulant may result in a decrease in floc strength so the possibility of a non-linear relationship between dose and $M_{R,opt}$ needs to be considered. Furthermore the coagulant demand may vary with influent turbidity. The greatest variability in coagulant dose occurred in the mass accumulation experiments. Alum doses for these experiments were shown in Figure 3.6.

9.3.3. Linear regression analysis

Model selection techniques utilizing multivariate linear regression provide a relatively simple way of determining which of a number of possible parameters are significantly correlated with filter backwash performance and whether the correlations are positive or negative. Matlab's stepwise linear regression tool (The Mathworks, 1999) was used to identify filtration and backwash parameters which were correlated with the mass retained after backwashing, M_R. Once a statistically significant model was identified, Microsoft Excel's linear regression tool was used to calculate the regression statistics (regression coefficients and confidence intervals).

9.3.3.1. Experiments with 1-1.4 mm sand (AU and ZU)

The AU series of experiments included 4 runs with M_{TF} held relatively constant (880 to 730 g/m^2) while the backwash rate was varied, and an additional three runs where the

backwash rate was held constant and the degree of clogging of the bed was varied. M_{TF} and M_R were not determined for AU77, so this experiment is not included in the following analysis.

In Section 9.2, it was established that backwash rate was the best predictor of backwash efficiency (mass retained) for similar filtration conditions and variable backwash rate. Consequently, the following model of the variability in M_R for the AU data was proposed

$$M_R = a_0 + a_1 v_b + a_2 p_{f1} + a_3 p_{f2} + ... \qquad 9.8$$

a_0, a_1,… = Regression coefficients

p_{f1}, p_{f2},… = Parameters relating to the filtration phase which reflect the floc characteristics and degree of clogging of the filter

Figure 9.9 compares the correlations between mass retained (M_R) and three measures of the degree of filter clogging: terminal headloss, filter run time and mass deposited for backwash at 61 m/h.

All three indicators of clogging are highly correlated with each other and with M_R but M_R is most strongly correlated with filter run time. This is consistent with the finding in Chapter 8 that floc became more difficult to remove the longer it remained in the filter. The best choice for p_{f1} therefore appears to be filter run time. Matlab's stepwise regression was used to look for additional parameters p_{f2}, … which might reflect other changes in floc properties. Average

influent and filtrate turbidity, raw and filtrate pH, temperature, average coagulant dose, ratio of filtrate to influent turbidity and rate of headloss development were considered but no further significant correlations were found.

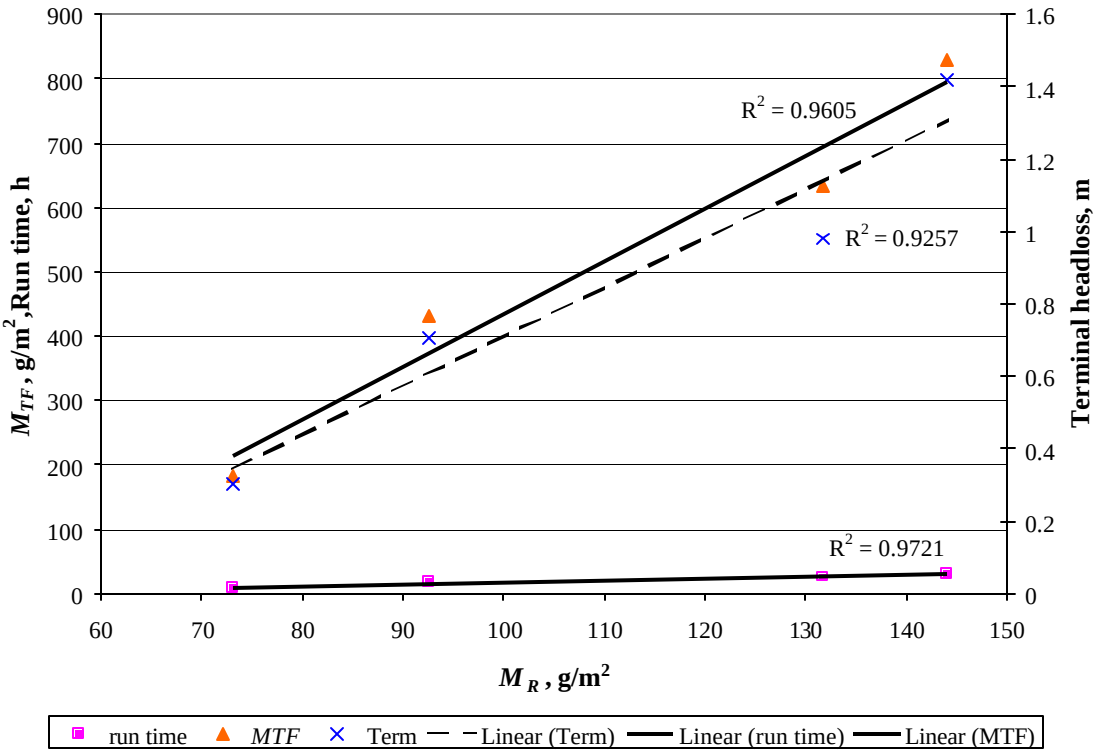

Figure 9.9 Relationship between mass retained and degree of clogging for alum coagulation and backwash at 61 m/h

The final result for the AU data set calculated using Excel's linear regression tool was

$$M_{R,AU} = -9.583 v_b + 3.545 runtime + 627.46 \qquad 9.9$$

$$R^2 = 0.965$$

Stepwise linear regression was then applied to the data for the ZU experiments. Once again, filter run time was the best choice for p_{f1} and no statistically significant correlations were found with any other variable. The model for the Z464N experiment was

$$M_{R,ZU} = -5.953 v_b + 4.777\, runtime + 350.56 \qquad 9.10$$

$$R^2 = 0.958$$

The 95 % confidence intervals for the regression coefficients (calculated using Excel's linear regression tool) are listed in Table 9.3.

Table 9.3 95 % confidence intervals for regression coefficients

	AU	ZU
A_0	(473, 782)	(532, 169)
A_1	(-6.9, -12.2)	(-4.8, -7.1)
A_2	(2.4, 4.7)	(0.9, 8.6)

In each case, the regression coefficients for the two data sets are not statistically different at the 95 % confidence interval.

Figure 9.10 shows the agreement between the predictions for Equation 9.10 (calibrated using the ZU data) and the measured values for both the AU and ZU experiments. The

apparently good agreement between the model predictions for alum and Z464N is somewhat surprising. Generally, one expects polymer flocs to be more difficult to remove. Furthermore, the floc composition is different for the two coagulants. Therefore, the fact that the two empirical models agree in this case may be coincidental.

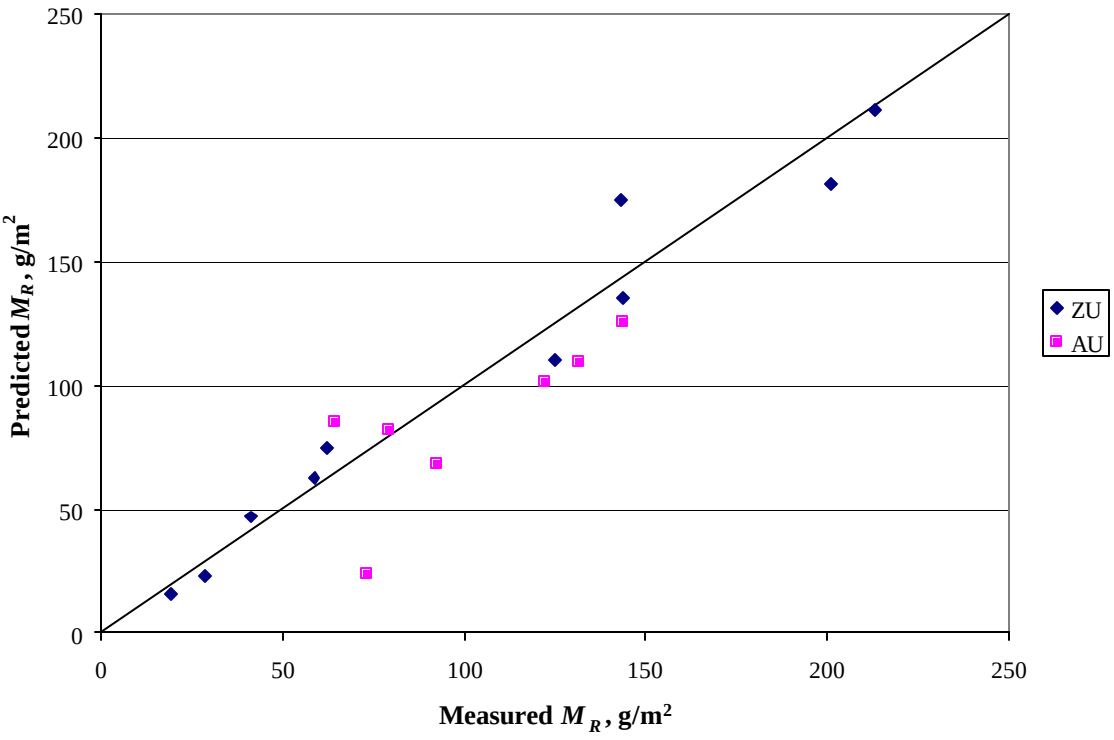

Figure 9.10 Agreement between measured mass retained and Equation 9.9

However, it should be noted that the strength of both alum and Z464N floc will vary depending on the dosing conditions. Polymeric coagulants are generally used to improve the filtrate turbidity. In this case, the filtrate turbidity was lower for the ZU experiments but this was at least partly due to lower influent turbidities. The filtration removal efficiencies were around 90 % in both cases. Therefore, the polymer floc was not necessarily inherently stronger than the

alum floc. However, one would not necessarily expect the strength of Z464N floc to increase at the same rate as alum. Since there was no direct comparison between backwash efficiency for alum and Z464N floc at the same run time, these results are inconclusive about the relative strengths of the two flocs. Nonetheless, overall the data highlights the importance of the effect of floc aging on backwash efficiency and indicates that more research in this area is needed.

The results obtained in the AU and ZU experiments did not support the view that the rate of headloss development should provide a useful indicator of floc strength – within the separate data sets for alum and Z464N and in comparing the two. Larger concentrations of floc lead to more rapid accumulation of deposits and higher rates of headloss development particularly in the top sections of the filter. This does not necessary indicate stronger floc.

9.3.3.2. Mass accumulation experiments

The data for the mass accumulation experiments proved more difficult to analyze than the AU and ZU experiments because: (a) none of the backwash or filtration parameters except for number of consecutive runs were varied in a systematic way; and (b) there was a substantial amount of uncertainty in the estimates of both the total mass deposited and the incremental mass retained for individual runs as discussed in Chapter 5. There was a clear correlation between delay time and backwash efficiency for the delayed backwash experiments but this result was not directly useful for analyzing experiments with no backwash delay. While floc aging during filtration and floc aging with no flow are both expected to affect backwash efficiency, they are

not necessarily going to have same impact. The following discussion refers to the experiments with 0 hours delay time, that is M0, M0D and M1R1-M9R9.

The one factor that was varied deliberately was the number of filter runs in a series. It was hoped that if other sources of variability could be identified and quantified, then it would be possible to determine conclusively whether the apparent decrease in rate of accumulation with run number implied in Figures 8.9 and 8.11 was physically significant or coincidental. The calculation of a set of estimates of the mass retained, M_{Ropt} was described in Section 5.3.

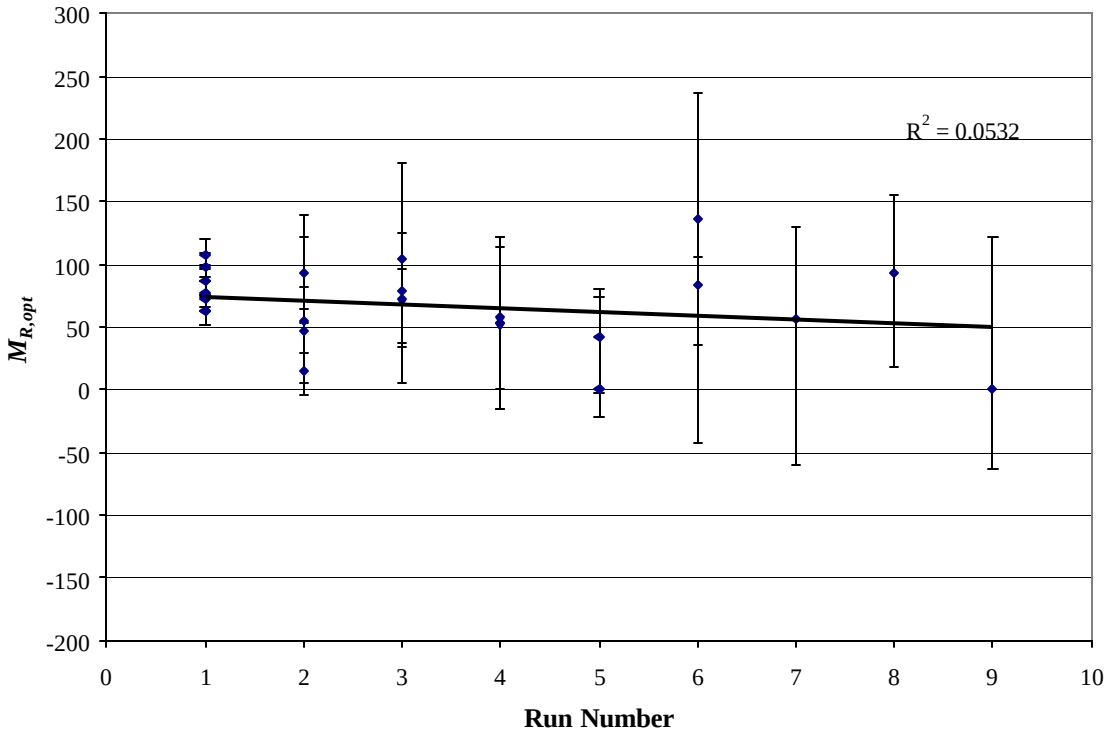

Figure 9.11 Best estimates of mass retained for individual filter runs as a function of run number

Figure 9.11 shows a very weak, statistically insignificant negative dependence of $M_{R,opt}$ on the number of runs. As discussed in Chapter 8, the incremental increase in mass retained from one run to the next might be expected to decrease as the mass of previously retained material increases. Figure 9.12 shows $M_{R,opt}$ for the k^{th} run plotted against the cumulative mass retained up to the previous run, $(\Sigma M_{r,opt})_{k-1}$. There is a slightly better negative correlation here than in Figure 9.11.

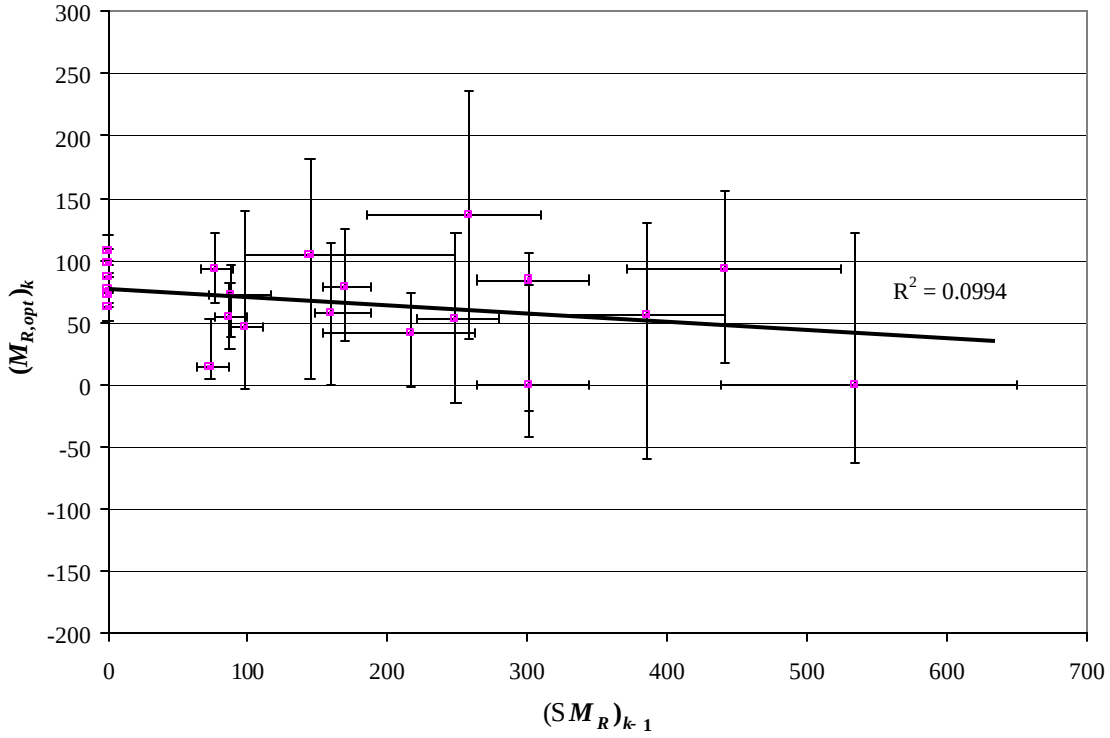

Figure 9.12 Incremental increase in mass retained as a function cumulative mass retained

Figure 9.13 shows $M_{R,opt}$ as a function of $M_{TF,opt}$, the best estimate of the total mass deposited in a given run. The correlation between $M_{R,opt}$ and $M_{TF,opt}$ appears to be substantially better than the correlation between $M_{R,opt}$ and n, and between $(M_{r,opt})_k$ and $(\Sigma M_{R,opt})_{k-1}$.

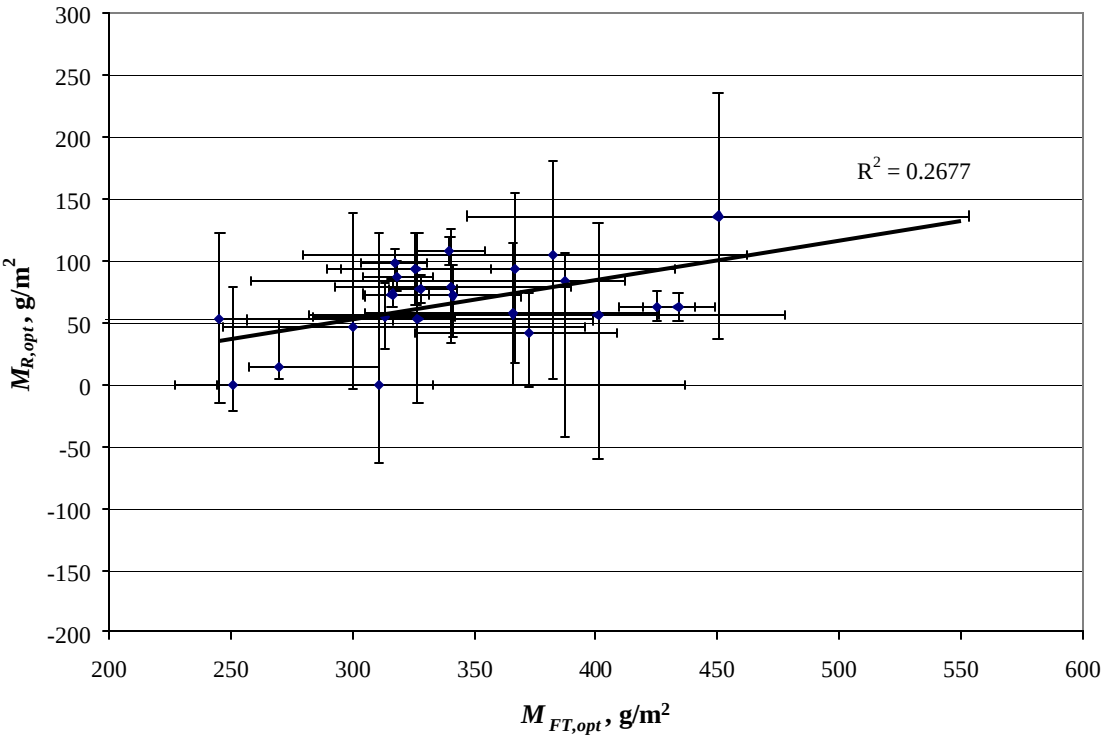

Figure 9.13 Incremental mass retained as a function of mass deposited

However, it must be remembered that Figure 9.13 shows the relationships between estimates of $M_{R,opt}$ and $M_{TF,opt}$ rather than their true values. Even if there were no relationships between the true values there must be some degree of covariance between the estimates since the $M_{R,opt}$ is the difference between $M_{TF,opt}$ and M_D, the measured mass detached. From Equation 5.4, it is evident that increasing the estimate of M_R increases the estimate of M_{TF} by the same amount.

In order, to get a better idea of the extent of the relationship between $M_{R,opt}$, the correlation between $M_{R,opt}$ and M_D should be calculated. It can easily be shown that if M_R tends

to vary in proportion to M_{TF} then M_D will also tend to vary in proportion to M_{TF} and consequently, M_R must tend to vary in proportion to M_D. A zero or negative correlation between $M_{R,opt}$ and M_D would indicate that there is no relationship between $M_{R,opt}$ and M_{TF} and therefore probably no physical relationship between the true values of M_R and M_{TF}. Figure 9.14 shows that there is in fact no apparent relationship between $M_{R,opt}$ and M_D.

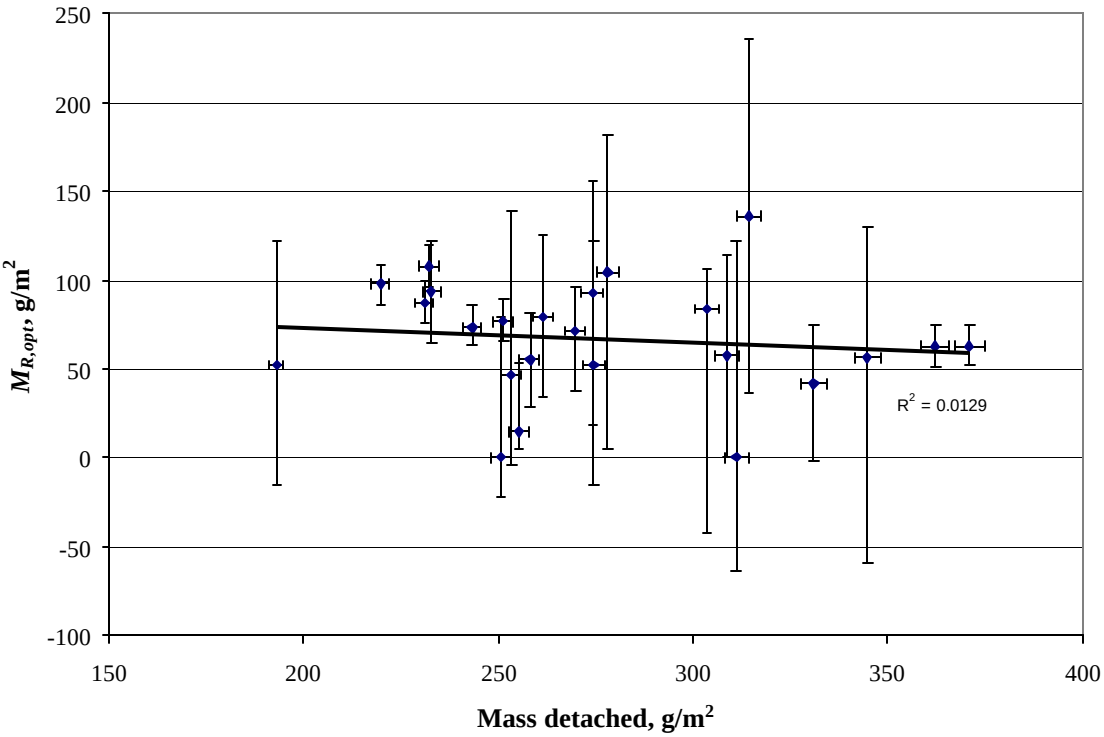

Figure 9.14 Estimated mass retained vs mass detached

Of all the possible correlations considered for this data set, none are statistically significant at the 95 % confidence interval. The most significant single factor relationships are between $M_{R,opt}$ and *rate1*, $(\Sigma M_R)_{k-1}$ and *dose* at the 87 %, 86 % and 83 % confidence levels respectively. In constrast to the AU and ZU experiments, there was essentially no correlation

between run time and mass retained. Figures 9.15, 9.16 and 9.17 show mass retained plotted against rate of headloss development, dose and run time.

Figure 9.8 showed a distinct step up in rate of headloss development during the series M9R1-M9R9. It was thought that this might explain the difference in backwash efficiency for experiments M0 and M0D and M1R1. Figure 9.15 shows that there was in fact a weak positive correlation between rate of headloss development and $M_{R,opt}$. The calculation of the upper and lower estimates of the rate of headloss development is discussed in Appendix 3.

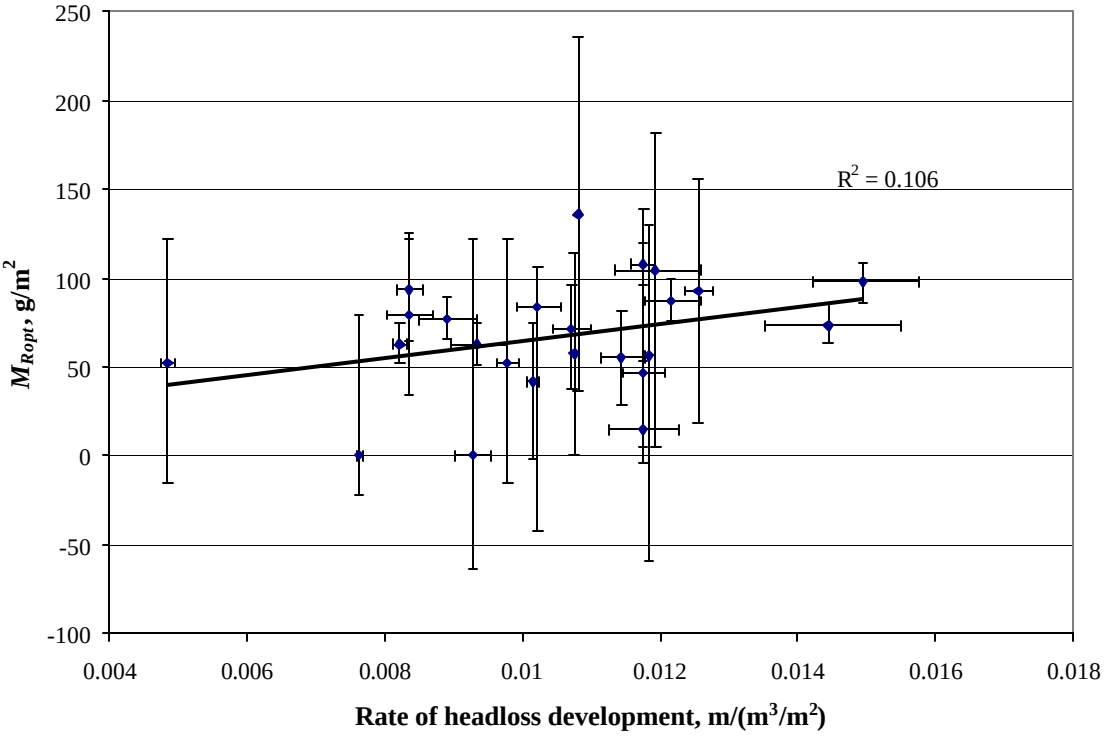

Figure 9.15 Relationship between incremental mass retained and rate of headloss development

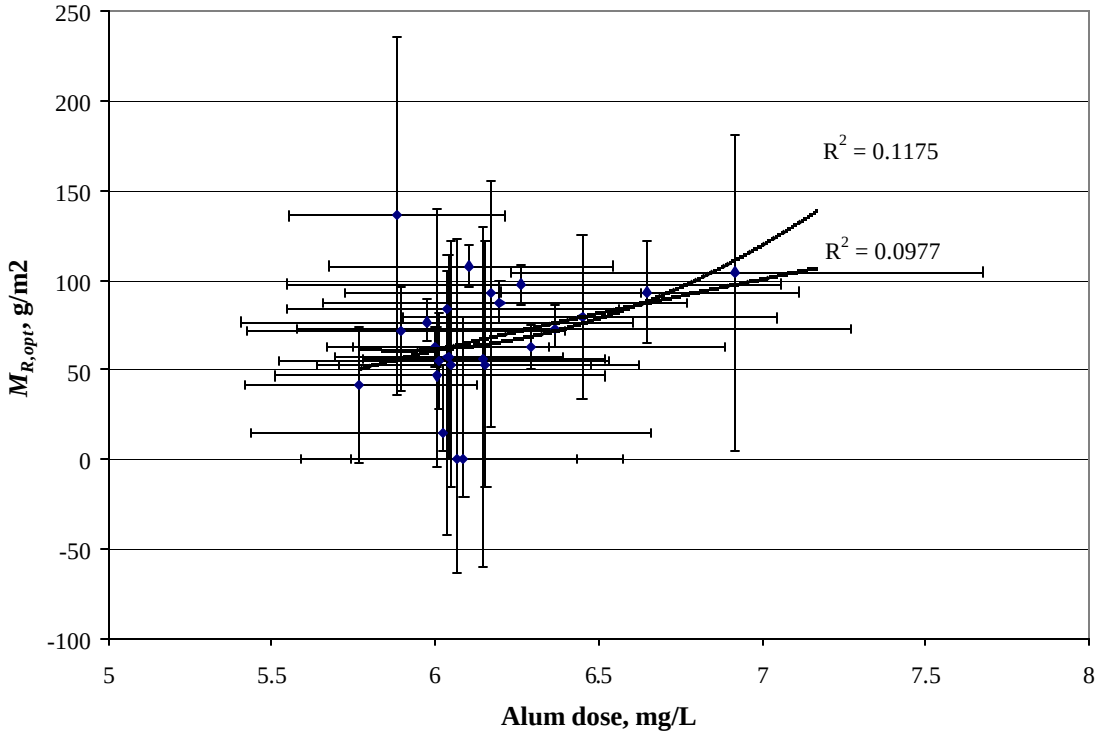

Figure 9.16 Incremental mass retained as a function of alum dose

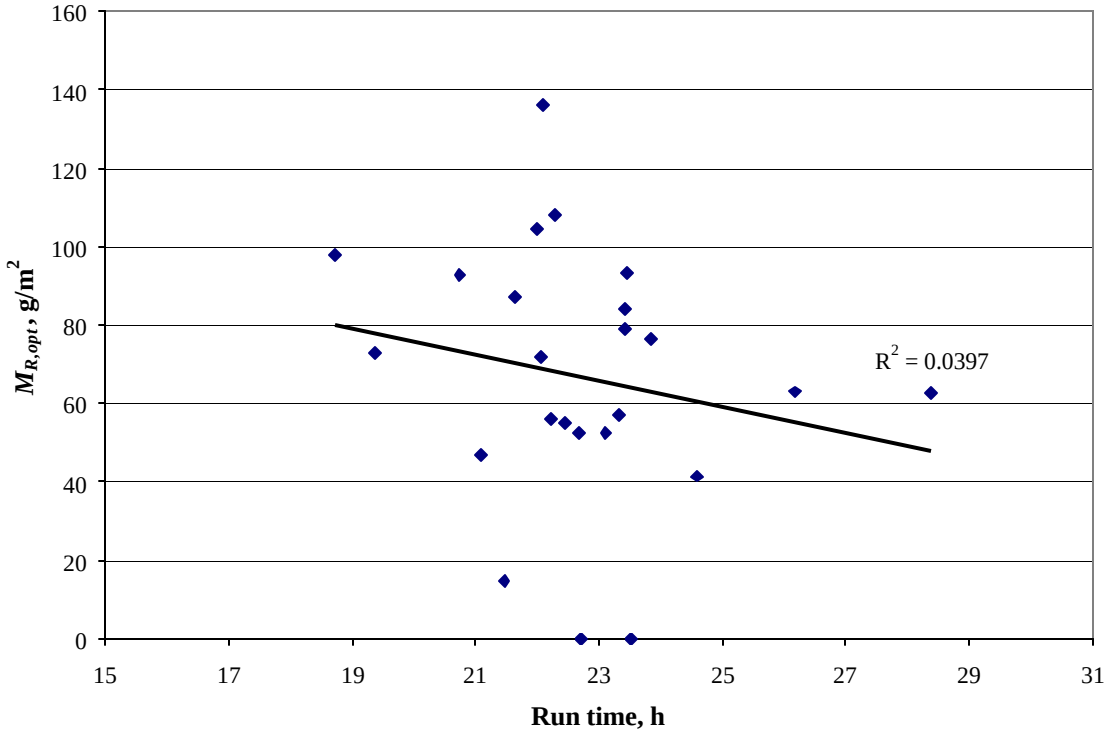

Figure 9.17 Estimated mass retained vs filter run time

Figure 9.16 shows $M_{R,opt}$ plotted against coagulant dose with linear and quadratic trendlines. The quadratic trendline was calculated to check whether there was a possible maximum point (since both under and overdosing can result in weaker floc) but none was detected. Figure 9.17 shows $M_{R,opt}$ plotted against filter run time.

The next question to be answered was whether any combination of these factors would yield a better, statistically significant correlation with $M_{R,opt}$. Matlab (The Mathworks, Inc, 1999)'s stepwise regression tool was used to look for relationships between $M_{R,opt}$ and various linear combinations of M_D, $(\Sigma M_R)_{k\text{-}1}$, $\frac{dh_f}{dV_f}$, *filt*, *filt/coag*, *temp*, *dose*, *dose*^{2} and run time. pH was not considered because the data set was not complete and the single factor correlation results were not particularly promising. Stepwise regression at the 77 % confidence level yielded a model of the form

$$\left(M_{R,}\right)_{k,est} = b_0 + b_1 \frac{dh_f}{dV_f} - b_2 \left(\sum \mathrm{M}_{\mathrm{R,opt}}\right)_{k-1} \qquad 9.11$$

b_0, b_1, b_2 Regression coefficients

with $R^2 = 0.169$. i.e. Equation 9.11 is only able to account for 17 % of the variation in $M_{R,opt}$. This does not seem unreasonable given the estimated uncertainties in $M_{R,opt}$ and the narrow range of conditions considered.

In Equation 9.11, the value of $(M_R)_{k,est}$ depends on the values of the estimates of M_R all for all previous runs in the series. Therefore the optimum values of the regression coefficients have to be determined iteratively. Using the first set of regression coefficients obtained for Equation 9.11, the values of $(\Sigma M_R)_{k-1}$ of were recalculated and the regression repeated. This procedure was continued until the estimates of M_R converged within 1 g/m^2.

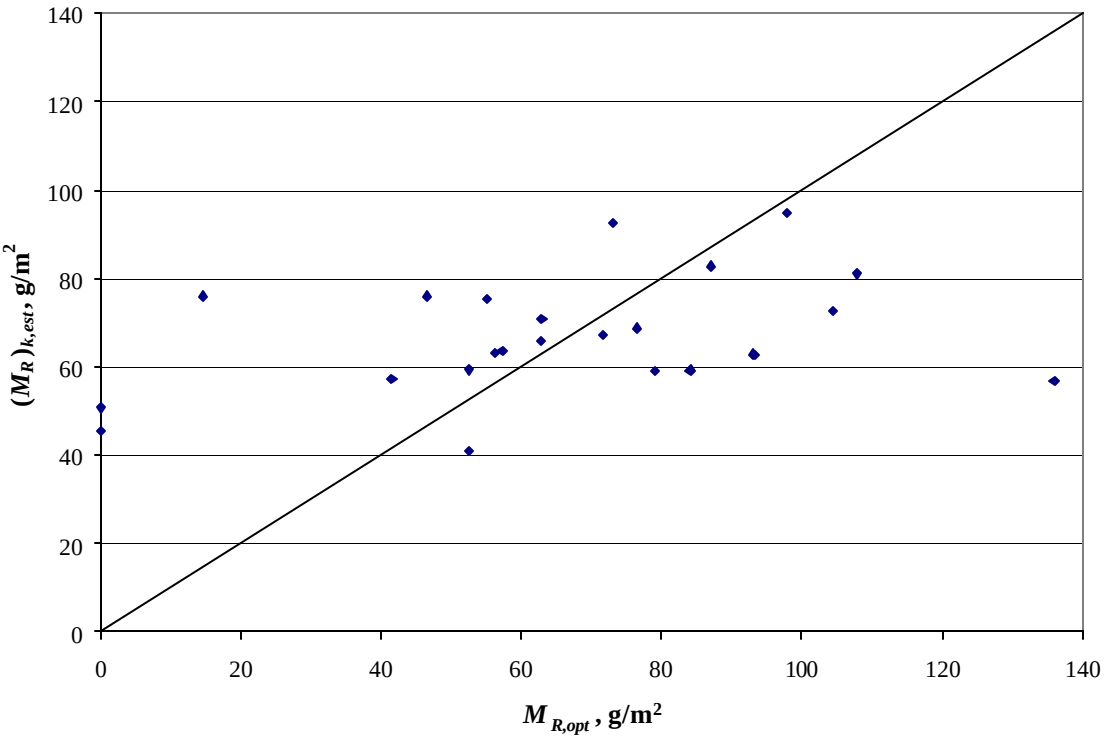

Figure 9.18 Comparing model predictions with $M_{R,opt}$

Figure 9.18 compares the results of Equation 9.11 with $M_{R,opt}$. Estimates from Equation 9.11 fall in a much narrower range of values than $M_{R,opt}$ (40 to 100 g/m^2 as compared to 0 to 140 g/m^2), suggesting that a substantial fraction of the variability in $M_{R,opt}$ was due to errors in the measurements on which these estimates were based. Comparing Figures 8.9 (cumulative

mass retained, measured) and Figure 5.9 (cumulative mass retained, estimates) reinforces this impression: the measured cumulative mass retained shows a much smoother increase with run number than the estimates $\sum M'_R$, $\sum M''_R$ and $\Sigma M_{R,opt}$ suggest. Figures 9.19 and 9.20 show the cumulative mass retained calculated from Equation 9.11 and $\Sigma M_{R,opt}$ vs the measured values. In Figure 9.20, the total mass retained is divided by the number of runs to give a better idea of the accuracy of the calculations for individual runs.

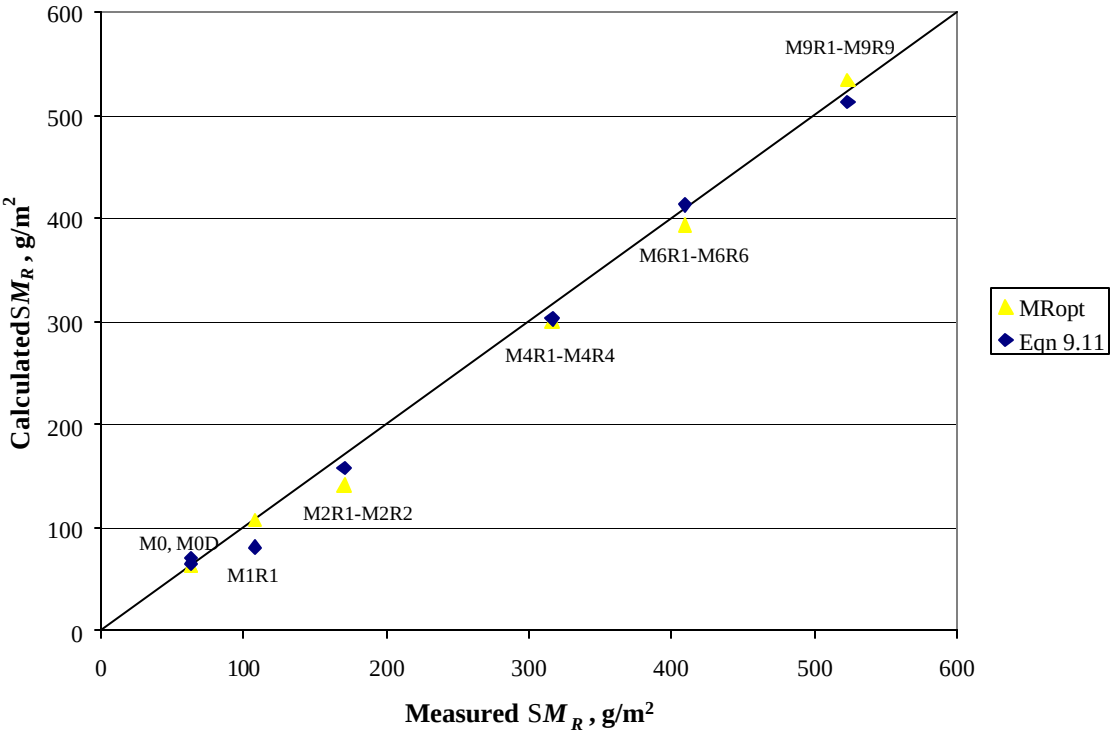

Figure 9.19 Calculated cumulative mass retained vs measured cumulative mass retained

The sum of square errors (differences between calculated and measured values of ΣM_R) for the Equation 9.11 estimates was slightly better than the sum of square errors for the

calculated data set $M_{R,opt}$. This is in spite of the fact that the data set $M_{R,opt}$ included three actual measurements (M1R1, M0, M0D).

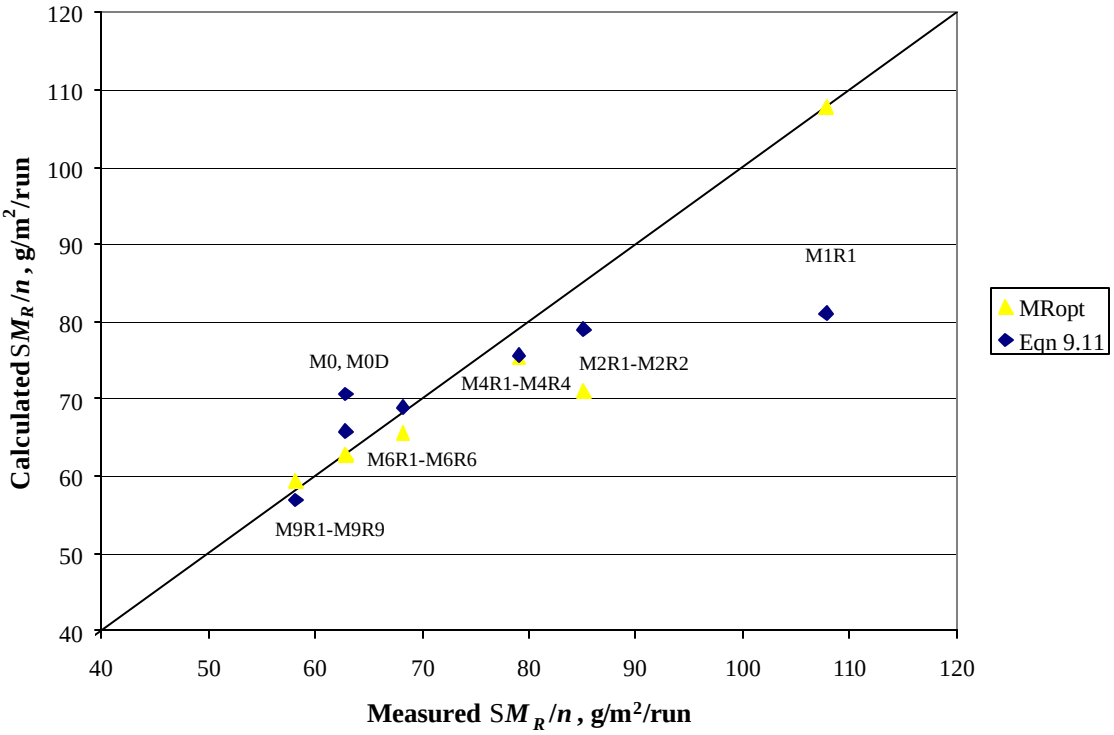

Figure 9.20 Calculated average mass retained per run vs measured mass retained per run

Not only does Equation 9.11 provide a reasonable accurate prediction of ΣM_R but it also shows the expected qualitative dependence of incremental mass retained on floc strength and retained mass already present in the filter. The negative coefficient for $(\Sigma M_{R,opt})_{k-1}$ is consistent with the results in Figure 9.11.

However, it must be noted that when when the average mass retained per run is plotted against the average rate of headloss development for each series, it is clear that at least part of the apparent dependence of mass retained on run number is due to changes in floc strength over the course of the experimental study. This is shown in Figure 9.21. Note that the regression line refers only to experiments M1R1 – M9R1 and not M0 and M0D.

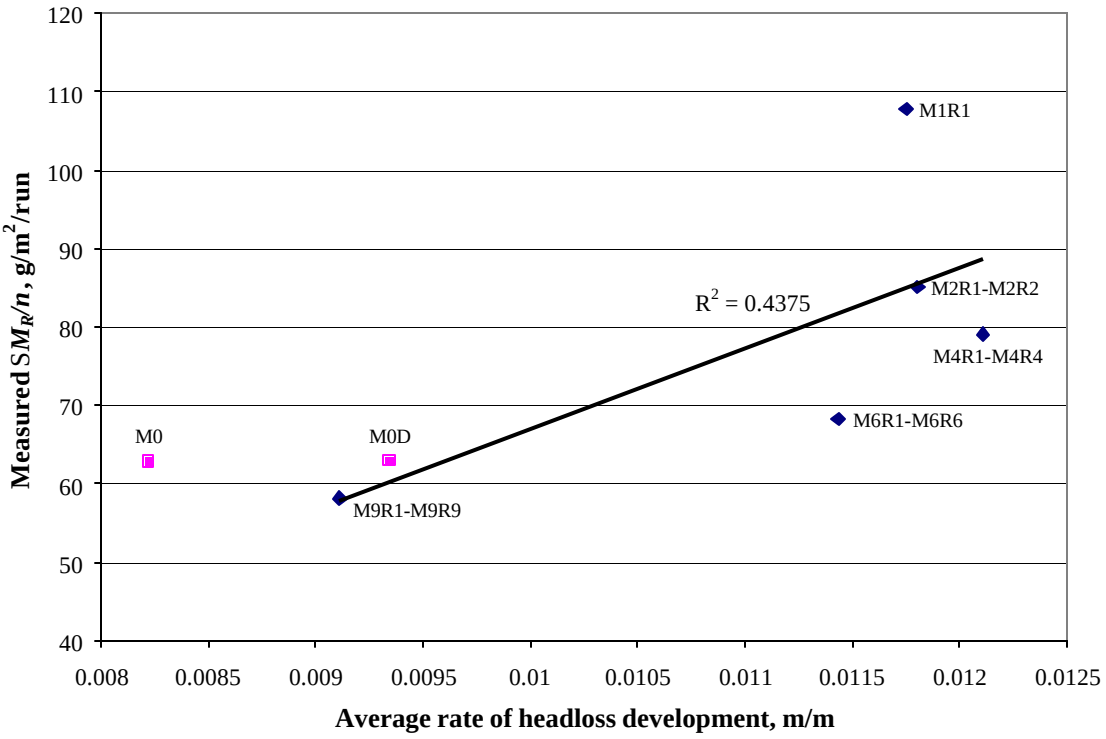

Figure 9.21 Average mass retained vs average rate of headloss development

The correlation between mass retained and rate of headloss development helps to explain the differences in backwashing efficiency for the single run experiments M0, M0D and M1R1. Equation 9.11 therefore appears to be a promising basis for the development of an accurate predictive model of backwash efficiency and filter mudballing.

9.3.4. Comparing the results for 0.7 mm and 1 to 1-1.4 mm sand

In the analysis of the AU and ZU experiments, backwash efficiency was found to be correlated with filter run time but not with rate of headloss development while for the 0.7 mm sand, the opposite result was obtained. This reason for this discrepancy appears to have been the different criteria used to determine when to end filter runs in each set of experiments. The AU and ZU experiments were typically run to a predetermined headloss, while for the mass accumulation experiments, the target filter run time was 22 to 24 hours. Figure 9.22 shows the relationship between filter run time and rate of headloss development for each set of experiments.

If a filter run is terminated when a particular headloss is reached then an increase in rate of headloss development results in a decrease in filter run time. The AU, ZU and backwash delay experiments (M0 to M48) were all run to a pre-determined terminal headlosses and consequently the filter run time was quite sensitive to the rate of headloss development. A relatively small change in $\frac{dh_f}{dV_f}$ in Figure 9.22 produced a relatively large change in filter run time. By contrast, the run times for the mass accumulation experiments were relatively insensitive to rate of headloss development so there was relatively large variation in $\frac{dh_f}{dV_f}$ and a relatively small variation in run time.

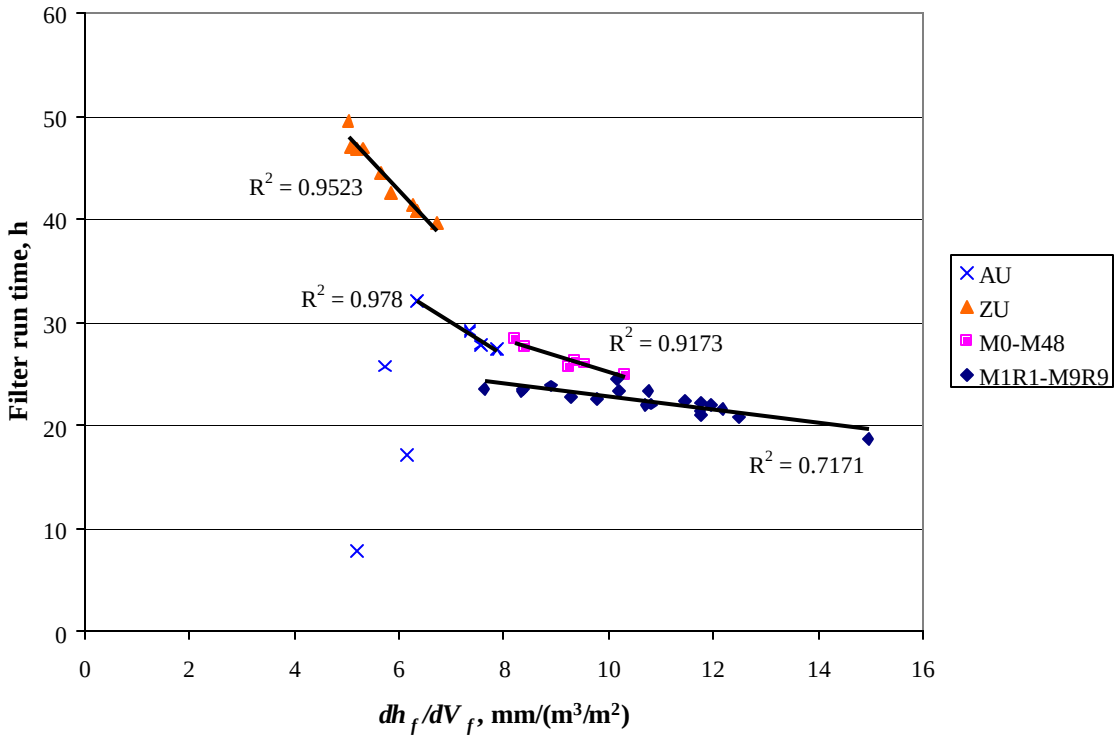

Figure 9.22 Relationship between filter run time and rate of headloss development

Therefore it appears that both rate of headloss development and filter run time are useful predictors of backwash efficiency but the one may mask the effect of the other in a regression analysis depending on how the experiments are run. Rate of headloss development may be a good indicator of floc strength when it is freshly deposited (although the effects of influent concentration and media size also have to be taken into account). However, the length of time that it remains in the filter is also important. If high rates of headloss development lead to shorter filter runs then higher rates could actually result in more efficient backwash.

Neither differences in filter run time nor rate of headloss development can explain why the mass retained in 0.7 mm sand filter tended to be less than the mass retained in the coarser

media filter (1-1.4 mm) washed at a higher backwash rate (See Figure 9.1). This was most likely due to the lower alum dose used in the mass accumulation experiments. The turbidity removal efficiency may be a useful basis for comparing results for different coagulants. However, in this case, the effect of media size and bed depth on turbidity removal would also have to be considered when comparing results from different filters.

9.3.5. Developing a predictive model of backwash efficiency

At the beginning of this chapter it was proposed that the rate of detachment and efficiency of backwash was a function of the ratio of the hydrodynamic detachment forces to the cohesive and adhesive forces of the floc deposits attached to the media grains. It was further suggested that since it is difficult to obtain values of the different forces for real systems, it would be more practical to attempt to relate backwash efficiency to readily determined filtration and backwash parameters which provide an indication of the relative strengths of the different forces.

Based on the experimental results presented in Chapter 8 and Chapter 9, the best indicators of floc deposit strength for a given filter bed were the rate of headloss development and filter run time. The mass retained after backwash did not generally appear to be strongly correlated with the mass deposited during the filter run. Floc strength is also expected to vary with coagulant dose and it possible that the turbidity removal efficiency would be a useful indicator of the relative strengths of different types of floc deposits, however, there was

insufficient data to confirm this. Data on filter run time and influent and filtrate turbidity should be available at any treatment plant. Rate of headloss development is recorded at many plants. Therefore, a model of floc strength based on these parameters could easily be applied to real world filtration plants.

Backwash rate appeared to be a better indicator of the hydrodynamic forces then the theoretical rate of power dissipation for the narrow range of conditions investigated. However, theoretical analysis and actual experience in the water treatment industry indicates that the hydrodynamic detachment forces are also a function of grain size, shape and temperature. Consequently, the theoretical shear stress $\Phi_{10\%}$ may turn out to correlate better with backwash efficiency over a wider range of conditions than were studied here, since it incorporates the effects of grain, size shape and water temperature as well as backwash rate.

In this study, the experimental results were modeled using linear regression models. These are adequate for modeling the effect of small changes in various parameters but are unlikely to be adequate over a wide range conditions. Further experimental work is required to derive an appropriate semi-empirical formulation for f_2 in Equation 9.1. The parameters identified in the current study as being useful indicators of floc deposit strength would be a good starting point for a future study to accomplish this. The effect of filter bed design (depth and size distribution) on turbidity removal efficiency and rate of headloss development would have to be included in the model if it was to be applied to different filter beds.

Equation 9.11 can be seen as a simplified version of Equation 8.5 for a single set of backwash conditions (p_{b1}) and a narrow range of filtration conditions ($p_{f1} = rate1$). In Chapter 8, it was suggested that the rate of mud accumulation would decrease as the finer fractions of the media became progressively mudballed. More experimental work looking at the effect of media size on mud accumulation would be required to confirm this. However, the experimental results did indicate an apparent decrease in rate of accumulation with number of runs and the forma of Equation 9.11 is consistent with this hypothesis.

CHAPTER 10

CONCLUSIONS AND RECOMMENDATIONS

10.1. Review of research objectives

The primary objective of the current study was to investigate the backwash behavior of filters under realistic operating conditions and to develop a quantitative model or models of the backwash process based on both fundamental and practical considerations.

Specific research objectives were as follows:

- Assess the assumptions on which existing backwash models are based and identify their limitations.

- Develop a better conceptual framework for understanding and modeling filter backwash, including the mechanisms by which inefficient backwash leads to filter mudballing

- Investigate the effect of filtration and backwash conditions on backwash efficiency.

- Develop a model for predicting backwash efficiency under realistic operating conditions.

- Develop a model of the long-term impact of inefficient backwash on the state of the filter media.

This chapter reviews the key findings of this study and discusses how they can be applied to modeling both the backwash concentration profile and rate of detachment as well as predicting the efficiency of backwash and the accumulation of mud over multiple filter cycles.

10.2. Summary of findings

10.2.1. Filter behavior during fluidized bed backwashing

In this study, two distinct phases of the backwash process were identified. The first phase is the transition from the fixed to the fluidized bed. In the second phase, the media is fully fluidized. Behavior of an initially clogged filter bed is different to that of a clean bed in both phases but particularly in the first phase. A dirty bed initially expands in a smooth and linear manner. Very little or no flow passes through the surface of the clogged bed so the velocity of the bed surface is approximately the same as the backwash velocity.

The clogged bed structure as a whole has essentially no tensile or flexural strength. As the media beneath a given layer of clogged media becomes fluidized, it tends to crumble and

disintegrate under its own weight. When the plug of remaining clogged media becomes sufficiently thin that it can be destabilized or broken up by irregularities in the filter wall or by flow maldistributions, the plug begins to tilt and buckle and the backwash flow breaks through its surface. Thereafter the plug erodes fairly rapidly depending on the backwash rate. In the process, a substantial amount of mixing of both detached floc and media occurs in the top layers of the bed. The scale and timing of the disintegration and mixing processes are a function of the degree of clogging of the bed, the depth of floc penetration and is specific to the equipment used.

The mechanisms, and in all likelihood also the rates of detachment are different for the two phases of backwash and therefore should be modeled differently. The bulk of the floc is detached during the expansion/disintegration phase. The mechanism here appears to be the fracture and erosion of the clogged bed structure. The rate of detachment in the second phase is determined by both the hydrodynamic forces in the fluidized bed and the cohesive and adhesive properties of the floc deposits.

The rate of detachment can be calculated from the backwash concentration profile if an appropriate model of the backwash flow is assumed. Mixing tends to die down fairly quickly after the end of the disintegration phase and the rate of detachment can be estimated from the backwash concentration profile after the floc detached during the disintegration and mixing phase is washed out of the filter. The amount of floc detached during the fluidization phase is

relatively small but significant because residual floc accumulates over multiple runs and can rapidly develop into filter mudballs.

The key to understanding the growth of filter mudballs is the observation that floc deposits become harder to remove or breakdown, the longer they remain in the filter. Therefore, mudballs can start off as a few floc coated grains and gradually grow into much larger composite structures than would otherwise be able to survive during backwash.

10.2.2. Factors affecting the efficiency of backwash

In this study, the age of floc deposits was found to be a major factor determining the efficiency of backwash. This has important implications for both the management of filters and design of experiments to study backwash processes. Treatment plant operators should not allow excessively long filter runs (> 24 – 36 h), especially if the backwash is not very efficient, and should minimize the delay time between the end of filtration and backwash. In experimental studies of backwash, the importance of using realistic filter run times should not be overlooked. Some researchers have tended to use concentrated influent suspensions to clog filters in relatively short periods of times (e.g. 6 hours). However, the backwash behavior of a filter clogged within 6 hours is likely to be different from the behavior of a filter that reaches the same terminal headloss or mass of deposits over 24 hours.

The rate of headloss development was found to be a useful indicator of the strength of cohesive deposits for filter runs of similar length. Comparison between backwash efficiencies for different experimental conditions suggested that the turbidity removal efficiency could also be used to predict backwash efficiency, particularly when different coagulants are used. However, the effect of filter bed design (depth and size distribution of media) on turbidity removal efficiency and rate of headloss development would have to be included in the model if it was to be applicable to different filter beds.

The experimental work on the effect of hydrodynamic conditions on backwash efficiency focused on variations in backwash rate for a single media design and a narrow range of temperatures. In this case, the backwash rate appeared to be a good indicator of the magnitude of the hydrodynamic forces. However, theoretical analysis and actual experience in the water treatment industry indicates that the hydrodynamic detachment forces are also a function of grain size, shape and temperature. Further experimental work in this area is recommended.

10.2.3. Accumulation of mud over multiple filter cycles

In this study, it was found that backwash efficiency decreased the longer the floc deposits remained in the filter and it was concluded that the deposits which survived one backwash would be unlikely to be removed in future backwashes. Experimental results did indicate a fairly steady increase in mass retained in the filter with increasing number of

consecutive runs for up to 9 runs. The rate of accumulation did however tend to decrease as the amount of residual mud in the filter increased. This was thought to be due to the change in size distribution of the media in the top section of the filter as the finest grains became encapsulated in mudballs. However, the abrading forces experienced by mudballs during backwashing would tend to increase with mudball size and this may also have been a factor. More research is required to study this phenomenon for greater numbers of filter cycles and different filter media designs.

10.3. Filter backwash modeling

10.3.1. Mechanisms and kinetics of detachment

The major limitation of existing models of the backwash effluent concentration profile is that they do not adequately account for the intense mixing which occurs at the beginning of backwash as the most clogged regions of the filter bed collapse and disintegrate. It is however extremely difficult to define a suitable flow model for the initial stages of fluidized backwash because the mixing conditions change very rapidly with time. Detailed analysis of the disintegration of the fixed bed structure and its impact on mixing indicated that the process was dependent on the scale of the filter, irregularities in the filter wall, the backwash rate and the degree of clogging of the filter. In other words, one would essentially need a different model for every experiment run or filter used.

Based on the experimental observations of fluidized water only backwash, it was concluded that it would most likely be easier to model the initial stages of backwash with auxiliary backwash than without, because mixing effects would be more uniform and predictable. Since most modern filters use some form of auxiliary backwash, it would be more useful to focus modeling efforts in this area.

Once the turbidity spikes generated by the disintegration of the clogged bed and resultant mixing were flushed out of the bed, the rest of the concentration profile could be described by a simple model of exponential decay

$$c = b\,\exp(-kt) \tag{10.1}$$

k = Rate of detachment constant, 1/s

If sufficient detachable floc remained in the filter after the residue from the intense mixing phase had washed out, then k was found to correlate with the efficiency of backwash or in other words, it was probably a characteristic of the intrinsic rate of detachment.

A model that only describes the tail of the backwash concentration profile, while less useful than a model of the full process, can be used to predict the impact of backwash remnants on filter ripening. The fitting parameter k may also be used as a crude estimator of backwash efficiency.

The main contribution of this work to the modeling of backwash kinetics was to identify of the effect of the various phases of backwash on the concentration profile and to highlight the difficulties involved in trying to obtain useful data on this aspect of backwash process.

10.3.2. Predicting the efficiency of backwash

A major aim of this research project was to develop a means of predicting backwash efficiency based on data that would be readily available at most filtration plants. The results of this study demonstrate that this quite achievable. Stepwise multiple regression was used to determine which of several experimental parameters were the best predictors of both the hydrodynamic detachment force and the adhesiveness of the floc deposits. This general approach is equally applicable to backwash with auxiliary wash.

For the range experimental conditions investigated, backwash rate was found to be the best predictor of hydrodynamic forces for a given filter, while rate of headloss development and filter run time were the best predictors of the adhesiveness of the floc. The experimental proof of the critical role of floc age in determining backwash efficiency was a particular important result since no previous attempts to model backwash have considered this type of time dependent effect. The simple linear correlations developed in this study provide an important first step towards developing and calibrating a more comprehensive model of backwash efficiency that could easily be integrated with existing models of filtration.

10.3.3. Modeling the accumulation of mud in the filter

The major original contribution of this work was the measurement of the rate of mud accumulation over multiple filter runs and the development of a theory and a model to describe it. The following model of mass accumulation was proposed (Equation 8.5).

$$\frac{\Delta\left(\sum M_R\right)}{\Delta n} = f\left(p_{f1}, p_{f2}, p_{f3},..., p_{b1}, p_{b2}, p_{b3},..., \left(x_i d_i\right)_n\right) \qquad 10.2$$

p_{f1}, p_{f2}, p_{f3} = Parameters relating to the filter run which affect the strength of deposits e.g. coagulant used, run duration, etc.

p_{b1}, p_{b2}, pb_3 = Backwash parameters which affect the hydrodynamic detachment forces e.g. backwash rate and temperature, etc.

$(x_i d_i)_n$ = Size distribution of media not incorporated in mudballs after n filter runs

As the volume of mudballs in filter V_{mb} increased, this would tend to also impact the hydrodynamics of backwash. This effect might also need to be included in the model for $n >> 1$. Once the model is calibrated, it can be used to predict the useful life of a filter bed with inefficient backwash.

In the current study, Equation 10.2 was calibrated for a limited range of conditions (constant backwash rate, narrow range of temperature, dosing conditions and run time, maximum of nine consecutive runs) and the following model was obtained (Equation 9.11).

$$\left(M_{R,}\right)_{k,est} = b_0 + b_1 \frac{dh_f}{dV_f} - b_2 \left(\sum \mathrm{M}_{\mathrm{R},}\right)_{k-1} \qquad 10.3$$

b_0, b_1, b_2 = Regression coefficients

$\frac{dh_f}{dV_f}$ = Rate of headloss development, mm/(m^3/m^2)

Here, the rate of headloss development is an indicator of floc deposit strength and $(\Sigma M_R)_{k-1}$ is the cumulative mass retained through previous backwashes.

Equation 10.3 can theoretically be calibrated for an application that includes auxiliary wash. The efficiency of detachment and the abrasion of mudballs would be expected to be much higher than for water only backwash.

10.4. Recommendations for future research

Based on the findings of this study, it is recommended that future work on backwash modeling should be focused on the following issues:

- Incorporating auxiliary backwash into models of the backwash concentration profile and detachment kinetics as described in Section 9.4.1

- Investigating the effects of media size distribution on backwash efficiency and mudball accumulation. This would be particularly relevant to the design of filters

that have to operate under conditions where optimum backwash is not guaranteed, for example in remote rural areas with few skilled personnel. Using coarser media requires deeper filter beds and higher backwash rates, which increases the cost of the filter. However, the filter bed may be less prone to mudballing, delaying the necessity of intervention such replacing the filter media.

- Developing a more comprehensive predictive model of backwash efficiency based on easily measured parameters such as rate of headloss development, turbidity removal and filter run time. Such a model would be easily integrated with existing models of the filtration phase of the filter cycle, including models of filter ripening.

APPENDIX 1

PRESSURE PROBE SIGNAL PROCESSING

A1.1. Introduction

During measurements of clean bed headloss transients it was noticed that pressure probe response included a distinct and reproducible oscillation in the first few seconds after the flow was turned up (see figure A1.1).

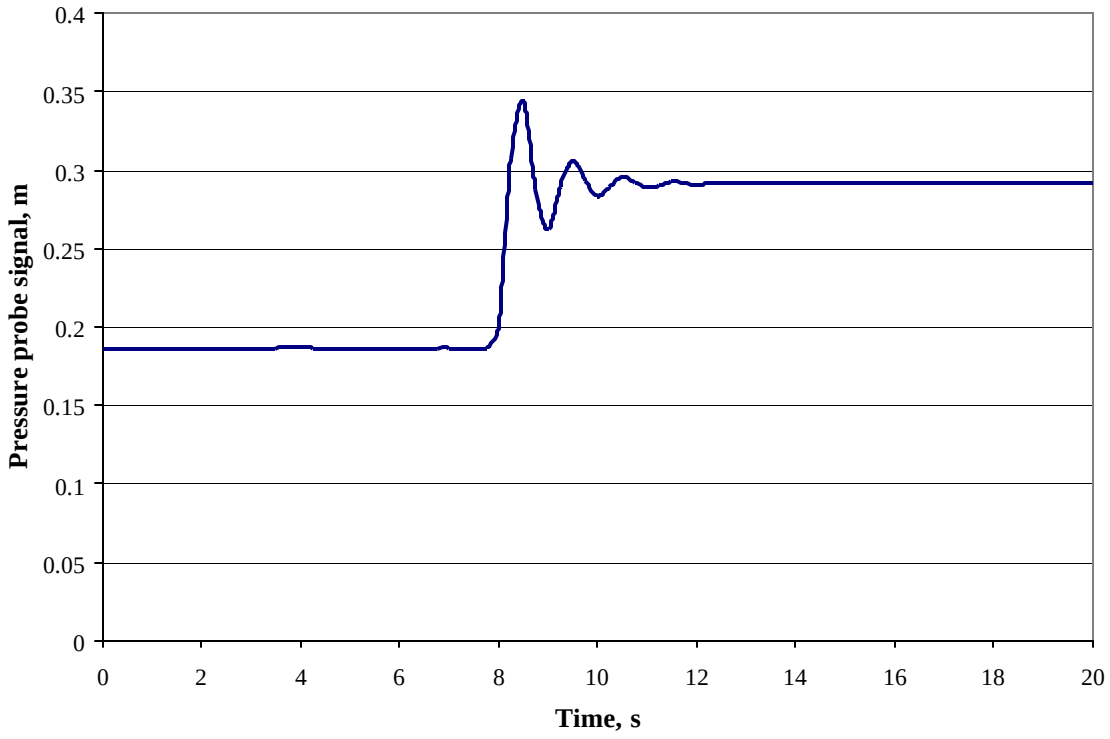

Figure A1.1 Response of the DP probe to step change in headloss

This did not appear to be related to any phenomenon observable in the fluidized bed. In order to check that the observed oscillation was not a function of the initial expansion of the bed, the probe was isolated until the fluidized bed had reached steady state by closing shut off valves on the pressure taps. The valves were then quickly opened and the dynamic response of the probe measured. Superficially, the probe response appeared to be identical to that measured when backwash was initiated with the pressure taps opened.

The vendor who had supplied the probe suggested that the oscillation could be due to vibration of the probe diaphragm under shock loading (typical of probes for low-pressure differentials because of the thinness of their diaphragms). He suggested that tiny orifice plates be inserted into the pressure taps to mechanically damp the response to a change in pressure. However, concern was expressed that this would slow down the probe response and possibly result in the loss of information. Since the dynamic response seemed to be quite reproducible, it was decided to try to model it to see if the measured response could be deconvolved to determine the actual media headloss.

A1.2. Determining the dynamic response of the DP cell to a step change in head

If the probe response to a given change in head was to mdoeled, the exact change in head had to be known. In order to eliminate any uncertainty about the effect of the response time of the pump on the result, the following procedure was adopted:

1. The probe was allowed to stabilize with the pressure tappings open at the initial flow rate and headloss (in some cases, zero) and the tappings were closed to isolate the probe.

2. The flow rate was changed and the bed allowed to stabilize at the new settings.

3. The pressure tappings were opened as quickly as possible and the dynamic response determined.

During these measurements, the manometer tubes were closed to prevent fluid flow into and out of the tubes affecting the measured response.

Multiple determinations of the response to each change in head were made so that signal stacking could be used to improve the time resolution and reduce the noise in the measurements. The datalogger was set at its maximum sampling frequency of 4 /s.

.

Since the actual time at which the head was stepped up did not necessarily correspond to a sample point, there was some uncertainty about the effective time zero for each signal. Small differences in start time relative to the nearest sampling point result in replicate signals being shifted along the time axis relative to each other. In order to stack these signals it was necessary to find a hypothetical time zero for each replicate signal that gave the same phase shift for the sinusoidal component of the response. For convenience, the start times were manipulated to produce a phase shift of zero as will be discussed below.

Mathcad 8.0 was then used to fit the stacked signals to the following model of under-damped vibrations:

$$h_{resp}(t) = C\exp(-at)\cos(wt - j) \qquad \text{A1.1}$$

For a linear system, C will be proportional to the actual change in head, Δh causing the response. In practice, the phase shift j is a function of the assumed time at which the step change in head occurred. As mentioned above, the assumed start times of all the component signals were adjusted to yield $j < 0.01$.

The results of the parameter fitting are summarized in Table A1.1 (a) and A1.1 (b). The assumption of linearity with respect to Δh appears to be justified. The characteristic frequency

of the cosine term was ~ 2 π in both cases however, the exponential decay coefficient, α, varied slightly.

Table A1.1(a) Fitting parameters for Δh = 0.278 m

	Run 1	Run 2	Run 3	Run 4	Run 5	Average	Stacked signal
C	-0.281	-0.269	-0.282	-0.271	-0.255	-0.2716	-0.273
α	1.061	1.036	1.071	1.041	1.057	1.0532	1.059
ω	6.284	6.283	6.283	6.284	6.283	6.2834	6.283
φ	-0.00494	2.55E-03	4.24E-03	-0.00251	1.76E-03	0.000219	1.95E-04
Δh	0.279878	0.276203	0.277778	0.275152	0.281664	0.278135	0.278135
$C/\Delta h$	-1.00401	-0.97392	-1.0152	-0.98491	-0.90534	-0.97667	-0.98154

Table A1.1(b) Fitting parameters for Δh = 0.103 m

	Run 1	Run 2	Run 3	Run 4	Run 5	Run 6	Average	Stacked signal
C	-0.098	-0.1	-0.098	-0.093	-0.102	-0.089	-0.09667	-0.101
α	1.197	1.229	1.227	1.159	1.248	1.116	1.196	1.245
ω	6.283	6.283	6.284	6.282	6.283	6.282	6.282833	6.285
φ	6.23E-04	-0.00122	-0.0054	9.64E-03	-1.1E-03	9.51E-03	0.00201	-0.008
Δh	0.105295	0.102449	0.100025	0.102765	0.104451	0.102133	0.102853	0.1029
$C/\Delta h$	-0.93072	-0.9761	-0.97976	-0.90498	-0.97653	-0.87142	-0.93992	-0.982

A1.3. Deconvolving the pressure probe response

The pressure probe response to a step a change of head (instantaneous pulse in Δh) at $t = 0$ is given by

$$h_{resp}(t) = 0.98\Delta h(0)\exp(-\alpha t)\cos(2\pi t) \qquad \text{A1.2}$$

In general, the pressure probe response to changes in head may be expressed in terms of the convolution integral

$$h_{resp}(t) = 0.98\int_{-\infty}^{t}\frac{dh}{dt'}(t')\exp[-a(t-t')]\cos[2p(t-t')]dt' \qquad \text{A1.3}$$

In discrete form, this becomes

$$hr_i = 0.98\sum_{j=0}^{i}\Delta h_j \exp[-\alpha\Delta t(i-j)]\cos[2\pi\Delta t(i-j)] \qquad \text{A1.4}$$

Δt = Sampling interval

This can be expressed in matrix form as

$$\overline{hr} = \overline{\overline{E}} \cdot \overline{\Delta h} \qquad \text{A1.5}$$

$\overline{hr}$ = Vector of n data points

$\overline{\overline{E}}$ = n x n matrix

$\overline{\Delta h}$ = Vector of n data points

Where

$$E_{ij} = 0.98 \exp\left[-\alpha \Delta t (i-j)\right] \cos\left[2\pi \Delta t (i-j)\right] \qquad \text{A1.6}$$

Therefore

$$\overline{\Delta h} = \overline{\overline{E}}^{-1} \cdot \overline{hr} \qquad \text{A1.7}$$

The convolution matrix and its inverse were calculated for n = 100 using Mathcad 8.0. The procedure was then tested by deconvolving various real and hypothetical signals.

A1.4. Deconvolution of the hypothetical response of the probe to ideal step and ramp changes in head

Consider the response to a hypothetical step change in head (impulse in Δh). If Δh falls exactly at a specific sampling time then the analysis and interpretation of the signal and its deconvolution is quite straightforward. This is illustrated in Figure A1.2.

h1r is the response to the step change at i = 40, Δh1r is the change in head calculated by deconvolution and $h1rr_i$ is the actual head reconstructed using Δh1r.

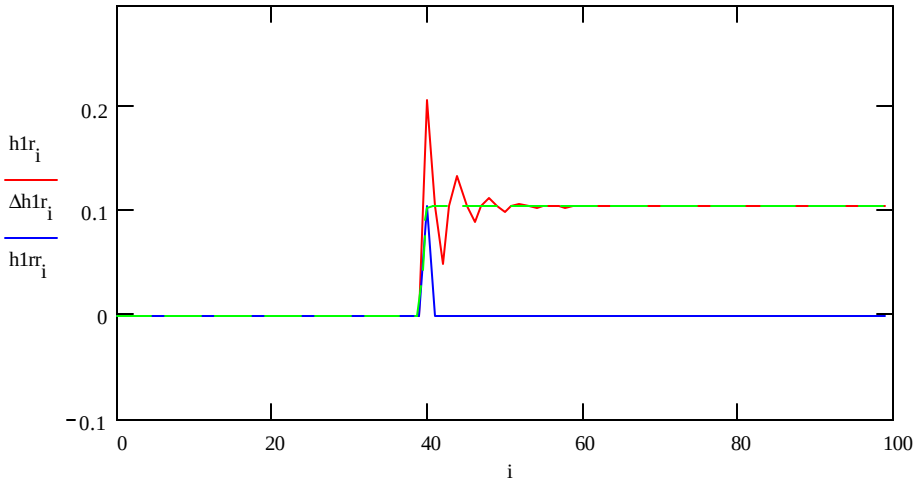

Figure A1.2 Response and deconvolution of response for step change in head at i = 40.

Problems arise if the step change occurs in the middle of a sampling interval, as is more likely to be the case. Equation A1.7 can only assign changes in head to integer values of i and j. However, the measured response at any given time t_i may relate to an event which occurred at a non-integer multiple of Δt previously. The measured response is to a step change in head at $t = \Delta t(j + \xi)$ where $|\zeta| < 1$, is given by

$$hr_i = 0.98\Delta h_{j+z} \exp\left[-a\Delta t(i - j - z)\right]\cos\left[2p\Delta t(i - j - z)\right] \qquad \text{A1.8}$$

In Figure A1.3, hr was calculated with $x = 0.5$ but deconvolved assuming $x = 0$.

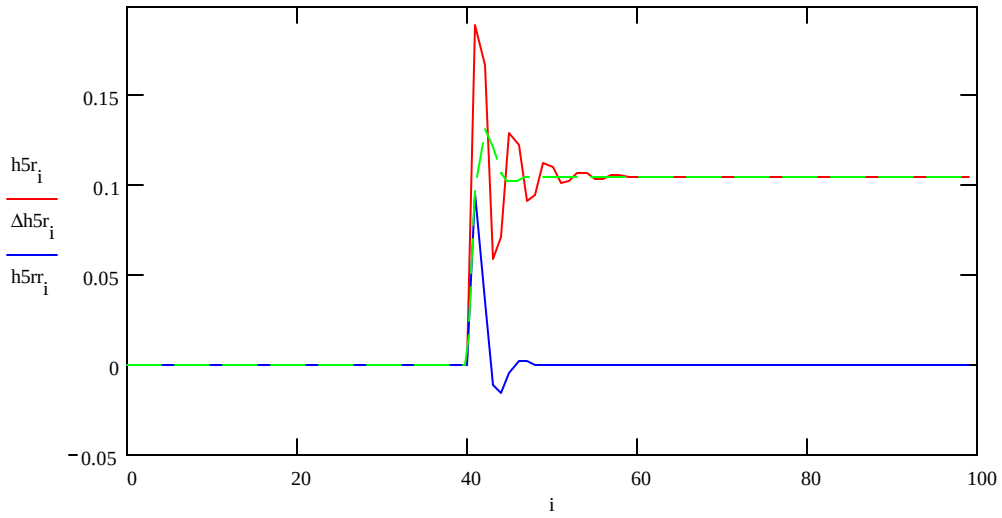

Figure A1.3 Effect of offset in start time on deconvolution of the pressure probe response to an ideal step change in head

Clearly, the ability of the procedure to detect the step change has been compromised. However, if the probe response and the deconvolution matrix are calculated with the same value of x, then a perfect step function can be retrieved.

In the backwash experiments, it is unlikely that turning on the backwash pump causes an instantaneous step change in head. Figure A1.4 shows the result of deconvoluting the response of a ramp change in head. The hypothetical response, h2r was calculated using equation A1.3, i.e. the continuous form of the convolution integral. h2 is the actual headloss, h2r is the calculated response and Δh2r and h2rr are the change in head and total head calculated by deconvolution. Clearly, the deconvolution procedure is not as good as detecting rapid continuous changes in head as it is at recovering instantaneous discrete changes in head.

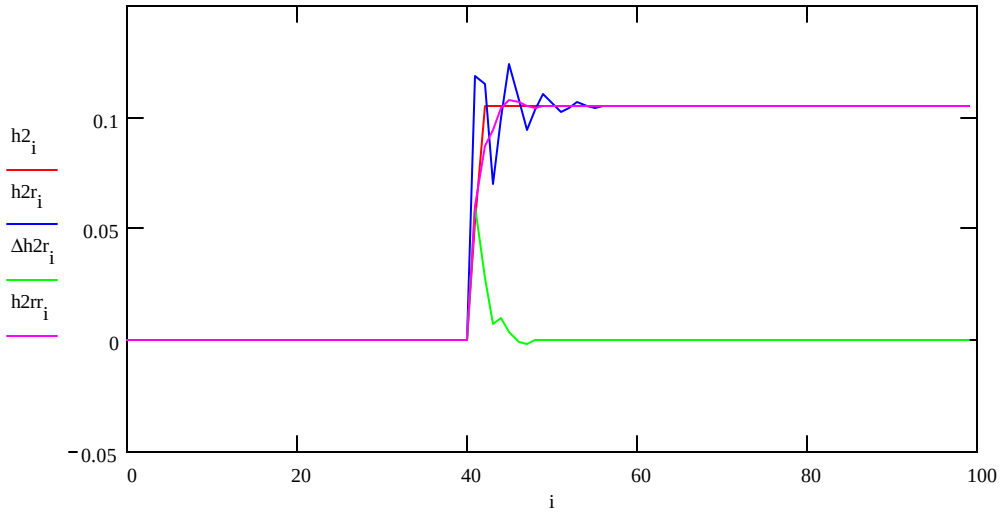

Figure A1.4 Deconvolution of the theoretical response to a ramp change in head

Figure A1.5 and A1.6 show the deconvolution of the response to the same ramp change as in Figure A1.4, but starting half a time interval earlier. The deconvolution matrices were calculated assuming x = 0 and -0.5 respectively.

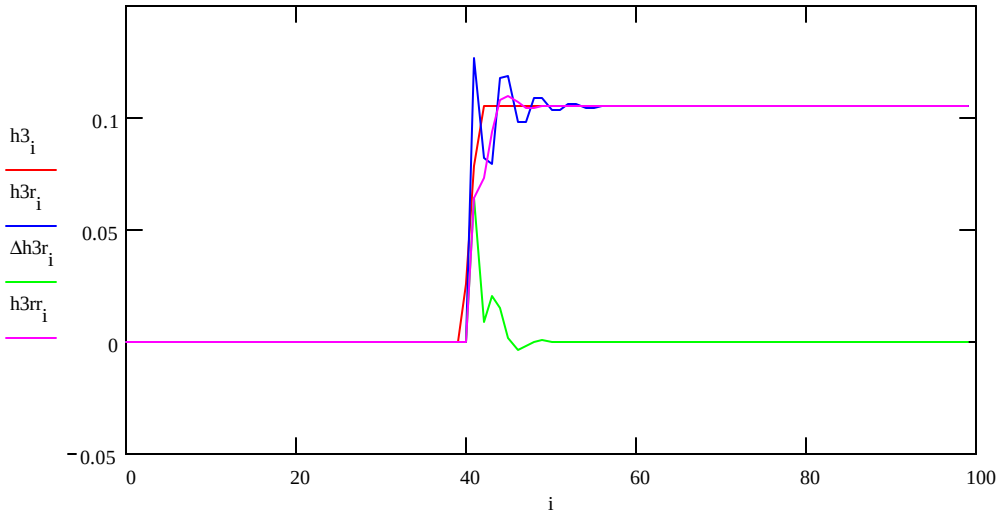

Figure A1.5 Deconvolution of the theoretical response to a ramp change in head between i = 39.5 and 41.5, deconvolution calculated with $\xi = 0$.

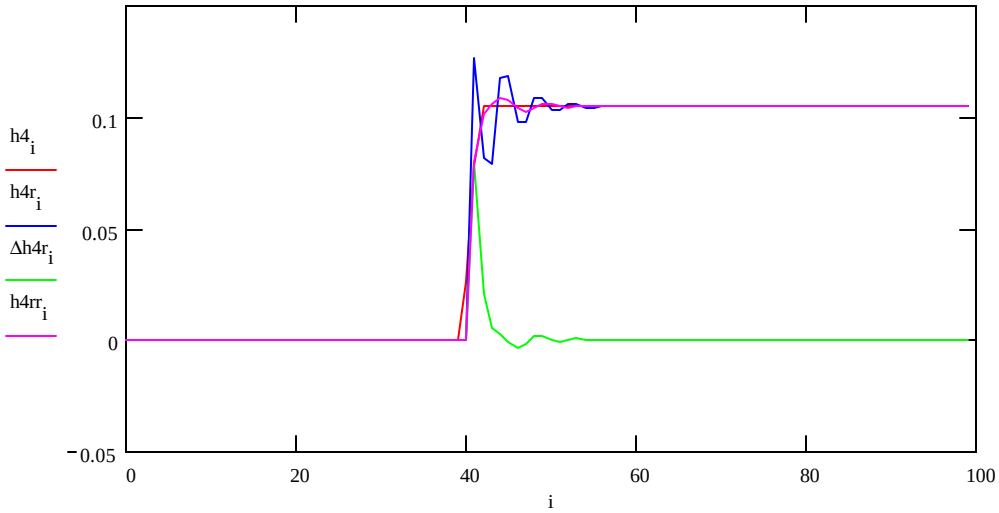

Figure A1.6 Deconvolution of the theoretical response to a ramp change in head between i = 39.5 and 41.5, deconvolution calculated with ξ = -0.5

In Figure A1.6, the hypothetical response was calculated using α = 1.24, however, it was found that adjusting α in the deconvolution matrix to 1.5 produced a slight (4 %) improvement in the sum of differences between the input headloss and the deconvolved headloss.

Based on these results, unless stated otherwise, the following parameters were selected for analysis of the backwash signals:

1. $C = 0.98\Delta h$
2. α = 1.00 –1.50, $|\zeta| < 1$, selected to produce a fairly smooth, clean step/sharp ramp increase in head at the beginning of backwash.

3. $\omega = 2\pi = 6.2832$

4. $\varphi = 0$

A1.5. Deconvolution of the probe response to real changes in head

Figure A1.7 shows the effect of trying to deconvolve an actual probe response measured after opening the pressure taps as described above, assuming $\xi = 0$. Here, hr is the measured response and h and Δh are the total head and change in head calculated by deconvolution. The two small peaks in head could theoretically be due to the flow of fluid in the pressure tappings once the valves are opened, however, the similarity to Figure A1.3 is marked. Figure A1.8 shows the same signal deconvolved assuming $\xi = 0.56$ (found by trial and error). The result is much closer to a perfect step function.

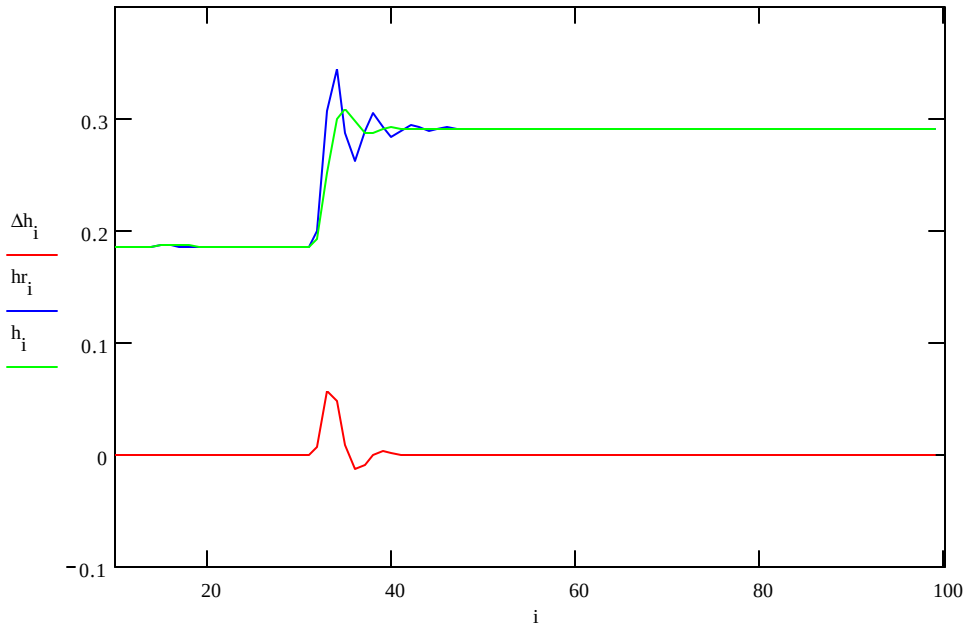

Figure A1.7 Deconvolution of pressure probe response to an actual step change in head, assuming $\xi = 0$, $\alpha = 1.24$

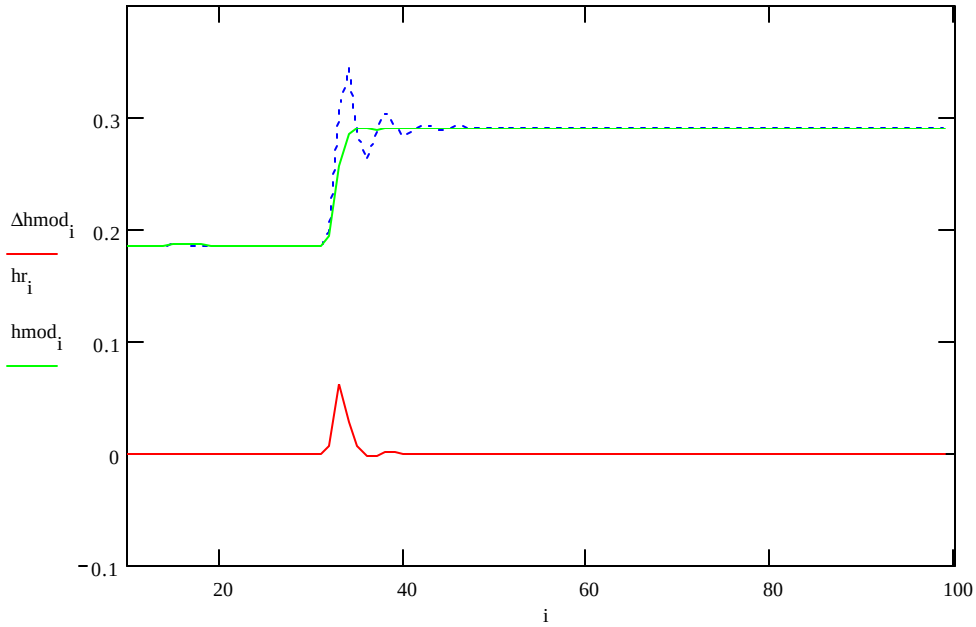

Figure A1.8 Deconvolution of pressure probe response to an actual step change in head, assuming $\xi = 0.56$, $\alpha = 1.24$

Figures A1.9 and A1.10 show the calculated headlosses for backwashing a clogged bed at 32 m/h (v_{mf} ~ 51 m/h) assuming $\xi = 0$ and 0.8 respectively. As before, a value of ξ can be found such that the solution is approximately a step increase in head. In this case, the total head declines slowly after the initial increase but the measured headloss signal and the calculated actual headloss are not significantly different after the first 5 seconds. Figures A1.9 and A.10 appear quite similar to Figures A1.5 and A1.6, implying a sharp ramp change in head rather than a step change, which seems reasonable.

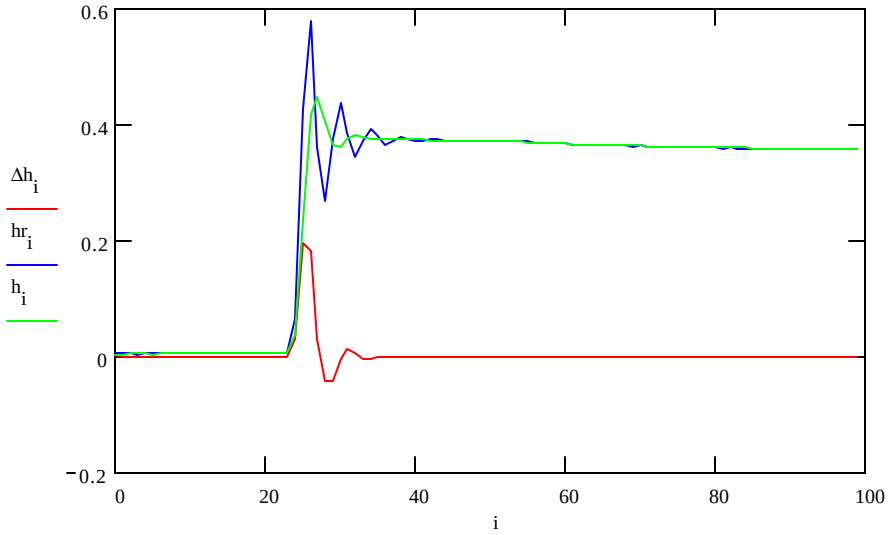

Figure A1.9 Calculated headloss for backwashing at 32 m/h, assuming $\xi = 0$, $\alpha = 1.066$

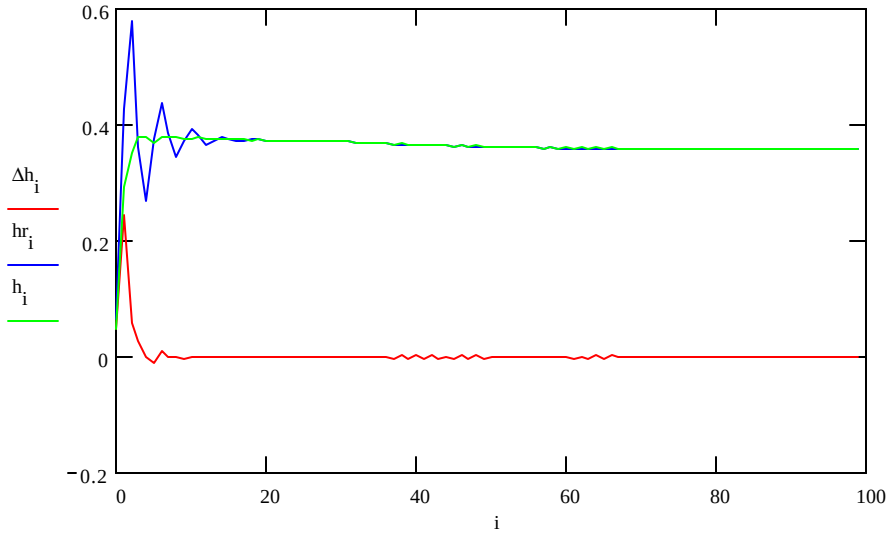

Figure A1.10 Calculated headloss for backwashing at 32 m/h, assuming $\xi = 0.8$, $\alpha = 1.066$

A1.6. Conclusions

Given the sensitivity of the solution to the time at which changes in headloss are assumed to occur, it has to be concluded that the details of the headloss in the first couple of seconds after the pump has been turned on cannot be resolved with any degree of certainty. However the deconvolution procedure presented here gives a reasonable estimate of what the headloss probably is. No selection of fitting parameters can perfectly recover a ramp change in head therefore the small ripples in the solution where the headloss initially peaks can be ignored.

APPENDIX 2

DETERMINING THE CONCENTRATION OF BACKWASH

A2.1. The Opacity Meter

A2.1.1. Set up

The operation of the opacity meter was described in Section 3.4.2. The opacity meter had two adjustable parameters: the voltage supply to the LED and a scaling factor on the voltage output to the datalogger. The latter was simply a variable resistor that was used to reduce the maximum voltage fed to the datalogger. At the beginning of each calibration or backwash experiment, the output resistor was set to 0 Ω and the output voltage set to approximately 10.60 V (measured using a Fluke Voltmeter) by adjusting the LED input voltage. The output voltage signal was then scaled down to just less than 10 V as the datalogger input was required to be −10 to 10 V. The voltages before and after scaling down the signal were recorded and the ratio between the two was used to calculate the actual output from the photodiode for subsequent measurements, i.e.

$$V_{PD} = V_{DL} \frac{V_{PD0}}{V_{Dl0}} \qquad \text{A2.1}$$

V_{PD} = Photodiode output voltage, V

V_{DL} = Voltage recorded on datalogger, V

V_{PD0} = Photodiode voltage prior to scaling down signal

V_{DL} = Datalogger voltage after scaling down signal

A2.1.2. Calibration procedure

During calibration, the variable resistor on the outlet was set to 0 Ω and the output voltage was read using a Fluke Multimeter rather than the datalogger.

The opacity meter was calibrated using backwash wastewater. The wastewater was allowed to settle and then concentrated sludge and supernatant were separated Samples for calibration were created by combining settled sludge and either supernatant or tap water in various proportions.

Sample for calibration was circulated between the detector and a 3 L sample reservoir using a small centrifugal pump until the reading on the voltmeter stabilized. The voltage and sample temperature were then recorded and a sample taken for turbidity analysis.

The maximum photodiode voltage was set to ~ 10.6 V using tap water, and then the settled sludge was used to determine the turbidity corresponding to the lowest voltage measured during the various backwash runs. The sludge was then sequentially diluted down with supernatant to determine the other points on the curve. Dilution with tap water was required to achieve turbidities < 10 NTU.

A2.1.3. Sensitivity to temperature

The calibration of the opacity meter was somewhat sensitive to temperature because the photodiode output voltage tended to drop as the detector heated up. Figure A2.1 shows an example of the variation of voltage reading for clean water plotted against water sample temperature. The water temperature was obviously not the same as the detector temperature and a consistent trend could only be obtained if the flowing sample and detector were given time to equilibrate before any readings were taken.

This was more difficult to achieve for the backwash experiments than for the calibration. In every experiment where the opacity meter was used, there was an increase in voltage between the beginning of the experiment, before detachment, and the end when all the floc had been flushed away. This was because the backwash sample flowing through the detector was cooling it down, causing the calibration to shift over the course of the backwash.

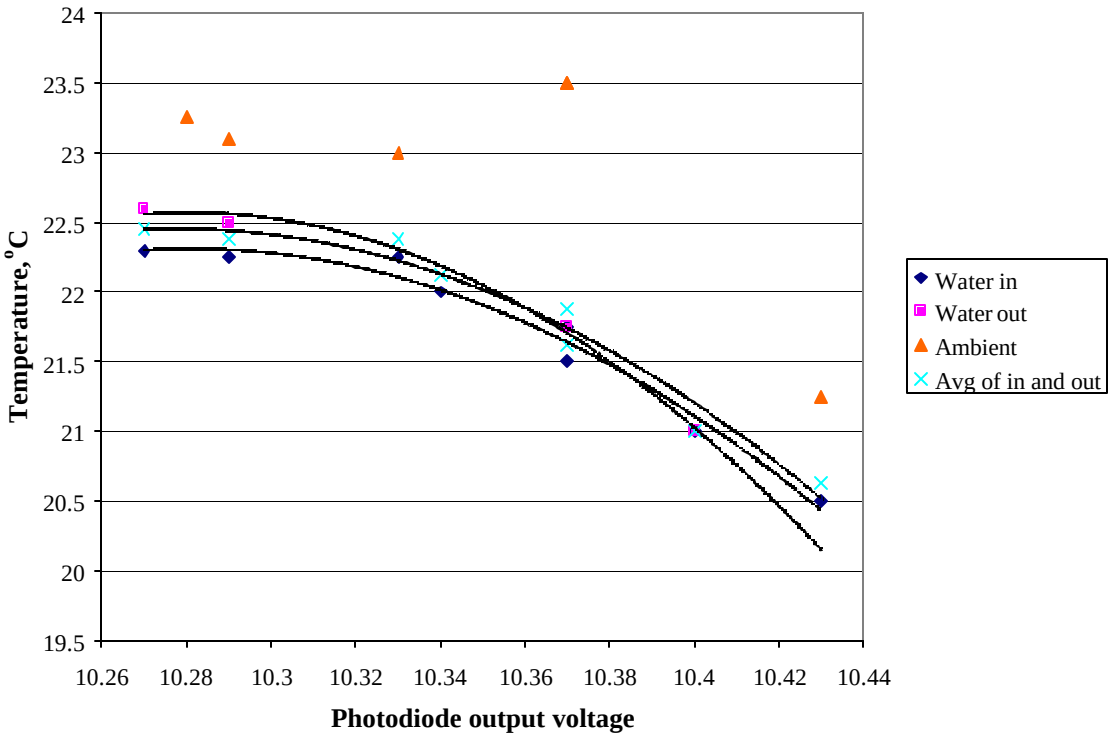

Figure A2.1 Effect of temperature on baseline reading

Once this problem had been identified an attempt was made to achieve thermal steady state before the start of the backwash by allowing water from above the filter to drain through the opacity meter while the preparations for backwash were underway. However, for most experiments there was a small increase in baseline voltage between the beginning and end of backwash. This translated into about a +/- 10 mg/L uncertainty in the concentration near the end of backwash.

A2.1.4. Calibration Results

The methodology for calibrating the opacity meter was developed using backwash sludge from experiments using alum. A separate calibration was then developed for the Z464N experiments. Initially, several calibration experiments were carried out on different days using alum backwash effluent. It was difficult to set the maximum photodiode to exactly 10.6 V, in part because of drift due to temperature and in part due to the limitations of the device. Different maximum voltages resulted in similar curves shifted along the voltage axis by various amounts, as shown in Figure A2.2.

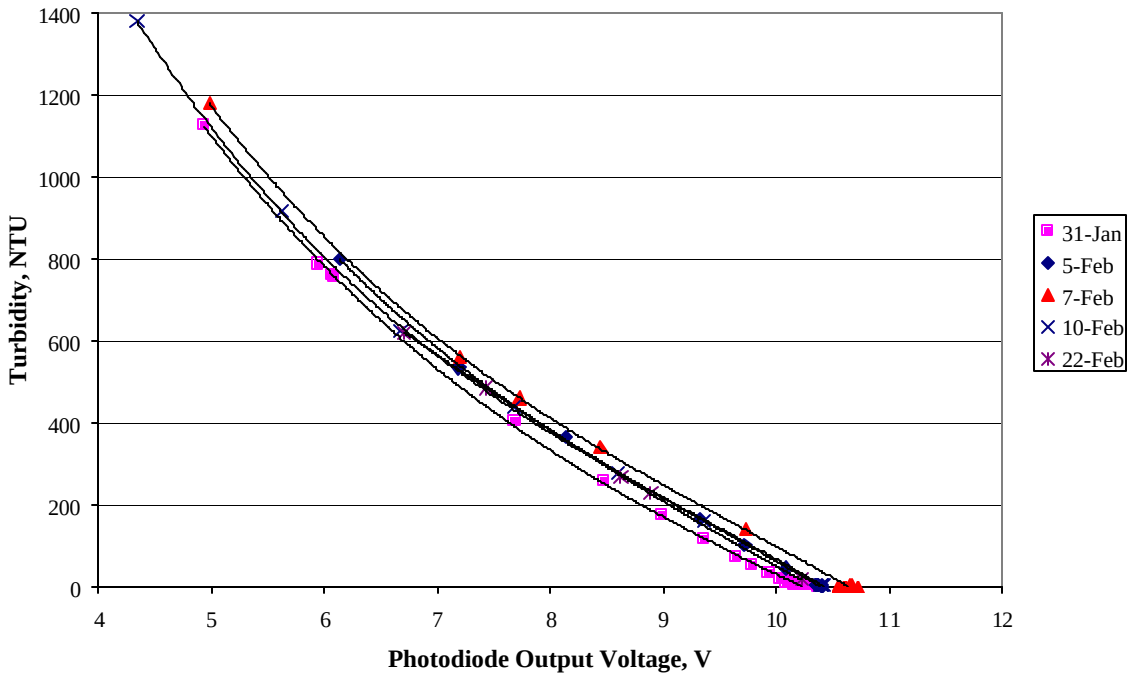

Figure A2.2 Opacity meter calibration curves obtained on different days – coagulation with alum

A single calibration curve including all data points could be obtained by shifting each individual curve along the voltage axis by an appropriate amount. The voltage shift for each curve was chosen to be the difference between 10.6 V and the average of the first and last reading for clean water for a given calibration run.

For example, if at the beginning of the calibration, the clean sample gave a voltage of 10.40 V and at the end of the exercise, clean water gave a voltage of 10.32 V then the voltage shift for that set of data would be

$$10.60 - \frac{10.32 + 10.40}{2} = 0.24$$

The resulting calibration curve is shown in Figure A2.3. A similar calibration curve was obtained for the Z464N sludge.

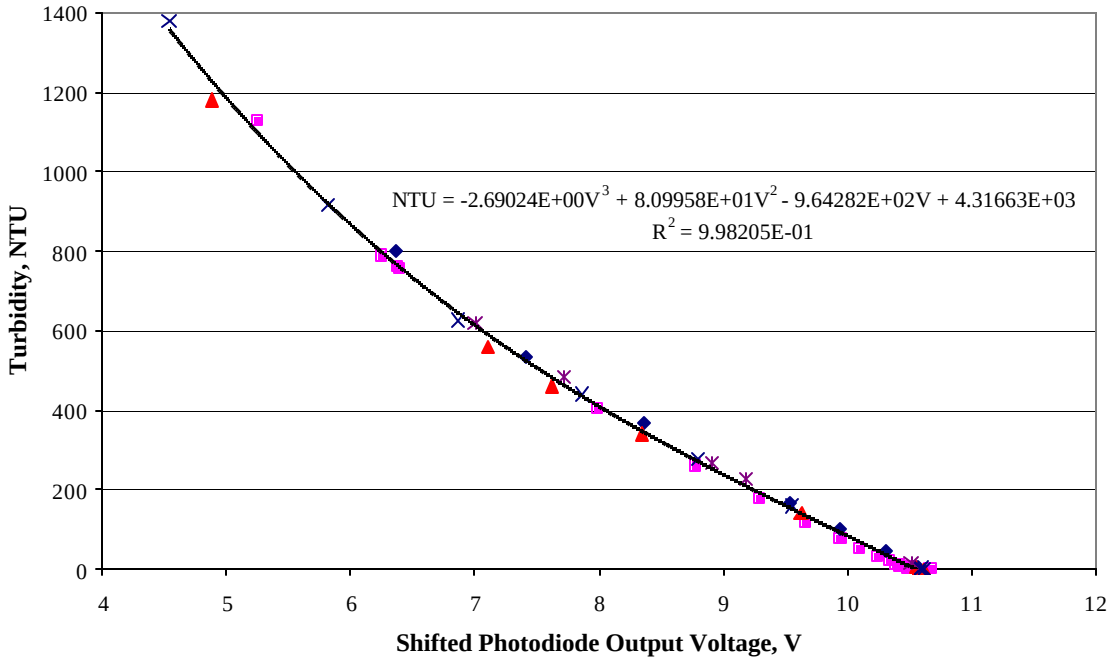

Figure A2.3 Opacity meter calibration for suspensions coagulated with alum

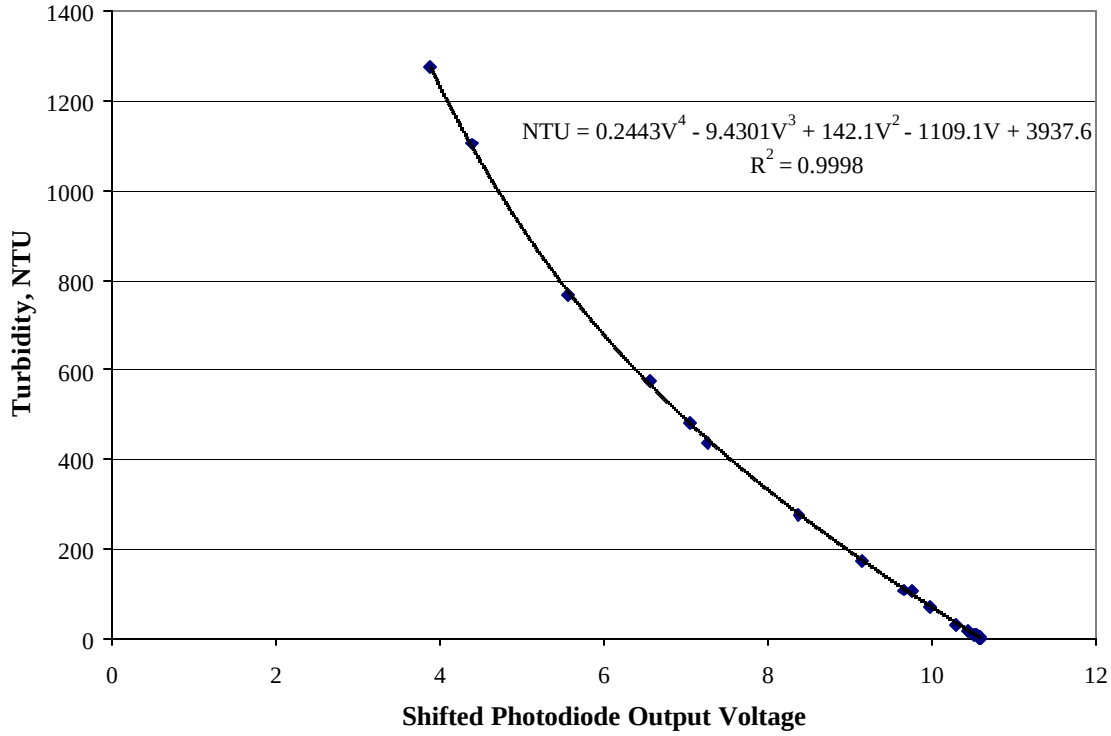

Figure A2.4 Opacity meter calibration for suspensions coagulated with Z464N

Over a wide range of turbidities, the calibration curve appears to fit the data very well. However, a closer look at the low turbidity end of the curve shows that the calibration gives large relative errors at low turbidities (Figure A2.5). This is in part due to the effect of variations in temperature, which have the greatest relative impact in the low turbidity range.

This is makes it more difficult to estimate the rate of detachment during the later stages of backwash. It also complicates the comparison between mass detached based on the opacity meter readings and the suspended solids analysis on the collected backwash effluent because a long low concentration tail can represent a significant portion of the total calculated mass detached from a backwash run.

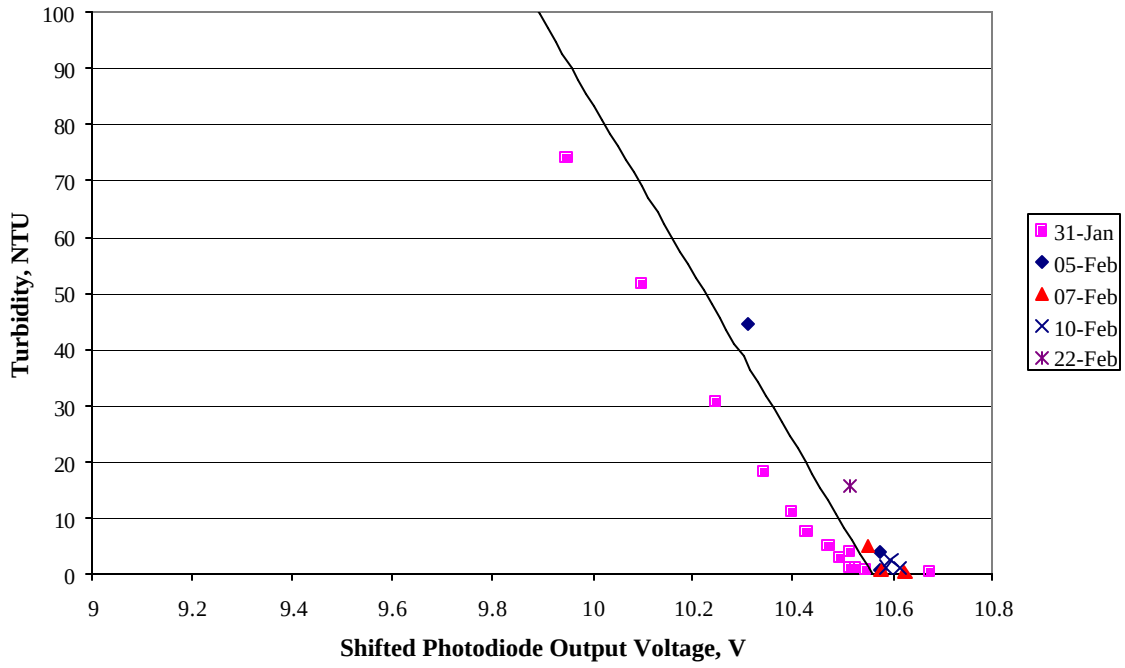

Figure A2.5 Calibration for turbidity < 100 NTU – suspensions coagulated with alum

A2.1.5. Calculating the backwash concentration - time profile and total mass detached

For each backwash experiment, the voltages recorded on the datalogger were converted back to the photodiode output voltage using Equation A2.1. The baseline voltage V_R for each backwash experiment was taken to be either the first voltage recorded or the voltage at the end of backwash, whichever was higher. The reference voltage was then subtracted from the output voltage to obtain the shifted voltage V_s.

$$V_S = V_{PD} - V_R \qquad \text{A2.2}$$

The backwash turbidity was calculated using V_S using the calibration equation in Figure A2.3 or A2.4. The backwash concentration was calculated from the turbidity using the correlations presented in Section A2.2.

The cumulative mass detached at time t_k was calculated by numerical integration.

$$M_{CD}(t_k) = \sum_{i=1}^{k} c_i Q_i \Delta t \qquad \text{A2.3}$$

$M_{CD}(t_k)$ = Cumulative mass detached at time t_k, mg

c_i = Backwash concentration at time t_i, mg/L

Dt = Sample interval = 0.25 s

The total mass detached calculated from Equation A2.3 was then compared to the measured mass detached, M_D (expressed in mg). The choice of V_R was revisited and if the alternate baseline voltage gave a better agreement with the measured mass detached then V_R was changed accordingly.

A2.2. Correlation between turbidity and suspended solids

The determination of suspended solids is time consuming and not very accurate at low concentrations therefore it was convenient to use turbidity as a surrogate measure of suspended solids for the calibration of the opacity meter. Correlations between turbidity and suspended solids were developed using the backwash samples used to determine M_D and M_R. Concentrated sludge samples were diluted as required to obtain samples corresponding to the highest concentrations in the backwash peak. Figures A2.6 and A2.7 show the correlations for alum and Z464N respectively.

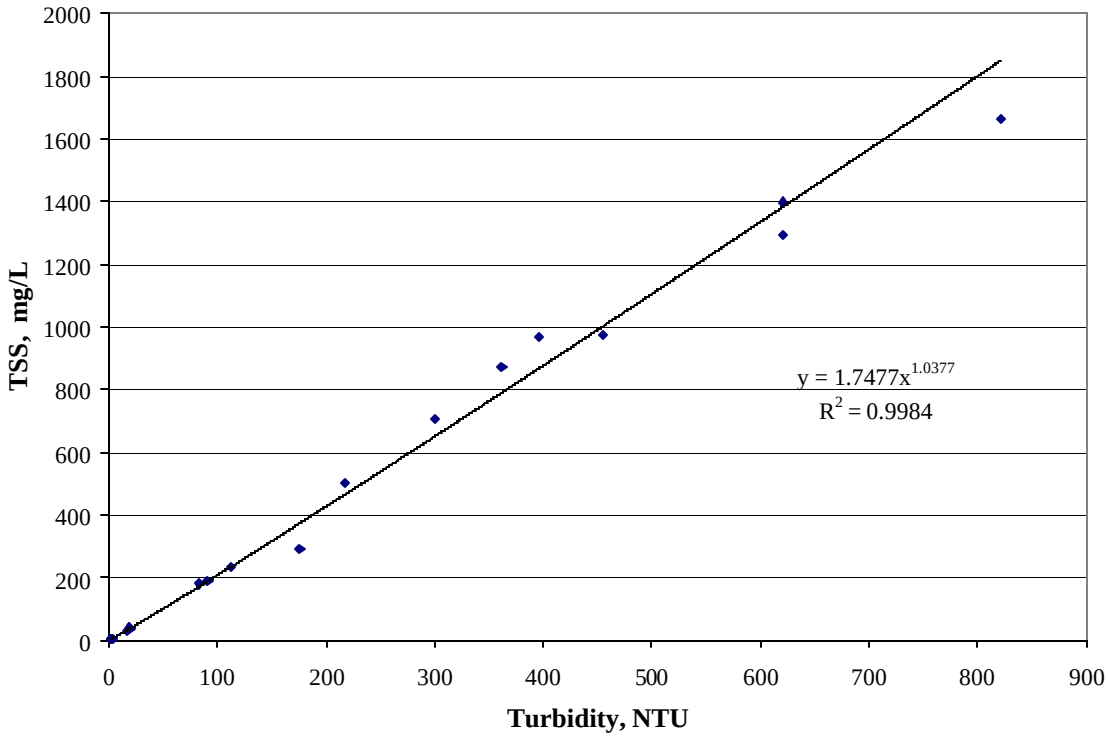

Figure A2.6 Correlation between turbidity and suspended solids for alum suspensions

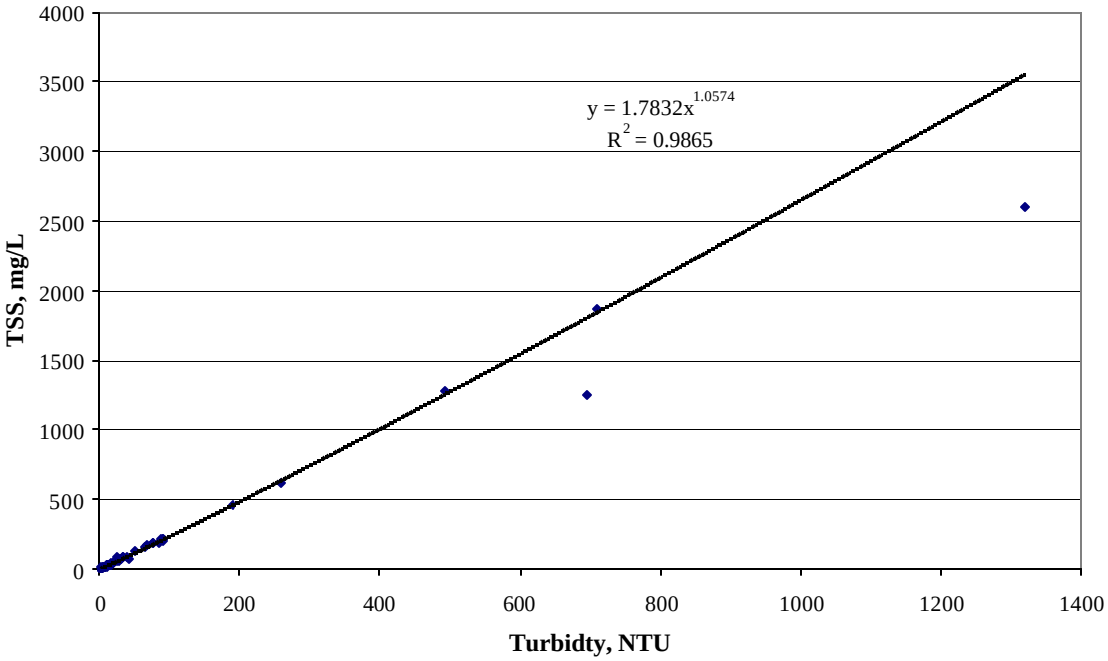

Figure A2.7 Correlation between turbidity and suspended solids for Z464N suspensions

APPENDIX 3

UNCERTAINTY CALCULATIONS

A3.1. Introduction

This Appendix provides additional information on the calculation of the margins of the uncertainty in the estimates of M_R and M_{TF} in Chapter 5 and the filter operating parameters in Chapter 9.

A3.2. Filter operating parameters

A3.2.1. Filtrate rate and volume filtered

The total volume filtered per filter run calculated by numerical integration (Trapezoidal Rule) of the measured flow rate vs time.

$$volf = \frac{\sum_{i=0}^{N-1} \frac{Q_{i-1} + Q_i}{2}\left(t_i - t_{i-1}\right)}{1000A} \qquad \text{A3.1}$$

$volf$ = total volume filtered during run, m^3/m^2

Q_i = filtrate flow rate measured at time t_i, L/h

t_i = run time at i^{th} measurement, h

A = filter area = 0.0314 m^2

The greatest source of uncertainty in the calculation of *volf* was the variation in flowrate overnight. Consequently, the maximum filtered volume was estimated by assuming that the flow remained constant overnight at the last measured flow in the afternoon while the minimum filter volume was estimated by assuming the overnight flow remained constant at the first flowrate measured the following morning.

$$volf_{\max} = volf + \frac{\frac{Q_{pm} - Q_{am}}{2}\left(t_{am} - t_{pm}\right)}{1000A} \qquad \text{A3.2}$$

$$volf_{\min} = volf - \frac{\frac{Q_{pm} - Q_{am}}{2}\left(t_{am} - t_{pm}\right)}{1000A} \qquad \text{A3.3}$$

$volf_{max}$ = maximum estimated total volume filtered during run, m^3/m^2

$volf_{min}$ = minimum estimated total volume filtered during run, m^3/m^2

Q_{pm} = last filtrate flow rate measured in the afternoon, L/h

Q_{am} = first filtrate flow rate measured the following morning, L/h

t_{pm} = time of last flow measurement in the afternoon, h

t_{am} = time of first flow measurement the following morning, h

The average filtration rate (*flow*) for a give filtration run was calculated as

$$flow = \frac{volf}{runtime} \qquad \text{A3.4}$$

flow = average filtration rate, m/h

runtime = total filter run time, h

A3.2.2. Influent and filtrate turbidity

The average influent (coagulated water) and filtered water turbidities were calculated by numerical integration of turbidity vs volume filtered, divided by the total volume filtered during the run.

$$coag = \frac{\sum_{i=0}^{N-1}\left[\left(V_{i+1} - V_i\right)\left(\frac{NTU_{in,i+1} - NTU_{in,i}}{2}\right)\right]}{volf} \qquad \text{A3.5}$$

$$filt = \frac{\sum_{i=0}^{N-1}\left[b_i\left(V_{i+1} - V_i\right)\left(\frac{NTU_{out,i+1} - NTU_{out,i}}{2}\right)\right]}{volf} \qquad \text{A3.6}$$

coag = Average coagulated water turbidity, NTU

filt = Average filtrate turbidity, NTU

V_i = Volume filtered at time of i^{th} turbidity measurement, m^3/m^2

$NTU_{in,i}$ = i^{th} coagulated water turbidity measurement, NTU

$NTU_{out,,i}$ = i^{th} filtrate turbidity measurement, NTU

b_i = weighting factor = 0.5, 0.75 or 1

The weighting factor b_i was used, where necessary, to compensate for low sampling resolution during the filter ripening stage, Here, the rapid initial drop in filtrate turbidity could result in large errors in the result calculated using Equation A3.6 if the filter ripening curve was not well defined. The value assigned to b_i for each increment depended on how far filter ripening had progressed.

A3.2.3. Coagulant dose

The average coagulant dosing rate (mL dosing solution per time) was calculated from the total volume consumed in one filter run divided by the filter run time.

$$dose\ rate = \frac{volc}{runtime} \qquad \text{A3.7}$$

dose rate = coagulant dosing rate, L/h

volc = volume of dosing solution consumed, L

The average coagulant dose for the run was:

$$dose = \frac{S \times dose\ rate}{A \times flow} \qquad \text{A3.8}$$

dose = Average coagulant dose, mg/L

S = dosing solution concentration, g/L

A3.2.4. Rate of headloss development

Two different measures of rate of headloss development were calculated. *rate*1 was calculated as

$$rate1 = \frac{term - h_0}{volf} \qquad \text{A3.9}$$

*rate*1 = rate of headloss development, m/(m^3/m^2)

term = terminal headloss, m

h_0 = initial headloss = 0.086 m

Note that *rate1* as defined in Equation A3.6 can be considered dimensionless. Headloss development was found to be non-linear with volume filtered near the beginning of the filter run, which implies that *rate*1 depends to some extent on the length of the filter run. Figure A3.1 shows the headloss development for a typical filter run. The large gap between the second and third data points corresponds to the overnight section of the filter run. *rate*1 corresponds to the slope of a straight line between the initial and final headloss.

*rate*2 was defined to be the slope of the linear regression line through all the measured headlosses excluding h_0. This is also illustrated in Figure A3.1. The value of rate2 depended somewhat on how far into the run the first headloss after h_0 was measured and therefore was not necessarily a superior measure of headloss development to rate1. Figure A3.2 shows the correlation between *rate*1 and *rate*2.

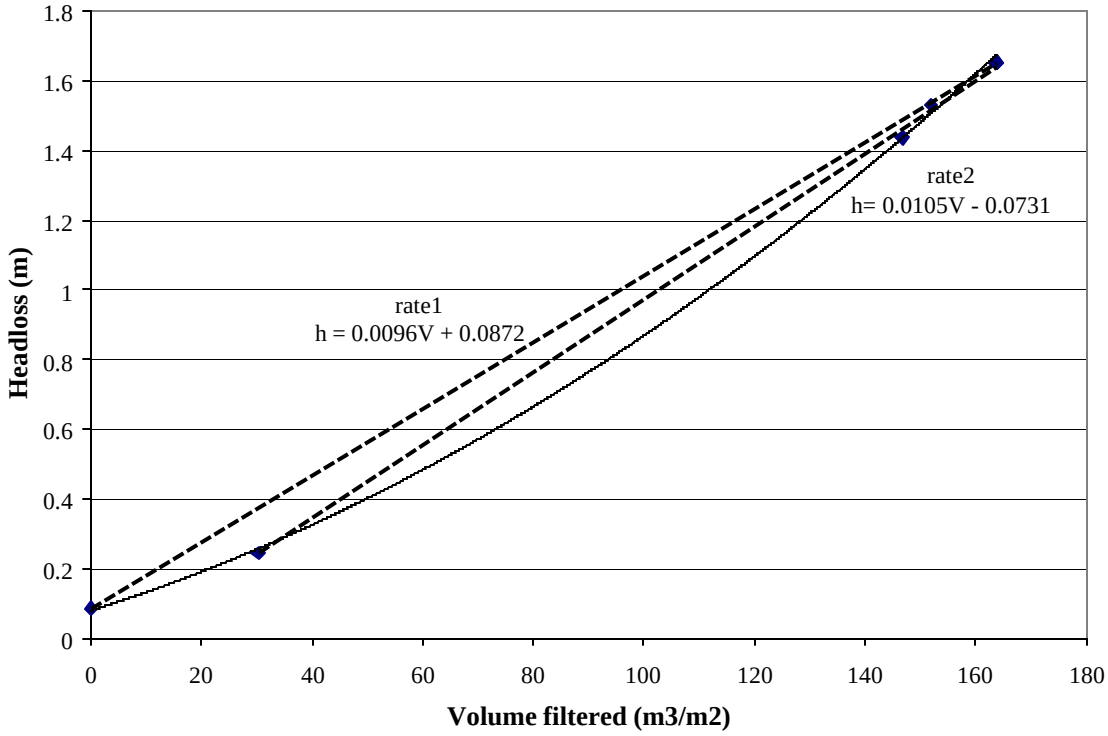

Figure A3.1 Rate of headloss development for run M48

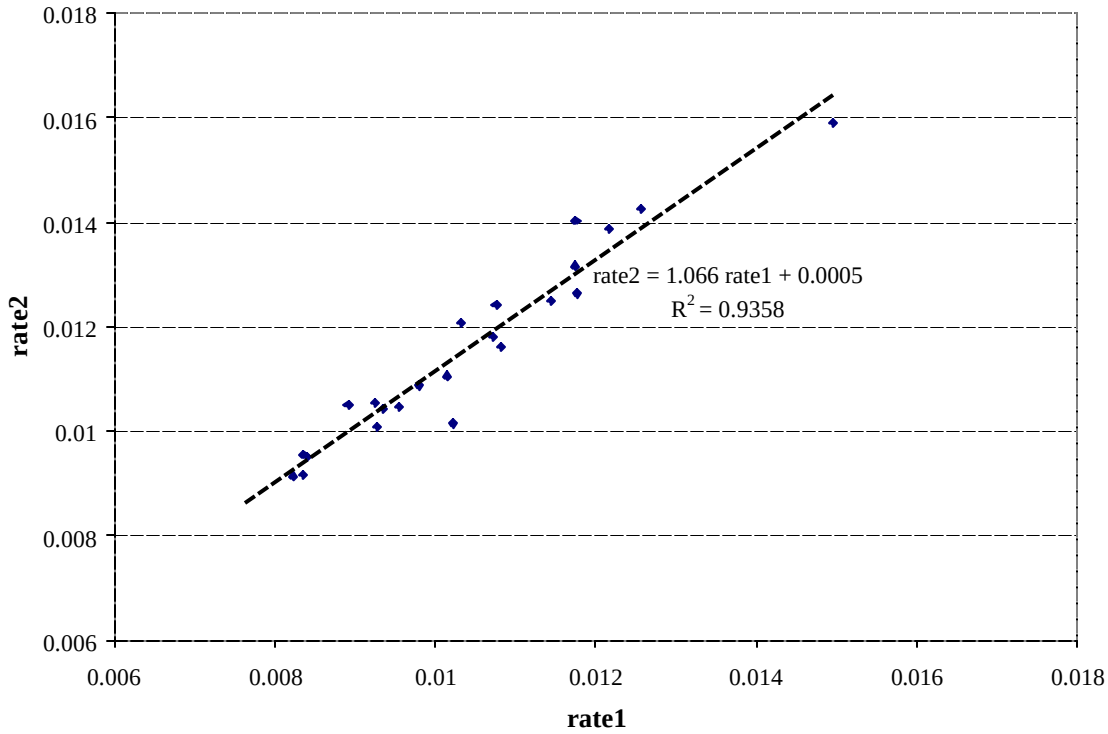

Figure A3.2 Correlation between *rate*1 and *rate*2 for runs M0 to M6R6

Given the close correlation between the two measures of rate, *rate*1 was selected to represent rate of headloss development in subsequent data analysis since values of *rate*1 were available for more of the filter runs than *rate*2.

A3.2.5. pH and temperature

The average temperature (*temp*), raw water pH (*rawpH*) and filtered water pH (*filtratepH*) used in the data analysis were the arithmetic means of all measurements of these variables in a given filter run. Upper and lower estimates of filtrate pH and average temperature are discussed in Section A3.1.3.1.

A3.3. Estimates of mass deposited and mass retained

A3.3.1. Calculations of mass of precipitate

For each filter run, the solubility of $Al(OH)_3(a)$ at the average operating conditions was calculated using MINTEQA2. Upper and lower limits of the solubility were calculated at the same time. The input for each run is summarized in Table A3.1

For each filter run the solubility at the average operating conditions was calculated using the variables *filtpH* and *temp* defined in Section A3.2.5. If no pH data was collected for a run, the pH from either the previous or the next run was used with the exception of runs from the series M9R1-M9R9.

Table A3.1 Inputs for calculation $Al(OH)_3(a)$ solubility using MINTEQA2

$$[Al]_T = 2 \times \frac{dose}{1000 \times M_{alum}}$$

$$[SO_4]_T = 3 \times \frac{dose}{1000 \times M_{alum}}$$

$[Al]$, $[SO_4]$	=	Total concentrations of aluminium and sulphate, mol/L
dose	=	Average alum dose defined in Equation A3.8, mg/L
M_{alum}	=	Formula weight of alum ($Al_2(SO_4)_3.14.3H_2O$) = 599.772382

Average solubility, $[Al]_{S,avg}$	Maximum solubility, $[Al]_{S,max}$	Minimum solubility, $[Al]_{S,min}$
filtpH	*filtpH MAX*	*filtpH MIN*
temp	*temp MAX*	*temp MAX*

Problems with the pH probe were experienced during this series of experiments and reliable pH data was only collected for two of the nine runs, M9R1 and M9R8. The pH was assumed to decrease linearly between runs M9R1 and M9R8, except for run M9R4. A pH of 8.76 was measured during this run but was initially assumed to be due to a malfunction of the pH electrode and rejected. However, there was also a sharp drop in rate of headloss development for this run. An increase in pH would have resulted in an increase in aluminium solubility and hence a decrease in precipitate deposited in the filter. This could have resulted in a slower headloss development. No other explanation for this anomaly in headloss development

was found, therefore it was assumed to be pH related. The measured value of 8.76 was probably too high since at this pH, no precipitate would have formed at all (See Figure 5.3) however, it is assumed that the problems with the pH electrode could have obscured a real, transient pH spike. Nevertheless, since there was no credible estimate of the actual pH, the mass of precipitate deposited for this run was assumed to be equal to the mass detached (i.e. in this case $M_R = 0$).

Upper and lower bounds for the solubility for each run were calculated by MINTEQA2 using the maximum and minimum temperatures measured during each run, and the maximum and minimum pH estimates respectively. Maximum and minimum pH estimates were based on measured variability in pH during individual runs where such data was available. This included measurements which were not considered reliable in themselves, but were included in the calculation of margins of uncertainty. For runs with only one pH measurement, the *filtpH MAX* and *filtpH MIN* were assumed to be the measured value +/- 0.05 units. For runs with no measured pH data, the margin of uncertainty on the assumed average pH was assumed to be +/- 0.1 units.

The mass of precipitate deposited was calculated using Equation 5.16. The upper and lower limits on M_{ppt} were calculated as follows: The maximum estimate of M_{ppt} corresponds to the maximum estimate of the dose and the minimum estimate of the solubility. The minimum estimate of M_{ppt} corresponds to the minimum estimate of the dose and the maximum estimate of the solubility.

$$M_{ppt,\max} = M_{ppt} \times \left(\frac{volc + 0.5}{volc} \right) \times \frac{\left(1 - \frac{[Al]_{S,\min}}{[Al]_{T,\max}} \right)}{\left(1 - \frac{[Al]_{S,avg}}{[Al]_T} \right)} \qquad \text{A3.10}$$

$$M_{ppt,\max} = M_{ppt} \times \left(\frac{volc - 0.5}{volc} \right) \times \frac{\left(1 - \frac{[Al]_{S,\max}}{[Al]_{T,\min}} \right)}{\left(1 - \frac{[Al]_{S,avg}}{[Al]_T} \right)} \qquad \text{A3.11}$$

Where

$$[Al]_{T,\max} = [Al]_T \times \frac{volc + 0.5}{volc}$$

$$[Al]_{T,\min} = [Al]_T \times \frac{volc - 0.5}{volc}$$

$M_{ppt,max}$ = Maximum estimated mass precipitate deposited in filter, g/m^2

$M_{ppt,min}$ = Minimum estimated mass precipitate deposited in filter, g/m^2

The upper and lower limits of the total cumulative mass deposited over a several runs was estimated slightly differently to account for the fact the relative uncertainty in the total volume of dosing solution consumed decreased with increasing number of runs. For $k > 1$, where k refers to the k^{th} run

$$\sum^{k} M_{ppt,\max} = \sum_{i=1}^{k-1} M_{ppt,\max,i} + M_{ppt,k} \times \frac{\left(1 - \frac{[Al]_{S,\min,k}}{[Al]_{T,k}} \right)}{\left(1 - \frac{[Al]_{S,avg,k}}{[Al]_{T,k}} \right)} \qquad \text{A3.12}$$

$$\sum^{k} M_{ppt,\min} = \sum_{i=1}^{k-1} M_{ppt,\min} + M_{ppt,k} \times \frac{\left(1 - \frac{[Al]_{S,\max,k}}{[Al]_{T,k}}\right)}{\left(1 - \frac{[Al]_{S,avg,k}}{[Al]_{T,k}}\right)} \qquad \text{A3.13}$$

For k = 1, $M_{ppt,\ max}$ and $M_{ppt,\ min}$ are calculated using equations A3.10 and A3.11 respectively.

The incremental mass retained for each run, M'_R, is estimated as the difference between M_{ppt} and the measured mass detached, M_D (Equation 5.17). The maximum of M'_R should therefore correspond to the maximum estimate of M_{ppt} and the minimum estimate of M_D. Hence

$$M'_{R,\max} = M_{ppt,\max} - M_{D,\min} \qquad \text{A3.14}$$

$$M'_{R,\min} = M_{ppt,\min} - M_{D,\max} \qquad \text{A3.15}$$

$$\left(\sum M'_R\right)_{\max} = \left(\sum M_{ppt}\right)_{\max} - \sum M_{D,\min} \qquad \text{A3.16}$$

$$\left(\sum M'_R\right)_{\min} = \left(\sum M_{ppt}\right)_{\min} - \sum M_{D,\max} \qquad \text{A3.17}$$

A3.3.2. Confidence intervals for the estimation of mass retained based on increase in bed height

The 95 % confidence interval on a prediction of a linear regression model is given by (Walpole and Meyers, 1985):

$$\hat{y}_0 - t_{0.025} s \sqrt{\frac{1}{m} + \frac{(x_0 - \bar{x})^2}{S_{xx}}} < y_0 < \hat{y}_0 + t_{0.025} s \sqrt{\frac{1}{m} + \frac{(x_0 - \bar{x})^2}{S_{xx}}} \qquad \text{A3.18}$$

where

$$S_{xx} = \sum_{i=1}^{m} (x_i - \bar{x})^2$$

$$s^2 = \frac{SSE}{m-2} = \frac{\sum_{i=1}^{m} (y_i' - \hat{y}_i)^2}{m-2}$$

x = Independent variable

$\bar{x}$ = Mean of x values used in the regression

y = Dependent variable

y_0 = True value of y at $x = x_0$

$\hat{y}_0$ = Predicted value of y at $x = x_0$

y_i' = i^{th} measurement of y

m = Number of data points used in the regression

SSE = Sum of square errors

$t_{0.025}$ = Value of the t distribution with m –2 degrees of freedom for $\alpha = 0.025$

In this case, $y = \ln(\Sigma M_R)$ and $x = \ln(\Delta Z_s)$. 95 % confidence intervals were calculated for $\ln(\Sigma M_R)$ and these were used to calculate upper and lower limits on ΣM_R. The incremental mass retained for individual runs, M_R were calculated as

$$\left(M_R''\right)_k = \sum_{i=1}^{k} M_R'' - \sum_{i=1}^{k-1} M_R'' \qquad \text{A3.19}$$

$\left(M_R''\right)_k$ = incremental increase in mass retained after kth run, g/m^2

The increase in settled bed height was not measured after runs M9R6 or M4R2. For these two runs $\sum M_R''$ was estimated as

$$\left(\sum M_R''\right)_{k,est} = \frac{\left(\sum M_R''\right)_{k-1} + \left(M_R'\right)_k + \left(\sum M_R'\right)_k}{2} \qquad \text{A3.20}$$

The upper and lower limits for individual values of M_R'' were calculated as

$$\left(M_R''\right)_{k,\max} = \left(\sum_{i=1}^{k} M_R''\right)_{\max} - \left(\sum_{i=1}^{k-1} M_R''\right)_{\min} \qquad \text{A3.21}$$

$$\left(M_R''\right)_{k,\min} = \left(\sum_{i=1}^{k} M_R''\right)_{\min} - \left(\sum_{i=1}^{k-1} M_R''\right)_{\max} \qquad \text{A3.22}$$

Note that

$$\left(\sum M''_R\right)_{\max} \neq \sum M''_{R,\max} \quad \text{A3.23}$$

$$\left(\sum M''_R\right)_{\min} \neq \sum M''_{R,\min} \quad \text{A3.24}$$

In several cases, negative values of $\left(\sum M''_R\right)_{\min}$ were obtained. This implies that in theory, there could be a net loss in mass retained after some backwashes. While this is possible, it is considered unlikely because no decrease in Z_S was observed after any of the water only backwashes.

The total mass of floc deposited during a given run was calculated as

$$M''_{TF} = M''_R + M_D \quad \text{A3.25}$$

$$M''_{TF,\max} = M''_{R,\max} + M_{D,\max} \quad \text{A3.26}$$

$$M''_{TF,\min} = M''_{R,\min} + M_{D,\min} \quad \text{A3.27}$$

The cumulative total mass deposited was calculated as

$$\sum M''_{TF} = \sum M''_R + \sum M_D \quad \text{A3.28}$$

$$\left(\sum M''_{TF}\right)_{\max} = \left(\sum M''_R\right)_{\max} + \sum M_{D,\max} \quad \text{A3.29}$$

$$\left(\sum M''_{TF}\right)_{\min} = \left(\sum M''_R\right)_{\min} + \sum M_{D,\min} \quad \text{A3.30}$$

REFERENCES

Ahmad, R. (1996). Filtration and Backwashing Performance of Biologically-Active Filters. Ph.D. Thesis. Georgia Institute of Technology, Atlanta. Georgia.

Amburgey, J.E., Amirtharajah, A., Brouckaert, B.M. and Spivey, N.C. (2003). An Enhanced Backwashing Technique for Improved Filter Ripening. J.AWWA, Vol. 95, No.12, pp.

Amirtharajah, A. (1971). Optimum Expansion of Sand Filters During Backwash. Ph.D Thesis. Iowa State University, Ames, Iowa.

Amirtharajah, A. (1978). Optimum Backwashing of Sand Filters. Journal of the Environmental Engineering Journal, ASCE, Vol. 104, No. 10, pp. 917-932.

Amirtharajah, A. (1984). Fundamentals and Theory of Air Scour. Journal of the Environmental Engineering Journal, ASCE, Vol. 110, No. 3, pp. 573-590.

Amirtharajah, A. (1985). The Interface Between Filtration and Backwashing. Water Research, Vol. 19, No. 5, pp. 581 – 588.

Amirtharajah, A. (1993). Optimum Backwahing of Filters with Air Scour: A Review. Water Science and Technology, Vol. 27, No.10, pp. 195-211.

Amirtharajah, A. and Cleasby, J.L. (1972). Predicting Expansion of Filters During Backwash. J.AWWA, Vol, No., 52 – 59.

Amirtharajah, A. and O'Melia, C.R. (1990). Coagulation Processes: Destabilization, Mixing and Flocculation. Chapter 6 in Water Quality and Treatment, 4th Edition, McGraw-Hill, Inc., USA.

Amirtharajah, A. and Giourgas, A.J. (1981).Theory for particle detachment from sand grains during backwashing of filters. International Symposium on Application on Fluid Mechanics and Heat Transfer to Energy and Environmental Engineering. University of Patras, Patras, Greece.

Amirtharajah, A. and Wetstein, D.P. (1980). Initial Degradation of Filter Effluent Quality During Filtration. J.AWWA, Vol 72, No., pp. 518-524.

Bache, D.H., Johnson, C., McGilligan, J.F. and Rasool, E. (1997). A conceptual View of Floc Structure in the Sweep Floc. Water Science and Technology, Vol 36, No. 4, pp 49 – 56.

Baylis, J.R. (1954). Washing and Maintenance of Filters. J.AWWA, Vol. 46, No. 2, pp. 176 – 186.

Baylis, J.R. (1959). Review of Filter Bed Design and Methods of Washing. J.AWWA, Vol. 51, No. 11, pp. 1433 – 1454.

Beek, W.J. (1971) Mass Transfer in Fluidized Bed, Fluidization, J.F. Davidson and D, Harrson eds., Academic Press, Inc. New York, N.Y. 1971, pp 431 – 470.

Bhargava, B.H., Ojha, C.S.P., (1989) Theoretical analysis of the backwash time in rapid sand filters. Water Research, Vol. 23, N 5 , pp 581- 587.

Buevich Y.A. and Markov, V.G., (1970). Pseudo-Turbulent Diffusion of Particles in Homogeneous Suspension, International Chemical Engineering, Vol. 10, pp. 570 – 575.

Brouckaert, B.M, Rajagopaul, R. and Pryor, M.J. (2003). Optimisation of an Autonomous Valveless Gravity Filter for the Cost Effective Production of Potable Water for Rural Areas. Water Research Commission, Pretoria, South Africa.

Cairns, E.J. and Prausnitz, J.M. (1960). Macroscopic Mixing in Fluidization, American Institute of Chemical Engineering Journal, Vol. 6, Dec. 1960, pp. 554 – 560.

Camp, T.R. and Stein, P.C. (1943). Velocity Gradients and Internal Work in Fluid Motion, Journal of the Boston Society of Civil Engineers, Vol. 30, pp. 219 - 237.

Camp, T.R. (1965). Theory of Water Filtration, Discussion. Proc. ASCE San. Div., Vol. 91, N0. SA.5, pp. 55 - 69.

Camp, T.R., Graber, S.D., and Conklin,G.F. (1971). Backwashing of Granular Media Filters. Journal of The Environmental Engineering Division, ASCE. Vol. 97, No. SA6, Proc. Paper 8605, December, pp. 903 –926.

Ceronio, A.D. and Haarhoff, J. (1994). Die Evaluasie van Suid-Afrikaanse Filtermedia vir Diepbedfiltrasie. Water Research Commission, Pretoria, South Africa.

Cleasby, J.L. (1977). Backwashing of Granular Filters. J.AWWA, Vol. 69, No. 2. pp. 115 - 126.

Cleasby, J.L. (1990). Filtration. Chapter 8 in Water Quality and Treatment, 4th Edition, McGraw-Hill, Inc., USA.

Cleasby, J.L and Fan, K.S. (1981). Predicting Fluidization and Expansion of the Filter Media. J. Environ. Eng. Div. ASCE, Vol. 107 (EE3), June, p. 455

Clerscerl, L.S.(ed), Greenberg, A.E. (ed.), Eaton, A.D. (ed.). (1999) Standard Methods for the Examination of Water and Wastewater, 20th Edition. American Public Health Association.

Corino E.R. and Brodkey R.S. (1969), A Visual Investigation of the Wall Region in Turbulent Flow. Journal of Fluid Mechanics, Vol. 37, Part 1, pp. 1 –30.

Cotruvo, J.A. and Vogt, C.D. (1990). Rationale for Water Quality Standards and Goals. Chapter 1 in Water Quality and Treatment, 4th Edition, McGraw-Hill, Inc., USA.

Dankwerts, P.V. (1951). Significance of Liquid Film Coefficients in Gas Absorption. Industry and Engineering Chemistry. Vol. 44, pp.1460-1467.

Dharmarajah, A.H. and Cleasby, J.L. (1986). Predicting the Expansion of Filter Media. J. AWWA, Vol. 78, No.12, pp. 66.

Fair, G.M. and Hatch, L.P. (1933). Fundamental Factors Governing the Streamline Flow of Water Through Sand. J.AWWA, Vol. 25, November. pp. 1551 – 1565.

Fair G.M. and Geyer J.C. (1954). Water Supply and Wastewater Disposal, John Wiley and Sons, Inc. New York, N.Y.

Fitzpatrick, C.S.B. (1990). Detachment of Fluid Deposits by Fluid Shear During Filter Backwashing. Water Supply, Vol. 8., pp. 177 – 183.

Fitzpatrick, C.S.B. (1991). Filter Backwashing Mechanisms. Ph.D. Thesis. University College of London, London, UK.

Fitzpatrick, C.S.B. (1993). Observations of Particle Detachment During filter Backwashing. Water Science and Technology, Vol. 37, No.10, pp. 213 - 221. IAWQ, Great Britain.

Gabilech, C.J., Ishida, K.P., Gerringer, F.W., Evangelista, R and Kaylan, M. (2004). Control of Residual Aluminum from Conventional Treatment To Improve Reverse Osmosis Performance. Proceedings. 9th World Filtration Conference. New Orleans, LA, April 18 – 22.

Getting, T.M., Geibel, J. and Eades, A. (2001). An American Approach to Designing and Rehabilitating Gravity Filter Systems. Proceedings: International Conference on Advances in Rapid Granular Filtration in Water Treatment, 4-6 April 2001, Chartered Institute of Water and Environmental Management, London, UK pp. 241 – 250.

Haarhoff, J. Filtration. (1997). Chapter 12 in Water Purification Works Design. F A Van Duuren, editor, Water Research Commission, Pretoria, South Africa. pp. 180 – 205.

Haarhoff, J. and Malan, W.M. (1983). The disturbance of sand filter supporting layers by air scouring. Water SA, Vol. 9 No. 2, pp. 41-48.

Hall, D. and Fitzpatrick, C.S.B. (1998). A mathematical filter backwash model, Wat. Sci. Tech., Vol. 37, N 12 pp 371 – 188.

Hall, D. and Fitzpatrick, C.S.B. (2000). Suspension concentration profiles during rapid filter backwashing, Chemical Engineering Journal, Vol. 80, pp 197 – 201.

Hanratty, T.J., Latinen, G., and Wilhelm R.H., (1956). Turbulent Diffusion in Particulately Fluidized Bed of Particles. American Institute of Chemical Engineers Journal, Vol. 2, pp. 372 – 380.

Hinze, J.O. (1975). Turbulence. 2nd Edition. McGraw-Hill, Inc., New York, U.S.A.

Huang, J.Y.C. and Basagoiti, J. (1989). Effect of Solids Property on Rates of Solids Detachment. Journal of Environmental Engineering, Vol. 115, No.1., pp. 3-19.

Ives, K.J. (1975). Mathematical Models of Deep Bed Filtration. In: the Scientific Basis of filtration, K.J. Ives (editor), Vol. 2, Series E, Noordhoff International Publishing, Leyden, pp. 203-224.

Kau, S.M. and Lawler, D.F. (1995). Dynamics of Deep Bed Filtration: Velocity, Depth and Media. Journal of Environmental Engineering, ASCE, Vol. 121, No. 12, pp. 850-859.

Kawamura, S. (1975a). Design and Operation of High-Rate Filters – Part 1. J. AWWA, Vol. 67, No.10, pp. 535 – 544.

Kawamura, S. (1975b). Design and Operation of High-Rate Filters – Part 2. J. AWWA, Vol. 67, No.11. pp 653 – 662,

Kawamura, S. (1991). Integrated Design and Operation of Water Treatment Facilities, 1st ed., John Wiley and Sons, Inc., New York.

Kawamura, S. (2001). Design and Operation of Filters with Granular Media. Proceedings: International Conference on Advances in Rapid Granular Filtration in Water Treatment, 4-6 April 2001, Chartered Institute of Water and Environmental Management, London, UK pp. 149 – 160.

Lang, J.S., Giron, J.J., Hansen, A.T., Trussel, R.R. and Hodges, W.E. (1993). Investigating Filter Performance as a Function of the Ratio of filter Size to Media Size. JAWWA, Vol. 85, No. 10, pp. 122-130.

Logsdon, G.S., Hess, A.F., Chipps, M.J. and Rachwal, A.J. (2002). Filter Maintenance and Operations Guidance Manual. AWWA Research Foundation and American Water Works Association, Denver, Colorado, U.S.A.

Martin, S.R. (1998). High Rate Granular Media Filtration. Chapter 8 in Water Treatment Plant Design, 3rd ed., American Water Works Association, pp 153 –192.

Mahmood, T. (1996). The Mechanics of Asymmetric Particle Release During Filter Backwashing and Migration of Colloids. Ph.D. Thesis. Georgia Institute of Technology, Atlanta. Georgia.

Mahmood T., Amirtharajah A., Sturm T.W. and Dennet K.E. (1998). A Micromechanics Approach for Attachment and Detachment of Asymmetric Colloidal Particles. Proceedings of the 72nd ACS Colloids and Surface Science Symposium, Penn State University.

McCabe, W.L. and Smith, J.C. (1976). Unit Operations of Chemical Engineering, 3rd ed. McGraw-Hill, New York.

McCune, L.K.. and Wilhelm, R.H. (1949). Mass and Momentum Transfer in Solid Liquid System, Industrial and Engineering Chemistry. Vol. 41, pp. 1124 – 1134.

Monk, R.D.G. and Willis, J.F. (1987). Designing Water Treatment Facilities. J.AWWA, Vol. 79 No. 2, pp 45 – 57.

Nozaic, D.J., Freese, S.D. and Thompson, P. (2001). Long Term Experience in the Use of Polymeric Coagulants at Umgeni Water. Water Science and Technology: Water Supply, Vol. 1, No. 1, pp. 43-50.

Raveendran, P. (1993). Mechanisms of Particle Detachment During Filter Backwashing. Ph.D. Thesis. Georgia Institute of Technology, Atlanta. Georgia.

Richardson, J.F. and Zaki, W.N. (1954). Sedimentation and Fluidisation: Part I. Transactions of the Institution of Chemical Engineers, Vol. 32, No. 1, pp. 35- 53.

Richman, M.T. (1999). Particle and Biomass Detachment During Biological Filter Backwashing : Impact of Water Chemistry and Backwash Method. Ph.D. Thesis. Georgia Institute of Technology, Atlanta. Georgia.

Sakkas , N.D. and Lekkas, T.D. (1989). Hydrodynamic Characteristics of the Solid-Liquid Fluidized Bed Developing During the Backwash of Filter Media. Environmental Technology Letters, Vol. 10, pp. 151 – 156.

Turan M., (1992). Velocity Gradient in Filter Backwashing, Journal of Environmental Engineering, Vol. 118, N 5, pp.776 – 790.

Wen, C.Y. and Yu, Y.H. (1966). Mechanics of Fluidization, Chemical Engineering Progress Symposium Series 62, Vol. 62, New York, N.Y., pp. 100-111.

Walpole, R.E. and Myers, R.H. (1985). Probability and Statistics for Engineers and Scientists, 3rd Edition, Macmillan Publishing Company, New York.

Water Department, City of Kyoto (1956). Effect of Filter Sand Size on Filter Performance. Journal JWWA, 262:8:32.

Zenz, F.A. and Othmer, D.F. (1960). Fluidization and Fluid Particle Systems. Rheinhold Publishing Corporation, New York, New York.

Ziskind, G., Finchman, M. and Gutfinger, C. (1995). Resuspension of Particulates from Surfaces to Turbulent flows – Review and Analysis. Journal of Aerosol Science, Vol. 26, pp. 613 – 644.

VITA

Barbara Brouckaert was born in Durban, South Africa in January 1973 to Chris and Heidi Brouckaert. She grew up in Durban and graduated with a Bachelor of Science Degree in Chemical Engineering from the University of Natal in December 1994. She enrolled in the Ph.D. program in the School of Civil and Environmental Engineering at Georgia Tech in September 1995 where she worked on several water quality and water treatment projects under her advisor Dr Appiah Amirtharajah. She graduated with her Master of Science degree in August 1999 before returning home to South Africa to complete her Ph.D. research at Umgeni Water under the International Student Co-op Program. She was employed by Umgeni Water as a contract scientist until June 2000 and then moved to the University of Natal while continuing to work with Umgeni as a consultant. In 2002 she became a Research Fellow and part time lecturer in the Pollution Research Group at the University of Natal. In August 2002 she married her husband Enrico Bellotti, then an Assistant Professor at Boston University. Since then she has divided her time between Boston and South Africa where she continues to work. In July 2004 she finally graduated from Georgia Tech with her Ph.D in Civil and Environmental Engineering.